Development of a novel bioreactor and systems for suspension cell culture in biopharmaceutical production

Rajesh Sharma

A thesis presented for the degree of

DOCTOR OF PHILOSOPHY

Supervisors: Dr. Siew L. Tai and Professor Susan T. L. Harrison

Department of Chemical Engineering
Faculty of Engineering and the Built Environment
University of Cape Town
March 2021

Plagiarism Declaration

1. I know that plagiarism is wrong. Plagiarism is to use another's work and to pretend that it is one's own.
2. I have used the Harvard system for citation and referencing. Each significant contribution to, and quotation in, this report from the work, or works, of other people, has been attributed and has been cited and referenced.
3. I declare that this thesis is my own unaided work, both in concept and execution and that, apart from the normal guidance from my supervisors, I have received no other assistance. Neither the substance nor any part of this thesis has been submitted in the past, or is being, or is to be submitted for a degree at this University or at any other university.
4. I have not allowed, and will not allow anyone, to copy my work with the intention of passing it off as his or her own work.

Signed by candidate

Signature

Abstract

Mammalian cells offer superior cellular machinery for the production of complex biological products. These cells provide proper post-translational processing machinery for recombinant protein expression to acquire the desired folding for optimal activity. With this advantage, mammalian cells have become the preferred choice for the production of biological products. These cells may grow either attached to a solid surface (adherent cells) or, where adapted, as suspension cultures. In order to grow these cells efficiently in suspension, a bioreactor is therefore required.

Bioreactors play a key role in the production of biologicals. Due to the continuous advancement of medicine and the healthcare industry, the demand for biological drugs has increased in the last three decades. This has placed a significant pressure on the biopharmaceutical industry to meet this increasing demand and has become a key driving force behind the need to develop better, safer and more economical bioreactor designs and culture processes.

Continuous stirred tank bioreactor is the norm for production of many bioproducts. However, these bioreactors exert high shear forces to cells due to the impeller speed, bubble disruption, and foam formation. In addition, at a large scale, improper mass transfer impairs the performance of cell lines and achieving high cell densities and prolonged viability with correct glycosylation of a secreted proteins is still a challenge during scale-up.

Many cell lines, for example Vero cells, which are widely used to produce human vaccines are difficult to adapt into suspension culture. Fixed-bed bioreactors and the use of microcarriers provide an alternative platform for their growth to produce biologicals. However, a high surface area is required to achieve the high cell density which leading to an elevated cost of production (mainly from microcarriers) and ensuing a costly and technically challenging scaling-up of these systems. Other designs such as single-use bioreactors and novel bioreactors based on different operating principles have been explored, but their utilisation is limited from laboratory to pilot scale. Hence, a comprehensive bioreactor design which would be suitable for a large variety of cell lines to produce high-yielding products in suspension culture with the lowest cost and risk in the shortest span of time is still sought.

In the current research, two approaches were investigated to address these challenges. Firstly, a horizontal tubular bioreactor (HTB) with a spiral impeller was designed and fabricated for the propagation of suspended mammalian cells with a focus to achieve middle to high cell density by improving mass transfer whilst reducing hydrodynamic shear and energy requirements through surface aeration.

The second approach is to test the adaptation of adherent Vero cells into single-cell suspension culture in serum-free media by treating them with an anti-cancer drug, Puromycin aminonucleoside (PAN). The absence of a supporting surface for cell growth (e.g. microcarriers) and serum-free conditions are expected to reduce the cost of manufacturing and to achieve higher productivity of biological production per unit volume of bioreactor.

In the first approach, the horizontal tubular vessel was designed to achieve the final volume of approximately 5.0 L. Design of the impeller is a key component that dictates the mixing patterns and mass transfer efficiency. Different geometric configurations were used to design the spiral impeller by considering various parameters such as impeller diameter, the pitch of the blade, pitch angle, height of the blade, the thickness of the blade, clearance efficiency and the position of the heating element. Another important aspect of the prototype design was incorporating an external magnetically-coupled motor drive which assisted in not only in aseptic handling but also reduction in mechanical stress and generation of fewer particles for cleanroom operations. The side plate was designed with the appropriate number of addition ports to allow execution of batches with minimum cross-contamination and for the ease of operation.

Thereafter, the engineering characterisation of the HTB was carried out. The performance of the HTB was evaluated for (i) oxygen mass transfer **($k_L a$)** through the dynamic gassing-in method, (ii) mixing time and fluid flow by tracer and phenolphthalein method, (iii) minimum stirring speed **(N_{js})** through alginate beads mimicking cell loading and modelling through modifying Zwietering equation, (iv) power consumption through heat calorimetry (temperature method) and (v) shear stress by determining specific death constant (k_d) at different impeller speeds.

The general characterisation profile of HTB has shown that at high agitation speed, homogeneity and mass transfer efficiency improved while power consumption increases with an increase in agitation speed. The bioreactor operated well at 2 L and 3 L capacity when the impeller is 40 - 90 % immersed in the liquid. The maximum mass transfer coefficient **($k_L a$)** of 16 h^{-1} was measured with a 3 L volume with an impeller speed of 500 rpm. These results are comparable with the other culture systems of the same scale.

The HTB was also tested for suitability to grow mammalian cells. Three batches were carried out, of which one was with the Chinese hamster ovary (CHO) cells expressing the somatic angiotensin-converting enzyme (sACE) and the two with plain CHO cells without expressing any recombinant protein. The maximum cell density achieved was of 5.48 x 10^6 cells mL^{-1} with plain CHO cells and 4.14 x 10^6 cells mL^{-1} with CHO cells expressing sACE with a maximum protein productivity of 465 mg mL^{-1}. The specific death rate constant of 0.025 (h^{-1}) was obtained when impeller speed was increase from 150 rpm (normal) to 300 rpm (induced shear) for 72 h.

In this study, CHO cells have been successfully adapted to suspension in serum-free conditions using the slow weaning of serum method and propagated in the HTB whereas Vero cells have been adapted successfully to serum-free media in adherent conditions. Attempt to suspend Vero cells based on literature using the weaning method remains timeous. Therefore, an alternative approach was explored using an anti-cancer drug (PAN) which is known to suppress the expression of integrin (cell adhesion receptors). The expectations from this approach were that the suppression of integrin would allow cells to detach and grow as a suspended culture (Krishnamurti et al., 2001). The results indicated that the anti-cancerous drug may have modulated the structure and function of the integrin which resulted in dislodging of the cells from the surface and form clumps which were viable for a week in

suspension culture without increase in cell density. The viability of the cell clumps and few suspended cells were tested by re-seeding of these cells back to tissue culture (TC) flasks in serum-containing media without the presence of PAN. The culture in the TC flask regained confluency in the 2-3 day which confirms the viability of the cells and the likeliness of integrin re-modulating itself in the absence of PAN. As the suspended Vero cells did not grow, they were not tested for growth in the HTB.

To investigate the biological activity of these Vero cells, Isothermal microcalorimetry was used to evaluate the heat generation profile of the Vero cells quantitatively before and after drug treatment. The heat flow data (metabolic heat) from the treated and normal cells showed a distinct decrease in the heat generation profile which indicated that the treated cells were viable but not as active as the normal (non-treated) cells. It was evident from the heat flow data obtained for the PAN-treated Vero cells (-0.13 μW) from that of non-treated cells (13.12 μW) and thereafter when PAN-treated Vero cells regrown in serum-containing media, they regain their metabolic activities which were indicated by their heat flow values as positive control (9.30 μW), 100 μg mL^{-1} (10.12 μW), 200 μg mL^{-1} (10.18 μW), and 250 μg mL^{1} (9.15 μW). It is recommended that dielectric spectroscopy and total DNA in the culture from the lysed cells could also be used to measure the bioactivity of the pre and post treated cells and data can be compared with IMC for more insight into the behaviour of the cells

It has been concluded that the horizontal tubular bioreactor (HTB) can sustain the middle to high cell density by imparting desired mixing and mass and heat transfer requirements whilst exerting minimum hydrodynamic shear. For the improvement of the design, it is recommended that more batches at different agitation speeds in combination with different airflow rate would further unravel the suitability of HTB to grow mammalian cells and stringently decode the optimum process conditions to achieve high cell densities with extended longevity. Additionally, changes in the pitch of the impeller blades could result in the improved fluid flow profile, mixing and mass transfer while drawing low power input. Subsequently, different modes of operation, e.g. fed-batch or continuous operation are suggested to investigate the suitability of the HTB for integrity, sterility, and possible higher productivities of products.

In suspending Vero cells, it has been concluded that the presence of serum-containing media reversibly stimulates the re-modulation of the integrin which poses hurdles in suspending Vero cells by reattaching the cells to the TC flasks. Therefore, it is recommended that a thorough investigation of the drug-treated cell integrin profile is examined through fluorescence-activated cell sorting (FACS) which would give details of the inhibition of the different integrin subunits. This information could form the basis of adapting cell-lines into suspension in a single step, which is otherwise difficult to adapt.

Dedication

This thesis is dedicated in the loving memory of my late mother Smt. Sneh Lata Sharma whose love, care, and strength made me the person I am today.

"All that I am or hope to be, I owe to my mother."

(Abraham Lincoln)

Acknowledgements

First of all, I would like to thank Dr Siew Tai and Prof. Sue Harrison for giving me the chance to undertake this research in the prestigious research group (CeBER) at the University of Cape Town. I would also like to acknowledge their full support in providing me scientific and professional guidance along with financial support. Without their guidance, it would have been impossible for me to complete this PhD journey. I would also extend my gratitude to NRF and CeBER (UCT) for their financial support for my research.

I would also like to thank Prof. Edward Sturrock and Sylva Schwager from IDM, UCT for their kind support to allow me to use their lab space when our lab was not ready at CeBER. I am also very grateful to both for sharing their sACE clone for the protein expression in HTB. Their valuable inputs have a great impact on my research. I would also like to thank Afolake Arowolo for playing a pivotal role in connecting me with Prof. Sturrock and Sylva. I would also like to thank Dr Suraj Parihar for assisting me in doing some of the experiments in his lab.

I would also like to thank and acknowledge the contribution of Dyasi Nontsikelelo and Machete Lebogang (2015) and Wesley Collair and Andrew Williams (2016) (undergraduate students) for carrying out the preliminary engineering characterisation experiments of HTB as a requirement towards the completion of their undergraduate studies.

Above all, I would extend my appreciation and thanks to all those researchers who were part of the Bioproduct and Engineering aspect discussion groups for their inputs and critical insight. There were some people who were part of CeBER but have moved on. They have also helped me in shaping my research. I would like to acknowledge their support and the time spent with them. Madelyn-Johnstone Robertson, Tobi Louw, Robert Pott, Caryn Fenner, Sarah Jones and Emmanuel, you guys are fantastic.

A special thanks go to CeBER staff especially Marijke, Thanos, Rob, Elaine, Mariette, Tich, Sharon, Lesley, Ruegshana and Sue J. Apart from these, I appreciate Muven, Qubekani, and Nosaibeh whose companionship I enjoyed during my research.

I sincerely thank my sisters, Vandana and Rajni with their respective families for their love and encouragement. I am deeply grateful to my brother, Brij Bhushan Sharma for always being there for me as a mentor and also as a pillar of strength. His wife (Neeraj Bala Sharma) and kids (Taveesh and Shreya) have always put smiles on my face with their unconditional love and support.

I don't have any words to describe the gratitude to my father, Raghubir Chand Sharma and late mother Sneh Lata Sharma. Their unparalleled love, support, and guidance has and will always strengthen me. I am also forever indebted to my children, Onir and Irit. They have sacrificed their playtime for me and turned out to be my greatest stress busters.

Finally, I thank with love to Jivashi Nagar, my wife, who herself is a PhD student. Jivashi has been a great companion in all respects and supported me to get through this hard journey of PhD.

The Novelty of the Project

The novelty of the project lies in the development of the bioreactor design and processes to achieve a single unified objective of attaining mid-range to high cell density and prolonged viability for shear-sensitive cell-lines. The following key points are novel in this research work.

- The design and use of **spiral impeller in a horizontal tubular vessel (HTB)** have not been reported for the propagation of mammalian cells. Various systems have however been reported using spiral or screw like agitators for moving Newtonian and non-Newtonian fluids e.g., ketchup, food juices, slurries.

- The CHO cells expressing somatic angiotensin-converting enzyme (sACE), firstly adapted to suspension culture from adherent culture and then propagated in HTB in batch mode. The novelty lies in the fact that sACE protein has not been expressed in a suspension cell set-up.

- The perspective of **suppressing integrin expression of Vero cells by using the anti-cancer drug** to bring Vero cells into suspension

- Isothermal microcalorimetry (IMC) was utilized to differentiate the biological activity of the normal mammalian cells from that of drug-treated cells by interpreting their metabolic heat profile chart.

Research Outputs

Journal papers in progress

Rajesh Sharma, Susan T.L. Harrison, Siew L. Tai. (2021). Advances in bioreactor systems for the production of biologicals in mammalian cells. Review article - Manuscript communicated to ChemBioEng Reviews

Rajesh Sharma, Wesley Collair, Andrew Williams, Susan T.L. Harrison, Siew L. Tai. (2021). Designing and engineering characterisation of Horizontal Tubular Bioreactor with spiral impeller - Draft in progress for Biochemical Engineering Journal

Rajesh Sharma, Sylva L. Schwager, Edward D. Sturrock, Susan T.L. Harrison, Siew L. Tai. (2021). Establishing the suitability of Horizontal Tubular Bioreactor with spiral impeller- A case study- Draft in progress for Biochemical Engineering Journal

Rajesh Sharma, Susan T.L. Harrison, Siew L. Tai. (2021). Vero cells adaptation into suspension culture - a novel way - Draft in progress for Current Opinion in Cell Biology

Rajesh Sharma, Susan T.L. Harrison, Siew L. Tai. (2021). Isothermal microcalorimetry and mammalian cells- a short review- Draft in Progress for Thermochimica Acta

Conference presentations

Rajesh Sharma, Susan T.L. Harrison, Siew L. Tai. (2017). Evaluating process parameters of surface-aerated horizontal tubular bioreactors for the growth of animal cells. 10th World Congress of Chemical Engineering, Barcelona, Spain, 1st – 5th October 2017.

Rajesh Sharma, Sylva L. Schwager, Edward D. Sturrock, Susan T.L. Harrison, Siew L. Tai. (2019). Evaluating bioreactor performance of a surface-aerated novel horizontal tubular bioreactor with spiral impeller for mammalian cells. 12th European Congress of Chemical Engineering and 5th European Congress of Applied Biotechnology, Florence, Italy, 15th – 19th September 2019.

Rajesh Sharma, Sylva L. Schwager, Edward D. Sturrock, Susan T.L. Harrison, Siew L. Tai. (2019). Evaluating bioreactor performance of a surface-aerated novel horizontal tubular bioreactor with spiral impeller for mammalian cells. International Conference on Biotechnology and Genetic Engineering (BioCon), Paris, France, 28th- 30th October 2019.

Table of Contents

List of Figures

List of Tables

Glossary of Terms

Axial flow	Movement of fluid or gas parallel to the axis of impeller rotation
Circulation time	The average time is taken for a fluid element to circulate around an entire vessel
Computational fluid dynamics (CFD)	The study of fluid dynamics using numerical algorithms
Conditioned medium	A medium where cultured cells secrete metabolites, growth factors, extracellular proteins, which are essentials for the propagation of cells
Convection	Movement of material by viscous drag forces between bulk fluid elements
Dimensional analysis	The use of dimensionless groups to model physical systems, dependent on Buckingham's π-Theorem
Dimensionless group	Group of physical parameters that produce the dimension of unity
Draft tube	A hollow tube concentric to another larger tube
Glycosylation	The process of functional folding of proteins by animal cells
Homogeneity	State of zero gradients within a system
Hydrodynamic forces	Viscous and shear forces acting within a fluid due to velocity gradients
Impeller	Rotating device in the bioreactor which accelerate the fluid motion
Impeller immersion	The ratio of impeller height covered with liquid to impeller diameter
Impeller zone	Fluid elements between submerged impeller blades and immediately surrounding the blades
In vitro	In a synthetic environment to mimic in vivo conditions
In vivo	Inside a living organism
Kolmogorov micro-scale	A scale for the measurement of hydrodynamic forces, based on the energy dissipated by turbulent eddies
Localized shear	Hydrodynamic forces generated in the impeller zone, and typically in the zone around a cell
Mixing time	Time is taken to achieve a state of 95% homogeneity in a vessel
Operating window	The range of operating parameters for meeting minimum performance criteria
Pitch	The axial distance between the two adjacent vanes on a screw
Helix angle	The angle between any helix/spiral and an axial line on its right
Pumping capacity	The amount of fluid circumscribed by the rotating impeller blades per unit time
Radial flow	Movement of fluid or gas normal to the axis of impeller rotation
Superficial gas velocity	Volumetric gas flow rate divided by cross-sectional area for flow
Surface renewal rate	The rate at which fluid elements with a high dissolved component concentration near the gas-liquid interface, replaced by fluid elements from the bulk liquid with a low dissolved component concentration
Thermogram curve	Graphical presentation of heat flow pattern in the sample

Symbols and Abbreviations

Symbols

$C*$	mmol L^{-1}	Oxygen Saturation Concentration
C_L	mmol L^{-1}	Actual Oxygen Concentration in Solution
C_x	Cells L^{-1}	Cell Density
Cp	J kg^{-1} K^{-1}	Specific Heat Capacity
D	M^2 s^{-1}	Molecular Diffusivity Coefficient
dm	m	Mean Diameter
E	J	Energy
k_d	s^{-1}	Cell Death Constant
k_La	h^{-1}	Volumetric Mass Transfer Coefficient
N_{js}	rev s^{-1}	Minimum Agitation Speed
N_P	Dimensionless	Power Number
N_Q	Dimensionless	Circulation Number
P	W	Power
P/V	Wm^{-3}	Power Density
qO_2	mmol $Cell^{-1}$ h^{-1}	Specific Oxygen Consumption Rate
Q	Mol s^{-1}	Mass Transfer Rate
R_e	[-]	Reynolds Number
R^2	[-]	Coefficient of Determination
θ_m	s	Mixing Time
τ_r	s	Response Time
UA	W k^{-1}	Overall Heat Transfer Coefficient

Acronyms and Abbreviations

AMPS	Ammonium Persulphate
ANOVA	Analysis of Variance
ATCC	American Type Culture Collection
ATF	Alternating Tangential Flow
ATP	Adenosine Triphosphate
BCIP	5-Bromo-4-Chloro-3-Indolyl Phosphate
BHK	Baby Hamster Kidney
BME	Beta-Mercaptoethanol
BTS	Bayer Technology Services
CAGR	Compound Annual Growth Rate
CEMMs	Cholesterol-Enriched Membrane Microdomains
CFD	Computational Fluid Dynamics

CHO	Chinese Hamster Ovary
CIP	Cleaning-in-Place
CSV	Comma-Delimited
2 D	Two Dimension
3 D	Three Dimension
DO	Dissolved Oxygen
DMA	Dynamic Membrane Aeration
DMEM	Dulbecco's Modified Eagle Medium
DMSO	Dimethyl Sulphoxide
DSPA	Desmodus Rotundus Salivary Plasminogen Activator
ECM	Extracellular Matrix
ECS	Extra-Capillary Spaces
EDR	Energy Dissipation Rate
FACS	Fluorescence-Activated Cell Sorting
FBA	Flux Balance Analysis
FBS	Fetal Bovine Serum
FDA	Food and Drug Administration
FMDV	Foot and Mouth Disease Virus
GMP	Good Manufacturing Practices
GPI	Glycosylphosphatidylinositol
GPT	General Performance Test
GVs	Gas Vehicles
HEK	Human Embryonic Kidney
HL	L-Histidyl-L-Leucine
HT	Hypoxanthine
HTB	Horizontal Tubular Bioreactor
ICS	Intracapillary Spaces
IgG	Immunoglobulin G
IL	Interleukin
IMC	Isothermal Microcalorimetry
IC_{50}	Inhibitory Concentration
ITC	Isothermal Titration Calorimetry
JEV	Japanese Encephalitis Vaccine
LDH	Lactate Dehydrogenase
MAbs	Monoclonal Antibodies
MBR	Membrane Bioreactor
MFC	Mass Flow Controller
µW	Microwatt
mU	Milli Unit

NADH	Nicotinamide Adenine Dinucleotide
NASA	National Aeronautics and Space Administration
NBT	Nitro Blue Tetrazolium
OSR	Orbital Shaken Bioreactor
OTR	Oxygen Transfer Rate
OUR	Oxygen Uptake Rate
pW	Picowatt
PAGE	Polyacrylamide Gel Electrophoresis
PAN	Puromycin Aminonucleoside
PAT	Process Analytical Technology
PBR	Photobioreactor
PE	Polyester
PFC	Perfluorocarbon
PIV	Particle Image Velocimetry
PTM	Post Translational Modifications
QbD	Quality by Design
RCCS	Rotary Cell Culture System
RGD	Arg–Gly–Asp
RI	Refractory Index
ROS	Reactive Oxygen Species
RTD	Residence Time Distribution
sACE	Somatic Angiotensin-Converting Enzyme
SDS	Sodium Dodecyl Sulphate
SF	Shake Flask
SFM	Serum-Free Media
SIP	Sterilization-in-Place
SOD	Specific Oxygen Demand
SSE	Sum of Square Errors
STR	Stirred Tank Bioreactors
SU	Single-Use
SUB	Single-Use Bioreactor
SV	Simian Virus
TBST	Tris Buffered Saline with Tween
TC	Tissue Culture
TCA	Tricarboxylic Acid
TEMED	Tetramethylethylenediamine
tPA	Tissue Plasminogen Activator
TFF	Tangential Flow Filtration
TME	Tumour Microenvironment

TWB	Travelling Wave Bioreactor
ULDPE	Ultra Low Density Polyethylene
URS	User Required Specifications
USP	Upstream Processing
VCD	Viable Cell Density
VLA	Very Late Antigen
WHO	World Health Organisation
WFI	Water for Injection
ZFHL	Z-Phenylalanine-L-Histidyl-L-Leucine
ZAR	Zuid-Afrikaans (South African) Rand

1 Introduction

1.1 Context of project

The integration of biotechnology is critical for the commercial production of useful products in the field of agriculture, food manufacturing, medicine, environment, and mining. In the context of South Africa, the biotechnology sector is still growing. The Government of South Africa initially adopted the National Biotechnology Strategy in 2001 and has given impetus to develop the biotech sector in the country and later in 2008 envisioned and published the Ten-Year Innovation Plan towards Knowledge based economy (2008-2018). The biotechnology canvas of the country in the 2000s were segmented into 50 % of companies in health-related activities, 8 % environmental, 9 % industrial biotechnology and around 13 % in support services (Cloete et al., 2006). Later, in 2013, The Government of South Africa embraced a comprehensive approach to push the bio-economy encircling sectors like agriculture, health, and industry for sustainable development in the coming future. The National Biotechnology Strategy (2001) was replaced by the Bio-economy Strategy in 2013 and then complemented with a white paper on Science, Technology, and Innovation in 2018 (Department of Science and Technology, 2018). Patra and Muchie (2017) later laid down the South African biotechnology sector according to the Sectoral System of Innovation (SSI) framework and compared the performance of South Africa among the BRICS countries. The SSI framework evaluated and provided indicators on innovation across sectors that are dynamic, integrated and multidimensional which primarily depend on the sources, participants and institutions (Malerba, 2017).

The central theme of these reports is to develop the South African economy as a “knowledge-based economy” which would produce skilled manpower and infrastructure not only in biotechnology sector but also include information technology, engineering, and a social science which would further assist in achieving the desired target of the self-reliant economy in health, agriculture and sustainable industry. The production of biopharmaceutical products falls under medical biotechnology or modern biotechnology which produces biological macromolecules that used to treat various diseases by modulating their physiological processes at a cellular level which pharmaceutical drugs are unable to do. (Research and Markets, 2017a). These products include vaccines, recombinant protein products, monoclonal antibodies, and small peptides which are produced by genetic manipulation of living organisms or animal/plant/insect cells (DaSilva, 2004; Zhang, 2010).

Over the last three decades, the production of biopharmaceutical products expressed in mammalian cells has gained paramount importance. These biological drugs are more efficacious than pharmaceutical drugs because of their biological origin (Research and Markets, 2017a). Proteins are translated from messenger ribonucleic acid (mRNA) with the help of transfer ribonucleic acid (tRNA) decoding and translating mRNA into a single amino acid chain, which further undergoes post-translational modifications (PTMs) to form a mature protein molecule. The PTM can be defined as changes to the protein due to the covalent bonds and enzymatic modification of the proteins. As a consequence, various functional groups would attach to the side chain of a polypeptide during protein biosynthesis which is

essential for the secreted proteins to infer proper conformation and size (Boehm, 2007; Knorre et al., 2009; Sidoli et al., 2004). These changes are necessary to increase the biological activity, immunogenicity and the serum half-life of the proteins (Duan and Walther, 2015; Fernandes, 2004; Knorre et al., 2009).

The increasing demand of biopharmaceutical products is due to the prevalence of many chronic diseases and the increase in the percentage of the population aged above 65, which leads to the increased investment in research and development activities and further induces the fast-track production of biologicals (Transparency Market Research., 2016). Since 2016, around 160 drugs have been approved by the Food and Drug Administration (FDA) and many more are in the pipeline from big companies. A total of 65 drugs were approved from 2000 to 2004 alone (Walsh, 2005), and a total of 96 recombinant proteins molecules produced in the mammalian cell culture were subsequently approved by 2011. This works out to an average of 15 drugs per year approved by the FDA from 2006 to 2011 (Lai et al., 2013). It has been reported that around 120 new products are currently in the pipeline and global vaccine markets alone have soared from $ 5 billion in 2000 to $ 24 billion in 2013 and are projected to reach $ 100 billion by 2025 (Kaddar, 2013). Overall, the biopharmaceutical market was valued at $ 162 billion in 2014 (Persistence Market Research, 2015), $ 176.9 billion in 2015, $ 192 billion in 2016 and $ 237.25 billion in 2018 (Mordor Intelligence, 2019). It is projected that with the Compounded Annual Growth Rate (CAGR) of 8.6 % per annum, it may reach $ 291 billion by 2021 and $ 389 billion by 2024 (Mordor Intelligence, 2019; Research and Markets, 2017a). It is also expected that the global biopharmaceutical market will grow at a CAGR of 10.1 % in the next decade, and the market may reach the mark of $ 459.81 billion by 2025 (Research and Markets, 2017b) as shown in Figure 1-1

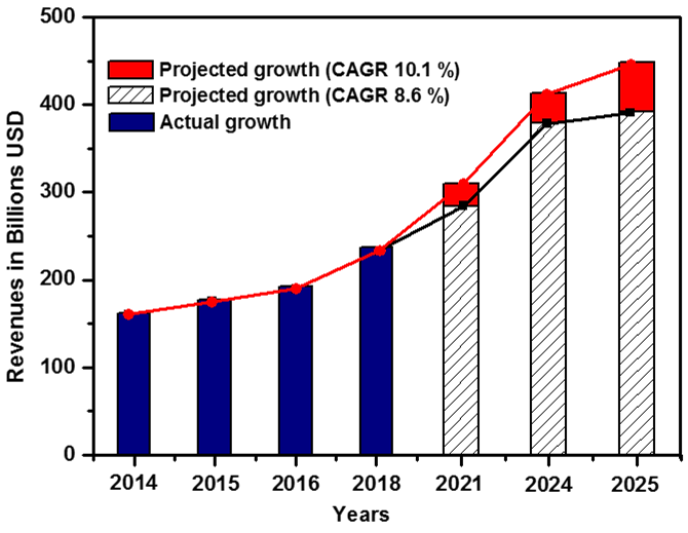

Figure 1-1 Overall biopharmaceutical growth - adapted from Mordor Intelligence (2017, 2019). Blue column represented the actual growth occurred in the indicated years and shaded column represented the projected growth at a rate of CAGR 8.6 % whereas additional red stacked column represented the difference between projected CAGR of 10.1 % to CAGR 8.6 %, denoted by red and black lines respectively

The demand for biopharmaceutical drugs has increased many folds as compared to other chemically synthesized pharmaceuticals. This is because of their ability to treat previously non-treatable diseases and also being a niche and novel market, increased the profit margins for their manufacturers (Research and Markets, 2017a). Therefore, in order to meet the rising demand for biopharmaceutical

drugs, innovative bioreactor designs and bioprocess strategies are required to continually improve yields and productivities of the product while maintaining a low production cost.

The bioreactor plays a pivotal role in the production of biologicals. Mammalian cells have semi-permeable outer cell membranes instead of a cell wall. Due to this, mammalian cells are shear-sensitive. Their fragility, large size, slow growth rates, and low oxygen consumption rates make them difficult to grow (Popović and Pörtner, 2012; Tolbert, 1990). Liquid shear forces from stirring, direct sparging of air and bubble formation inside the bioreactor have adverse effects on the growth of cells thus making it difficult to achieve optimum cell density, viability, and productivity. In addition, small changes in the macro and microenvironment during fermentation such as temperature, pH or solute concentrations can produce a protein with heterogeneity in structure and varying biological activity (Hu and Aunins, 1997). This leads to batch-to-batch variations and inconsistent product quality (Anicetti, 2009; Fernandes, 2004; Tolbert, 1990). Therefore, there is a need to develop strategies that would provide adequate mass and heat transfer with low shear stress on the growing cells.

Various bioreactor designs have been developed and tested since the 1940s, which works on different operating principles. The primary function of the bioreactor is to supply oxygen in sufficient amount to meet the oxygen demand of cells. This is an important parameter as the solubility of the oxygen in the liquid is low (7.8 mg L^{-1}) at ambient temperature. Failure to meet the oxygen demand would trigger apoptosis *i.e* cell death (Godoy-Silva et al., 2010). Therefore, the cardinal point of selecting a bioreactor for a process depends on its efficiency to deliver sufficient oxygen for the required cell density with minimum shear stress.

In case of conventional stirred-tank bioreactors, the combination of aeration and agitation plays a crucial role in achieving homogeneity in the vessel. For pneumatically driven bioreactors such as airlift, fluidised bed, and bubble column, oxygenation, mixing, and homogeneity are achieved by rising bubbles in the column. Hydrodynamic shear, bubble bursting and foaming in the bioreactor have a deleterious effect on the growth of cells, in both stirred tanks (STR) and pneumatic bioreactors (Chisti, 2000, 1993; Hambor, 2012; Sánchez Pérez et al., 2006). Fixed or packed bed bioreactors have also been in use for the growth of adherent cell lines. Due to low hydrodynamic shear, packed bed bioreactors attain high cell densities with few free cells in suspension as compared to STR (Zhou et al., 2010). The disadvantage of packed bed bioreactors is their low mass and heat transfer due to low velocity of medium circulation. This limits cell growth due to low availability of oxygen, nutrients and removal of toxic metabolites (Warnock and Al-Rubeai, 2006).

Surface aeration provides another route to deliver oxygen with low shear conditions through the surface of the liquid. It has been reported that surface aeration alone cannot cater to the oxygen demand of the high cell density cultures at commercial scale. This is because of low surface area available for oxygen transfer to the volume of medium (Henzler and Kauling, 1993; Nienow, 2006; Ozturk, 1996). There are bioreactor models available such as the wave type bioreactor, and orbital shaken bioreactor which exploit the surface aeration to deliver the oxygen to the cells. The demand for oxygenation can be

supplemented by intensifying the motion of the liquid by increasing the rocking or orbital shaking and this has been achieved up to pilot scales (Pörtner, 2015).

Alternatively, oxygen can be supplied to cells by the means of membrane aeration (porous silicone tubing with bubble-free aeration), perfluorocarbons (PFCs) and oxygen carrier. These methods have been established to work up to pilot scales. The disadvantages of these methods are in the high cost and safety concerns during downstream processing especially on the removal of perfluorocarbons, the availability of little design information and the difficulty in maintenance of silicone tubing at large scale (Godoy-Silva et al., 2010).

New technologies have also been developed based on novel principles such as the disposable CelCradle system, mimicking the functionality of the lungs, doughnut-shaped bioreactor with travelling wave as a medium of mass and heat transfer and dynamic membrane aeration (DMA) technology where,microporous silicone tubing wrapped around an oscillating stator, which when rotates, aid in mixing and oxygen mass transfer to the medium. These designs move away from conventional systems where air sparging draw high power, generate bubbles, and impellers causing hydrodynamic shear. These designs have been tested at laboratory and pilot scale but the scalability of these designs is still a challenge at a commercial scale (Czermak et al., 2009; Kaiser et al., 2016; Pörtner, 2015).

Many companies dealing in bioreactor developments are still seeking a comprehensive design that can minimise energy utilisation, increase mass transfer and mixing, monitor real-time cell growth and viability, and monitor and control the microenvironment (Wang et al., 2005). Henzler and Kauling (1993) reported that the mass-transfer efficiency ($k_L a$) mainly depends on the stirring speed and it has to be kept low to avoid shear conditions but sufficient enough to keep the cells into suspension. Therefore, it is evident that the aeration-agitation configuration of the bioreactor is a key factor in deciding the success of bioreactor design.

CHO and Vero cells are the primary mammalian cell-lines usually used to produce recombinant proteins and vaccines respectively. CHO cells are fibroblasts in nature and are derived from the ovary of the Chinese hamster whereas Vero cells are epithelial in nature and derived from the kidneys of African green monkey. CHO cells have an ability to grow well under adherent conditions and in suspension culture in serum-free medium (Bandaranayake and Almo, 2014; Lai et al., 2013) whereas Vero cells are adherent in nature and require a surface to grow. Currently, most of the viral vaccines produced using Vero cell lines are either adhered to solid surfaces (static) or onto microcarriers (suspension) which hugely elevate the production cost and a major limitation towards scale-up and commercialisation.

With advanced medium and feed development strategies and molecular biology techniques, scientists have developed many CHO cell variants through cell engineering that are compatible with various expression systems (Bandaranayake and Almo, 2014) and replaced serum-containing medium with serum-free and animal component-free formulations (Rourou, 2009). With the advances in mammalian expression systems and genetic manipulations of host cell lines, many more cell-lines derived from mammalian origin such as HEK, BHK, NS0, COS-1, COS-7, PER.C have shown a good prospect

to produce recombinant proteins and vaccines in terms of PTM profiling of the expressed proteins and productivity (Coco-Martin and Harmsen, 2008).

Many researchers have successfully adapted Vero cells to grow in the serum-free and animal component-free medium as an anchorage-dependent culture (Butler et al., 2000; Rourou, 2009; Rourou et al., 2009). It has also been reported that Vero cells can grow as cell aggregates in suspension culture, however with reduced culture age as oxygen mass transfer, nutrient availability to cells and difficulty in infecting with the virus for the production vaccine becomes an issue (Litwin, 1992). Daelli (2007) and Paillet et al., (2009) adapted Vero cells in suspension in batch and perfusion mode with the production of virus but unfortunately these processes could not be further exploited. Recently, Kiesslich and Kamen, (2020) reported that two research groups have successfully adapted the Vero cells in suspension in serum-free media through a sequential method (Rourou et al., 2019; Shen et al., 2019). Although, various researchers have endeavoured to bring Vero in suspension and indicate successful progress, the mechanism of adaptation of Vero cells into suspension is still unknown. So, a strategy to bring Vero cells into a single cell suspension in serum-free conditions needs to be developed which will not only reduce the doubling time and aggregate formation but also increase the growth rate.

Krishnamurti et al. (2001) have demonstrated the use of Puromycin aminonucleoside (PAN) as a suppressor of integrin on the glomerular epithelial cells, which has similar integrin subunits as of Vero cells. Integrins are heterodimeric, bidirectional, cell surface protein receptors, which play an important role in various cellular processes by mediating cell-to-cell interaction cell adhesion to the extracellular matrix, and act as a signalling hub for the normal cellular processes of the cell (Hynes, 2004, 1992; Schmidt et al., 2013). As the origin of Vero cells are kidney cells of the African green monkey and have the same subunits of integrins as of glomerular epithelial cells, it is predicted that PAN may exhibit the similar phenomenon of cell detachment as in the case of glomerular epithelial cells.

The physiological health of the cells can be determined by monitoring and analysing the heat generation profile of the living cells. A heat generation profile of a population of cells is directly related to growth stoichiometry and metabolic activity of the cells (Maskow and Paufler, 2015), which was measured through IMC. This is a versatile technique where heat flow calorimeter channelises the heat produced or consumed by the sample through the heat flow sensor which is made of the thermoelectric module. One side of the thermoelectric module is connected with the sample and another one with the heat sink which is kept at constant temperature by TAM III thermostat. When the temperature gradient is formed by the activity of the sample under investigation across the thermoelectric module, a voltage is produced as per the Seebeck effect, which is proportional to the rate of heat production or consumption by the sample (TA Instruments, 2012). Therefore, this technique is helpful in determining the changes in metabolic activity occurring in the cells before and after treatment with the anti-cancerous drug (PAN). The data obtained would assist in determining the biological activity (cell division and viability) of the cells before and after treatment (Garcia et al., 2017; Maskow and Paufler, 2015; Wadsö et al., 2017).

1.2 Research gap

To achieve middle to high cell densities (10 - 100 x 10^6 cells mL^{-1}) of mammalian cells, it is essential to provide a conducive growth environment inside the bioreactor without compromising (i) homogeneity of the culture and nutrients, (ii) optimum mass and heat transfer, and (iii) low shear conditions. Direct sparging in combination with agitation causes physical damage to the cells while surface aeration (bubble-free) with varying low-speed agitation methods does less damage to cells than high agitation speeds with a low flow rate of air (Chalmers, 1994; Chisti, 2000; Marks, 2003; Nienow, 2006; Pörtner, 2015). Mixing is necessary to keep cells in suspension and to provide optimum heat and mass transfer. Therefore, there is a window of opportunity to investigate a new design of a novel bioreactor that can address the issues in current bioreactors.

In conjunction, adapting adherent cells into suspension culture would also potentially reduce the production cost by eliminating the usage of microcarriers and low surface to volume ratio constraints for cell growth. The role of integrins in cell attachment and cell signalling has extensively been studied and published in literature. The exploitation of integrins subunits by exposing to an anti-cancer drug, could lead to bringing adherent cells into suspension by downregulating or suppressing the expression of integrins. The effects of this exploitation can thereafter be monitored using an isothermal microcalorimeter.

1.3 Objectives of the study

The primary aim of this project is to grow shear-sensitive cell lines in suspension to achieve cell densities in the range of 5 - 10 x 10^6 cells mL^{-1} for an extended duration of the batch by maximising mass transfer whilst minimising hydrodynamic shear. This thesis is focused on primarily two methods to maximise cell densities:

1. Designing a novel bioreactor with a specifically designed spiral impeller for shear-sensitive suspended cells for recombinant protein production
2. Adaptation of strongly adherent mammalian cells into suspension in serum-free media by using anti-cancerous drugs. (developing a proof of concept)
    a. Biological activity of Vero and CHO cells would be established using IMC technique to evaluate the heat generation profile of the cell lines w.r.t drug treatment before and after exposure, where CHO cells were used as a control.

1.3.1 Hypothesis 1

Surface aeration and agitation provide adequate mixing and mass transfer with the absence of high hydrodynamic shear for mammalian cell culture when a high surface area to volume ratio is achieved using the horizontal tubular reactor and a high surface renewal rate is achieved using a low shear, spiral impeller design.

1.3.1.1 Research Questions

- How would the spiral impeller contribute to the mass transfer efficiency, and will that be sufficient to support high-density culture in the horizontal tubular bioreactor (HTB)?
- What would be the effect of reactor fill volume on engineering parameters of the bioreactor?
- What will be the effect of low turbulence generated in the HTB by spiral impeller, on mixing, mass transfer and homogeneity of the culture?
- What would be the power utilisation profile of the spiral impeller in the HTB in comparison to wave type bioreactor
- What will be the effect of horizontal spiral impeller on hydrodynamic shear for mammalian cell culture?
- How would mass transfer efficiency of the HTB differ from the existing bioreactor at the same scale?

1.3.2 Hypothesis 2

To achieve Vero cells in suspension, it is necessary to suppress cell surface receptors (Integrin). Suppression of Integrin can be achieved by exposing the cells with anti-cancer drugs like Puromycin aminonucleoside.

1.3.2.1 Research Questions

- What would be the range of Puromycin aminonucleoside concentration that would suppress the expression of integrins but keeping the cells viable?
- What culture conditions would be suitable for Puromycin aminonucleoside to act?
- What operating factors would be responsible for the adaptation of Vero cells into suspension?
- What would be the growth profile of suspension-adapted cells as compared to adherent cells?

1.3.3 Hypothesis 3

The effects on the biological activity of mammalian cells treated with anti-cancerous drugs to suppress integrin can be monitored from the heat generation profiles of cells using an isothermal microcalorimetry.

1.3.3.1 Research Questions

- What will be the appropriate cell number that can generate sufficient metabolic heat flow (µW) for Vero and CHO cells?
- How would the heat generation profile differ for adherent and suspended cells?
- How would the heat flow signal correlate with the number of viable cells?
- How would heat flow data from the normal and treated cells elucidate the difference in biological activity?

- How would the heat profile pattern of normal and treated cells show a detectable difference in metabolic activities?

1.4 The scope of the thesis

The primary focus of this research was to design a novel horizontal tubular bioreactor (HTB) and formulate other strategies that would enhance cell growth and minimise the hydrodynamic shear.

The thesis explained the designing and commissioning of the HTB and later abiotic characterisation of engineering parameters such as oxygen mass transfer efficiency ($k_L a$), mixing time and fluid flow pattern, power consumption and minimum speed (N_{js}). The performance of this novel bioreactor with engineering parameters was compared to the literature values of stirred-tank and wave-induced bioreactor of the same scale. The suitability of the prototype was then evaluated by cultivating CHO cells in batch mode. The data obtained from CHO batches (cell density, viability, protein productivity) was then be compared to literature values of stirred tanks, wave-induced bioreactor, and CelCradle. Shear sensitivity was determined through the estimation of the death rate constant (k_d).

CHO and Vero cell-lines have been chosen for this study because of their usefulness to produce biologicals. Firstly, the adaptation of both the cell-lines in serum-free conditions was carried out and later, CHO cells were adapted to suspension culture. The suspension adapted CHO cells were then be used in the HTB to investigate its suitability to grow mammalian cells in batch mode.

Puromycin aminonucleoside was selected as a suppressor of Integrin to adapt Vero cells into suspension culture in serum-free media. The aim of adapting Vero cells in suspension was to achieve high cell density which is difficult to achieve with adherent culture. Furthermore, the adaptation reduced the risk of using serum and serum-associated contamination of adventitious agents. The comparative study of the behavioural changes that occurred in the Vero cells after treating with anti-cancer drug from that of normal cells were determined through IMC.

1.5 Structure of the dissertation

This thesis begins with the introduction (Chapter 1) which sheds light on the importance of mammalian cell line in the manufacturing of biologicals. Chapter 1 then identifies the knowledge gap, formulates the hypotheses and key research questions. Thereafter, the scope of the research is laid out.

The introduction chapter is followed by Chapter 2 on literature review, which extensively focusses on the identified knowledge gaps. This chapter lays the foundation by establishing the fact that the bioreactor is a key element for the development of various biologicals in mammalian cell culture. Later, it gives a chronological account of the development of different types of cell culture bioreactors since 1940s. It also touches upon various fundamental issues such as types of impellers and modes of sparging and their effects on cells during batch operation. Additionally, the chapter further described the advantages and disadvantages of commercially available cell culture bioreactors.

This chapter also review the methods that could be used to bring cell-lines into suspension e.g. encapsulation of Vero and CHO cells and exploiting integrins using anti-cancer drug, their role in virus entry and cancer research. Furthermore, the chapter touches on the use of IMC with mammalian cell culture. This chapter is concluded by identifying the areas where further study is required.

Chapter 3 defines the approaches of conducting the current research with materials and methods used in detail. This chapter explains the conceptualisation of the prototype idea, its designing strategies and the working principle of spiral impeller. The chapter also furnishes information on cell-lines used for the studies and the selection of appropriate media by carrying out media screening from various commercially available media. Thereafter, the chapter lays impetus on defining the methodology of characterisation of HTB, analytical methods used for adopted during the analysis of secondary metabolites alongside qualitative and quantitative analysis of the recombinant protein. Additionally, the methodology of Vero treatment with PAN is also discussed, the biological activity of Vero cells post drug treatment is then analysed with isothermal microcalorimetry along with CHO cells as control. The working principle and operational procedure of the IMC instrument is also covered in the chapter. A chapter summary is given in the end.

The results and discussion of the HTB with spiral impeller are divided into Chapters 4 and 5. Chapter 4 deals with the results obtained through abiotic characterisation of the HTB which includes the discussion on fluid flow pattern and mixing time mass transfer efficiency and its power consumption and determination of minimum agitation speed required to off-bottom the solid loading. The results obtained from abiotic characterisation are given at the end.

Chapter 5 deals with the biotic aspect of characterisation. Initially, an account of media screening is given for selection of appropriate media for the growth of CHO cells. Upon selecting the optimal media available, the details of three batches are furnished. During the batches, the results obtained for dynamic mass transfer (with cells) and shear stress experienced by cells during batches are also discussed. A comparative account of different surface aerated culture systems is also discussed. The metabolite analysis of the batches is given which sheds light on the pattern of glucose consumption, lactate and ammonia production, and osmolality, as culture biomass and age increase. Thereafter, an operational window is purposed for the HTB.

Chapter 6 discusses the results obtained by exposing the Vero cells to PAN. At the start of the chapter, time-dependent IC_{50} concentration of PAN is looked into, thereafter a vast spectrum of drug concentrations was evaluated to determine concentrations where the cells are dislodged from the substratum. The visual inspection of the cells under the microscope was carried out to elucidate the effect of PAN on Vero cells. A section has been dedicated to ***reasoning and analysis*** to discuss the behavioural changes that occurred to the Vero cells under the influence of PAN and a summary of the chapter is given at the end.

Chapter 7 investigates the applicability of IMC in determining the biological activity of CHO cells as a control. Thereafter, IMC profile of Vero cells grown in medium containing 1 % FBS, Vero adapted in serum-free medium (adherent) and Vero cells that came into suspension after dislodging from the surface

under the influence of PAN were analysed and discussed. This chapter is concluded with suggestions for further work in this arena.

Chapter 8 discusses the significant findings of the overall research and proposes the recommendations on current design of the HTB which may further improve the performance. Additionally, it is also recommended to explore other anti-cancer drugs (PAN) to suppress integrin's expression and explore the applicability of IMC to be used effectively for monitoring the health of mammalian cells.

2 Literature Review

The scope of this chapter is to cover the relevant literature on cell culture systems and bioreactor designs used to produce biologicals in mammalian cells both in adherent and suspension cultures. The chapter also covers the strategies to adapt mammalian cell lines into suspension, which is otherwise difficult to achieve, owing to its nature to remain adherent. Finally, the literature will be accessed to determine the biological activity of the cell-lines post-drug treatment, mainly focusing on the use of isothermal microcalorimetry (IMC).

2.1 Bioreactors and mammalian cell culture - the key elements of bioprocessing

Historically, humans exploited microorganisms for their use in making cheese, bread, wine, and beer with little mastery and understanding of the actual processes. The success of the process was merely by chance than by design (Williams, 2002). In present days, many biotherapeutics are produced in mammalian cells with quality by design (QbD) approach. Various cell lines have been deployed such as Chinese hamster ovary (CHO), baby hamster kidney (BHK), mouse myeloma cells (NS0, SP2/0) and human embryonic kidney cells (HEK). These cell lines are engineered to produce desired proteins with high volumetric productivity and biological activity. CHO cells alone accounted for 60 % of biologics produced with mammalian cells (Kantardjieff and Zhou, 2014). Vero cells are the preferred host for the production of vaccines. Hence, various cell lines and bioreactor processes are key elements of bioprocessing.

2.2 A brief history of mammalian cell culture

Cell culture is a century-old science. In 1885, researcher Wilhelm Roux managed to maintain the neural plate of chick embryos alive in saline for a few days (Rodríguez-Hernández et al., 2014) and later on, Ross Harrison in 1907 grew frog nerve fibre on lymph fluid in vitro for weeks on coverslips. These coverslips were placed inverted in an empty hollow grounded glass slide, thoroughly sealed with paraffin wax in a hanging drop method. The results obtained through this experiment demonstrated that cells can be grown in-vitro, which then laid the foundation for modern cell culture (Kretzmer, 2002; Tissot, 2011). Developmental work with plasma clot as a medium for the growth of chick embryo by Carrel and Burrows in 1910 led to the development of the first continuously growing cells. Up to the late 1930s, cell culture encountered many difficulties such as frequent contaminations and lack of growth media (Freshney, 2005; Rodríguez-Hernández et al., 2014). The commercial use of penicillin (antibiotic) in the early 1940s accelerated the cell culture work and later development of synthetic media by Eagle, who analysed the nutritional requirements of the cultured cells that transformed and intensify the cell culture work. The establishment of HeLa and BHK cells paved the way to produce vaccines (Polio). Additionally, the gradual advancements in media and feed developments made cell work easier than before. The advances in recombinant DNA (rDNA) technology and the discovery of monoclonal antibodies in the 1970s (Kohler

and Milstein, 1975), opened a new chapter of the cell culture applications in the health sector and increased knowledge of genes and expression systems in the production of genetically modified cell lines. Furthermore, with the advances in cryobiology, the preservation of biological samples (microbes, cell-lines, fungal and other specimens) became possible. The foundation of a repository such as American Type Culture Collection (ATCC) in 1992 played a significant role in specimen storage in an organized manner with full collection history and passages. Researchers can source strains/cell lines with authentic collection history with the guaranteed purity of the strain, which further assists in achieving reproducible results (Cypess and Simione, 2016). Another landmark was achieved in 1986 when tissue plasminogen activator (tPA) was produced in CHO cells and subsequently approved by the Food and Drug Administration (FDA). This technology revolutionized the area of medicine and broaden the horizon of using mammalian cells as a host cell line for the production of various recombinant protein products (Kunert and Reinhart, 2016; Lai et al., 2013). The launch of the process analytical technology (PAT) framework in 2004 by the FDA made bioprocessing a reality with robust, repeatable and reproducible results (Hinz, 2006). These breakthrough activities have further accelerated the production of biologics in mammalian cells. In more recent years, high-throughput technologies and the advances in “omics” tools such as proteomics, genomics, metabolomics further improved the process development strategies which later translated into high production yields and productivity (Cuperlović-Culf et al., 2010; Kretzmer, 2002; Lai et al., 2013; Omasa et al., 2010). Figure 2-1 showcasing the major milestones achieved in cell culture on time scale.

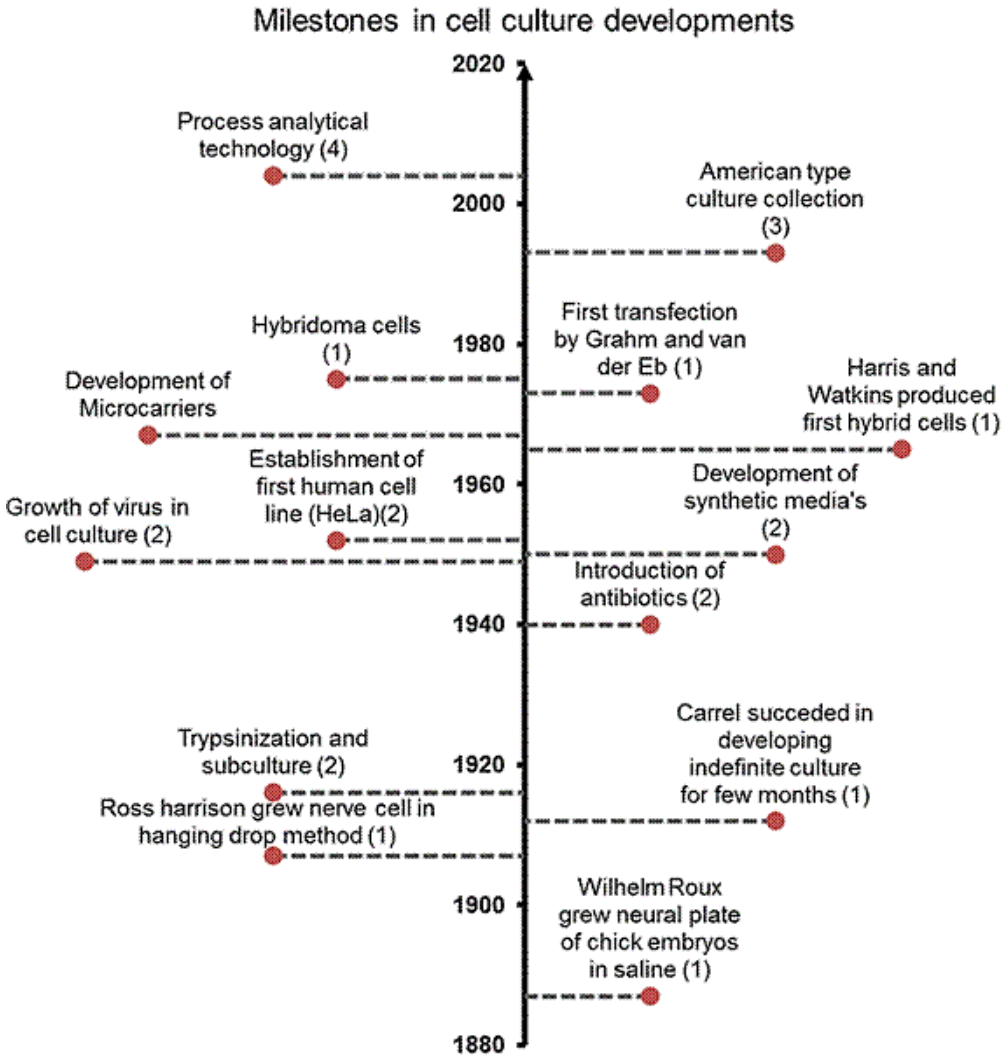

1. Rodríguez-Hernández, C.O., Torres-Garcia, S.E., Olvera-Sandoval, C., Ramirez-Castillo, F.Y., Muro, A.L., Avelar-Gonzalez, F.J., Guerrero-Barrera, A.L., 2014. Cell culture: History, development and prospects. Int. J. Curr. Res. Acad. Rev. 2, 188–200
2. Freshney, R.I., 2005. Culture of animal cells-A manual of basic Technique. Fifth. ed. Wiley-Liss, New York
3. Cypess, R.H., Simione, F.P., 2016. Transformation of an icon: ATCC and the new business model for science. First. ed. American Type Culture Collection (ATCC).
4. Hinz, D.C., 2006. Process analytical technologies in the pharmaceutical industry: the FDA's PAT initiative. Anal. Bioanal. Chem. 384, 1036–1042

Figure 2-1 Major milestones in cell culture process development

2.3 Mammalian cells and their application in biotherapeutics production

Since the production of tPA in the early 1980s in CHO cells, mammalian cell cultures have grown many folds and have become a major field in modern biotechnology for the production of biologicals (Eibl et al., 2009). This is primarily because of the increasing knowledge of gene expression systems, protein structures and their relationship to the protein activity, advances in cell engineering, and more importantly the development of stringent process development techniques (Eibl et al., 2009). The canvas of biological production has spread across many fields namely vaccines, monoclonal antibodies (MAbs), recombinant proteins, Fc-fusion proteins, interferon and other small peptides like interleukins (IL), growth factors and blood factors (Eibl et al., 2009; Godoy-Silva et al., 2010; Kantardjieff and Zhou, 2014).

The demand for biologicals and their approvals per year have grown many folds as discussed in Chapter 1. Moreover, 68 MAbs were approved by US-FDA until 2017 (Cai, 2017; Dangi et al., 2018). This is essential because of their ability to produce proteins with accurate post-translational modifications (PTMs) which ensure proper biological activity and efficacy to treat diseases. Furthermore, from an economic perspective, effective proteins are efficient in treatment and therefore increase profit margins for their manufacturers (Bleckwenn et al., 2004; Kantardjieff and Zhou, 2014; Research and Markets, 2017b). Anicetti (2009) reported that the current protein production processes consistently produce protein products with 99.9 % purity with uniform size and charge. This is essential to ensure that the protein products acquire proper 3 D conformation for high potency and activity which later triggers an immune response.

The key functions of a bioreactor are to provide optimal cell growth conditions for high cell densities, prolonged longevities, and high product yields and productivities. Many bioreactor designs have been tested for the growth of mammalian cells since the 1940s. These bioreactors fall under five major categories; namely, (1) bioreactors without control (e.g. tissue culture flasks, multi-tray cell factories, roller bottles, spinner flasks), (2) reusable bioreactors (e.g. conventional glass vessels, stainless steel stirred tank bioreactor, packed-bed, pneumatically-driven bioreactors), (3) single-use bioreactors (e.g. disposable stirred tank, wave mixed, orbitally shaken, pneumatically driven and fixed bed bioreactors), (4) novel bioreactor designs with different operating principles (e.g. CelCradle, Travelling wave, Nucleo bioreactor with tumbling impeller, Pad bioreactor, Vertical wheel and Rotating wall bioreactor) and (5) membrane bioreactors (CELLine flask, Super spinner).

2.4 Bioreactors: the foundation of the upstream processes

The primary aim of the upstream processing (USP) is to create an environment for the mammalian cells to express and excrete the desired proteins into the growth media. Significant improvements in the optimisation of USP have been carried out in the last two decades (Gronemeyer et al., 2014), which include several aspects of the biomanufacturing upstream process as depicted in Figure 2-2.

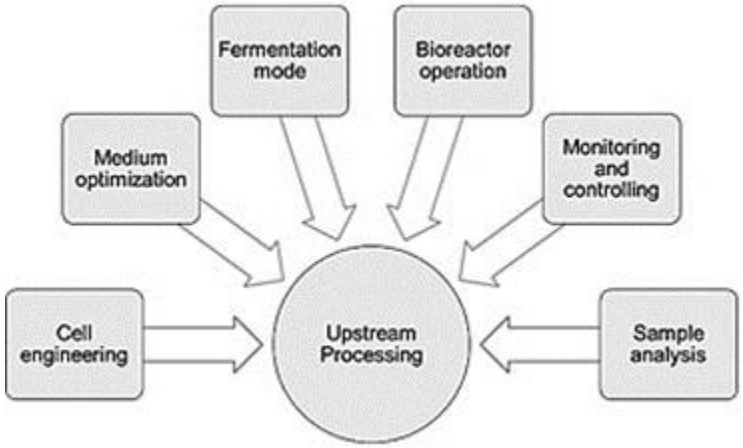

Figure 2-2 Steps in upstream processing- adapted from Gronemeyer et al (2014)

A bioreactor plays a dominant role in the production of biologicals, and it has been regarded as the central production wheel for the biopharmaceutical industry since the discovery of hybridoma technology in the 1970s. Traditionally the term “Bioreactor” has been synonymous to a stirred tank bioreactor which is the most commonly used reactor for bacterial, yeast, insects, plants and mammalian cells to produce valuable biological products. Yeast (*Pichia pastoris*), fungus (*Aspergillus niger*) and bacteria (*E. coli*) have been used to express small peptides/antibody fragments (Dangi et al., 2018; Kunert and Reinhart, 2016; Li et al., 2010). These expression platforms lack in human-like post-translational modification (PTMs) and forms inclusion bodies which further have a negative impact on the target product yield (Dangi et al., 2018). Therefore, mammalian cells are the preferred platform for the manufacturing of biopharmaceutical products predominantly because of their inherent ability to perform human-like PTMs and the ability to produce a large volume of target proteins at large scale in suspension culture (Demain and Vaishnav, 2009; Kunert and Reinhart, 2016). At present, various major biopharmaceutical companies have bioreactors with the maximum capacity in the range of 20 to 25 m^3 such as the large-scale cell culture bioreactors at Genentech, Vacaville with a capacity of 25 m^3 (25,000 L) and at Lonza, Singapore with a capacity of 20 m^3 (20,000 L) (Ozturk, 2014).

The Chinese hamster ovary (CHO) cells are the preferred host cells for the commercial production of biologicals because of its proven track record in manufacturing since its first use in the production of recombinant proteins (tPA). Various other cell lines such as Vero, MRC-5, BHK, NS0, Sp2/0, and PER.C6 are also used to develop recombinant proteins and vaccines. Vero and MRC-5 are predominantly used in the production of vaccines and CHO cell variants used for the production of biotherapeutic proteins (Butler, 2005; Kang et al., 2015). With the steady advances in the expression systems, process development techniques and production processes quality and quantity of the secreted proteins in CHO cells have improved over the years which resulted in high yields and purities (Anicetti, 2009). Media optimisation and the development of various bioreactor designs provide a conducive environment to the growing cells to achieve high cell density (10 - 100 x 10^6 cells mL^{-1}) for an extended period of time in a perfusion culture with high specific productivity (Butler and Meneses-Acosta, 2012; Kunert and Reinhart, 2016; Pörtner, 2015).

Upstream processing optimisation has the ability to achieve the required cell density with extended longevity, desired product titre and process efficiency at low cost (Gronemeyer et al., 2014). It could be achieved by manipulating several aspects included selecting a high producer clone, optimising media composition and feed regimens, establishing clonal stability which further aid in deciding the mode of fermentation with appropriate culture system, monitoring and controlling of process parameters, and finally in-line sample analysis for the desired product, host cell DNA and protein, and spent media .The advancement in control systems and instrumentation of bioreactors have allowed for an optimised macroenvironment leading to higher productivity, favourable growth kinetics and metabolic activity of the cells (Marks, 2003).

2.5 Chronological advances in mammalian cell culture systems: growth wheel of the biologicals Industry

Cell culture was traditionally done in glass tissue culture flasks (TC-flasks) and spinner flasks. Later, in the 1960s, disposable culture flasks made their way to the market (Eibl et al., 2014). The first use of stirred-tank bioreactors for mammalian cell culture was reported in 1965 when BHK cells were grown at 30 L scale in suspension for the production of inactivated foot and mouth disease vaccine (Hu et al., 2011; Nienow, 2006; Telling and Elsworth, 1965).

Product quality, yields and productivity depend on a variety of key parameters including the choice of the host cell system, culture medium, feeding regimen, process control, the efficiency of downstream processing of the product and the bioreactor design (Löffelholz et al., 2013a). Bioreactor systems to grow mammalian cells that have been developed over the last 60 or more years can be categorised in several ways. A major categorisation is whether the bioreactors are reusable or single-use bioreactors (SUBs). Reusable bioreactors are vessels with rigid walls constituted of glass and/or stainless steel and are cleaned and re-sterilised after use. Disposable reactors, on the other hand, are polyplastic vessels which normally constitute a collapsible bag which is discarded after use. Reactors are also classified in terms of the method by which energy is introduced for mixing. Examples include mechanically agitated systems with internal energy delivery such as stirred tank reactor; reactors with external pumping of liquids such as the fluidised bed bioreactor or packed bed reactor; reactors driven by external energy input such as the wave bioreactor or orbitally shaken reactors; and aerated systems such as the airlift reactor or bubble column. Table 2-1 details the major reactor types and the development of bioreactors from the 1940s to 2020. Trends in the development include single-use technology and impeller free systems.

Table 2-1 Chronological advancements of the bioreactors for the cell culture systems

Bioreactor categories	Bioreactor sub-categories	1940s-1950s	1960s-1970s	1980s-1990s	2000-2004	2004-2008	2008-2012	2012-2021
Without control		Disposable blood bags (Fenwel), Glass Spinner flasks	Glass Petri plates and Roller Bottles, SU-TC flasks, SU-Multi-layered TC factories			Super spinner D1000 (Sartorius)	Sensolux Flasks	
Reusable	The magnetically driven rigid vessel		Stirred tank-stainless steel					
	Pneumatically driven		Cell Maker Felix (Cellexus)				PBS3 (PBS biotech)	
	Hollow fibre		Cellmax				CelliGen BLU (Eppendorf)	iCELLis, Xpansion 200 (Pall)
	Packed or Fixed Bed			Solid glass beads, Macroporous glass beads (SIREN), Ceramic cylinders with the uniform square channel, PE non-woven fibre (FibraCel)				
	Bioreactor for Microcarrier Culture			Spin filter		DE53, (Whatman) (FibraCel, Eppendorf		
Single-Use	Wave mixed			Wave Bioreactor (GE)		AppliFlex, (Applikon), Biostat RM (Sartorius)	CellTainer, (CELLution Biotech)	Multi-layered Tsunami Bioreactor, Allegro XRS 20 (Pall), Smart Rocker (Finesse)
	Rotationally/Orbitally shaken bioreactor				Tube spin (TPP)	Orbitally shaken helical track	CultiBag ORB (Sartorius), Orb Shake (Kuhner), BayShake (BTS)	
	Mechanically driven stirred tank							Custom Single Run (CSR) (ABEC), Mobius 2000 (Millipore), Allegro XTR 200 (Pall)
Novel Design	Novel designs with the different operating principle			Rotary Cell Culture System (RCCS), (Synthecon)	Bello cells (Cesco Bioengineering)	Pad and Nucleo Bioreactor (Pall)	Dynamic Aeration System (BTS), Tide cell (Cesco Bioengineering)	Travelling Wave Bioreactor
Membrane								CELLine flasks (Integra Biosciences)

2.6 Aeration - Agitation regimen - a pivotal role in bioreactor designing

Aeration and agitation supply energy to the culture system to achieve uniformity in cellular and nutritional distribution as well as the growth environment including fluid flow, pH, DO and temperature (Orton, 1993). In cell culture, cell death occurs either by necrosis (passive cell death) or by apoptosis (active cell death). Necrosis happens due to the change in macroenvironment surrounding the cells such as accumulation of toxic metabolites and mechanical shear which destroy the cell membrane. On the other hand, in the case of apoptosis, a sequentially regulated signal cascade triggered within the cells in response to stress stimuli (change in growth conditions and accumulation of toxic metabolites) which ultimately lead the cells to programmed cell death (Mollet et al., 2007; Velez-Suberbie et al., 2013).

The suitability of the bioreactor essentially depends on the mass and heat transfer efficiency of the bioreactor where aeration-agitation regimen plays a vital role in cell growth by providing conducive hydrodynamic conditions to the cells. In other words, the bioreactor must maintain the oxygen demand of the growing cells above their critical oxygen level to prevent oxygen limitation as oxygen is essentially required as an electron acceptor for energy metabolism of the cells. Lack of oxygen, push the cells toward anaerobic metabolism for their energy demand and produces toxic metabolite in the culture which eventually leads to cell death by apoptosis (Grilo and Mantalaris, 2019). In the case of high oxygen concentration (hyperoxia), it has been reported that cells may produce reactive oxygen species (ROS) such as free radicals, which negatively alter the macromolecules like DNA, proteins and lipids, thus impairing the cell growth and trigger apoptosis (Godoy-Silva et al., 2010; Nayar, 1995). Therefore, the culture media must provide sufficient buffering capacity to neutralise the toxic component produce during the culture (Pol and Tramper, 1998), thus it is evident that oxygen is a primary nutritional component required for cellular growth and energy production. As oxygen is sparingly soluble in water/ water-based media (7.8 mg L^{-1}), the dissolved oxygen (DO) present in the media gets consumed rapidly (Godoy-Silva et al., 2010). During the exponential phase of the cellular growth in the culture system, the oxygen demand goes up and can only be met by delivering a continuous supply of oxygen primarily through direct sparging or by surface aeration (Godoy-Silva et al., 2010). There are many aeration methods such as direct sparging, surface aeration, membrane aeration (diffusion), medium perfusion, and high oxygen partial pressure to deliver oxygen to the shear-sensitive cells (Czermak et al., 2009), which are discussed in detail in section 2.7 with their pros and cons.

2.6.1 Oxygen mass transfer

The environment in the bioreactor is a multiphasic system where transport phenomena between the liquid and gaseous phase play a vital role in its functioning. Oxygen molecules, nutrients and toxic molecules have to be taken-in or driven-out of cells and are the prime examples of the need for efficient mass transfer (Carcano, 2010). For the scope of the current research, the focus will be on oxygen mass transfer.

As oxygen has low solubility in aqueous media, the transport of oxygen in the gas-liquid phase is a limiting step. The oxygen transfer rate (OTR) is determined by the mass transfer coefficient ($k_L a$) and

the concentration gradient across the gas-liquid interface (Garcia-Ochoa and Gomez, 2005). The gradient near to the gas-liquid interface is a complex phenomenon which vary from turbulent flow in the bulk phases and comparatively stagnant flow near the interface (Carcano, 2010).

The widely described model on gas-liquid mass transfer is **Two-Film theory** (Lewis and Whitman, 1924). Mass transfer in gas-liquid systems may be modelled by a two resistance theory in which the dominant transport mechanisms for a component from the gas phase to the liquid phase are through convection from the bulk gas to the gas-liquid interface, followed by diffusion through one or more stagnant 'films' exist at either side of the interface (Figure 2-3).

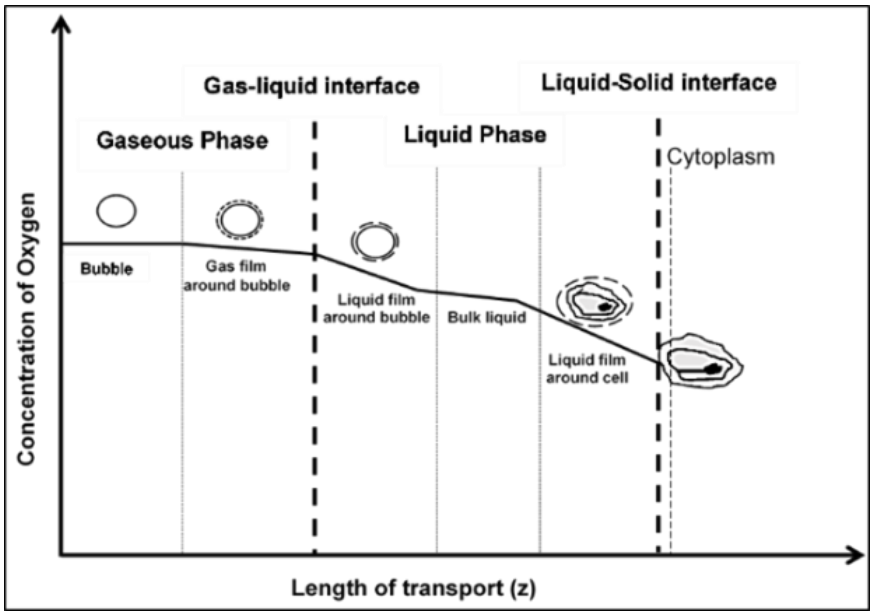

Figure 2-3 Phases of oxygen transport from gas bubble to cell with interfacial resistances (i) formation of gas bubble and gas film; (ii) transfer of gas bubble across the gas-liquid interface; (iii) diffusion through the relatively stagnant liquid film surrounding the bubble; (iv) transport through the bulk liquid; (v) diffusion through the relatively stagnant liquid film surrounding the cells; (vi) movement across the liquid-solid interface; and (vii) transport of oxygen to the cells via cytoplasm - adapted from Garcia-Ochoa and Gomez (2009)

It is assumed that there is no resistance to mass transfer at the interphase and the concentration across the interfaces $\boldsymbol{C_{gi}}$ and $\boldsymbol{C_{li}}$ are at equilibrium with each other. All the resistances occurred within the films (Carcano, 2010). According to Fick's Law, The concentration of the flux $\boldsymbol{j_A}$ (mol.m^2.s^{-1}) of component A, is given by molecular diffusion as Equation 2-1.

$$\boldsymbol{j_A} = -D\left(\frac{dC}{dZ}\right) \qquad \text{Equation 2-1}$$

Where, D is the molecular diffusion coefficient (m^{2}s^{-1}) and $\frac{dC}{dZ}$ is concentration gradient at equilibrium (mol.m^3.m^{-1}). Applying Equation 2-1 to both gas and liquid side diffusion across two films, we obtained Equation 2-2

$$\boldsymbol{j_A} = \boldsymbol{D_G}\left(\frac{\boldsymbol{C_G} - \boldsymbol{C_{Gi}}}{\boldsymbol{Z_G}}\right) = \boldsymbol{D_L}\left(\frac{\boldsymbol{C_L} - \boldsymbol{C_{Li}}}{\boldsymbol{Z_L}}\right) \qquad \text{Equation 2-2}$$

Where $\boldsymbol{D_G}$ and $\boldsymbol{D_L}$ are the effective molecular diffusivity ($m^2\ s^{-1}$) across each gas and liquid film respectively and $\boldsymbol{Z_G}$ and $\boldsymbol{Z_L}$ are the thickness of gas and liquid film (nm) respectively where the local mass transfer occurred due to the driving force.

As the interfacial concentrations $\boldsymbol{C_{Gi}}$ and $\boldsymbol{C_{Li}}$ are difficult to measure, the overall mass transfer coefficient can be written in terms of $\boldsymbol{k_G}$ and $\boldsymbol{k_L}$ for gas and liquid films ($m^2.s^{-1}$), $\boldsymbol{A}$ depicts the total interfacial area availble for mass transfer and Q (mol s^{-1}) represent total mass transfer rate as shown in Equation 2-3

$$Q = \boldsymbol{k_G} A(\boldsymbol{C_G} - \boldsymbol{C_G^*}) = \boldsymbol{k_L} A(\boldsymbol{C_L} - \boldsymbol{C_L^*}) \quad \text{Equation 2-3}$$

Where $\boldsymbol{C_G^*}$ and $\boldsymbol{C_L^*}$ are the steady state concentrations represent the bulk phase concentrations of gas phase ($\boldsymbol{C_G}$) and liquid phase ($\boldsymbol{C_L}$).

Using Henry's gas law, which states that at the gas-liquid equilibrium, the mass of dissolved gasses in liquid phase concentration ($\boldsymbol{C_{LA}^*}$) has a linear relationship with partial pressure ($\boldsymbol{pA}$) (Carcano, 2010) as shown in Equation 2-4

$$\boldsymbol{pA} = \boldsymbol{H_A}\, \boldsymbol{C_{LA}^*} \quad \text{Equation 2-4}$$

Where $\boldsymbol{H_A}$ is a Henry's gas law constant for component A in the liquid phase ($bar.m^3.kg^{-1}$). Henry's law predominantly hold true for the gasses with low solubility, hence the concentration gradient is low within the thin film (interface between gas and liquid) as that of bulk liquid, therefore, overall mass transfer coefficients are equal to the local coefficients (Carcano, 2010; Garcia-Ochoa and Gomez, 2009a). The overall mass transfer coefficient, (k_L) is a single parameter to describe all the combined resistances to mass transfer of species A from the bulk gas phase to the bulk liquid phase. It is often difficult to accurately measure the specific interfacial area, 'a' (interfacial area per unit liquid volume), so it is common to report the combined term $k_L a$ which represent the transport of A from gas to liquid, thus Equation 2-3 becomes

$$\boldsymbol{Q} = \boldsymbol{k_L a}\, (\boldsymbol{C_L^*} - \boldsymbol{C_L}) \boldsymbol{V_L} \quad \text{Equation 2-5}$$

The mass transfer coefficient in the bioreactor is generally represented by $\boldsymbol{k_L}$.or $k_L a$ (h^{-1}). This is an essential parameter in developing an adequate aeration design for a bioreactor to overcome the mass transfer resistances occurred in the liquid side (Carcano, 2010; Garcia-Ochoa and Gomez, 2009a; Nienow, 2015, 2006).

The value of $\boldsymbol{k_L a}$ is important to evaluate the bioreactor efficiency and determine the effect of the various operating parameter to deliver the oxygen to the end consumers, (cells/ microorganisms) (Garcia-Ochoa and Gomez, 2009a). The general equation applied to denote the well mixed aerated liquid phase is Equation 2-6

$$\frac{\boldsymbol{dC_L}}{\boldsymbol{dt}} = \boldsymbol{k_L a} * (\boldsymbol{C_L^*} - \boldsymbol{C_L}) - \boldsymbol{qO_2} * \boldsymbol{C_x} \quad \text{Equation 2-6}$$

Where, $\frac{\boldsymbol{dC_L}}{\boldsymbol{dt}}$ is the rate of oxygen concentration with time in the liquid phase, $\boldsymbol{k_L a}\, (\boldsymbol{C_L^*} - \boldsymbol{C_L})$ represent the oxygen transfer rate (OTR) across the liquid and $\boldsymbol{qO_2} * \boldsymbol{C_x}$ denote the oxygen uptake rate

(OUR) by the achieved cell density at a particular time during the batch. If water is used as a medium to determine the mass transfer efficiency of the bioreactor, then there will be no oxygen uptake by cells (OUR=0), Equation 2-7 becomes

$$\frac{dC_L}{dt} = k_L a * (C_L^* - C_L) \qquad \text{Equation 2-7}$$

Multiple methods have been evolved over time such as sulphite oxidation, dynamic gassing-in, hydrogen peroxide, oxygen balance and dynamic pressure method (Kadzinga, 2015). Only the dynamic method is discussed here

2.6.1.1 Dynamic method

The dynamic method is a classical physical method, where a change in dissolved oxygen concentration is measured with the oxygen probe in agitated conditions (non-stationary). The composition of gas has a negligible effect on the measurement, therefore, it is cheap to carry-out and widely used method (Villadsen et al., 2011). The rate of change of oxygen concentration mainly depends on the stirring speed, airflow rate and the volume of the liquid (Nienow, 2015, 2006).

In practice, at an operating condition *e.g.* stirring speed (rpm) and airflow rate (vvm), nitrogen is sparged into the medium inside the bioreactor until the dissolved oxygen concentration is zero in the medium. The bioreactor is then sparged with air over time to step-up the DO concentration in the medium until the medium is fully saturated with oxygen concentration denoted by C*. The change of DO concentration is thus a function of time as depicted in Equation 2-7

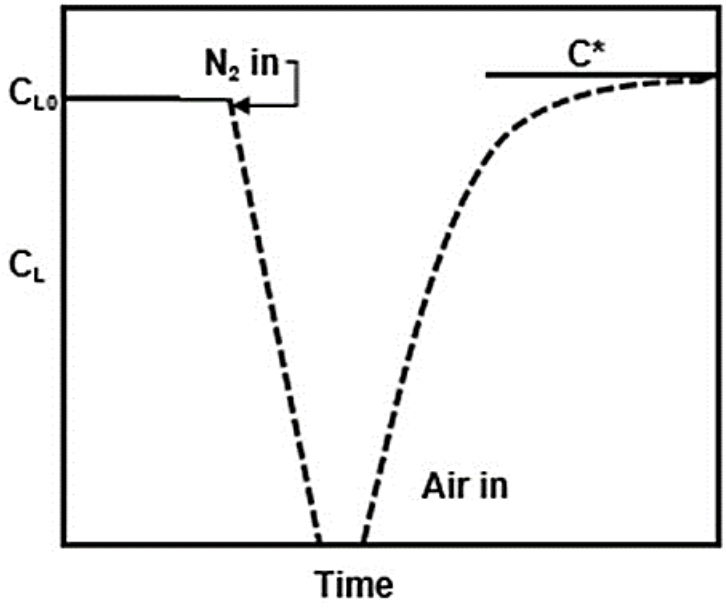

Figure 2-4 Schematic illustration of a dynamic method for the measurement of dissolved oxygen (DO) concentration – adapted from Uzir and Don, (2007)

Assuming that water is used as a medium to determine the $k_L a$ of a system, where OUR= 0, then, integrating the general mass balance Equation 2-7 becomes

$$ln\frac{C^* - C_L}{C^* - C_0} = -k_L a * (t - t_0)$$ Equation 2-8

Where, C_0 is a starting DO concentration at a time t_0. The $k_L a$ is given by the slope of the graph between $ln\frac{C^* - C_L}{C^* - C_0}$ and $(t - t_0)$. Precaution must be taken while recording the changes in DO concentration because few residual bubbles of nitrogen may be present in the medium which could alter the reading. The change of gas sparging may also alter the bubble regimen which have negative effects on the DO measurement because of the transition period, therefore, the system has to be at the steady state before recording the DO concentration and only the linear part of the slope is taken into consideration (Garcia-Ochoa and Gomez, 2009b, 2009a; Ruchti et al., 1981). This technique of measuring the mass transfer coefficient ($k_L a$) is well documented and widely practised across the research laboratories due to its simplicity and accuracy as compared to other methods (Chang et al., 1989; Gauthier et al., 1991; Koizumi and Aiba, 1984; Linek et al., 1991; Merchuk et al., 1990; Van't Riet and Tramper, 1991).

The success of this technique mainly depends on the response time of the probe otherwise inaccurate DO measurements result in false $k_L a$ value (Garcia-Ochoa and Gomez, 2009a; Uzir and Don, 2007). The delayed response of the dissolved oxygen (DO) probe is due to the sum of all the resistances faced by the probe from the surroundings and from inside (no/low electrolyte). The response time constant (τ_r) is the time taken by the DO probe (electrode) to reach the 63 % of the final value of the saturation point during the step-up stage (Garcia-Ochoa and Gomez, 2009a; Tribe et al., 1995; Van't Riet, 1979). Experimentally, the response time of the DO electrode can be measured by initially transferring the electrode into 0 % DO solution (sulphide solution in the presence of Co^{2+}) and then immediately transferred into the solution saturated with air (C*-100 % DO). The electrode is considered fast enough if the response time falls within 5s. The response time of a DO electrode can affect the determination of the mass transfer coefficient significantly if the response time constant (τ_r) is of the same order as ($1/k_L a$), however, the probe can still be used with appropriate correction in the $k_L a$ value (Garcia-Ochoa and Gomez, 2009a).

The electrode with extended response time has to be corrected with first-order modelling as shown in Equation 2-9, Where C_m is the DO value measured through the electrode, while C_L is the actual DO concentration in the liquid and τ_r is the response time

$$\frac{d\,C_m}{dt} = (C_L - C_m)/\tau_r$$ Equation 2-9

The combination of Equation 2-7 and Equation 2-9 results into Equation 2-10 which allow the measuring of the dissolved oxygen (DO) concentration in the case of saturation while considering the delayed response of the electrode (Tribe et al., 1995)

$$C_m = C^* + \frac{(C^* - C_{L0})}{(1 - \tau_r\, k_L a)}\left[\tau_r\, k_L a\, exp\left(-\frac{t - t_0}{\tau_r}\right) - exp(-k_L a\,(t - t_0))\right]$$ Equation 2-10

Where, C_m is the oxygen concentration measured by the electrode (DO) and while C_{L0} is the actual DO concentration in the liquid at the start of aeration.

The success of this method mainly depends on the fast response time of the DO probe and the residence time of the gas in the liquid phase, particularly, when the bioreactor is sparged with air Figure 2-4, while nitrogen is still present in the system. It is noted that this method is also not suitable for high viscosity medium merely because of extended hold-up time of the gas bubble in the medium (Uzir and Don, 2007).

2.7 Methods of oxygen delivery

Cells require an optimum supply of oxygen for metabolism. Mammalian cells have low oxygen demand as compared to microbial cultures, however, oxygen is still a limiting factor for high-density cell cultures. The oxygen mass transfer coefficient (k_La) value of sparged stirred tank bioreactor for mammalian cell growth conditions falls between 1 - 15 h^{-1} (Nienow, 2006). It is the new normal for industrial batches to achieve cell densities ranging from 5 - 10 x 10^6 cells mL^{-1}. Some systems reported to achieve even higher cell densities, especially in perfusion cultures. The typical oxygen uptake rate (OUR) of mammalian cells is in the range of 0.5 - 8.0 x 10^{-10} mmol $cell^{-1}$ h^{-1} (Pörtner, 2015). Oxygen requirements increase as the cell density increases during the bioreactor run. Most of the industrial applications accept cell lines operating at a wide range of oxygen concentration (15 - 90 %), whereas primary cell lines prefer to grow at low oxygen concentrations (< 20 %) mimicking the in vivo conditions (Czermak et al., 2009). Generally, to meet the oxygen demand of a middle to high cell density, the operational conditions of a batch fall in the range of 20 - 50 % of air saturation (Xie et al., 2011), therefore, there is a need to select for an effective method of oxygen delivery to the cells to control the desired range of DO % during the batch to ensure the required cell density and target product titre. Oxygen delivery has a direct relationship with the aspect ratio of the vessel (h/d ratio), sparger type, impeller type, number of blades, the position of the blades in the vessel, gas flow rate and, speed of the stirrer (Chalmers and Ma, 2015). These relationships are then optimised for the many ways in which oxygen is delivered in the bioreactor. The methods are discussed below.

2.7.1 Direct sparging

Direct sparging is considered as the method of choice at large scale cell cultivation as it represents a conventional and inexpensive mode of aeration to provide oxygen to the large-scale culture (Nayar, 1995). Generally, the sparger is placed under the agitator at the bottom of the bioreactor, which aids in bubble break-up, removal of the toxic gases from the culture media and provides adequate oxygen mass transfer necessary for the cells (Czermak et al., 2009; Godoy-Silva et al., 2010; Henzler and Kauling, 1993). The gas sparged into the bioreactor is usually measured in, the volume of gas flow per unit volume of the bioreactor per minute (vvm) or in litre per minute (LPM) displayed on rotameters.

Various types of spargers are employed for aeration such as point, frit, ring, and pipe sparger. The type of sparger plays an important role in delivering the desired mass transfer coefficient for high cell density culture without impacting on the overall cell growth and in determining the hydrodynamic patterns

of the bioreactor. For mammalian cell culture, ring sparger and microporous frit sparger are common in use which has 7 - 10 holes of 0.5 - 1.0 mm diameter and 10 - 20 µm pore size respectively (Bowers, 2008; Sandadi et al., 2011).

Usually, a microsparger have pore sizes of 2 - 30 µm and come in different shapes and sizes (Ozturk, 2014). Microspargers provide a large surface area and high mass transfer efficiency to the high-density culture. It is estimated that to maintain the same cell density, microsparger required 1/10 gas flow rate as compared to macrosparger (Ozturk, 2014). The downside of using the microspargers is that it also generates small bubbles (< 2mm), which create foaming and bubble bursting at the surface of the liquid (Chisti, 2000). To prevent foam formation, the gas flow rate through microspargers is usually pulsed at regular intervals. At large scale, the formation of small bubbles does not pose foaming problems as small bubbles will dissolve in the liquid before reaching to the surface and moreover, the small bubbles get saturated with CO_2 easily hence not suitable for stripping CO_2 which could, therefore, accumulate in the media to a toxic level (Pörtner, 2015).

In the case of macrospargers (ring, pipe and “L” shaped), large bubbles are formed with the size of 1 mm to few centimetres (Ozturk, 2014). The size of the bubbles formed during aeration has a significant impact on the mass transfer efficiency of the reactor. If the size of the bubbles formed is around 6 - 8 mm, they do not cause foam formation and cell death, because they travel faster upwards toward the surface and carry fewer cells attached to the bubble surface. However, they are not suitable at scale due to their small interfacial area for mass transfer (Czermak et al., 2009; Godoy-Silva et al., 2010; Ozturk, 1996). High mass transfer efficiency can be achieved by providing higher gas flow rates of oxygen-rich air as compared to the microsparger to achieve the same cell density. Additionally, increasing stirrer speed could enhance the mass transfer but the additional shear can cause cell death, therefore, the addition of surfactants such as Pluronic F68, poloxamer 188, and kollipore could minimise the shear effect of bubble rupture and foaming (Nienow, 2015; Pörtner, 2015). The recommended approach is to use both the sparger in combination, microspargers for aeration and macrospargers for CO_2 stripping (Godoy-Silva et al., 2010; Ozturk, 2014, 1996).

In the case of microcarrier cultures, where anchorage-dependent cells adhere onto the small beads (microcarriers) in suspension, the cells experience localised frictional forces due to the collision among beads, against impeller blades, reactor walls and rising bubbles, and as a result cause damage to the cell (Godoy-Silva et al., 2010). In other words, microcarriers are exposed to local hydrodynamic forces in the same region where the bubble is rising. The rising bubbles also carry microcarriers on the surface of the foam where it formed a thick layer and inhibits cellular productivity as shown in Figure 2-5

Figure 2-5 Effect of the foaming on microcarrier culture (Courtesy Panacea Biotec Ltd.)

2.7.2 Surface aeration

Surface aeration can be explained as a method of aeration where oxygen diffuses from the headspace into the medium through the liquid phase, and as a result, there is almost no cell-bubble interaction. Initially, surface aeration was designed for small scale culture systems only such as shake flask and bench-top lab-scale bioreactors but currently, many surface-aerated bioreactors are commercially available up to a scale of 2000 L (single-use wave-induced culture systems) (Eibl and Eibl, 2009; Pörtner, 2015; Singh, 1996).

As a principle, in the case of shake flask, the primary hindrance to oxygen transfer from the gas phase to the liquid phase is the liquid phase boundary layer at the gas-liquid interphase. The rate of oxygen transfer in surface aeration mainly depends on the surface area available for mass transfer and other factors such as liquid velocity, viscosity, diffusion coefficient, surface mobility at phase boundary and oxygen concentration gradient; ($\boldsymbol{C_L - C_{Li}}$- the driving force), apart from that the composition of the medium also affects the solubility of oxygen at the interface (Doran, 2013).

The crucial factor in surface aeration is the area available for oxygen transfer, which changes with an increase in agitation. The mass transfer coefficient $k_L a$ mainly depend on the agitation rate (Henzler and Kauling, 1993). Doran, (2013) explained that when a shake flask is rotationally moving on the orbital shaker, liquid form a thin film along the walls of shake flask after each rotation, which contribute significantly to the oxygen transfer thus agitation/ frequency of rotations play a key role in replenishing liquid thin film after each cycle and enhances overall mass transfer.

Therefore, increasing agitation rates for small culture systems such as shake flasks and spinner flasks, or increasing rotational speeds for roller bottles, or increasing rocking speeds in the case of wave-type bioreactors enhances the mass transfer efficiency (Ozturk, 2014). If the increase is within the optimum range to avoid hydrodynamic shear. The major limitation of this aeration system is the decrease in relative surface to volume ratio at large scale bioreactors and suboptimal ability to strip CO_2 from the culture broth.

2.7.2.1 Surface renewal theory

Surface renewal theory attempts to explain mass transfer coefficients based on the movement of liquid at the gas-liquid interface. Surface renewal theory was first given by Higbie in 1935 (Penetration theory) and later modified by Dankwerts in 1951 (Random surface renewal model). Thereafter, several methods were proposed to illustrate the mass and heat transfer phenomena at the gas-liquid interface and against the solid wall surface. Harriott, (1962) considered random distribution of eddies at random time with varied contact time, Wasan and Ahluwalia, (1969) proposed consecutive film and surface renewal mechanism, and Kermani and Shen, (2009) considered surface age (elapsed time between two consecutive surface renewal), a crucial parameter to determine mass and heat transfer. Surface renewal can be explained in a simplistic way by assuming that elements of liquid (a hypothetical small part of bulk fluid) is replaced by the bulk fluid at a regular interval at the gas-liquid interface. Alternatively, assume a bulk fluid consists of small balls having invariably different residence time and a surface concentration profile (mass) as shown in Figure 2-6 (a). Due to turbulent eddies, the surface is replaced by these water balls having varying residence time and concentration gradient at the gas-liquid interface Figure 2-6 (b), mimicking the upwelling and downwelling movement of fluid in the ocean (Asher and Pankow, 1991). Because of the concentration gradient at the surface of the liquid, passive scalar quantities such as temperature, oxygen, enthalpy homogeneously mixed by interfacial molecular diffusion (Kermani and Shen, 2009). At industrial scale, Gimbun et al., (2009) explained that at highly turbulent fluid conditions (high stirring speed and high power input), there is low resistance to oxygen transfer and other scalar quantities due to high surface renewal rates at the gas-liquid interface.

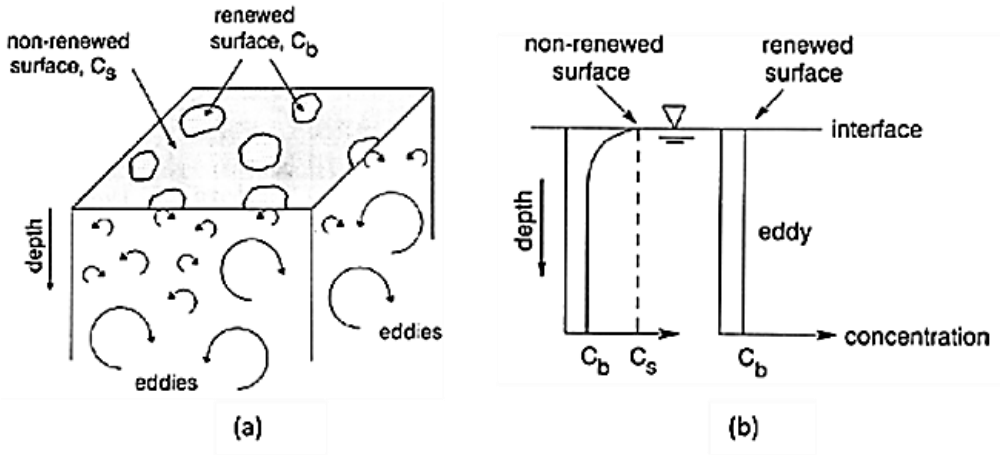

Figure 2-6 Theoretical representation of (a) surface renewal (b) concentration gradient in the liquid phase – taken from Asher and Pankow (1991)

2.7.3 Membrane aeration

Membrane aeration is useful to mitigate the issues related to hydrodynamic shear occurred during bubble-cell interaction by providing an option to separate the cells from the shear forces and provide them bubble-free aeration (Godoy-Silva et al., 2010). Hydrophobic gas permeable membrane such as silicone tubing and microporous nylon polypropylene, polyvinylidene fluoride, and polyester tubing are available commercially with pore sizes ranging from 0.01 - 20 µm (Godoy-Silva et al., 2010; Nayar, 1995). Ma et al., (2006) further categorised this membrane tubing as microporous or diffusional type. In the

microporous type membranes, the medium is in direct contact with air within the micropores of the tubing and the gas-liquid interface is held steady through the hydrophobic forces and internal gas pressure. In diffusional type, oxygen passes through the membrane, firstly from the gas phase to highly permeable oxygen soluble membrane and then to liquid phase (medium). These membranes are placed inside the liquid to provide a gas-liquid interface for oxygen transfer. Oxygen transfer primarily depends on the diffusion coefficient of oxygen, concentration gradient across the membrane, wall thickness and air pressure inside the tubing. Additionally, the fluid flow of the medium due to agitation also affects the liquid boundary layer resistance to diffusion (Nayar, 1995). As a matter of the fact, the mass transfer (diffusion) happening across the length of the membrane tube, is driven by the concentration gradient between the membrane and bulk fluid (Nayar, 1995; Pörtner, 2015). At larger scales, where the length of the tubing required is increased, it is essential to increase the gas flow rate inside the tube to maintain the concentration gradient for effective diffusivity (Nayar, 1995).

Although membrane aeration systems mitigate the problem of cell damage by hydrodynamic shear by the introduction of a stationary gas-liquid interface, they also have some inherent limitations. Firstly, scale-up is practically difficult. This is because of the requirement of large membrane area (approximately 1 - 3 meters of membrane per litre of reactor volume). Apart from that, wrapping of the membrane tubing around the aeration basket or around the stator, installing it in the bioreactor, and performing sterile operations are tedious tasks at large scale. Moreover, it is hard to maintain the large amounts of tubing and controlling the pH of the medium due to the differences in gas diffusion rates (Czermak et al., 2009; Nayar, 1995; Pörtner, 2015). Additionally, the deposition of cellular debris and protein have the potential to alter the hydrophobicity of the membrane (Ma et al., 2006). Frahm et al., (2009) has demonstrated dynamic membrane aeration (DMA) at 200 L scale, even then this method is restricted to small scale culture systems such as super spinner explained in section 2.12.2.

2.7.4 Other oxygen delivery methods

Apart from direct sparging, surface aeration and membrane aeration as discussed above, there are other methods which can be used for oxygen delivery such as perfluorocarbon (PFC) and oxygen carriers.

Perfluorocarbon is a non-polar, highly fluorinated and biochemically inert compound (Dias et al., 2004). The peculiar characteristics of this compound such as the capacity to dissolve oxygen, hydrophobicity and lipophobicity have much application in the medical and therapeutic field (Dias et al., 2004; Riess, 2005). Due to high hydrophobicity, PFC forms an emulsion in water which creates four-phase (two liquids, one solid and one gas phase) because of this it exhibits high solubility of oxygen (Godoy-Silva et al., 2010). Therefore, the addition of PFC in the liquid medium assist in delivering oxygen molecules to the cells and aid in removing CO_2. The drawback of using PFC at industrial scale is costly and poses a problem in downstream (Godoy-Silva et al., 2010). Another class of oxygen carrier are haemoglobins and cyanobacterial gas vehicles (GVs). Although they have shown the promising result in oxygen delivery, due to the high cost and issues in sterilisation has made them a difficult option to implement (Godoy-Silva et al., 2010).

2.8 Agitation

Agitation plays a crucial role in mixing and achieving homogeneity in the culture system. Direct sparging enhances mixing and homogeneity through fluid bubbling (aeration), but to obtain effective mixing and oxygen dispersion, incorporation of a mechanical agitator is essential, where mechanical energy supplied by the agitator to the liquid transforms into kinetic energy of the fluid and generate turbulent motion (Godoy-Silva et al., 2010; Kuncewicz et al., 2005).

Physical damage to the mammalian cells can be caused by hydrodynamic shear forces generated by agitation and foam formation due to high aeration in the cultured media (Chisti, 2000; Marks, 2003; Nienow, 2006). Surface aeration alone (bubble-free) with varying agitation speeds does not damage the free suspended cells but agitation with a low flow rate of air can significantly damage the cells (Chisti, 2000). Mixing is absolutely necessary to keep cells in suspension and to provide optimum heat and mass transfer, therefore the combination of aeration and agitation regimen (mode of aeration and choice of the impeller) to deliver effective oxygen transfer rates is necessary for the design of a bioreactor (Moutafchieva et al., 2013). The design criteria of STRs for mammalian cells have generally been modified from microbial cell cultivations to meet the requirements of the more sensitive mammalian cells. This includes changes in impeller design, use of baffles, aspect ratios and oxygenation methods. However, these changes do not necessarily overcome important parameters to keep mammalian cultures optimised for growth and production.

Hydrodynamic shear largely depends on the agitation of fluid inside the bioreactor. The important parameters are impeller design, number of impellers on the shaft, design of sparger and the geometry of the vessel (Varley and Birch, 1999). The main objective of the impellers is to create homogeneity in a cell population, nutrients distribution, gas dispersion in the liquid phase, bubble break-up, oxygen transfer to the liquid medium, heat transfer, CO_2 stripping, and to avoid gradient formation at large scales. Additionally, agitation also prevents the settling of the biomass at the bottom and maintains a uniform temperature for better growth conditions (Mirro and Voll, 2009; Nienow, 2010).

Based on the choice of impellers, fluid flow can either be radial or axial. Various impeller configurations have been employed for mammalian cells grown in suspension and on microcarriers as depicted in. Figure 2-7. Radial flow impellers such as Rushton turbine are used extensively in processes where strong mixing is required and when the local shear rates are of not a primary concern. In the case of axial-flow impellers such as marine/ propeller types exhibit bulk motion of the broth (Godoy-Silva et al., 2010; Mirro and Voll, 2009). When the impeller pushes the fluid away from its axis towards the bioreactor walls is called radial flow and when the fluid moves up and down along the axis of the impeller shaft is called the axial movement of fluid (Mirro and Voll, 2009).

The criteria for impeller selection are dependent on their power number N_p and pumping number (N_Q). It has been said that impeller with high (N_Q / N_{p}) induce adequate bulk mixing with low shear rate and impeller with the high impeller diameter (D_i) to vessel diameter (D_v) ratio (D_i/D_v) have high

pumping capacity i.e. amount of liquid discharged/circumscribed by the impeller per unit time that further enhances mixing, mass and heat transfer (Godoy-Silva et al., 2010).

Table 2-2 elaborated the type of impellers and the fluid flow generated by them with their advantages and disadvantages for the cultivation of mammalian cells. In nutshell, Rushton turbine produces unidirectional radial flow whereas pitched blade, marine, elephant ear and hydrofoil are the few impeller types that produce axial flow.

Table 2-2 Various impeller types with their fluid flow pattern, advantages and disadvantages- adapted from Godoy-Silva et al., (2010) and Mirro and Voll, (2009)

Various impeller type and their advantages and disadvantages			
Axial Flow	**Impellers**	**Advantages**	**Disadvantages**
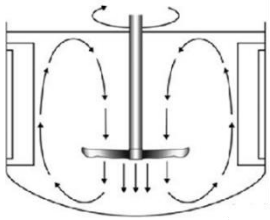	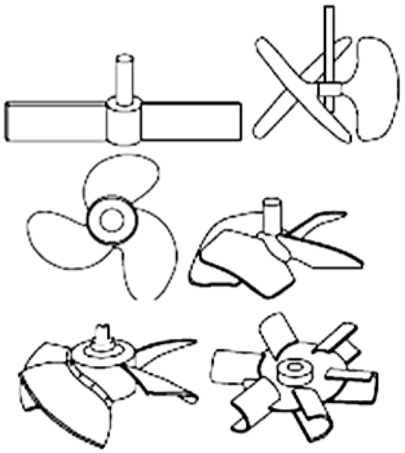	• Used for shear-sensitive cells. • The blades of the marine impeller are mostly concave, and their backsides are convex which assist in producing gentle axial flow by drawing low energy inputs. • Wider blade aid in rapid uniformity and gas dispersion • At high speed, induce dispersion and at low speed keep solids in suspension • Low energy demand • Cell lift impeller is specially used for microcarriers culture	• Only suitable for shear-sensitive mammalian cells • Not suitable for the processes where high oxygen mass transfer is required at large scale • Not appropriate for delivering high oxygen transfer rate
Radial Flow 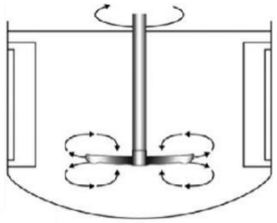		• Common for large scale fermentation with the non-shear sensitive organism • Maximise gas-liquid mass-transfer • Provide high OTR	• Creates dispersion and shear due to radial flow • Draw more power than axial flow impellers • Poor top-bottom mixing • Not suitable for mammalian cells

2.8.1 Cell lift impellers

Generally, most of the cell lines are inherently anchorage-dependent, few cell lines have been adapted to grow in suspension culture in the previous years. Still, many cell lines require a surface which can be in the form of microcarriers to grow in suspension culture. Various hydrodynamic conditions play a major role in cell damage such as direct interaction of turbulent eddies and microcarrier beads having cells, collisions between beads and internal moving and stationary parts of the bioreactor (Cherry and Papoutsakis, 1988, 1986; Chisti, 2000; Croughan et al., 1987; Croughan and Hu, 2006; Ibrahim and Nienow, 2004; Murhammer and Goochee, 1990; Nayar, 1995; Nienow, 2006).

Due to hydrodynamic shear conditions in traditionally stirred tank bioreactor, the new design of impellers and tank geometries have been tested in the past. Cell lift impellers from New Brunswick Scientific, (now Eppendorf) have been in use for the cultivation of anchorage-dependent cells in suspension such as Vero cells.

Cell lift impeller assists in providing uniform circulation of medium to the microcarriers. the low-shear impeller at the bottom of the tube lifts the microcarriers up and discharged from the discharge ports present at the impeller shaft, helped in uniform distribution of microcarriers in the tank (Mirro and Voll, 2009). The ring sparger is employed for oxygenation of the medium where bubbles travel inside the impeller tube between the exterior of the inner tube and outer membrane, which collectively called caged aeration. The mesh lining of the impeller tube has a pore size of 85 µm which prevent between microcarriers - bubbles direct interaction and gas exchange occurred at the membrane-medium interface. Bubbles then removed from the top ports on the impeller shaft (Mirro and Voll, 2009).

2.9 Mammalian cells and Hydrodynamics

Mammalian cells are known to be shear-sensitive because they are large in size (10 - 100 µm) and lack a protective cell wall. Due to this, small adverse culture conditions inside the bioreactor can be lethal and may force the cells towards apoptosis or necrosis. It can also show sub-lethal effects such as changes in doubling time, cell viability, OUR, cell morphology, cell-specific productivity (Nienow, 2006).

The combination of aeration-agitation regimen determines the hydrodynamic shear forces inside the bioreactor. Many factors contribute towards the shear-sensitivity of the culture which primarily depend on the cell type (freely suspended/microcarriers), vessel type, aeration-agitation, media formulation, the fluid flow, age of the cells and the exposure time to turbulence (residence time) as depicted in Figure 2-7 (Chisti, 2001; Nienow, 2006; Schnitzler et al., 2016).

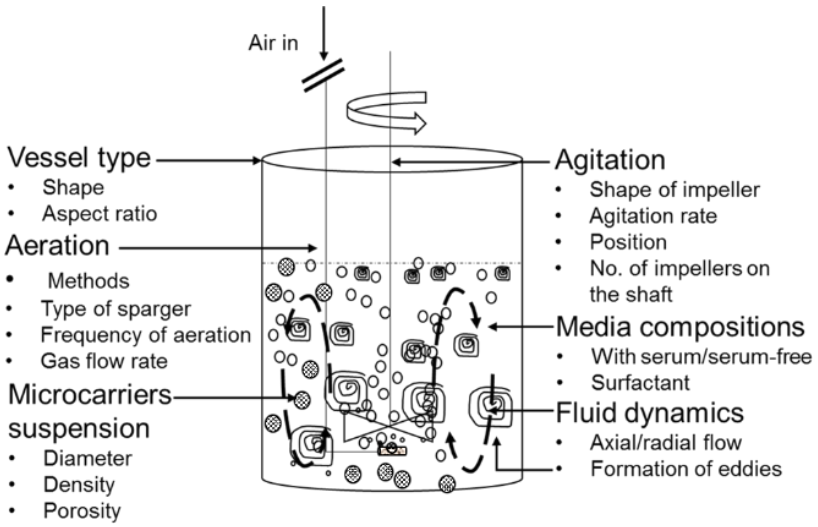

Figure 2-7 Factors responsible for hydrodynamic shear in the stirred tank- adapted from Schnitzler et al., (2016)

2.9.1 Mechanism of Hydrodynamic damage in mammalian cells

The choice of impeller type, speed of agitation and mode of aeration (sparging/surface) dictate the fluid flow regimen in the conventional stirred tank bioreactor. Usually, the fluid flow is turbulent with Reynolds number (R_e) above ≥ 10^4 which is given by Equation 2-11

$$\boldsymbol{R_e = (\rho N d^2)/\mu} \qquad \text{Equation 2-11}$$

Where ρ is the density of the fluid, N is agitation speed, d is the impeller diameter and μ is the fluid viscosity.

The formation of the turbulent eddies is a peculiar feature of the agitating fluid. The turbulent kinetic energy encompassed by the agitating fluid forms the large-sized eddies which disintegrate into smaller eddies and dissipates the energy in the form of heat to the fluid (Godoy-Silva et al., 2010; Illing, 1996; Tran et al., 2016). This is a continuous flow of energy from large eddies to smaller eddies, where the kinetic energy is transformed into heat energy in the form of the smallest eddies on the microscale called Kolmogorov' microscale of eddies (η), which is represented by Equation 2-12.

$$\boldsymbol{\eta = \left(\frac{\nu^3}{\varepsilon}\right)^{1/4}} \qquad \text{Equation 2-12}$$

Where ν kinematic viscosity and ε is the local rate of turbulence energy dissipation per unit mass of agitating fluid, in other words, local energy dissipation rate (EDR).

The theory of isotropic turbulence given by Kolmogorov in 1941, advocates that the kinetic energy introduced to the fluid by impellers forms the large eddies which undergo a series of disintegration of eddies to the smallest scale, therefore, in a given turbulent fluid flow, a range of eddies exists which are characterized by energy inputs and heat dissipation and result in hydrodynamic shear to the cells (Chisti, 2000; Godoy-Silva et al., 2010; Illing, 1996; Nienow, 2006). The damage to the cells occurs primarily by two mechanisms. Firstly, the interaction of the cells with turbulent eddies of the same size in the zone of high shear near the impeller and secondly by interacting with an air bubble at the gas-liquid interface and in the region of the sparger. Eddies which are larger than cells entrain the cells and move them in the direction of

eddies. Small-sized eddies with similar (or smaller) sizes than those of cells are deleterious due to local energy dissipation to the cell membrane.

2.10 Shear Stress

As mentioned earlier, mammalian cells are large and fragile and lack a protective cell wall. Due to this, small adverse culture conditions inside the bioreactor can be lethal and may force the cells towards apoptosis or necrosis. It can also show sub-lethal effects such as changes in doubling time, cell viability, oxygen update rate (OUR), cell morphology, and cell-specific productivity. Therefore, preventing premature cell death has become a core issue in bioprocessing (Nienow, 2006).

Various factors, for instance, a change in surrounding environment due to the lack of essential nutrients, accumulation of by-products, oxygen limitation at high cell densities and changes in pH, temperature or osmolality over the run-time of the batch contributes collectively in overall cell death. Additionally, the shear effect due to impeller agitation and bubble bursting also impart significantly to cell death by destroying the cell membrane. These changed conditions trigger the signalling pathways which pushes the cells towards apoptosis (Krampe and Al-Rubeai, 2010; Mollet et al., 2007). There are mainly two types of cell death pathways namely necrosis and apoptosis.

2.10.1 Necrosis

It is called passive cell death which is ATP-independent. Cell membrane exhibits certain morphological changes when exposed to external stress such as swelling, membrane blebbing, DNA breakage, membrane disruption and cell lysis (Krampe and Al-Rubeai, 2010). It is usually caused by the deteriorating condition of the culture medium over the batch cycle. It is due to the accumulation of excessive toxic metabolite and depletion of nutrients which caused cytotoxicity to the cells. In addition to that, bubble rupture and mechanical injuries also contributing the leakage/ or destroying of the cell membrane integrity that increases permeability and release of intracellular content (Cummings et al., 2004; Grilo and Mantalaris, 2019; Mollet et al., 2007).

2.10.2 Apoptosis

Apoptosis is a programmed cell death which contributes majorly (80 %) in cell death in bioprocesses especially in CHO cells (Grilo and Mantalaris, 2019). It is an active form of cell death where ATP is being utilised to carry out processes (signal transduction pathways) that finally leads to cell death (Krampe and Al-Rubeai, 2010). It is primarily denoted by chromatin condensation, DNA breakage, and plasma membrane integrity increased cytosolic concentration of Ca^{2+} ions and cell shrinkage. Apoptosis is triggered by two pathways mainly cysteine-containing, aspartate-directed proteases called caspases and another one is the expression of *BCL2* gene which comprises several check-points which regulate the apoptotic cell death (Cummings et al., 2004; Krampe and Al-Rubeai, 2010).

2.11 Mammalian cell bioreactors

Cells require an optimum supply of oxygen for metabolism. Mammalian cells have low oxygen demand as compared to microbial cultures, however, oxygen is still a limiting factor for high-density cell cultures. The oxygen mass transfer coefficient ($k_L a$) value of sparged stirred tank bioreactor falls between 1 - 15 h^{-1} (Nienow, 2006). Eibl et al., (2014) also outlined that for typical mammalian cell culture processes, oxygen mass transfer of 6 - 10 h^{-1} is sufficient to cater the oxygen demand for middle (5 x 10^6 cells mL^{-1}) to high cell densities (100 x 10^6 cells mL^{-1}), with a mixing time below 1.0 min and power input of 70 - 80 Wm^{-3}. Table 2-3 outlines the $k_L a$ requirements at various cell densities (ranging from 1 - 100 x 10^6 cells mL^{-1}) based on the percentage of air saturation.

It is the new normal for the industrial batch to achieve cell densities ranging from 5 - 10 x 10^6 cells mL^{-1}. Some systems were reported to achieve even higher cell densities, especially in perfusion cultures where culture supernatant is withdrawn continuously at a rate equal to the medium feeding rate. The typical oxygen uptake rate (OUR) of mammalian cells are in the range of 0.5 - 8.0 x 10^{-10} mmol $cell^{-1}$ h^{-1} (Pörtner, 2015). Based on these above-mentioned OUR values, the $k_L a$ for different cell densities were estimated at various percentages of air saturation as shown in Table 2-3. For example, the oxygen mass transfer coefficient ($k_L a$) for 10 x 10^6 cells mL^{-1} at 40 % air saturation would fall in the range of 4.2 to 66.7 h^{-1}. The percentage of air saturation is also known as percentage dissolved oxygen (% DO) in the liquid phase which is given by Equation 2-13

$$\% \boldsymbol{DO} = \left(\frac{\boldsymbol{C_L}}{\boldsymbol{C^*}}\right) * \boldsymbol{100} \qquad \text{Equation 2-13}$$

Where, C_L is actual oxygen concentration in the liquid phase, C^* is oxygen saturation concentration at equilibrium with air (Czermak et al., 2009).

Table 2-3 Estimated $\boldsymbol{k_L a}$ values for various cell density at 20 % - 50 % of air saturation

	$k_L a$ (h^{-1}) with air							
Cell Densities	20 % Air Saturation		30 % Air Saturation		40 % Air Saturation		50 % Air Saturation	
	Low	High	Low	High	Low	High	Low	High
100 x 10^6 cells mL^{-1}	31.3	500	35.7	571.4	41.7	666.7	50	800
10 x 10^6 cells mL^{-1}	3.1	50	3.6	57.1	4.2	66.7	5	80
5.0 x 10^6 cells mL^{-1}	1.6	25	1.8	28.6	2.1	33.3	2.5	40
1.0 x 10^6 cells mL^{-1}	0.3	5	0.4	5.7	0.4	6.7	0.5	8

Oxygen requirements increase as the cell density increases during the bioreactor run. Most industry application grow cell lines at a wide range of oxygen concentrations (15 - 90 %), however, cell lines prefer to grow at low oxygen concentrations mimicking the *in vivo* conditions (Czermak et al., 2009). Generally, to meet the oxygen demand of middle to high cell density, the operational conditions of a batch fall in the range of 20 - 50 % of air saturation (Xie et al., 2011). The $k_L a$ values for 20 to 50 % air saturation at various cell

densities are listed in Table 2-3. The cell density of 10 x 10^6 cells mL^{-1} is considered as an industrial benchmark for an optimised process, while 40 % air saturation is considered as the median oxygen saturation concentration range for established mammalian cell lines. These values are required because of the specific oxygen consumption rate (qO_2) of different cell lines, impacted by the cell type, cell density, medium composition, and the state of the batch (macroenvironment surrounding the cells). Therefore, oxygen mass balance is given as Equation 2-14

$$\frac{dc}{dt} = OTR - OUR * Cx \qquad \text{Equation 2-14}$$

Where $\frac{dc}{dt}$ is the rate of change of oxygen concentration during the batch, OTR the oxygen transfer rate into the culture medium, OUR, the oxygen uptake rate of the cell, and Cx is the total number of cells at a given time. OTR is further given by Equation 2-15

$$OTR = k_L a(C^* - C_L) \qquad \text{Equation 2-15}$$

The mass transfer efficiencies of different culture systems obtained through literature have been compared with respect to their mode of aeration in Figure 2-8. Mass transfer efficiency of a culture system primarily depends on the mode of aeration, mode of agitation, power input and the volume of the culture.

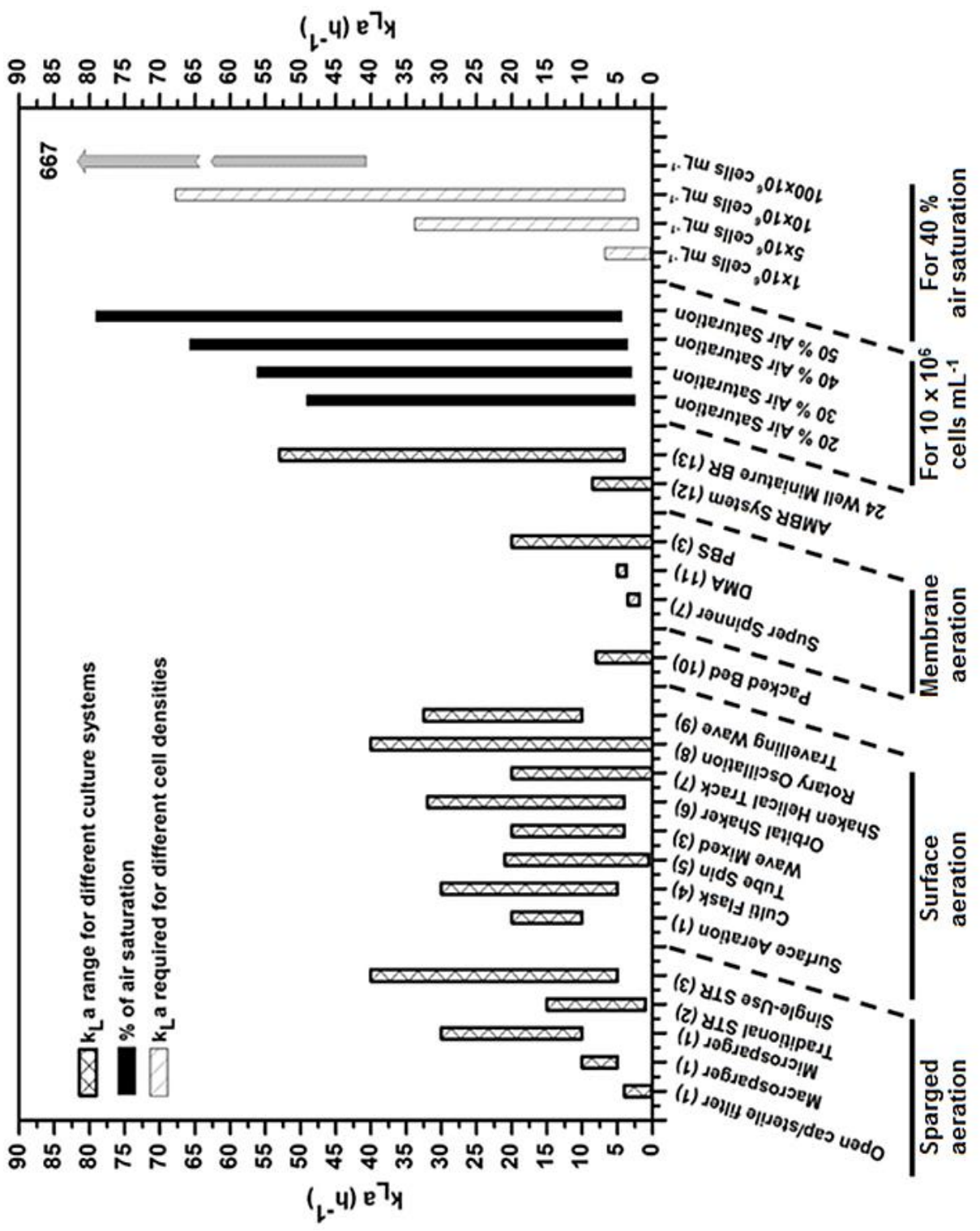

Figure 2-8 Indicative (k_La) values of different culture systems based on the methods of their aeration. Crossed columns represent (k_La) values of the various culture systems. Black column represents the (k_La) range for 10 x 10^6 cells mL^{-1} with varying air saturation

1 (Pörtner, 2015), 2 (Nienow, 2006), 3 (Löffelholz et al., 2013b), 4 (Eibl and Eibl 2009), 5 (de Jesus and Wurm 2011), 6 (Klöckner et al., 2013), 7 (Zhang et al., 2008), 8 (Kauling et al., 2013), 9 (Kaiser et al., 2016), 10 (Shakibaie et al., 2011), 11 (van Hecke et al. 2014), 12 (de Wilde et al. 2014), 13 (Betts et al., 2014)

2.12 Bioreactors without the control unit

Preliminary cell culture work is performed in culture systems without any integrated control systems. The physiological condition of the growing cells is maintained by keeping the culture system inside an incubator. Such culture systems are broadly divided into the static system grown in tissue culture flasks, multi-tray culture vessels and dynamic systems have typically grown in Erlenmeyer shake flasks, roller bottles and spinner flasks. These systems are typically used for initial process development such as the adaptation of cell lines, clonal selection, media and feed screening, and developing a proof of principle for the process (Brecht, 2009).

2.12.1 Static culture

All static cultures require a humidified CO_2 incubator to maintain suitable physio-chemical conditions for the growth of mammalian cells (Eibl et al., 2014). The CO_2 incubator would provide the physiological temperature of 37 ^oC and around 60 - 80 % relative humidity. The CO_2 is used for the maintenance of pH of the culture media at 7.0 ± 0.2. The percentage of the CO_2 purged into the incubator generally falls between 5 - 10 % and is dependent on the concentration of bicarbonate used in the growth medium. Static cell culture work was initially carried out by using glass tissue culture flasks. In the 1960s and 70s, glass tissue culture flasks were replaced by polystyrene which led to single-use technology. These flasks provide high volume to surface area ratio and are available from 25 cm^2 to 225 cm^2 in a single layer or up to a 5-layer format. Multi-stacked cell culture systems were then introduced for the growth of adherent cultures for the vaccine development at large scale. CellSTACK® from Corning and Cell Factory™ from Nunc are available in 10 and 40 layered closed systems. They also provide a high volume to area ratio similar to tissue culture flasks (T-flask) but are very difficult to handle due to their large size and volume (Schnitzler et al., 2016). The HYPER Flasks® system from Corning offers multi-layered culture system with 1720 cm^2 of surface area which is around 10 folds higher than a T-175 cm^2 TC-flask (Corning, 2008). Since there is no mixing involved in the tissue culture flasks (TC-flasks), oxygenation of media occurs through diffusion from the headspace to the media layer. At high cell density, oxygenation is a limiting factor and accumulation of metabolic wastes have negative effects on cell growth (Ozturk, 2014). To overcome the limitation of surface area for mass transfer, Corning introduced the 100-layered Cell Cube system, which provides a surface area of 85,000 cm^2. The liquid medium is continuously circulated through the multiple chambers of the cell cube through a media circulation pump for nutrient and oxygen supply through an inlet port at the lower corner of the plate and the media flow-out of the system from the outlet port at the top corner of the cell cube system (Corning, 2011). However, it has been reported that due to the large surface area, improper fluid flow across the different layers of the cell cube can result in non-uniform cell growth and shear stress (Aunins et al., 2003; Rodrigues et al., 2010). Integra Biosciences then introduced the CELLine disposable two-compartment flask system, a system for cultivation of cultured cell lines by separating the media from the growing cells using a 10 kDa semipermeable membrane (Integra Biosciences, 2014), hence reducing the effects of fluid motion and shear stress on the cells.

2.12.2 Dynamic culture

Six decades ago, the Polio vaccine became the first vaccine to be produced commercially where monkey kidney cells were infected with Salk poliovirus on adherent surfaces (Blume and Geesink, 2000; Kretzmer, 2002). Subsequently, the success of adapting baby hamster kidney (BHK) cells into suspension culture triggered the use of mammalian cells for the production of vaccines in a stainless steel stirred vessel (Telling and Elsworth, 1965). Development of spinner flasks further aided the growth of mammalian cells in suspension culture. Spinner flasks and roller bottles provide the starting platform for the development of seed cultures and are available as reusable and disposable units. The spinner flasks consist of a culture vessel with side arms; these side-arms are used for the addition of media and cells and withdrawal of samples and for the harvesting of the culture aseptically. These flasks are kept on the magnetic stirrer inside a CO_2 incubator to provide mass and heat transfer. The oxygen mass transfer coefficient ($k_L a$) in spinner flasks is reported to be in the range of 0.1 - 4.0 h^{-1} (Eibl and Eibl, 2009). Roller bottles, on the other hand, provide a much larger surface area for adherent cultures. The roller bottles are rotated horizontally such that gas exchange occurs through the liquid thin layer formed on the surface of the rotating roller bottles by diffusion (Eibl and Eibl, 2009; Ozturk, 2014).

The new advanced culture systems developed in the first decade of the 2000s by Sartorius, such as the Sensolux flask and Super spinner D1000 listed in Table 2-1, incorporate the pre-calibrated pH and dissolved oxygen (DO) sensors for real-time monitoring of these critical process parameters. The Sensolux flasks contain pre-calibrated pH and DO sensor patches on it which would be placed on a shaker tray platform. This shaker tray platform has optical sensors which aid in actual measurement optically and non-invasively through fluorescence.

In the case of the Super spinner D 1000, a magnetic stirrer covered with a hollow fibrous membrane provides bubble-free aeration with gentle mixing. It has been reported by Zhang et al., (2008), Eibl and Eibl, (2009) that these Super spinner flasks support higher cell densities compared to the standard spinner and can achieve a $k_L a$ of 1.9 - 3.5 h^{-1} as shown in Figure 2-8

2.13 Reusable bioreactor systems

Reusable systems are those in which culture vessels are made up of stainless steel and/or glass with a fixed vessel design and addition ports. At the pilot and commercial scale, the requirements for water for injection (WFI), piping for clean steam and plant steam, cascade sparging, cooling system and cleaning-in-place/sterilisation-in-place (CIP/SIP) is mandatory for the smooth operation of a large bioreactor. Reusable bioreactors typically start from 1 L (benchtop) and extend to 25,000 L in commercial scale to produce biologicals from mammalian cells. The stirred tank, bubble column, airlift, fixed or packed bed bioreactors are examples of reusable bioreactors.

2.13.1 Stirred tank bioreactors (STRs)

Stirred tank bioreactors are the most conventional bioreactors in which energy for contacting and mass and heat transfer is introduced into the reactor mainly through the impeller shaft, driving fluid motion, and partially by sparging of gases. STRs have been engineered quite extensively. Most of the bioprocesses

in the biopharmaceutical industry use stirred tank bioreactor because of its proven and well-established track record for upstream process development and scale-up. They are the preferred production platform for the biopharmaceutical industry (Chu and Robinson, 2001; De Wilde et al., 2009).

Owing to the sensitivity of mammalian cells to shear stress caused by bursting of air bubbles (Meier et al., 1999; Murhammer and Goochee, 1990), many methodologies have been developed to provide sufficient oxygen to the mitotic cells through micro and macrosparger, microporous silicone tubes and aeration through the headspace (surface aeration). High-density cultures require a high amount of oxygen supply, which is not often met by surface oxygenation methods alone (Berdugo, 2010; Ozturk, 1996). Therefore, direct sparging at large scale has proven, conventionally, to be the best suitable method of supplying oxygen to the growing cells. Ozturk, (1996) also reported that high cell density in the bioreactor depends on the mode of aeration. Surface aeration alone (headspace) is not adequate for catering the high oxygen demand of the cells whereas membrane aeration is the most suitable mode of aeration at high density. Oxygenation of the culture media can be done internally or externally with the help of a basket (silicone tubing coiled around a stainless-steel casing) and a gas exchanger respectively. The rate of oxygenation depends on the length of the tubing per volume. The membrane aeration has the limitation that it can only be manageable up to 200 L and support the cell density up to 10 x 10^6 cells mL^{-1}.

In the case of direct sparging, as discussed in 2.7.1, the type of sparger plays an important role in delivering the desired mass transfer coefficient for high cell density culture without impacting on the overall cell growth. A microsparger provide a large surface area and high mass transfer efficiency to the high-density culture. The downside of using the microsparger is that it also generates small bubbles (< 2 mm), which create foaming and bubble bursting at the surface of the liquid (Chisti, 2000). In the case of macrosparger, high mass transfer efficiency can be achieved by providing higher gas flow rates as compared to the microsparger to achieve the same cell density. The bubbles formed in case of macro-sparger are around 6 - 8 mm in size and do not take part in foam formation and cell death, because they travel faster upwards toward the surface and carry fewer cells attached to the bubble surface (Czermak et al., 2009; Ozturk, 1996).

The oxygen uptake rate (OUR) of high-density cultures determines the required $k_L a$ or oxygen transfer threshold of a system to support the growing cells, below which respiration becomes growth limiting. To meet the high demand of oxygen, different combinations of the aeration-agitation regimen were tested to meet the operating window while avoiding hydrodynamic shear, bubble damage and foam formation as indicated in Figure 2-9. The dotted lines in Figure 2-9 represent the system boundaries and, these boundary walls are flexible. The flexibility of these boundaries depends on the type of bioreactor system used, cell type, aeration-agitation regimen and process conditions. Woodley and Titchener-Hooker, (1996) explained this operating window for the microbial system and Mersmann et al., (1990) and Marks, (2003) for mammalian cells.

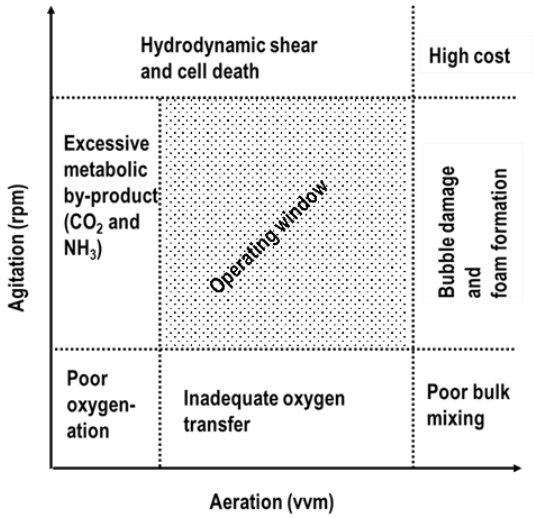

Figure 2-9 Sparging and agitation regimens for mammalian cells in stirred tank bioreactors: adapted from Mersmann et al. (1990), Woodley and Titchener-Hooker (1996); Marks (2003)

Mixing is necessary to keep the cells in suspension, provide homogeneity and to provide optimum mass and heat transfer. The choice of the impeller type is important in designing bioreactors for different types of cell systems. The Rushton turbine impellers typically exhibit radial flow which is used to maximise gas-liquid mass-transfer but this creates dispersion and shear in the reactor, hence negatively impacting the growth of shear-sensitive mammalian cells. Usually, axial flow impellers (marine or pitched blade) is used for the cultivation of mammalian cells which induces axial flow. The motion of the fluid moves up and down along the shaft/axis assisting in effective mixing from top to bottom with low shear conditions (Hu et al., 2011; Sandadi et al., 2011). Inappropriate mixing creates dead zones in bioreactors which would lead to low cell density and accumulation of undesired by-products which triggers necrosis and cell death by apoptosis during the bioprocesses. This would result in inconsistent batches and poor overall productivity (Collignon et al., 2010; Mirro and Voll, 2009). The selection of the suitable impeller type and agitation rate mainly depend on the cell type used, aspect ratio of the culture vessel, scale of the bioreactor and more importantly, the oxygen demand of the cells and the stripping of the carbon dioxide (CO_2) at the same agitation rate without compromising the shear-sensitivity of the cells (Nienow, 2010). The removal of CO_2 from the culture system is an important parameter for the selection of the agitator while designing a bioreactor. It has been reported that the specific production rate of CO_2 for CHO cells is 4 - 6 pmol cell^{-1} day^{-1} and for the efficient removal of CO_2 from the system requires a CO_2 mass transfer coefficient ($k_L a_{CO_2}$) of 40 - 50 h^{-1} for a cell density of 10 x 10^6 cells mL^{-1} (Oosterhuis and Junne, 2016).

An approach to mitigating (accumulation of undesired by-products, is continuous culture systems. The continuous bioprocessing generally requires a more complex integration of multiple unit operations, where the output of one unit is being successfully handled by others in a systematic way. Continuous bioprocessing can be extended to perfusion systems. In this case, fresh media (containing nutrients, non-essential amino acids, growth factors and trace elements) are continuously fed to the bioreactor at a constant rate simultaneously with the withdrawal of the product at a rate equal to medium addition to avoid nutrient limitation and minimise metabolite accumulation but with cell retention in the bioreactor (Challener, 2016;

Langer and Rader, 2014). Perfusion culture has gained attention from the biopharma industry to manufacture various biologicals products such as monoclonal antibodies, vaccines and growth factors due to better process monitoring and control, high productivity, and conducive environment to the cell as compared to batch and fed-batch system (Zeng and Deckwer, 1999). The other benefit of perfusion culture is achieving industrial-scale productivity from the pilot-scale facility without using large equipment (Marks, 2003; Woodside et al., 1998). However, the considerable issue regarding the use of perfusion system depends on the reliability of the cell retention devices such as spin filters, crossflow membrane, inclined settlers, continuous centrifuges and ultrasonic separators which aid in easy product harvesting and down streaming (Eibl and Eibl, 2009; Merten, 2006; Tapia et al., 2016). The efforts should be made to use these devices optimally during the continuous operation by optimising the perfusion rate and cell density to avoid clogging.

2.13.2 Air-lift and bubble column bioreactor

The airlift and bubble column bioreactors operate pneumatically, where both oxygenation and mixing are done by rising bubbles. The stochastic movement of rising bubbles results in mass and heat transfer and mixing in these bioreactors. The bubble column systems represent a column with a much larger height than the diameter of the column with an internal sparger to inject gas flow inside the column. The mixing is achieved by stochastic movement of bubbles inside the column and hydrodynamic conditions mainly depend on the type of sparger, gas flow rate, column geometry and the medium rheology (Eibl and Eibl, 2009). The bubble column bioreactor has been used to cultivate the shear-sensitive cell lines such as a hybridoma, lymphoma, BHK 21 and insect cell line Sf 21. It was concluded that in suspension culture, cell death is linked to the bubble rupture at the surface of the liquid-gas interface and significantly at the orifice of the sparger where the bubble is formed (Handa-Corrigan et al., 1989; Tramper et al., 1988). Due to poor mixing, as compared to a stirred tank, the cultivation of mammalian cells in bubble column bioreactor has not been reported as yet at commercial scale (Eibl and Eibl, 2009; Varley and Birch, 1999).

Though the air-lift bioreactor is driven pneumatically, it has been in use for the propagation of mammalian cells (Warnock and Al-Rubeai, 2006). In airlift bioreactors, the air is sparged into only a compartment of the reactor, ascending through a riser before disengaging such that the un-aerated liquid returns to the bottom of the reactor via the downcomer as a result of the density gradient, driving the recirculation of the cells and nutrient components in a circular motion. The fluid flows in the defined circular loop (Eibl and Eibl, 2009). Figure 2-10 shows the bubble column (a) and airlift bioreactors with internal and external draft tube (b, c) respectively. Without impellers and a mechanical seal, these bioreactors have lower the chances of contamination and facilitate easy cleaning (Warnock and Al-Rubeai, 2006). Hydrodynamic properties of these bioreactors mainly depend on the type of sparger, gas flow rate, and liquid circulation velocity, rheology of the culture broth and most importantly the aspect ratio of the bioreactor. The typical aspect ratio of these bioreactors (height/diameter) is in the range of 14 for small-scale and 6 - 7 with larger scales (Eibl and Eibl, 2009). Airlift bioreactors have been scaled up to 2000 L for the production of monoclonal antibodies in fed-batch mode (Merchuk, 2008; Warnock and Al-Rubeai, 2006) and it has also been reported to a scale up to 5000 L for the cultivation of mammalian cells (Eibl and Eibl, 2009). Despite good mixing and mass transfer, the design faces some limitation such as back mixing between gas and liquid phase, high-pressure drop, foaming, dead zones, bursting bubbles and bubble coalescence (Hambor, 2012).

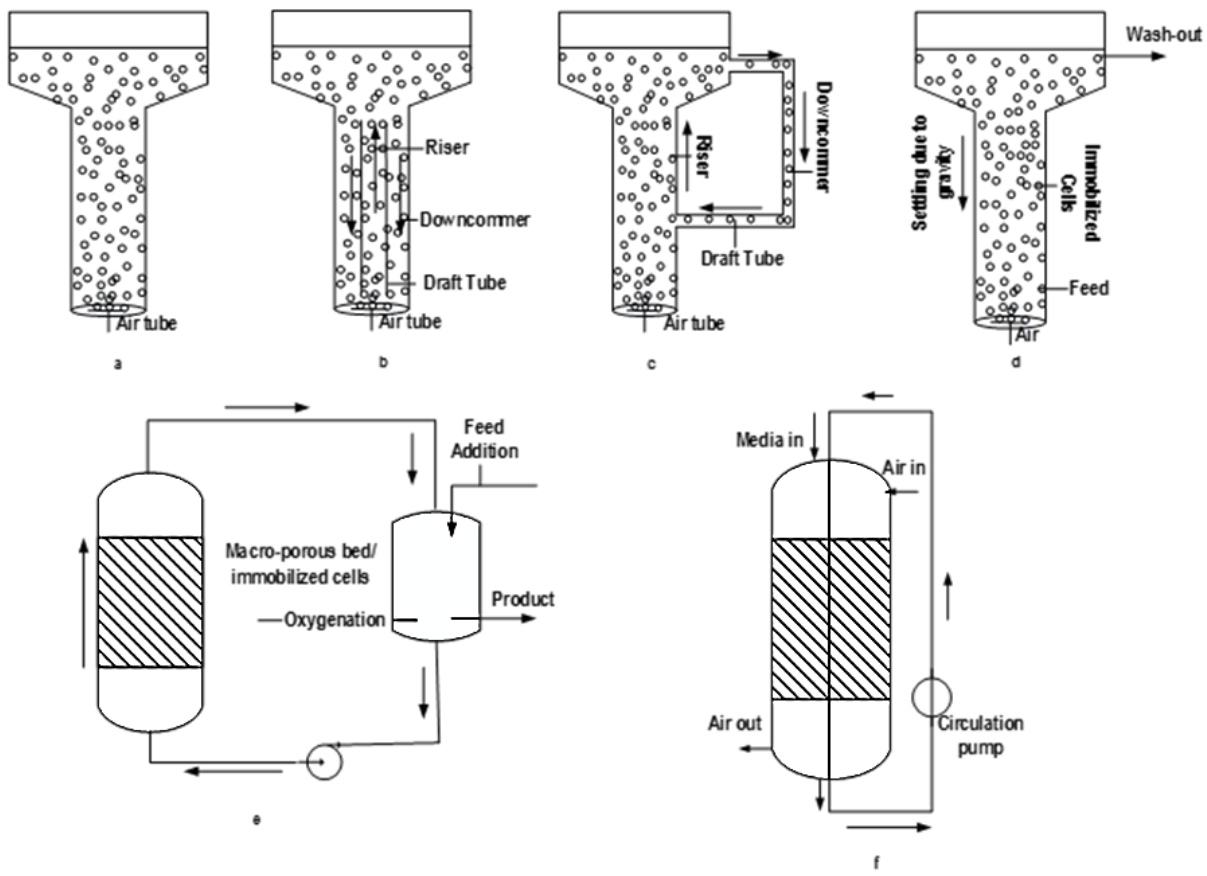

Figure 2-10 Schematic diagrams of various pneumatic and packed bed bioreactors. (a) Bubble column (b) Air-lift bioreactor with an internal loop (c) Air-lift bioreactor with external loop (d) Fluidised bed (e) Internal packed bed bioreactor (f) External packed bed

2.13.3 Fluidised bed bioreactor

The Fluidised bed bioreactor Figure 2-10 (d) is used for the cultivation of mammalian cells in suspension culture, where cells are immobilised on porous microcarriers or beads. The working principle of this type of bioreactor is that the beads with a higher density than the culture medium will be kept in suspension by the upward flow of the growth medium (Warnock and Al-Rubeai, 2006). Fluidised bioreactors are vessels with a high aspect ratio, where solid-fluid mixing is vastly homogenous. It exhibits good mass and heat transfer due to the large surface contact area between the gas and liquid phases, hence showing good mixing and relatively low power requirements. The unique feature of fluidization of the immobilised cells depends on their settling velocity and density of the cells per bead. Heavy cells would be retained in the bioreactor due to gravity whereas free cells and debris will be washed out if their settling velocity is less than the liquid velocity (Andrews, 1988). Due to the high aspect ratio, the formation of oxygen gradient is a hindrance in scale-up. In an upward flow of the medium, the concentration of oxygen decreases from the bottom of the bed to the top (Eibl and Eibl, 2009). Fluidised bioreactors exert low shear forces on the growing cells, making them a good choice for the propagation of animal and plant cells (Margaritis and Wallace, 1984; Popović and Pörtner, 2012). Commercially available fluidised bed bioreactor systems of, up to 400 L scale are available which can support the cell density of 2 x 10^6 cells mL^{-1} but there are yet no licensed production processes that use the fluidised bed as their production platform (Warnock and Al-Rubeai, 2006).

2.13.4 Fixed or packed bed bioreactor

Mammalian cells may grow either attached to a solid surface for their propagation (adherent cells) or adapted, as suspension cultures. Suspension cultures of CHO, BHK21 and NS0 are used in the development of vaccines and the expression of recombinant protein products (Boehm, 2007; Wurm, 2004). Many cell lines are difficult to adapt to suspension cultures, for example, Vero cells. Fixed bed bioreactors have been used for the propagation of such adherent cells for the production of monoclonal antibodies, vaccines, biotherapeutics proteins, retroviral vectors and the propagation of tissues for artificial organs (Hu et al., 2000; Kaufman et al., 2000; Meuwly et al., 2007; Pörtner and Barradas, 2007). Cells are immobilised or fixed either inside or outside the carrier structure (microcarriers, macroporous beads, fibrous bed) and the oxygenated medium is recirculated from the reservoir to the vessel continues to feed the growing cells Figure 2-10 (e, f). There are two aspects of the packed bed bioreactor configuration wherein one the packed beds are outside the reservoir and the oxygenated medium is recirculated with a pump across the external bed whereas in the other configuration, the packed bed is located inside the vessel and the oxygenated medium is circulated continuously across the internal bed (Wang et al., 1992).

Due to low hydrodynamic shear, high cell densities are attained in the packed bed bioreactor with few mammalian cells in suspension compared to stirred tank bioreactor (Zhou et al., 2010). The disadvantage of packed bed bioreactors is their low mass and heat transfer due to the low velocity of medium circulation. This low availability of oxygen, nutrients and the limited removal of toxic metabolites limits cell growth (Pörtner et al., 2007; Pörtner and Barradas, 2007; Warnock and Al-Rubeai, 2006). Pörtner et al., (2007) reported that in small scale fixed-bed bioreactor with bed length up to 15 cm, media flow axially across the bed to eliminate the issue of oxygen limitation. In the case of larger fixed bed height, media was pumped radially to the bed width to overcome the oxygen demand for the growing cells (Pörtner et al., 2007; Pörtner and Barradas, 2007). This problem can also be overcome by enhancing intra-particle convective flow where nutrients and oxygen are delivered to growing cells immobilised in the porous beads as illustrated in Figure 2-11. This fluid flow is improved by applying pressure and controlling bulk fluid flows to enhance convection and diffusion of nutrients and oxygen into the porous bead (Park and Stephanopoulos, 1993). Immobilised mammalian cells have been carried out in fixed-bed bioreactors at cell densities of 1.0 - 5.0 × 10^8 cells mL^{-1} and these reactors support $k_L a$ values of 8.0 as reported in Figure 2-8. The maximum scale of fixed bed bioreactor reported to date is 30 L bed volume for the biotransformation using immobilized enzyme and in waste-water treatment (Meuwly et al., 2007).

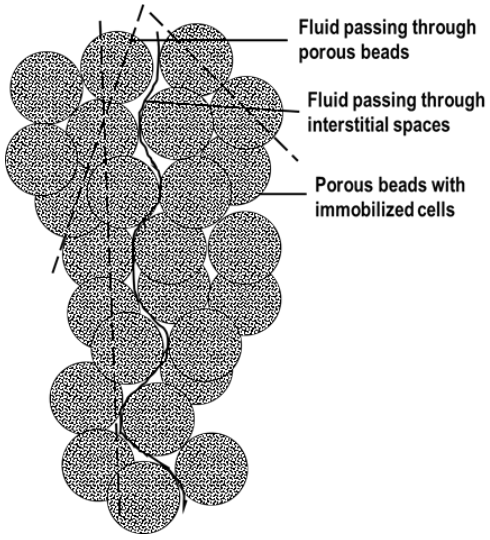

Figure 2-11 Pictorial description of intra-particle convective flow where solid line represents bulk fluid flow through interstitial spaces and dotted line represent intra-particle convective flow-adapted from Park and Stephanopoulos, (1993)

Zhang et al., (2015) introduced a novel fixed bed cell tank bioreactor for CHO cells expressing IgG monoclonal antibody developed by Perfuse Cell, Denmark as shown in Figure 2-12. The peculiar feature of the cell tank bioreactor is that it can support both adherent and suspension-adapted cell lines. The growing cells are retained in a non-woven polyester matrix placed in a chamber and immersed in a reservoir containing growth medium. The growth medium is delivered to the growing cells in the matrix with the help of a magnetic stirrer bead placed at the bottom of the bioreactor. The bioreactor is placed on a magnetic stirrer and the stirrer bead acts as a centrifugal pump by force circulating liquid from the media reservoir into the cassette where the matrix is suspended. The maximum cell density achieved across different runs was 200 x 10^6 cells mL^{-1} and the titre of the monoclonal antibody achieved was 1.42 g in the matrix of 15 mL volume (Zhang et al., 2015).

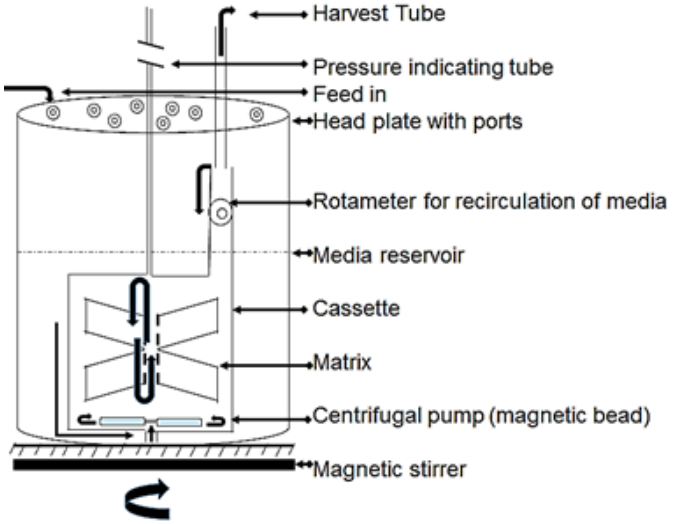

Figure 2-12 Schematic diagram of the Cell Tank: adapted from Zhang et al. (2015)

2.13.5 Membrane bioreactor

The use of membranes has been reported in the upstream and downstream bioprocesses. These include membrane bioreactors, ultrafiltration, microfiltration, membrane chromatography and membrane contactors (Charcosset, 2006). This article focuses only on the use of membranes in the development of bioreactor for the upstream process. The design of the membrane bioreactor includes a membrane which divides the vessel compartment into two zones, where cells are cultivated on the extra-capillary spaces (ECS) to form a biofilm, and the growth media is circulated inside the lumen or intracapillary spaces (ICS) as depicted in Figure 2-13. Conventionally, a membrane bioreactor consists of thousands of porous tubes, packed in a cylinder as shown in Figure 2-13 (a). The structure of the bioreactor depends on the type of membrane packing. It can be a hollow fibre, tubular in shape or in sheets and a spirally woven style membrane (Huang and McDonald, 2009; Kargi, 1992). Generally, membranes used in such bioreactors are usually polysulfone, polyamide, polyacrylate, cellulose acetate and cellulose derivatives (Kargi, 1992; Wolff et al., 2013). The simplistic operational principle of the bioreactor is that as the oxygenated media containing nutrients enters the ICS (lumen), it develops positive transmembrane pressure which assists the diffusion of the media through the micropores of the membrane tubes to the ECS and thereby providing growing cells with nutrients. This positive transmembrane pressure decreases along the length of the column channel (hollow fibre) hence develops a negative pressure towards the end of the fibre, resulting in media permeating back to the ICS from the ECS Figure 2-13 (b). Secondary metabolite (toxic substances) are hereby taken away from the cells through the ICS, thereby improving the performance of the product inhibited bioprocesses (Warnock and Al-Rubeai, 2006; Wolff et al., 2013). As the membrane bioreactor separates the adherent cells from direct stirring and fluid flow, it exhibits low hydrodynamic shear The benefit of this technology lies in the fact that it provides a high surface per unit volume and minimum shear environment to the growing cells while achieving high cell density by selectively controlling the culture conditions by supplying nutrients and removing waste through membranes (Charcosset, 2006). However, poor oxygen mass transfer, not-supportive to complex cell systems, membrane fouling, a diffusional gradient across the length of the column, lack of sensors, difficulties in sampling and scale-up limitations are few short-comings of membrane bioreactors in general (Fraser and Endres, 2013; Warnock and Al-Rubeai, 2006; Wolff et al., 2013). Membrane bioreactors have previously been used in the production of monoclonal antibodies and recombinant proteins but have not been used in any commercial bioprocesses (Warnock and Al-Rubeai, 2006).

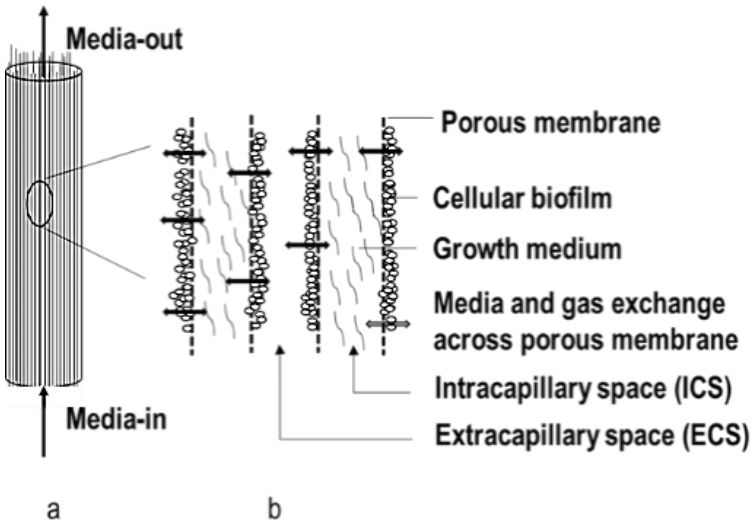

Figure 2-13 Tubular membrane bioreactor type (a) column of tubular membrane bioreactor (hollow fibre) (b) magnifying pictorial diagram of membrane bioreactor

2.14 Single-use Technology (S.U.T.) - broadening the horizon of biological manufacturing

Disposable bioreactors use a culture bag or vessel made up of flexible plastic material (Ding and Martin, 2010; Eibl, 2012). In the last decade, this technology has emerged as an alternative cost-effective and flexible platform for both laboratory-scale process development and commercial-scale manufacturing of biologicals. It has been estimated that setting up a new production facility based on single-use systems could lower the capital cost by 40 % as compared to commissioning a conventional hard pipe facility and it could also lower the operating cost by around 22 % per batch as compared to a batch taken in a conventional facility. The savings are mainly because of the elimination of the CIP and SIP step, which reduces the utilisation of WFI and chemicals such as phosphoric acid and sodium hydroxide which are used in conventional bioreactors. It has also been reported that the water usage in the single-use plant is 46 % lower and the carbon footprint by 35 % lower than in the traditional stainless-steel plant (Davis, 2001; Levine et al., 2013; Rentschler Biotechnologie, 2015; Rogge and Müller, 2014; Shukla and Gottschalk, 2013). Single-use technology is not only confined to the reactor component through cultivation bags but also liquid media storage bags, sampling devices, and modular facility design which includes downstream unit operation accessories like depth filters, ultrafiltration and disposable chromatography columns (Sandstrom, 2009).

Disposable bioreactor systems work on a variety of operating principles such as static culture systems (single and multi-layered tissue culture flasks, multi-stack culture vessels, CELLine bioreactor) and dynamic culture systems (which includes wave-induced mixing, use of the tumbling impeller or vibromixer to mimic stirring as in the case of STR, pneumatically-driven mixing, and shaking vessel systems). Disposable technology has many advantages over conventional bioreactors as there are no requirements for CIP (cleaning in place) and SIP (sterilization in place), low initial Capex investment, easy handling, reduced turnaround time between batches, ability to take multiple products in the same facility, minimum cross-contamination, reduced validation requirements, minimum usage of WFI and have a low carbon and energy footprint. SU technology, like hard piped facilities, is also easily integrated with process analytical tools (PAT)

for the development of repeatable and robust processes by implementing quality by design (QbD) approach. However, compared to hard-piped stainless-steel facility which has limited scope for modularity, SU facility can be fully modular and therefore allows for quick campaign changes, increased flexibility and improved equipment utilisation. which further assist in easy validation and regulatory approvals (Huang and McDonald, 2012; Rawlings and Pora, 2009; Read et al., 2010; Riley, 2016; Whitford, 2010a)

In pre-existing manufacturing plants with hard pipe structured facilities, there is scope for the transition to disposable technologies single-use even with the involvement of prior capital investments, facility design and facility approval from the competent authorities. Companies carry out a step- by- step integration of the permanent hard structured facility to disposable accessories by incorporating the use of tubing, air vent capsules, TFF cassettes, preparation of seed inoculum in small bags and /or complete disposable unit operations. It has been reported that if the product has less than 50 batches annum^{-1}, single-use technology will prove economically beneficial otherwise reusable technology would still be the best option alongside hybrid facilities where part of the unit operations are carried out with disposables (Ziemlewski, 2009). Small and start-up companies have a greater interest in adopting single-use technology for a speedy pre-clinical and clinical trial material generation without compromising the sterility of the product and with a reduced product delivery span.

The use of disposable technology further aids in simplifying regulatory requirements for product and facility approvals, increase in the return on investment by reducing the cost of hard structure installation, reducing the requirements for utilities, provide flexible facility for multi-product development, and reduce the excessive validation requirements frequency associated with conventional plants (Lopes, 2015). The use of disposable technology is 50 % more energy-efficient than reusable technology (Rawlings and Pora, 2009) because of the minimum utility requirements for cleaning and sterilisation, low demand for WFI, requirements for smaller kill tanks as wastewater produced is much less compared to reusable bioreactors as shown in Figure 2-14. The only energy-intensive operation is the disposal of used biohazardous bags with either incineration, chemical treatment, or through autoclaving and inactivation.

In spite of all the benefits of disposable technology, there are concerns from industry leaders concerning the strength of the plastic material for scaling up, the accuracy of disposable non-invasive sensors, the integrity of bioreactor accessories such as sampling devices and the increased probability of extractable and leachable in the final product. Additionally, disposable technology is not environmentally friendly as it generates a large amount of non-biodegradable plastic waste (Shukla and Gottschalk, 2013).

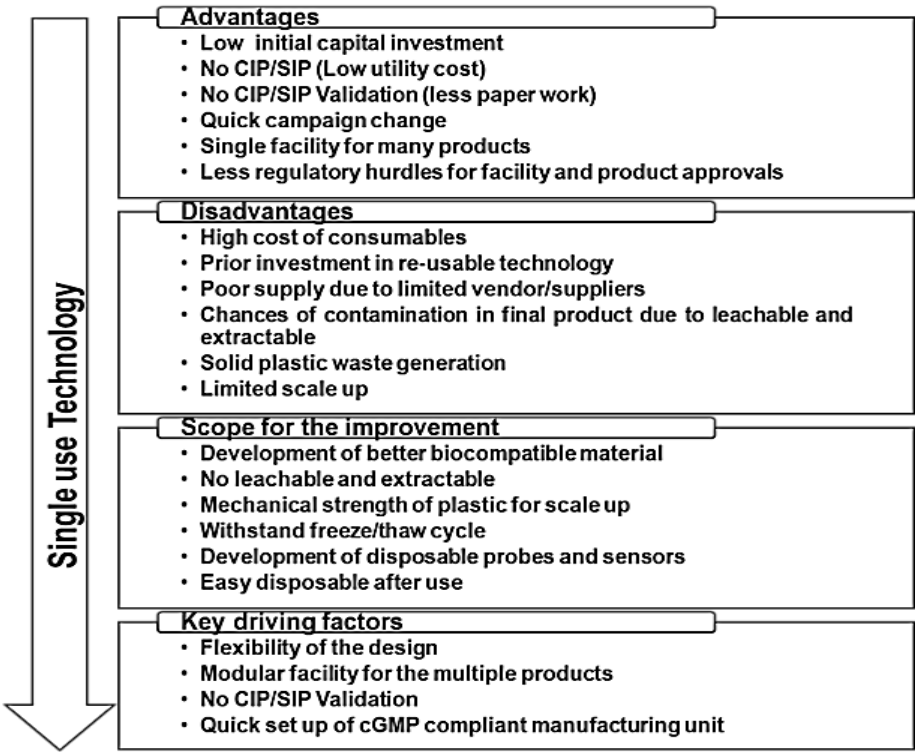

Figure 2-14 Advantages and disadvantages of Single-use technology - adapted from Brecht (2009); Shukla and Gottschalk (2013

Major companies dealing in SU technology have started addressing the various drawbacks to broaden the scope of their usability. For example, Cytiva has invested $ 5 million to set up a lab for the testing of extractable and leachable from the single-use consumables for the on-going support to their products (Mirasol, 2018).

The key driver for the expansion of SU technology in biomanufacturing is their ability to extend modularity in biologicals manufacturing. Most of their components are simply “plug and play”, which assists in manufacturing multiple products in the same facility by reducing the downtime. Many big companies have shifted their processes from traditional units to SU manufacturing units. In December 2014, Amgen inaugurated its fully modular single-use technology-based biomanufacturing facility at Tuas, Singapore and Cytiva expanded its SU technology portfolio by acquiring Xcellerex, a biotechnology company dealing in single-use bioreactors (XDR series) and its accompanying Flex factory technology for modular manufacturing platform manufacturing. Abzena has also joint-ventured with Sartorius-Stedim Biotech to equip their two integrated facilities based in Bristol, PA and San Diego, CA with single-use biomanufacturing units (Mirasol, 2018; Yeo, 2014).

Many companies have ventured into the space of disposable bioreactors for the propagation of mammalian cells by developing innovative new technologies using various operating principles. The disposable stirred tank, wave-induced, orbitally shaken bioreactors have become the dominant systems and are available in mL scale to m^3 scale. Table 2-4**Error! Reference source not found.** showed an overview of companies dealing in a single-use bioreactor in an alphabetical order adapted from (Löffelholz et al., 2013a). Other designs have also demonstrated their suitability for mammalian cell culture based on various novel principles e.g. pneumatically driven PBS bioreactor, Cell tumbler (CerCell), Pad reactor with cubical design, and Bio-t bag with vibromixer technology (Löffelholz et al., 2013a). The main players in the space of

disposable bioreactors are Sartorius-Stedim (Biostat CultiBag STR), Cytiva (WAVE Bioreactor), Xcellerex (XDR), Hyclone (SUB-Single-use Bioreactor), PBS Biotech (PBS Bioreactor), and Bayer Technology (BayShake). Table 2-4 depicts the different single-use bioreactor designs developed over the years and made available to produce biologicals not only for mammalian cells but also for different animal and plant cells.

Table 2-4 Overview of companies dealing in a single-use bioreactor in alphabetical order adapted from Löffelholz et al. (2013a)

Companies deal in SUBs	Commercial system	Total Volume	Description	References
Applikon	AppliFlex	10-50 L	AppliFlex bags can use reusable, single-use and fluorophore sensors for pH and dissolved oxygen measurements. It supports CHO cells, Hybridoma cell lines and insect cells like Sf-9, Sf-21 cells. Suitable for propagating seed culture for large-scale batches.	Eibl et al. (2009)
ABEC	Custom Single Run	3500 L	Stirred tank bioreactor (Data not available yet)	Stanton (2015)
Bayer Technology	BayShake	1000 L	Vertical orbital shaking cube-shaped bag bioreactor with the pyramidal bottom for low starting volume & full drainage, equipped with optical and fluorescence-based sensors for pH & DO measurements.	Kauling et al. (2013)
CerCell	Cell Tumbler	0.5-10 L	A rocking platform cabinet which can accommodate any commercially available wave-type bag up to 10/20 L with common drive and independent heating unit with the manually operated gas unit for air and CO_2	CerCell (2014)
	Cell Vessel 21 & 23 Series	2.1 -75 L	Single-use bioreactor with flexibility in design customization as per the application, offering different types of impellers for mixing and mass transfer.	CerCell (2012)
CELLution Biotech	CELL-tainer bag bioreactor	20-200 L	Wave style rocking platform with a box or pillow-like a bag with a pre-fixed pH & DO sensor.	Zijlstra and Oosterhuis (2010)
Cellexus	Cell Maker	8 -50 L	Airlift single-use bioreactor without agitator/rocker, suitable for a variety of cell systems	Auton (2010)
CatchMAbs	Tsunami Bioreactor	6x160 L	Series of wave mixed bioreactor with a multi-layer platform with the same wave hydro dynamicity for cell growth.	Houtzager et al. (2010)
Eppendorf	Celligen BLU Fixed Bed	3.75 L	Single-use stirred tank with pre-loaded Fibre-cell disks, suitable for adherent & suspension cells	Hatton et al. (2012) Application note
	Celligen BLU	5-50 L	Single-use bioreactor with pre-attached pitched blade impellers and Microsparger with all the other accessories required to run the batch.	Wang et al. (2012) Application note
Finesse	Smart Glass Vessel	0.5-2.2 L	The bioreactor provides axial and radial fluid flow by using down pumping segmented blade and bottom-mounted Rushton turbine.	Kaiser et al. Application note
	Smart Rocker Bioreactor	10-50 L	Wave platform support from gentle to vigorous rocking motion based on cell lines. The system is coming with pre-loaded SmartPuck sensors for monitoring & controlling of process parameters, also have optional load cell for fill control	Perepelitsa et al. Application note
Cytiva	Wave Bioreactor systems	0.2-500 L	Well established wave systems suitable for various animal cell lines	Singh (1999)
	Ready to process Wave 25	0.3-25 L	It provides the option of single or dual culture cultivation on a single platform with different working volume. The pH, DO and pump speed can be controlled independently.	G E-healthcare LifeSciences Data file

	Xcellerex XDR range	10-2000 L	Modular stirred tank disposable bioreactor system with batch, fed batch and perfusion applicability. Provide excellent mass Transfer and mixing mimicking reusable system	G E-healthcare LifeSciences Data file
Hangzhou Am protein Bioengineering	Current bioreactor	5-300 L	Orbitally shaken single-use bioreactor with bubble and sparger free oxygen transfer from vessel surface which is made up of EVA	Li et al. (2009), Regine and Dieter (2011b)
Kuhner	Orb Shake Bioreactor	10- 200 L	A well-established system for mammalian and plant cell cultivation	Anderlei et al. (2009)
Merck Millipore	Mobius Cell Ready Bioreactor	3-2000 L	Mobius CellReady 2000L joins 3, 50 & 200 L bioreactor series on June 15, 2015.	Millipore (2015) (Press release)
Meissner Filtration Inc.	Saltus Bioreactor	2-500 L	The bioreactor has a vertical hollow, conical perforated disk on the shaft which provides axial motion without vortex and provides mixing and mass transfer. Due to high power consumption, it is not suitable for shear-sensitive cells.	Eibl et al. (2011) Application note
Pall Life Sciences	Allegro XRS 20	0.1-20	Rocker system with bi-axial motion provide shorter mixing and high mass transfer, suitable for seed development to full GMP production	Henry et al. (2015) Application note
	Allegro STR	60-200 L	Squarely designed vertical bioreactor similar to Stainless steel bioreactor	Pall Life Sciences Application note
	Pad Reactor	10-1200 L	Cubical design bag with paddle impeller and dynamic sparger for shear-sensitive cells. Impeller and sparger is covered with ULDPE membrane	Pall Life Sciences Application note
	Xpansion multiplate	0.06-12.2 m^2	Plate system	Pall Life Sciences Application note
	Nucleo Bioreactor	1000 L	It offers similar functionality as of stainless-steel bioreactor, in addition to that it has paddle impeller and dynamic sparger covered with ULDPE membrane	Collignon et al. (2015)
PBS Biotech	Vertical wheel Bioreactor	20 mL-500 L	Airlift bioreactor where bubble aerates the vessel thus provide mixing and mass transfer. Agitation is provided by the buoyancy of gas bubble in case of air drive and magnetically coupled drive for MAG drive	Hashimura (2011) Application note
Sartorius-Stedim	Biostat CultiBag RM	300 L	Wave mixed bioreactor	Herholdt et al. Application note
	Biostat CultiBag STR	25-2000 L	Vertical stirred tank bioreactor similar to the reusable counterpart, housed in a stainless-steel chamber	Wilde et al. (2014), Müller et al. (2015) Application note
	CultiBag ORB	50-2500	Orbitally shaken bioreactor with surface aeration & without impeller and agitator, suitable for adherent and suspension cells	(Sartorius Stedim) Application note
	UniVessel SU	0.6-2.0 L	Single-use stirred tank with pre-loaded pH & DO probes, ready to use, compatible with any bio-controller brand	NA
Thermo Scientific	HyPerforma S.U.B. Range	25-2000 L	1st stirred tank bioreactor in the industry having the conventional geometry of the vessel. The system is compatible with other systems from Applikon, finesse etc.	NA
Terumo BCT	Quantum Cell Xpansion	2.1 m^2 culture surface	Automated flask scale cell culture process development platform based on hollow fibre system for adherent cells	Hanley et al. (2014)
ZETA Holding Gmbh	Bio-t Bag	3L-1875 L	Culture bag uses vibromixer technology for mixing and aseptic handling of the process while maintaining the integrity of the bag	Brecht (2009)

2.14.1 Wave mixed bioreactors

The first wave-induced bioreactor was designed by Dr Vijay Singh in 1999. Dr Singh demonstrated that wave-induced motion provides good mixing and mass transfer with minimum shear stress to the growing mammalian cultures such as Sf 9, HEK 293 and NS0 cell lines (Singh, 1999). Wave bioreactors are made up of a culture bag, typically rectangular in shape, which is partially filled with growth medium and cells and inflated with a gas mixture or air. The bag is placed on a rocking platform which moves at an optimised angle and speed as illustrated in Figure 2-15. The rocking movement of the platform provides sufficient agitation, mixing, heat and mass transfer. Wave and undertow bioreactors have also been developed for the production of biologicals that use different host cell systems like plant cells (Terrier et al., 2007). Oxygen is transferred from headspace to the cultured broth through entrainment of air by wave motion. It has been reported that the wave-induced culture bag has shown lower mass transfer efficiency than a stirred tank with $k_L a$ falling in the range of 4 - 20 h^{-1} (Löffelholz et al., 2013b). However, in a micro algal system, Jones et al., (2017) demonstrated that the gas-liquid mass transfer in the wave bioreactor exceeds and is more energy efficient than the airlift bioreactor, with $k_L a$ values in the range of 9 - 150 h^{-1}. With the technological advancement of the design, new cell lines have been adapted to grow in this bioreactor configuration supporting both suspension and adherent cell cultures (Namdev and Lio, 2000; Zhong, 2010).

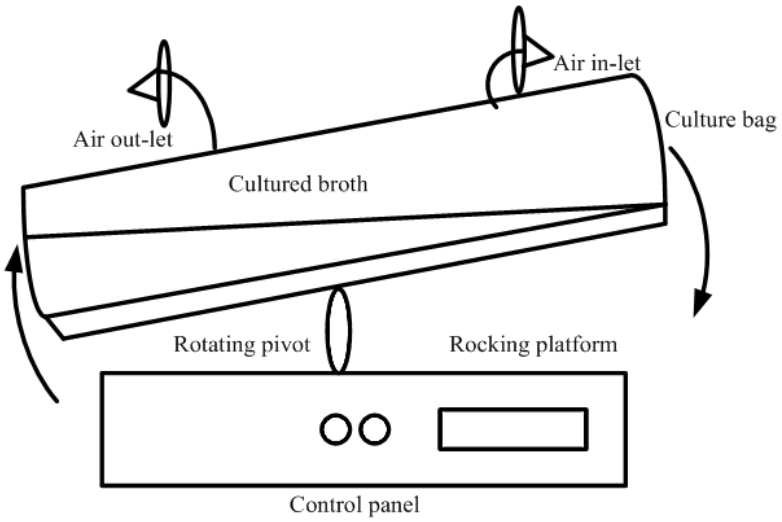

Figure 2-15 Wave mixed bioreactor

2.14.2 Rotationally/orbitally shaken bioreactor

Orbitally shaken bioreactors work on the principle of rotational motion of the culture vessel around a central axial shaft. Mass transfer of oxygen happens through surface aeration similar to shake flask culture systems. Zhang et al., (2008) used helical tracks to improve the mass transfer efficiency of the bioreactor by placing these tracks inside the wall of the culture vessel and with orbital motion, liquid media travels upwards along the track, thus increasing surface area for enhanced gas to liquid transfer. An increase of 5 - 10 fold of volumetric mass transfer coefficient has been reported due to increased liquid-gas interface, and at 1000 L scale with 39 rpm, the mass transfer coefficient of the orbitally shaken reactor with the helical track was 10 h^{-1} with air (Zhang et al., 2008). The $k_L a$ value in orbitally/rotationally moving bioreactor primarily depend on the shaking speed and fill volume which increase the oxygen transfer rate. The mass transfer coefficient $k_L a$ is inversely proportional to the working fill volume (Klöckner et al., 2013; Zhang et al., 2008). Commercial

orbital shaken bioreactors are available up to 200 L by Kuhner. The peculiar feature of this bioreactor is that it has no provision for a dissolved oxygen probe and oxygen transfer is controlled through surface aeration (Tissot et al., 2011). Bayer technology (Germany) has developed the BayShake® disposable bioreactor which works on the mechanism of rotary oscillation around its vertical axis, which relies purely on surface aeration for the propagation of high cell densities in low shear conditions, without moving internal parts (Kauling et al., 2013).

2.14.3 Disposable stirred tank bioreactors

As stirred tank bioreactors have an established track record in the biomanufacturing sector, the development of single-use STR bioreactor systems is an inevitable progression. Here, a plastic culture bag is mounted inside a cylindrical cabinet to support the bag as a vessel for growth. Many companies have ventured into the development of single-use stirred-tank bioreactors with internal disposable impellers such as Thermo fisher (SUB-Single-use Bioreactor), Xcellerex (XDR) and the recently launched custom single run bioreactor from ABEC which can be custom made in the range of 50 L to 3500 L working volume. Thermo fisher's SUB bioreactor is equipped with a motor on the top head plate for mixing and agitation whereas XDR has a bottom driven impeller. Disposable STR bioreactors have been tested for the propagation of CHO cells. A comparative study of performance between SUB (Thermo fisher) and stainless steel STR has been done by growing CHO and NS0 cell lines. It has been demonstrated that SUB systems (Disposable technology) successfully reproduce similar metabolic growth and product quality at production scale (Smelko et al., 2011). Disposable bioreactors have supported 20 x 10^6 cells mL^{-1} in fed-batch operations with the enhanced product titre of around 6.0 g L^{-1} at 1000 L scale (Smelko et al., 2011).

2.14.4 Pneumatically driven single-use bioreactor

A new addition on the canvas of single-use technology is pneumatically driven single-use bioreactors which primarily uses gas buoyancy as a tool for mixing and mass transfer. PBS Biotech® is the first to introduce a pneumatically driven vertical air-wheel bioreactor where a vertical wheel moves inside the liquid chamber mimicking a "merry-go-round" (Almo and Love, 2014; Lee et al., 2011). Another addition in this class is the CellMaker series of bioreactors from Cellexus Limited. These bioreactors use the principles of airlift and mechanical agitation in unison to achieve high mixing and low shear conditions (Eisenstein, 2006; Shukla and Gottschalk, 2013).

2.14.4.1 Vertical wheel™ bioreactor

The vertical air wheel bioreactor is an airlift bioreactor made up of single-use components. It is an impeller-less, pneumatically mixed U-shaped bioreactor, which uses gas bubbles as a mixing device by rotating the air-wheel like a "merry-go-round" with the buoyant force of the bubbles (Almo and Love, 2014; Sousa et al., 2015; Wilson, 2011). This technology is patented by PBS Biotech, which uses the theory of radial-axial tangential fluid flow around a vertical rotating wheel during cell cultivation. The rotating wheel covers 85 % width of the U-shaped vessel which revolves in a vertical plane on a horizontal shaft. It generates radial and axial fluid motion in the bioreactor simultaneously; radial flow in a vertical plane and the axial flow component along the horizontal axis which further supports homogeneous mixing. The energy dissipation rate (EDR) and maximum wall shear stress are reported to be 2 x 10^3 Wm^{-3} and 1.7 Nm^{-2} respectively, which is under the tolerance limit for mammalian cell growth (Sousa et al., 2015). The advantage of the air wheel

is that it requires a lesser amount of air thus increases the working volume of the batch while reducing compressor requirements. This type of bioreactor is suitable for the growth of shear sensitive mammalian and insect cell lines and is available from 3 L to 2500 L in working volume (Lee et al., 2011; Shukla and Gottschalk, 2013).

2.14.4.2 Cellexus system

This is a pneumatically driven (airlift) bioreactor where rising bubbles provide effective mixing, oxygen delivery and enhance mass transfer to the growing cells without a mechanical agitator. Cellexus Biosystems has introduced a novel bag geometry which facilitates the mixing. CellMaker Regular (previously CellMaker Lite) is an inverted "L" shaped bag, where air passes through the long vertical stem and hits the deflector to provide good oxygenation and mixing. Due to the design, Cellexus systems also allows the system to be pressurized above the culture level (Overlay pressure), which in single-use systems is unique for suppressing foaming (Eisenstein, 2006; Scott, 2007). Cellexus Biosystems offers systems which can be operated on the airlift principle alone or as a hybrid system. In hybrid systems, internal impellers are fitted to give similar mixing and aeration conditions as seen in stirred tanks but with the benefits of low shear conditions similar to an airlift bioreactor (Auton, 2010; Brecht, 2009). It has been reported that this bioreactor can provide aeration more efficiently than a very vigorously shaken culture flask. The oxygen transfer rate (OTR) is in the range of 15 - 30 mmol O_2 L^{-1} h^{-1} (Auton, 2010). Cellexus bioreactors are available in 3 L to 50 L scale (Auton, 2010; Cellexus, n.d.; Löffelholz et al., 2013b).

2.15 Novel cell culture systems

Novel bioreactor technologies are essential for the continual improvement and innovation of the bioprocess platform. Many novel bioreactors explore the concepts of biomimicry as a basis for their design. In this respect, designs are moving away from traditional air sparging which is energy-intensive and from impellers which create high hydrodynamic shear.

2.15.1 Bello cells / CelCradle / FibraStage cell culture system

Cesco Bioengineering Co. (Hsinchu, Taiwan) developed Bello cells which were later acquired by ESCO, VacciXcell (Singapore) and named CelCradle. These are benchtop disposable bioreactors and come in a set of four bellow bottles with each bottle operating to a volume of 500 mL. Their working principle resembles the functionality of lungs. This bioreactor is impeller-free that works without air sparging thus provides a low shear environment and reduced foam formation. The bioreactor consists of two parts: lower hollow bellow and an upper chamber with cells immobilised on BioNOC II® made of polyester fibres. The operational mechanics of the system works in such a way that it creates cyclic oscillations by compression and release of the bellow. The oscillatory motion of the bellow moves the medium upward and downward with minimum hydrodynamic shear which is ideal for the growth of shear sensitive cell lines. One CelCradle system with four bellows equates to the surface area of 80 roller bottles (Vaccixcell, 2016). Increase in the headspace on the upper chamber helps in gaseous exchange and high oxygen mass transfer and have achieved cell densities of 4 - 6 x 10^9 cells $bottle^{-1}$ 500 mL^{-1} (Cesco Bioengineering, n.d.). Research has been published on using these systems to grow Vero cells for the production of Japanese Encephalitis virus and

swine virus as well as insect cells for the production of recombinant Baculovirus (Hu et al., 2003; Lu et al., 2005; Toriniwa and Komiya, 2007; Wu et al., 2013).

Like BioNOC II® polyester fibres, New Brunswick Scientific (NBS, now Eppendorf) have also developed FibreCel disks, which are made up of polyester non-woven fibres crosslinked with polypropylene mesh. Cells are either attached to the matrix or entrapped within, therefore, meant for both adherent and suspension cell lines. Based on this technology, NBS has developed Fibra Stage cell culture system similar to CelCradle. Apart from the advantages of a packed bed or fixed bed bioreactor as listed in section 2.13.4. FibraCel has additional advantages also such as reduced time for the attachment of the cells as compared to microcarriers. In the case of FibraCel, 15 - 60 minutes are usually sufficient whereas, in microcarriers, it may take 6 hours. Other than that, they are autoclavable and do not lose their shape and integrity (Vyas and Cino, 2007). It has been claimed by the NBS that due to the 3 D porous structure of the disks, it not only protects the cells from the shear environment but also increased the productivity by 10 folds as compared to microcarriers (Eisenstein, 2006).

2.15.2 Dynamic membrane aeration system (DMA system)

Bayer Technology Services (BTS) developed a novel aeration method, the Dynamic Membrane Aeration method (DMA) as reported by Frahm et al., (2009) using surface aeration for the cultivation of shear sensitive cell lines with the use of microporous silicone tubing wrapped around a centrally placed star-like oscillating/ tumbling stirrer. They combined rotor and stator to form a rotary oscillating stirring unit. Traditionally, the stator is a cylindrical shaped unit fixed to the head plate, onto which gas permeable silicone tubing is wrapped thoroughly. Bioreactor stirrer is placed within the hollow cylindrical space. The conventional rotor-stator combination has some limitations such as poor mass transfer capacity at high cell densities and poor scalability. These limitations have been overcome by DMA technology where mixing is generated by rotating the stator platform by 180^{o} in a clockwise and anti-clockwise motion. This setup gives high mass transfer and a low shear condition, conducive for high cell density due to the high surface area for gaseous exchange. This DMA technology has been tested for the production of blood coagulation factor VIII at 12, 20,100 and 200 L scale. It has been reported that with the same power input of 6.0 Wm^{-3}, which is typical for cell culture applications, the mass transfer coefficient for DMA system is 35 % higher than the conventional systems (stirred tank) and the cell density achieved during continuous culture at 12 L was around 15 - 20 x 10^{9} cells mL^{-1} (Frahm et al., 2009).

2.15.3 Travelling wave bioreactor

Toroidal bioreactors work on the mechanism of the orbital motion of the bioreactor which creates travelling waves inside a hollow toroidal shape vessel. This travelling wave bioreactor (TWB) provides a high surface area and high surface renewal rates for oxygen mass transfer and mixing (Selker and Paldus, 2008). A CFD model of fluid flow has been developed with different geometries and consideration of parameters like shaking frequency, filling volume and amplitude of the moving liquid. The outcome of the computational studies has shown that travelling waves could provide a high specific surface area, low hydrodynamic shear and high mass transfer efficiency (Kaiser et al., 2014). A study of growing CHO cells in the TWB achieved a cell density of 5.4 x 10^{6} cells mL^{-1} with the viability of 95.5 %. The maximum oxygen mass transfer coefficient of 32 h^{-1} was reported, which is sufficient to cater to the mean specific oxygen uptake rate of 2.5 x 10^{-12} mgO_2

cell^{-1} s^{-1}. The maximum power input was reported to be 82.2 Wm^{3} for un-baffled TWB and 86.0 Wm^{-3} for baffled TWB whereas oxygen mass transfer coefficient was 10 - 12 h^{-1} for both baffled and un-baffled bioreactor types (Kaiser et al., 2016).

2.15.4 Rotary cell culture system (RCCS)

RCCS was developed by Synthecon for the National Aeronautics and Space Administration (NASA) for the growth of stem cells and 3 D cell culture (Schwarz et al., 1991). This bioreactor consists of a horizontal rotating vessel filled completely with culture media and a central axis shaft covered with microporous silicone tubes for gaseous exchange. The reactor has a zero headspace, zero gravity condition for the growing cells thus exerting low hydrodynamic shear. The continuous slow rotation of the vessel keeps all cells in suspension in low shear conditions and aid in forming small aggregates and cell clumps of sizes in the range of centimetre in diameter (Haut et al., 2003). This technology, however, has some limitations with cell aggregates which limits mass transfer to cells in the inner core leading to necrosis and eventually cell death (Hambor, 2012; Mitteregger et al., 1999; Schwarz et al., 1991).

2.16 Cell culture systems and accessories for microcarriers culture

Cell culture is naturally adherent and is initially grown in tissue culture flasks, where single-layered tissue culture flasks (TC flasks) can provide a maximum surface area of 225 - 300 cm^{2}. Therefore, large numbers of TC flasks are required to achieve the desired cell density for a seed tank. Roller bottles and multi-stacked cell factories (10/40 tray) have provided the next generation two-dimensional (2 D) culture platform, but this is laborious and time-consuming at large scale. Cell attachment, non-uniform cell distribution, difficulty in trypsinization, loss of cells, the requirement of large volumes of media and poor mass transfer are key problems in 2 D platforms (Whitford, 2010b). The initial concept of growing adherent cells on microcarriers as suspension culture was demonstrated by van Wezel (wezel 1967; Warnock and Al-Rubeai, 2006). Microcarriers are small spheres with a 90 - 300 µm diameter in different geometrical shapes like cylindrical (DE53, Whatman) and disk-shaped (Fibra-Cel, Eppendorf). They provide a large surface area to volume (cm^{2} mL^{-1}) ratio and enhance mass transfer efficiency and deliver consistent product quality over static culture systems (Schnitzler et al., 2016; Szczypka et al., 2014). Different types of microcarriers have different coating material which enhances the efficient attachment and distribution of the cells around the microcarriers over a large surface area (LifeSciences, 2013; Szczypka et al., 2014). Microcarriers are used to grow adherent cells for large-scale suspension culture in stirred tank bioreactors. These microcarriers are divided into two subtypes, macroporous and solid. Macroporous carriers provide a larger surface area, hence support higher cell density than solid microcarriers but yield fewer products than solid carriers. This is mainly due to poor mass transfer capabilities which include limited diffusion of nutrients into the centre of the macroporous carrier and difficulty in removing toxic metabolite, which negatively impacts the cell density and longevity of the culture (Warnock and Al-Rubeai, 2006).

2.17 Encapsulation of mammalian cells and its application

In bioprocess development, hydrodynamic shear forces, low cell density and low productivity are a huge problem with suspension cultures. Encapsulation of mammalian cells has opened a new window of opportunity in developing new bioprocesses for the shear-sensitive cell-lines. A microcapsule entraps viable cells within the boundary of a semi-permeable membrane and provides a conducive environment to the shear-sensitive cells. This microcapsule separates the cells from direct contact with turbulent eddies and the adverse conditions of the medium while providing the desired permeability for optimum oxygen and nutrient mass transfer (Goosen, 1988; Grigorescu and Hunkeler, 2003; Uludag et al., 2000). In addition, encapsulated cells also prevent the cells from wash-out in the case of continuous culture with high medium flow rate (Goosen, 1992).

The material of encapsulation plays a key role in encapsulation technology. There are four major properties a material should possess (i) Capsule permeability (ii) Mechanical strength (iii). Immune protection and (iv) Biocompatibility (Uludag et al., 2000). There are several types of materials (Synthetic and biological) available for encapsulation. Synthetic polymers such as water-insoluble poly (2-hydroxyethyl methacrylate), poly (2-hydroxyethyl methacrylate-co-methyl methacrylate, poly (ethylene glycol), polyvinyl alcohol, polyurethane, poly (ether sulfone), polypropylene, sodium polystyrene sulphate, polyacrylate poly (acrylonitrile-sodium methallylsulfonate), and dolomite based are few mentioned here whereas natural (Biological) alginate, agarose, chitosan, cellulose, collagen, and xanthan based are used (de Vos, 2014; Morikawa et al., 1997; The Dolomite Centre Ltd, n.d.).

Mammalian cell encapsulation has grown many folds since its first use reported back in the 1950s since then different types of cells have been microencapsulated for drug delivery, tissue engineering and regenerative medicines (Orive et al., 2002; Uludag et al., 2000). The CHO cells have also been successfully encapsulated for the production of recombinant protein products. It has been reported that CHO cells, encapsulated in the CellMAC capsule produced a similar amount of erythropoietin whilst attaining high cell density as compared to non-encapsulated cells (Weber et al., 2004). In another study, recombinant CHO cells expressing Desmodus rotundus salivary plasminogen activator (DSPA) in stirred tank bioreactor achieved comparative high cell densities as compared to non-encapsulated cells. The rate of product formation was 4.8 times higher and product accumulation was reported to be 3.3 times higher than non-encapsulated cells (Wang et al., 2015).

Apart from many disadvantages, cell encapsulation technology has some limitations in terms of the material used. Natural material obtained from seaweed have been used in encapsulation which pose safety issues and have found difficulty in clearing regulatory hurdles for human use in cell delivery-based therapeutics. Synthetic polymers have an edge over these natural polymers. They can be synthesized rapidly without a lot-to-lot variation, with increased bio-tolerability and mechanical strength (de Vos, 2014; de Vos et al., 2014).

2.18 Vero cells as a substrate for the production of the vaccines

The Vero cell line is the most universally acknowledged, continuous cell line which is approved by World Health Organisation (WHO) for their consistent successful track record of vaccines manufacturing (Bouquet, 2013; Paillet et al., 2009). Vero cells are derived from the renal cells of normal, adult African green monkey (*Cercopithecus aethiops*). These cells are epithelial in nature and grow on a solid surface, which classifies them as anchorage-dependent cells (Ammerman et al., 2008; Sheets, 2000). They are very susceptible to infections from a variety of viruses such as flavivirus, arboviruses, reoviruses, Simian virus 40 (SV-40), SV-5, Polioviruses, and parainfluenza. Vero cells are suitable for the development of several viral vaccines such as influenza, Japanese encephalitis, dengue, yellow fever, polio, and rotavirus. Vero cells grow as a static culture in tissue culture flasks which require a humidified CO_2 incubator to control and maintain suitable physio-chemical conditions for their growth as discussed earlier in section 2.12.1.

In brief, there is no provision for mixing in the tissue culture flasks and oxygenation of media occurs through diffusion from the headspace to the media layer. Hence, the required oxygenation of media is a limiting factor at high cell density and accumulation of metabolic waste have deleterious effects on cell growth (Ozturk, 2014). The two-dimensional (2 D) culture platform such as TC flasks, cell factories, roller bottles also have limitations such as non-uniform cell distribution, difficulty in trypsinization, loss of cells, the requirement of large volumes of media and poor mass transfer. Apart from that, it is also laborious and time-consuming to work on these culture systems at large scale (Whitford, 2010b).

To mitigate these surface constraints and mass transfer issues related to 2 D culture systems, many attempts have been made to grow Vero cells as a dynamic culture on microcarriers albeit elevated cost as discussed in section 2.16.

To reduce the cost and reliance on microcarriers, cells are adapted in suspension with emphasis on serum-free medium because sera have many drawbacks such as being a potential sources of contamination, having lot to lot variation, and difficult to remove in downstream processing (Daelli, 2007; Rourou et al., 2009). Many cell-lines have shown a tendency for easy adaptation to suspension cultures such as Chinese hamster ovary (CHO), Baby hamster kidney (BHK21) and 293 cells (Coco-Martin and Harmsen, 2008; Negrete et al., 2008). Vero cells are difficult to adapt to suspension due to the high expression level of structural proteins (Integrin) which have strong electrostatic binding to the attachment surface (Schmidt et al., 2013).

2.19 Integrins: Structural and communication network of the cells

Integrins are cell adhesion receptors, belonging to the widely expressed large family of multifunctional, multi-domain heterodimeric glycoproteins. They are an integral part of the cytoskeleton of all metazoans and are involved in the evolutionary changes occurring during developmental and pathological processes (Barczyk et al., 2010; Danen and Yamada, 2001; Hynes, 2002; Xiao et al., 2004; Zent and Srichai, 2010). The term “Integrin” indicates that this group of receptor proteins bind to the extracellular matrix (ECM)

of the cytoskeleton to establish communication to the surrounding cells (Campbell and Humphries, 2011; Hynes, 2004).

Integrins belong to the superfamily of Type 1 transmembrane cell adhesion receptors which bind to the ECM ligands, cell-surface ligands and soluble ligands. They act as a communication hub for bidirectional communication (inside-out and outside-in) between the intracellular environment and the extracellular environment (Takada et al., 2007; Tolomelli et al., 2017; Zent and Srichai, 2010). On the surface of the resting cells, integrin is present in the form of non-adhesive inactive protein which is reversibly regulation for quick activation for cell adhesion (Chigaev et al., 2011). Apart from that, integrins play a significant role in immune response, wound healing, tissue re-modelling and haemostasis. In response to undesirable conditions for cellular growth, integrins re-modulate and trigger various cellular processes through signal transduction such as cell migration, proliferation, cell adhesion, cell differentiation and programmed cell death (Seguin et al., 2015; Zent and Srichai, 2010). These cellular processes are supported by integrin role in modulating the cytoskeleton through rearrangement of actin filament, cell adhesion on stable ECM, rolling adhesion in shear conditions and cellular signalling which lead to gene expression regulation (Delon and Brown, 2007; Staunton et al., 2006).

Primarily, integrins are non-covalently bound heterodimers which are constituted by α and β subunits. A total of 24 heterodimers are reported in humans, which includes the 18α and 8β subunits present in Vero cells (Hynes, 2002; Takada et al., 2007; Zent and Srichai, 2010) and the general structure consists of a large extracellular domain which communicates with the extracellular environment by binding to a protein, a transmembrane domain and a cytoplasmic tail (Hynes, 2002; Zent and Srichai, 2010). The complete heterodimer structure plays a crucial role in the structural integrity of the cells.

The environment inside and outside the cell dictates the overall cellular behaviour. Integrin recognises and sense the extracellular molecules with the aid of cell surface receptors and transmit a signal for cellular phenotype regulation and behavioural changes (Humphries et al., 1993). Integrins convert physical signal from outside to chemical signal inside of the cell. The factors such as microenvironment inside the cells, the environment outside the cell, mechanical shear-stress have an impact on the cell adhesion, actin polymerisation, regulation of cellular activity and overall cell shape which further impact the cell cycle (Barczyk et al., 2010; Moreno-Layseca and Streuli, 2014). In the case of a tumour, the tumour microenvironment (TME) on integrin plays a crucial role in cancer progression and have a significant impact on drug efficacy which further influence the therapeutic response (Klemm and Joyce, 2015).

2.19.1 Role of anti-cancer drugs or inhibitors in suppressing the expression of integrin

Integrins play a key role in regulating various cellular functions such as controlling leukocyte traffic, generating an immune response, maintaining homeostasis and programming of cancer cell onset (Chigaev et al., 2011). Many companies have attempted to develop antagonistic drug molecules (around 120) which could alter/modulate or suppress the integrin function (Goodman and Picard, 2012). The difficulty encountered in creating specific inhibitors are because many integrin subunits recognise the consensus amino acid sequences Arg-Gly-Asp (RGD) in the matrix protein. The combination of various αV and β units play a crucial role in various disease progression (i) αVβ1 responsible for tissue fibrosis *in vivo* ocular melanoma and neurological cancer (ii) αVβ5 especially in fibroblast and epithelial cells play a role in

angiogenesis (iii) αVβ6 a receptor for fibronectin and vitronectin which amplify carcinoma progression (vi) αVβ3 in, melanoma and glioblastoma (Li et al 2010; Das et al., 2018). Various inhibitor molecules/ antibodies and peptides have been developed which specifically target various subunits of the integrins to suppress and control the progression of cancer as shown in Figure 2-16

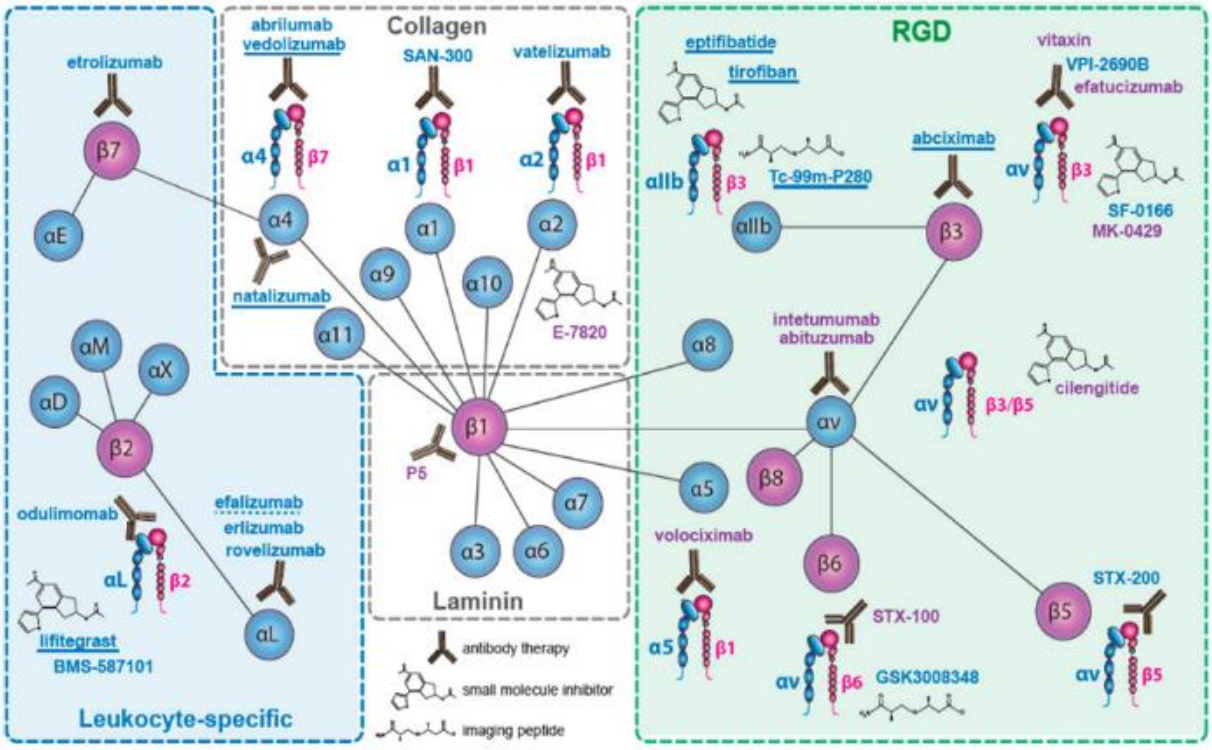

Figure 2-16 Integrin targeted by antibodies, small inhibitor molecules and peptides. Drugs named in violet have been used in cancer trials. Non-cancer drugs are named in blue. Marketed drugs are underlined; withdrawn drug indicated with a broken underline -taken from Raab-Westphal et al., (2017)

Chigaev et al., (2011) reported that exploitation of Nitric Oxide/cGMP signalling pathway down-regulate the adhesion efficiency of α4β1-integrin and very late antigen 4 (VLA 4) binding to the ECM which is expressed on leukocyte, stem cells and hematopoietic cancer cells. LM609 (Vitaxin) is an anti-angiogenic molecule which exhibits the antagonistic activity of αVβ3 (Mousa, 2002).

Krishnamurti et al., (2001) has also reported that the use of Puromycin Aminonucleoside (PAN) suppresses the expression of α3β1 in a dose-dependent manner when cells were exposed to PAN, resulting in glomerular epithelial cells detaching from the basement membrane. As glomerular cells and Vero cells have the same origin (kidney cells), they express similar integrin subunits (surface receptors) (Guo et al., 2014). Therefore, it can be postulated that use of PAN may suppress the expression of integrin on the Vero cells and assist in bringing cells in suspension by exhibit the similar phenomenon of cell detachment as in the case of glomerular epithelial cells.

2.19.2 Role of Integrin in virus entry for vaccine manufacturing

The first step of the virus attachment to the host cell is to identify the favourable cell-surface receptors that have an important role in triggering outside-in signal. Integrins are generally exploited by the viruses for entry into the host cells (Stewart and Nemerow, 2007). Advances in technology to elucidate the detailed

structure of integrin and their ligand's interaction with various viruses have paved the way to understand the molecular level interaction and mechanism of virus entry into host cells. With the advances in cell imaging techniques, it is evident that upon attaching to the cell-surface receptors, viruses bring conformational and structural changes to the cytoskeleton by exploiting integrins which then facilitates the virus entry through virus internalisation by rearranging the cytoskeletal (Stewart and Nemerow, 2007).

The process of virus entry facilitated by different subunits of integrins depending upon the affinity of viral proteins with the surface receptors. In the case of foot and mouth disease virus (FMDV), αvβ6 play a crucial role in virus entry and infection through clathrin-dependent endocytosis (Berryman et al., 2005), whereas, in the case of rotavirus, the surface receptor αvβ3 subunit of integrin plays a pivotal role in virus entry due to enhanced cellular susceptibility (Guerrero et al., 2000). Other integrin subunits such as α2β1, αxβ2 and α4β1 have shown to interact with capsid proteins VP4 and VP7 of rotavirus which mediates the entry into the host cell (Coulson et al., 1997). West Nile virus (WNV) and Japanese encephalitis virus (JEV) recognise the αVβ3 integrin subunit which is associated with signalling pathways responsible for virus entry into host cells (Chu and Ng, 2004).

In the event that Vero cells are treated with an anti-cancer drug to supress integrin expression and resulting in a suspension culture, consideration needs to be taken on the effect of this suppression on viral infection if the suspended cells are intended to be used in vaccine manufacturing as a host for viral replication.

2.20 IMC as a tool for measuring bioactivity of mammalian cells

2.20.1 Principle of Isothermal Microcalorimetry

Isothermal microcalorimetry (IMC) is a branch of calorimetry which deals with the concept of measuring and monitoring change in heat fluxes during chemical and physical processes. IMC is able to measure accurately extremely small heat signals (power < 1 μW) produced from the specimen sample (Said et al., 2015). The fundamentals of the technique are to record the change in heat fluxes from the specimen sample through conduction either into or from a heat sink whose temperature is kept at constant temperature (isothermal) (Buckton, 1995).

The response of the instrument is recorded as the power which is a rate of change of heat ($\frac{dq}{dt}$) as a function of time (t). Figure 2-17 explains the set-up of IMC instrument where an ampoule is lowered inside the oil bath for the reaction to happen and the heat flux changes logged per second.

The main advantage of this technique lies in the variety of samples it can undertake for investigation irrespective of their physical appearances (solid, liquid or heterogeneous samples) which broadens its applicability across various disciplines (Braissant et al., 2015; Said et al., 2015). It has been in use to quantify the microbiological activities in various samples not limited to soil ecology and sewage sample (Bravo et al., 2011; Dziejowski and Białobrzewski, 2011), determining the efficacy of compounds / drugs exhibits anti-microbial, anti-viral and anti-protozoans activities (Tan and Lu, 1999; von Ah et al., 2009; Wenzler et al.,

2012), identifying the vitality and viability of yeast (Myers, 2017) and to elucidate the microbial activities of mixed cultures on the mineral surfaces (Ghadiri et al., 2018; Makaula et al., 2017b, 2017a).

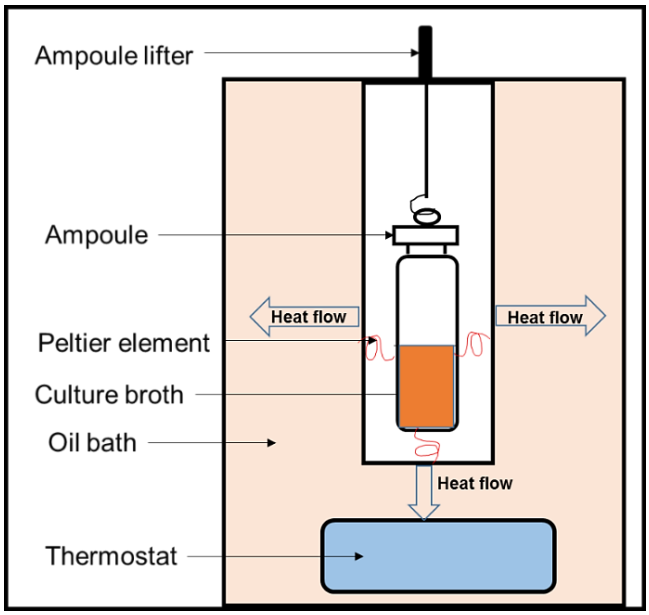

Figure 2-17 Schematic representation of the IMC instrument with essential parts (TAM III).

2.20.2 IMC and mammalian cells

The isothermal microcalorimetric technique has not been used with full potential for measuring the real-time biological activities of mammalian cells. Nedergaard et al., (1977) reported using microcalorimetry to measure the heat produced by brown adipose tissue. Since then, little work has been carried out on mammalian cells. With the advancements in IMC instrumentation and capacity, coupled with the need to measure protein and other macromolecule affinities to various ligand activity, Isothermal titration calorimetry (ITC) has extensively been in use (Bravo et al., 2011). ITC is a technique which computes the thermodynamic activity (heat activity) of various molecules/drugs which assist in determining their molecular interaction with ligands and establishing thermodynamic stability. Apart from this, Braissant and Daniels, (2011) detailed the measuring of the continuous real-time activity of cultured mammalian cells in a closed ampoule and reported that 2,000-20,000 cells are necessary to produce a detectable signal. In the present research, the applicability of the IMC instrument to measure the biological activity of the CHO and Vero cells was investigated especially when Vero cells were exposed to PAN.

2.21 Summary of literature review

This chapter emphasized on the role of a suitable mammalian cell bioreactor to produce biologicals. Therefore, an account of the chronological advances in the area of mammalian cell culture development and bioreactor designs were showcased. The impetus was given to the need to develop more comprehensive bioreactor designs that can accommodate various shear-sensitive cell lines to achieve high cell density with extended longevity.

The chapter further pinpoints the critical parameters which play a pivotal role in the optimum performance of the bioreactor i.e. the aeration-agitation regimen. Aeration and agitation regimen dictates the mass and heat transfer efficiency, power consumption, mixing and fluid flow profile which directly affect the hydrodynamic conditions of the bioreactor.

Additionally, a brief outline of different methods of delivering oxygen to the bioreactor was reviewed followed by a summary of impellers used for the propagation of mammalian cells. This exercise assists in weighing the pros and cons of various aeration-agitation regimen for the growth of mammalian cells which is directly responsible for the hydrodynamic conditions of the bioreactor. Apart from this, various other factors responsible for hydrodynamic shear were also accounted for in section 2.9.

Furthermore, a detailed review of relevant literature was carried on the various types of bioreactors such as static and dynamic culture, traditional and single-use bioreactor, use of microcarriers and novel designs of bioreactor available, their working principles, geometry and their advantages and disadvantages. This assisted in deciding the appropriate bioreactor design for the current study.

The significance of suspension culture was established therefore various methodologies were reviewed to bring the cells into suspension which are otherwise difficult because of the high expression of integrin in mammalian cells such as in Vero cells. The Vero cell line is a substrate/host cells for many vaccine production processes. In order to grow mammalian cells in suspension, encapsulation is one method, which has been done by various researchers for CHO cell but this technique has many drawbacks related to the material used for the encapsulation. A better understanding of the material used for the encapsulation may define the capsule properties (strength and compatibility) and its effects on the growth and behaviour of the cells hence the product produced from these encapsulated cells may get acceptance from the regulatory bodies and industry. Another method reviewed was exploiting the expression of integrin to bring the cells into suspension by detaching the cells from the ECM by using anti-cancer drug or integrin inhibitors. A brief background of integrins structure and their role in cancer and virus entry was explored.

In the end, the use of isothermal microcalorimetry was explored in mammalian cell cultivations and how it can assist in analysing the viability and vitality of the cells when subjected to sub-optimum growth conditions, such as when treated with anti-cancer drugs.

3 Approach to Project and Methodology

The focus of this chapter is to describe the methodology of designing and fabrication of the prototype bioreactor and its abiotic and biotic characterisation. Additionally, procurement of cell lines, their adaptation to suspension culture, maintenance, culture conditions, and media screening is also covered in this chapter. Furthermore, the chapter will also discuss the methodology of the treatment of Vero cells with anti-cancer drugs and the exploitation of Isothermal microcalorimetry to establish the bioactivity of the cells post drug treatment. Further details on specific experiments are described in subsequent sections.

3.1 Context of designing of a novel bioreactor

Various bioreactor designs (reusable, single-use and novel culture system) have been developed over time, which have their advantages and disadvantages, which are discussed in the sections 2.13, 2.14 and 2.15 of the previous chapter. Therefore, there is a need to develop a bioreactor which would mitigate the current issues in bioreactor designs and provide an alternative for the growth of mammalian cells. In this thesis, the focus was to develop a horizontal tubular bioreactor (HTB) with a novel spiral impeller. This prototype bioreactor not only exploited the advantage of using surface aeration (bubble-less) method but also induced continuous fluid flow and mixing by using a spiral impeller (Screw impeller). The horizontal vessel with spiral impeller provides high surface renewal rate, consequently allowing sufficient mass transfer and mixing with low power consumptions to be achieved.

3.2 The conception of an idea and role of biomimicry

Most of the bioreactor designs whether reusable or single-use have vertical geometries with various design options and aspect ratios. This would include the conventional stirred tank, disposable stirred tank, shaken bioreactor and the CelCradle. Few designs explore a horizontal setup, which include the bag and pillow type, doughnut and cubical in shape type bioreactors. The Rotary Cell Culture System (RCCS) is the only horizontal design reported so far to produce stem cell and 3 D culture for tissue engineering.

In the current research, we focussed on a horizontal design instead of a vertical design. The horizontal design gave a large surface area and low liquid height for the same volume (the surface area to volume ratio) for efficient mass and heat transfer (Šantek et al., 2006).

The design of the spiral impeller was inspired by nature and considered as an example of biomimicry. (Benyus, 2002). The objective of biomimicry is to exploit and translate nature and natural phenomena and getting cues from it to solve current problems related to technical, environmental and social challenges which affect every square of life without using biological material (Kennedy et al., 2015; Marshall and Lozeva, 2009). In other words, it is just not copying nature for our benefit but learning and understanding from nature, their processes, mechanisms, and structures which sustained and refined by the course of evolution (Lurie-Luke, 2014).

DeLuca (2016) gave emphasis on the power of the spiral biomimicry design and supported the argument and explained that nature's preferred way of working is in the form of spiral. Spiral (curved structure) is present everywhere, from DNA, mitochondrial cristae, deep in the ear, flowing rivers, the structure of leaves, the arrangement of leaves on the trees to galaxies. Most objects in some way follow the spiral form, which means that this spiral form is more sustainable in terms of stability and requires lower energy levels to acquire the shape and drive the processes (DeLuca, 2016).

The various kinds of spiral/anchor impeller have been in-use in the food industry to move Newtonian and non-Newtonian fluids such as thick slurries, sauces and ketchup but it has not been employed in any type of cell culture bioreactor for the growth of mammalian cells. The use of spiral impeller in the horizontal tubular bioreactor is unique. although researchers have used a static helical track in a shaken bioreactor (Zhang et al., 2008), it has not been reported yet in a horizontal vessel.

3.3 Materials and Methods

3.3.1 Cell lines and media

3.3.1.1 Cell lines

Chinese hamster ovary (CHO) cells (Item no. CCHO-C; CHO-K1) and Vero cells (Item no. CVER-C) were obtained from Cellonex (Johannesburg, South Africa). Both the cell lines were adherent in nature and were received as a frozen cryovial. Another adherent CHO cells (Item no. CHO-sACE-CHO-K1) was obtained in one T-75 cm^2 tissue culture (TC) flask from Prof. Edward Sturrock, Division of Medical Biochemistry, Institute of Infectious Disease and Molecular Medicine (IDM), University of Cape Town, South Africa. The aforementioned CHO cells were transfected with somatic angiotensin-converting enzymes (CHO-sACE).

3.3.1.2 Cell culture medium

Initially, both cell lines CHO and Vero cells were grown in Dulbecco's Modified Eagle Medium (DMEM-D6546-500 mL) with 10 % foetal bovine serum (FBS) (Hyclone-South American origin-SV30160.03IR). Transfected CHO cells were received in DMEM/Nutrient Mixture F-12 Ham medium supplemented with 10 % FBS. Thereafter, CHO cells were adapted to grow in suspension culture (CHO-S) in SFM4CHO, a serum-free media (G.E. Hyclone-SH30518.01), which were prepared as per manufacturer's guidelines. Similarly, Vero cells were also adapted to grow in two different media namely SFM4-MegaVir (Hyclone- SH30587.01) and Vero Express (Hyclone - RR16207.01) in serum-free condition as an adherent culture. Vero express medium was under developmental stage from the manufacturer, which later commercially available as Vaccine Xpress from G. E. Hyclone.

Various media were also screened to achieve optimum cell density for extended longevity with high protein productivity for already adapted suspended CHO cells (transfected and normal). The media samples were donated by Separations, Johannesburg, South Africa. All the six media were from G. E. Hyclone. The list of media screened as given below in Table 3-1

Table 3-1 List of commercially available media used for screening purpose

Media IDs	Media	Description of media	Cat. Number
M1	HyCell CHO	HyCell CHO medium with poloxamer188 and w/o glutamine	SH30934.01
M2	HyCell CHO	HyCell CHO medium with poloxamer188 and w/o glutamine w/o hypoxanthine, w/o thymidine (HT)	SH30949.02
M3	CDM4PERMAb	CDM4PERMAb without Glutamine	SH30871.02
M4	Actipro	HyClone ActiPro	SH31039.02
M5	ActiSM	Hyclone ActiSM with Poloxamer 188, w/o glutamine/ insulin	SH31040.02
M6	SFM4 CHO	Dry powder media reconstituted in autoclaved double distilled water with poloxamer188 and stable glutamine	SH30518.01

3.3.1.3 Sub-culturing and maintenance of cells

There are slight modifications of the sub-culturing method of adherent and suspension cell lines. Unless otherwise stated, the sub-culturing and cell line maintenance procedure was the same for all the cell lines mentioned earlier.

The criteria for sub-culturing and maintenance were defined when the monolayer is 70 - 90 % confluent and the suspension culture reached ~ 2 x 10^6 cells mL^{-1}. The spent media from the TC flask was aspirated aseptically with the help of serological pipette under a biosafety cabinet II. Then, an equal amount of pre-warmed 1 x PBS (phosphate-buffered saline), which was prepared as per CeBER protocol (unpublished) was added onto the monolayer, swirled thoroughly onto the monolayer and then aspirated to remove the traces of serum from the flask. Thereafter the monolayer was treated with cell dissociating solution Accutase® (Biowest-L0950-100). Total of 1 mL solution of accutase was added on the monolayer and the solution was swirled again onto the monolayer. Care was taken while adding the Accutase solution onto the monolayer for the solution must cover the monolayer before storing the flask inside the incubator for 3 - 5 minutes at 37 ^oC with 5 % CO_2. After incubation, the flask was gently tapped from the sides of the TC flasks to dislodge the cells. A fresh complete media of 5 mL was added inside the flask, the cell suspension was triturated well to dislodge the cells completely from the walls of the flask and reconstituted the cell suspension. The cell counting was done using 0.4 % trypan blue (Sigma-T8154) exclusion method using a bright-line haemocytometer to determine the cell count and % viability. The cell suspension was divided as per requirements in 1:2 or 1:3 split ratios. New TC flasks were kept in incubator again at 37 ^oC with 5 % CO_2. The culture was monitored the next day for their attachment and morphology. The TC flasks like T-25 cm^2, T-75 cm^2, and T-150 cm^2 can accommodate 5, 10 and 20 mL of culture media after sub-culturing.

The method adopted to subculture the suspended cell line do not require accutase treatment. Shake flask was taken from the incubator. Cell counting and viability of the culture was determined as mentioned earlier. The culture was divided as per requirement in the form of 1:2, 1:3 and 1:4 split ratios to maintain the

desired initial cell density of 0.2 – 0.3 x 10^6 cells mL^{-1} by adding pre-warmed complete serum-free media (Hyclone-SFM4 CHO). Thereafter, each flask was kept at 100 rpm on the orbital shaker (Lasec-Stuart SSL-1) inside the ESCO CO_2 incubator at 37 ^oC with 5 % CO_2.

3.3.1.4 Cryopreservation of cell lines and revival

A freezing mix was prepared for cryopreservation of adherent cell lines like CHO and Vero cells. The freezing mix contained 90 % FBS supplemented with 10 % Dimethyl sulphoxide (DMSO) (Sigma, Cat No.4540-100 mL). The freezing was done at each step of serum reduction during serum-free adaptation of the cell lines.

In the case of serum-free cells, whether adherent or suspended, the freeze mix constitutes 45 % fresh complete medium (Medium + 4 mM stable glutamine + 0.1 % Poloxamer 188), 45 % conditioned media and 10 % DMSO. The details of the cryopreservation method was described by Sinacore et al., (2000). All the cell lines were stored at -80 ^oC in staggering mode at two different places (one at CeBER (-80 ^oC) and another one at IDM, UCT Medical School at (-80 ^oC) with the viable cell density of 2.0 x 10^6 cells mL^{-1}.

The revival procedure was the same for all the cell lines. In the case of adherent culture TC flasks were used and for suspension culture shake flasks were used. The volume of the media was also adjusted accordingly. One vial was taken out from -80 ^oC freezer. The vial was quickly thawed in a 37 ^oC water bath before adding 9 mL of pre-warmed complete media (based on the cell line) in a T-25 cm^2 flask/125 mL Erlenmeyer vented conical shake flask with 0.22 µm vent filter in the cap (Corning Limited). Slowly, thawed cells were added drop by drop into the flask with complete media. Flasks were kept in the incubator at 37 ^oC with 5 % CO_2. Next day, cells were observed for their growth under microscope.

3.3.1.5 Adaptation of adherent CHO and Vero cells into serum-free conditions

As the aforementioned cell lines (non-transfected CHO cells, transfected CHO cells, and Vero cells) are inherently grown as adherent cells and into complete basal media as mentioned before, their method of adaptation to serum-free conditions is the same unless otherwise stated.

The original TC flask (T-75 cm^2) was split into two to maintain the culture in parallel. The first set of TC flasks was maintained with original medium with 10 % FBS throughout the adaptation process, whereas in the second set of TC flasks, the serum concentration was serially reduced from 10 % to 0.3125 %. Sub-culturing was repeatedly done every 3 days, after observing the TC flasks under an inverted microscope for an approximate 70 - 90% confluency and for cellular health. Thereafter, the TC flasks were split into 1:3 to maintain the cell density ≥ 0.2 x 10^6 cells mL^{-1} in TC flasks. The low cell density aided in coping with stress-related factors. At each serum concentration, at least three sub-culturing were done to achieve fully acclimatised cells in similar cell concentration to the cells maintained with 10 % FBS. When the serum concentration was at 2.5 %, fresh serum-free media was added in 1:1 ratio in the culture flask. Thereafter, at every third passage, the serum concentration in the medium was reduced by 50 % from the previously used concentration and the concentration of the serum-free medium was increased in the culture flask until the cells were fully adapted to serum-free conditions with similar growth rate as showed in serum-containing media (ATCC, 2012).

For adapting CHO (adherent) cells into suspension culture, the first step is to dissociate the monolayer from the attachment surface by using Accutase as discussed in section 3.3.1.3. The viable cells were counted using 0.4 % trypan blue exclusion dye and the shaker flasks were seeded with a starting cell density of 0.5 x 10^6 cells mL^{-1}. The culture was observed every day and the viable cells counted.

After every three days, the cells that survived in suspension culture were collected. The cells were centrifuged at 700 rpm for 5 minutes and resuspended in fresh complete medium and the new shaker flask was re-seeded with the adapted suspended cells based on the number of cells obtained. Cells that form clumps were dispersed in the cell suspension. During the subsequent passages, suspended clumps were broken down to small clumps or eventually into a single-cell suspension. The suspended cells were sub-cultured repeatedly to acquire similar and constant growth rate as that of adherent cells.

3.3.2 Process conditions

For the static culture such as adherent CHO and Vero cells, all the TC flasks were kept inside the incubator at 37 ^oC with 5 % CO_2 with more than 80 % humidity. For dynamic culture without process control, an orbital shaker was kept inside the CO_2 incubator at 37 ^oC and was used in the adaptation studies as well for the preparation of seed inoculum for the bioreactor batches. The shaker flasks were mounted on the orbital shaker and kept at 100 rpm.

In the case of bioreactor batches, specific parameters were maintained during the batch process Table 3-2

Table 3-2 General process parameters for CHO batches taken in HTB

Parameters	Process conditions	Phase
Temperature	37 ^oC	Growth phase
Temperature	35 ^oC	Stationary phase
pH	7.0 - 7.2	Growth phase
pH	6.9 – 7.0	Stationary phase
Stirring speed	150	Growth phase
Stirring speed	150 - 500 rpm	Based on batches, described individually in section 5.2
Airflow rate	0.2 LPM	Throughout batch

3.3.3 Media screening

The commercially available media were screened (Table 3-1) for their support to achieve optimal cell density with extended viability and high productivity. For this experiment, different media were screened which vary with respect to their composition to optimise protein production. The different media were screened for the growth of CHO cells expressing somatic ACE (sACE). All the media were additionally supplemented with 4.0 mM stable glutamine. The media without surfactant (poloxamer 188) were supplemented with 0.1 % poloxamer 188.

For the media screening experiment, cells were collected from the seed shake flask and centrifuged at 1000 rpm for 5 minutes. The supernatant was discarded, and the pellet collected was triturated well with 1 x PBS. Cells were centrifuged again at 1000 rpm for 5 minutes.

The supernatant was discarded, and the pellet was resuspended in 5 mL SFM4 CHO media. Cell counting was done. For the experiment, six 125 mL shake flasks were seeded with an initial cell density of 0.3 x 10^6 cells mL^{-1} with a maximum of 30 mL volume. Each flask was labelled from number M1 to M6 (Table 3-1). Samples from each shake flask were taken every day for cell density, viability and protein production.

3.4 The methodology of abiotic engineering characterisation of HTB

3.4.1 Fluid flow pattern and Mixing time

Fluid flow plays a crucial role in achieving homogeneity and determining the shear conditions and eddy formation inside the bioreactor. Fluid flow pattern and mixing time was determined by using phenolphthalein and conductivity methods respectively. Phenolphthalein method primarily aims to visualize the pattern of fluid flow whereas conductivity method aid in measuring accurate mixing time and in return assist in calculating circulation time.

For fluid flow, 2 mL of phenolphthalein (Merck) was added to every 1 litre working volume (deionized water) under investigation. As the phenolphthalein is a pH indicator, 1 mL of 1.0 M NaOH per litre working volume was added to increase the pH of the solution which produced the bright pink colour. A Canon EOS-600 DSLR camera was set up facing the reactor, and images of 1 - 2 frames per second (fps) were taken of the reactor contents throughout the experiment. Thereafter, 1 mL of 1.0 M HCl (32 %) per litre working volume was added to neutralize the pH of the solution so that the colour of the solution turned pink to colourless.

The experiments of fluid flow pattern and mixing time of HTB was carried out at 4 % (1 L.), 42 % (2 L), 79 % (3 L) and fully immersed impeller (121 %) at 4 L. The fluid flow and mixing time at each impeller immersion was then evaluated at 100, 200, 300, 400, and 500 rpm. For the accurate measurement of mixing time, a conductivity test was performed.

For the conductivity method, the bioreactor was filled with the working volume under investigation at a particular impeller speed. 5.0 M of sodium chloride (NaCl) was used as a tracer salt for the studies. 1 mL L^{-1} of tracer salt was injected into the bioreactor at a working volume with a particular impeller speed. A conductivity probe was immersed at one end of the bioreactor (a normal place for DO probe in HTB) which was connected to an *AZ-86555* bench-top multi-meter (AZ Instruments). The change in conductivity of water was logged-on to a computer-aided software (Handheld Version 3.0) as mS cm^{-1} at every 1-second interval. The time taken to reach the 95 % homogeneity was calculated as follow

$$h_{95} = \left(\frac{C_t - C_0}{C_\infty - C_0}\right) \quad \text{Equation 3-1}$$

Where h_{95} is 95 % homogeneity, an indicator of the extent of mixing in the bioreactor, C_0 is the initial concentration of the tracer if any, C_t is the uniform tracer concentration at time (t) and $C\infty$ is the final tracer concentration (Wang et al., 2010). Each experiment was repeated in triplicate. The response time of probe played a crucial role in measurement; therefore, the response time of the conductivity probe was also measured by moving the probe from the beaker filled with D.I. water to the beaker filled with 0.0125 M NaCl.

The average response time of 3.5 seconds was recorded and was taken into consideration when determining h_{95} by combining the errors associated from the probe response time and standard deviation.

3.4.2 Minimum agitation speed

The minimum agitation speed (N_{js}) was calculated at different reactor volumes resulting in varying impeller immersion percentages. Solid's loading was done by varying the solid suspension by mass which mimic the mass of medium to high cell density suspension cultures. For the experiments, the bioreactor was operated at volumes 2 L, 3 L, and 4 L resulting in 42 %, 79 % and 121 % impeller immersion. Solids loading considered was 0.25 %, 0.50 %, 0.75 % and 1.00 % (mass/volume). Due to the low contact between impeller blades and liquid surface, 1 L reactor volume was not considered for the current studies.

The bioreactor was filled with D.I. water at the required volume (% impeller immersion) and loaded with approximately uniform sized (200 ± 50 μM) sodium alginate beads (Lee et al., 2013), which had been stained with Rhodamine-B dye (Sigma-Cat. No. R6626 – 25 G). The solid loading (alginate beads) was added, and the starting impeller speed was set at 100 rpm. The bioreactor was visually observed throughout the length of the vessel for flow pattern adopted by the beads and the upliftment of the beads from the bottom of the vessel. The impeller speed was step-up gradually to see the beads lifted off the bottom of the vessel. Criteria was set as suggested by Zwietering (1958) that the minimum agitation speed is achieved when no beads settle on the bottom of the vessel for more than 1 second.

3.4.3 Oxygen mass transfer efficiency

The oxygen mass transfer efficiency of the HTB was determined by the dynamic gassing out method (Finn, 1954; Van't Riet, 1979; Wise, 1951) at impeller rotational speeds from 100 to 500 rpm with an increment of 100 rpm. Each speed was tested at aeration rates of 0.2, 0.3, 0.4 and 0.5 LPM of compressed air passed through the headspace. These experiments were repeated at liquid volumes of 2 L and 3 L with D.I. water. The experimental matrix of Table 3-3 has dimensions of 2 x 4 x 5, resulting in 40 different experiments. The $k_L a$ value at each operating point was measured in duplicate. The method was as discussed in the section 2.6.1.1.

Table 3-3 Experimental matrices for oxygen mass transfer

Volume		**2 L**				**3 L**			
Airflow rate [LPM]		0.2	0.3	0.4	0.5	0.2	0.3	0.4	0.5
Impeller Speed (rpm)	100	x	x	x	x	x	x	x	x
	200	x	x	x	x	x	x	x	x
	300	x	x	x	x	x	x	x	x
	400	x	x	x	x	x	x	x	x
	500	x	x	x	x	x	x	x	x

3.4.4 Power utilisation

The power consumption of the HTB was determined through the temperature method as described by (Kato et al., 2004; Raval et al., 2007). This method is based on the energy balance of the bioreactor. This method was used to determine the heat generation in the bioreactor due to the energy supplied to the liquid

through impeller agitation. The method measured the heat flow out of the reactor by measuring the heat produced by viscous dissipation of energy by agitating the fluid. The bioreactor was insulated thoroughly by wrapping it with sheets of cotton wool. Two temperature sensors were used, one placed inside and one outside of the bioreactor (surroundings) to measure variations in the temperature of the bulk fluid compared to that of the temperature of the surrounding (Figure 3-1). Both temperature measurements were logged on to a computer system.

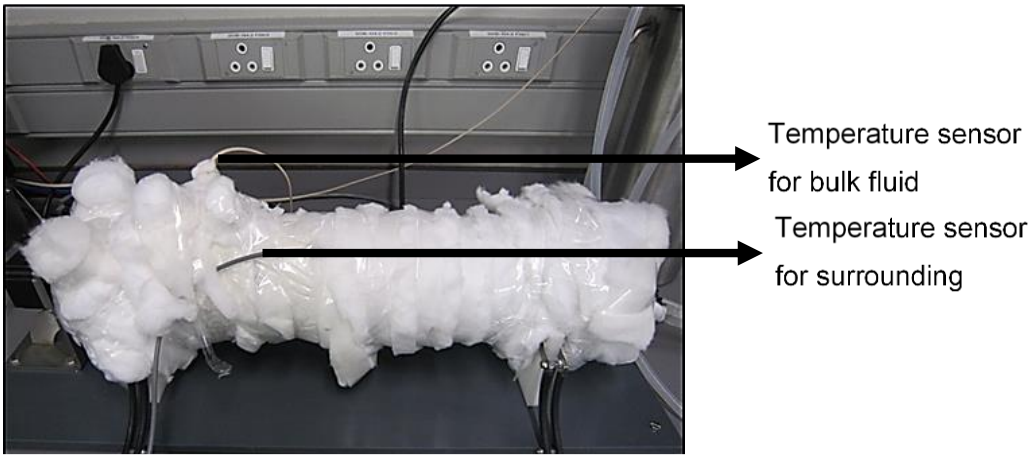

Figure 3-1 Bioreactor wrapped with cotton for the determination of power consumption

For the current study, the working volumes of 2 L, 3 L and 4 L were used to determine the power consumption at different impeller speed ranging from 100 rpm to 500 rpm with the increments of 100 rpm. The water was heated to 35.5 ^{o}C and was added inside the bioreactor which was thoroughly insulated with the sheets of cotton wool. The temperature inside and outside of the bioreactor was continuously logged on the system till the inside and outside temperature reached an equilibrium temperature (steady-state). According to Raval et al, (2007) the energy balance was defined by Equation 3-2

$$-mC_p\frac{dT_f}{dt} = UA\left(T_f - T_\infty\right) - P \qquad \text{Equation 3-2}$$

Where $-mC_p\frac{dT_f}{dt}$ represents the cooling rate of the heated liquid in the bioreactor, where m (kg) represent the mass of the fluid, C_p indicated the specific heat capacity (J kg^{-1} K^{-1}) and $\frac{dT_f}{dt}$ denoted the rate of change of temperature. $UA\left(T_f - T_\infty\right)$ represents the heat loss to the environment, which is represented by overall heat transfer coefficient UA (W K^{-1}) and P (W) denotes the power dissipation to the liquid. Two temperatures T_f and T_∞ (K) are the temperature of the fluid inside the bioreactor and the surroundings (outside the insulating cotton sheets) respectively.

During this experiment, firstly, the stirrer was kept off, in order to prevent any additional source of energy going into the system, therefore Power (P) was zero Equation 3-3.

$$-mC_p\frac{dT_f}{dt} = UA\left(T_f - T_\infty\right) \qquad \text{Equation 3-3}$$

Equation 3-3 was solved for the determination of overall heat transfer coefficient (U) and area of heat loss (A). The same experiment was repeated for the 2 L, 3 L and 4 L volumes to get the value of UA. Thereafter, experiments were set up with the stirring on at different speeds to calculate the value of Power imparted by the impeller to the bulk fluid. The Power (P) was calculated numerically by solving Equation 3-2

The value of P and UA are unknown for a given set of volume and stirring speed. Therefore, the value of P and UA were optimally guessed to minimise the sum of square errors. This temperature method requires experimental data of T_f and T_∞ over the time when the system is in equilibrium. The value of $T_f(t)$ was calculated numerically by using the input of $T_\infty(t)$. With the help of Solver add-on from the Excel (MS office 2013), the experimental and predicted values of $T_f(t)$ was compared for the lowest value of the sum of square errors (SSE) by varying the initial values of (UA) and (P) simultaneously (Jones et al., 2017).

3.5 The methodology of biotic characterisation of HTB

3.5.1 Mass transfer studies-dynamic gassing out method

The dynamic gassing out method was adopted to measure the volumetric mass transfer efficiency (k_La) of the HTB. The procedure to measure k_La was implemented during the stationary phase of the batch. As the batch had attained their peak cell density and protein activity was also optimally achieved during the stationary phase, the air supply to the bioreactor was stopped. The DO concentration started coming down as the viable cells started consuming dissolved oxygen (OUR) present in the media. The air supply was resumed before the dissolved oxygen concentration touched the critical level Figure 3-2. The general equation applied to denote the aerated liquid phase is

$$\frac{dC_L}{dt} = k_La * (C_L^* - C_L) - qO_{2.} * C_x \qquad \text{Equation 3-4}$$

Where, $\frac{dC_L}{dt}$ is the rate of oxygen concentration with time in the liquid phase, $k_La(C_L^* - C_L)$ represent the oxygen transfer rate (OTR) across the liquid and $qO_{2.} * C_x$ denote the oxygen uptake rate (OUR) by the achived cell density at a particular time during the batch, in this case, it was a stationary phase.

The modelled DO value was calculated from the value of $qO_{2.}$ (cell mL^{-1} min^{-1}) and the known value of C_x (cell density) thereafter the sum of square errors was minimised by using Excel solver to find the value of mass transfer coefficient (k_La).

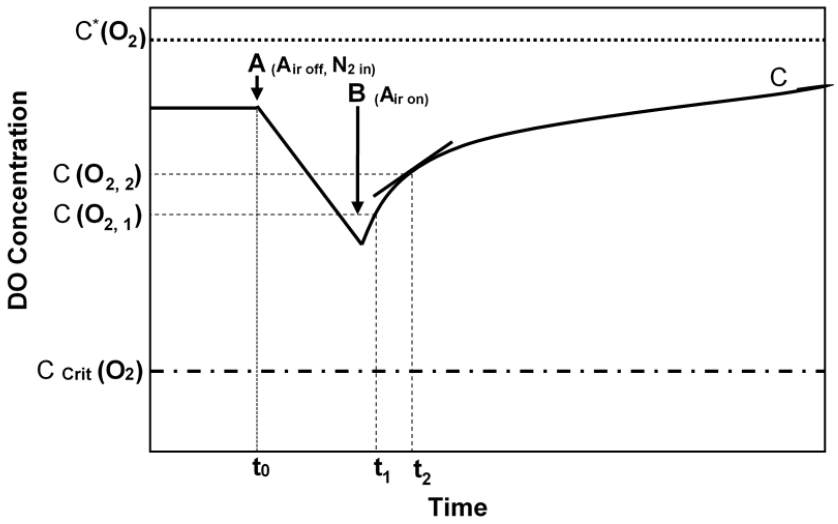

Figure 3-2 Measuring dissolved oxygen (DO) concentration through the dynamic gassing out method. At point A, the air is turned off till the point B, then the air was again turned on and allowed to reach the saturation point C. The point C*(O_2) represented the 100 % air saturation and C crit (O_2) indicate the critical oxygen level below which cells activities would be compromised - adapted from Uzir and Don, (2007)

3.5.2 Shear stress through cell death constant

Cell death kinetics was used to evaluate the mechanical stress induced due to the spiral impeller on the CHO cells during the stationary phase of their growth. It mainly followed the first-order kinetics which is described Equation 3-5

$$\frac{dVCD}{dt} = -k_d * VCD \qquad \text{Equation 3-5}$$

Where VCD is a viable cell density. Equation 3-5 was integrated for VCD (t) and VCD (t_0) to get Equation 3-6

$$VCD\ (t) = VCD(t_0) * e^{-k_d t} \qquad \text{Equation 3-6}$$

Here, k_d (day^{-1}), was measured by plotting the logarithmic VCD ($L_n\ VCD$) against time (t) (Blaschczok et al., 2013). The best fit of the curve was obtained by the linear regression method, calculating the R^2 value which indicate the accuracy of the predicted cell death constant as shown in Equation 3-7

$$lnVCD\ (t) = ln\ VCD(t_0) * -k_d * t \qquad \text{Equation 3-7}$$

3.5.2.1 Segregation of overall cell death from the impeller induced cell death

Efforts have been made to distinguish between the death from impeller stirring (hydrodynamic shear) in HTB to that of natural cell death which constitutes cell death from culture age, metabolite toxicity, oxygen and nutrition depletion. The specific cell death (k_d) was used as an indicator to depict the rate of cell death with an increasing impeller speed.

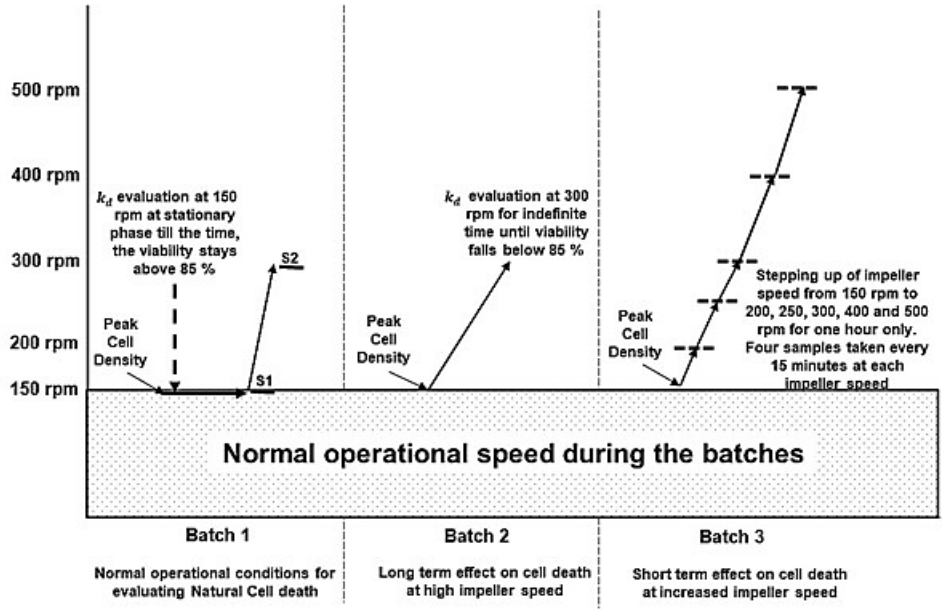

Figure 3-3 Experimental plan for determining the impeller-induced cell death in the HTB after achieving peak cell density. Batch 1 indicated the natural cell death occurring at the stationary phase when the viability would be still above 85 %. S1 and S2 samples were taken after one hour each at 150 rpm and 300 rpm to see short term –effect of increased impeller speed. Batch 2 elaborated the long-term effect of increased impeller speed at 300 rpm until the viability dropped below to 85 %. Batch 3 detailed the short-term effect of impeller speed at each rpm when the speed of the impeller was increased from 150 to 500 rpm for one hour each. Samples were taken after 15 minutes at each rpm.

The total of three batches with CHO cells were grown in the HTB and each batch was seeded with an initial cell density of 0.3 x 10^6 cells mL^{-1} and grown to stationary phase. The detailed experimental plan is described in Figure 3-3.

Batch 1 was grown with CHO cells expressing a heterologous proteins somatic angiotensin-converting enzyme (sACE protein) and Batch 2 and 3 were taken with plain CHO cells without any heterologous protein expression. The total volume of each batch was 3.0 L. The operating conditions were given in section 3.3.2. Each batch was run at 150 rpm till the batch attained peak cell density thereafter cells were subjected to shear stress as elaborated in Figure 3-3.

In Batch 1, the CHO cells expressing somatic ACE protein (sACE) was seeded in the bioreactor with an initial cell density of 0.3x 10^6 cells mL^{-1} and the batch ran at 150 rpm till the end of the stationary phase The aim of the batch was to determine the specific cell death constant at 150 rpm, which was assumed as natural cell death of the batches during normal operation. The impeller speed of the bioreactor was stepped up from 150 rpm to 300 rpm for one hour. Samples S1 and S2 were taken at each rpm after attaining the peak cell density for the determination of short-term effect of the increased impeller speed on culture health during stationary phase.

In Batch 2, when the cells reached peak cell density, the impeller speed was step-up to 300 rpm indefinitely until viability of the culture slipped between 80 - 85 %. The reason to step-up the impeller speed to 300 rpm was to determine the long-term effect of high impeller speed on the overall cell health as compared to when ran at 150 rpm during the growth phase which was considered as natural death. Samples were taken every day for cell counting on a haemocytometer with the trypan blue exclusion method.

Similarly, in Batch 3, the bioreactor ran until the end of the stationary phase while cell viability was above 85 %. To determine the effect of a gradual increase in impeller speed on the cells' health, the impeller speed of the bioreactor was stepped-up gradually starting from rpm 150, 200, 250, 300, 400 and 500 for one hour each as illustrated in Figure 3-3. Samples were collected aseptically every 15 minutes resulting in 4 data points for each rpm for determination of the cell death constant (k_d). The cell counting was performed in duplicate with the trypan blue exclusion method on a haemocytometer.

Two types of datasets were collected from all the batches. First dataset was at stationary phase during normal operation with stirring speed of 150 rpm, prior to the stress experiments. This data was to determine the natural cell death rate due to cell ageing. The second dataset was collected during the stress experiment where the cells were exposed to increased short-term or long-term increase of impeller speed. However, the cell death rate from the second set of data combines both the effects of natural cell death and from the increase in impeller speed. Therefore, in order to determine the death constant because of increased impeller speed, the following was determined:

k_d (due to impeller speed) = k_d (calculated from second dataset) – k_d (calculated from first dataset)

3.6 Mammalian cells and HTB

The suitability of the horizontal tubular bioreactor (HTB) was established by taking three batches as described in Figure 3-3. The process adopted to run the batches followed the sequence of (i) assembly and setting-up of the bioreactor, (ii) seed inoculum preparation and seeding, (iii) monitoring and controlling of the bioreactor as per process demand and (iv) harvesting of the bioreactor.

3.6.1 Assembly and setting-up of bioreactor

The glass vessel was thoroughly cleaned with tap water to remove dust and any other particulate impurities. Thereafter, the glass vessel was siliconized with Sigmacote® (Sigma-SL2) to avoid attachments of cells onto the glass surface. The spiral impeller was carefully fitted with the protruding centre from the glass wall from one end and other end fitted with the stainless-steel side plate. The pictorial representation of all the ports is shown in Figure 3-4.

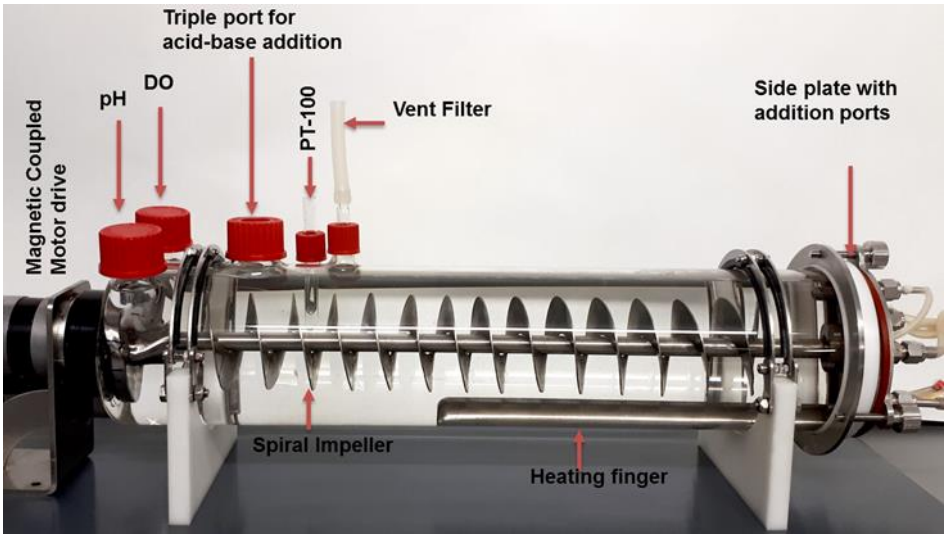

Figure 3-4 HTB assembly scheme with labels of the parts

The pH sensor was calibrated while the DO probe was checked for DO membrane integrity by visual inspection before insertion into their respective ports. Few drops of O_2 electrolyte were added into the DO probe for enhanced response time. Master Flex silicone tubing L/S 16 was used with a female MPC connector for the addition/harvesting port on the side plate. Sampling was done carefully with the help of 50 mL syringe from the sample port. Two vent filters (Millipore-0.2 μ) were connected with 'Y' connector for inlet and outlet of gases. The bioreactor probes and ports were wrapped with aluminium foil before autoclaving the bioreactor at 121 ^{o}C for 30 minutes. After autoclaving and cooling to below 70 ^{o}C, the bioreactor was taken out from the autoclave and kept inside the biosafety cabinet throughout the batch length as a presumptive measure to avoid contamination. Air was supplied to the bioreactor at a flowrate of 0.2 LPM to create a positive pressure in the vessel. The assembly scheme has given in Figure 3-4 and the detail of the positions of the addition ports are shown in Figure 3-5.

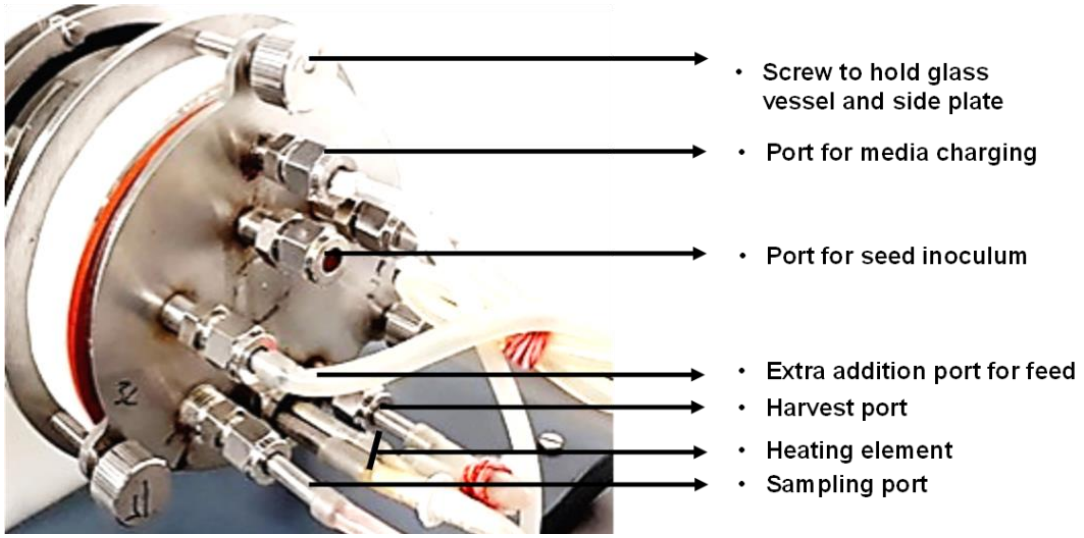

Figure 3-5 Illustration of the positions of the addition ports on the side plate

3.6.2 Inoculum seed preparation

A fresh vial from -80 ^{o}C deep freezer was taken out. Cells were revived as per the method mentioned in section 3.3.1.4. The shake flasks were kept inside the CO_2 incubator at 37 ^{o}C on the orbital shaker at 100 rpm as per scheme shown in Figure 3-6 which took approximately 11-12 days The total of 900 x 10^6 cells were required to inoculate the single batch of 3 L with the initial cell density of 0.3 x 10^6 cells mL^{-1}.

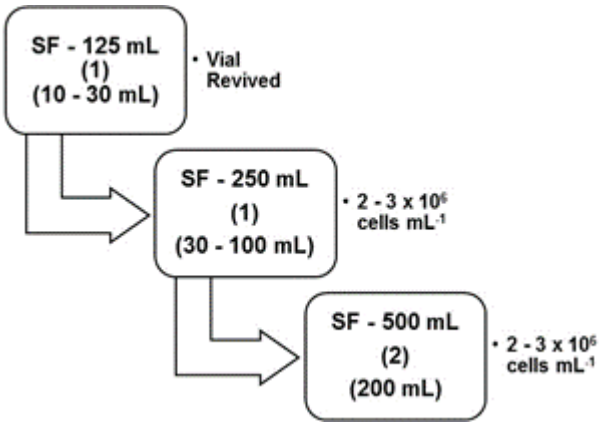

Figure 3-6 Schematic process for the development of seed inoculum for the batches from shake flasks

3.6.3 Batches with CHO cells with or without expressing somatic Angiotensin-converting enzymes (sACE)

The procedure adopted to run the batches was same in all the three batches. When the temperature of the autoclaved vessel came down to less than 50 ^{o}C, the connection of the vessel to the water bath was done to maintain the temperature at 37 ^{o}C. The initial volume of 2.5 L of complete media (medium with 4 mM stable glutamine and 0.1 % Poloxamer 188) was charged aseptically inside the bioreactor and the bioreactor was kept at 37 ^{o}C overnight for sterility check.

After the sterility test (i.e. media remains clear and no contaminants are observed visually), the DO probe was calibrated between 0 % to 100 % saturation of the air. Thereafter, prepared seed inoculum was charged inside the bioreactor from the seed addition port as described in Figure 3-5. The process conditions were maintained stringently as explained in section 3.3.2. Samples were taken after every 24 h for cell culture health and spent media profiling.

3.7 Analytical Procedures

3.7.1 Determination of Cell count and viability

The procedure of the cell counting and percentage viability was determined as per protocol given in (Freshney, 2005). This method was applicable to both adherent and suspension culture for CHO and Vero cells. Adherent cells were brought into suspension after exposing the monolayer to cell detachment reagent (Accutase®) as discussed in section 3.3.1.3.

Suspended cell culture samples were appropriately diluted in 1.5 mL microcentrifuge tubes with 0.4 % Trypan Blue to achieve 80 ± 20 cells in each counting chamber. The dilution range was kept between 1:2 to 1:30. The method was carried out for all TC, shake flask and bioreactor samples.

Cell suspension was maintained in trypan blue for at least one minute to allow non-viable cells to stain properly for clear differentiation. Cells were not left for more than 4 minutes in the stain to avoid non-specific staining of viable cells.

A freshly prepared sample was gently swirled and tapped with the index finger before loading on to the Haemocytometer. A thoroughly mixed sample was critical for accurate cell counting.

The suspension (~10 µL) was introduced into one of the V-shaped wells of the Bright-Line haemocytometer (Sigma) with the help of a 2 - 20 µL micropipette. Precautions were taken while loading the culture suspension onto the haemocytometer so that enough culture suspension was introduced just to cover the mirrored surface and the counting chamber should not be over-filled.

The charged counting chamber was then placed on the inverted microscope stage (Zeiss - Primo Vert) and the counting grid was brought into focus at low power. Focus was increased to 20 X and 40 X for counting. The cells were counted in four large corner square, separating the viable from the non-viable cells. Each corner square is divided into a 4 x 4 grid with an area of 1 mm^2.

Therefore, volume of single large corner square = 1 mm^2 x 0.1 mm = 0.1 cm x 0.1 cm x 0.01 cm = 10^{-4} cm^3, which is equal to 10^{-4} mL. The cell counting was done, and the cell concentration and viability were measured as follows:

The average number of cells in four large square x dilution factor x 10^4

10^4 = conversion factor to convert 10^4 mL to 1.0 mL

Calculation of Cell Viability:

% Viability= Number of viable cells/Total number of cells (viable +dead) x100

3.7.2 Glucose and lactate through HPLC

Glucose and lactate concentrations were analysed by HPLC (Thermo-Fisher) using an Aminex column (HPX – 87H (300 mm x 7.8 mm) from Bio-Rad, Ion exchange column. The instrument was equipped with UV and Refractive index (RI) detector. Separations were done at 40 ^oC. The mobile phase used in the analysis was 5 mM sulphuric acid which was prepared in deionised (D.I.) water, thoroughly filtered through 0.45 µM membrane filter and de-gassed with an ultrasonic water bath (PowerSonic405) for 30 minutes at 45 ^oC. A single vial was used to detect glucose and lactate concentration and the injection volume used for each analysis was 10 µL and each sample was analysed in triplicate. Standard solutions for glucose and lactate were also prepared in D.I. water and later serially diluted with the mobile phase and filtered through a 0.22 µM syringe filter. The concentration used for glucose standard curve was 2, 4, 6, 8 and 10 g L^{-1} whereas, for lactate, Sodium DL Lactate (50 %) (Sigma-71723-1L) was 0.2, 0.4, 0.6, 0.8 and 1.0 g L^{-1}. The mobile phase was kept as blank which was intermittently run throughout the analysis. The run-time for a single analysis was kept at 20 minutes with the flow rate of 0.5 mL $minute^{-1}$.

3.7.3 Osmolality

The 10 mL of culture broth from the bioreactor batch was centrifuged at 4000 rpm for 5 minutes after determining cell count and viability. 1 mL supernatant was taken in a 1.5 mL micro centrifuge tube to determine the osmolality by using freezing point Osmometer SLAMED 800 CL. The D.I. water was taken as a negative control and complete media was taken as a positive control. D.I was used to set the instrument at zero and fresh media was used as reference control for the initial osmolality of the medium. The normal cell culture medium osmolality ranges from 260 - 320 mOsmol kg^{-1}, which mimics the osmolality of serum at 290 mOsmol kg^{-1} (Zhu et al., 2008).

3.7.4 Ammonia

Ammonia was measured in the spent media by a colourimetric method (Cramp et al., 1997). A standard curve was made by using ammonium sulphate with concentrations of 0.2, 0.4, 0.6, 0.8, and 1.0 mg L^{-1}. Analytical grade chemicals were used to carry out the assay. Reagents A (0.59 M Phenol and 1.0 mM Sodium Nitroprusside) and reagent B (110 mM Sodium Hypochlorite and 2.0 M Sodium Hydroxide) were prepared. Bioreactor samples were appropriately diluted with D.I. water. 100 µL sample was added into the microcentrifuge tube. Thereafter, 350 µL of reagent B was added into the micro-centrifuge tube rapidly followed by 350 µL of reagent A. The tube was vortexed briefly and incubated at 37 ^{o}C for 30 minutes. After incubation, vortex the sample again and transfer 200 µL of reaction mix for each sample to a flat bottom 96 well plate. The absorbance of the reaction mix was observed at 600 nm by using a microtiter plate reader (BMG Labtech-FLUOstar Omega).

3.7.5 Characterisation of ACE protein

A fluorimetric assay was carried out to determine the enzymatic activity of the somatic ACE protein. In this assay, Z-Phenylalanine-L-histidyl-L-leucine (ZFHL) (BACHEM) was used as a substrate, which was catalysed by the ACE. ACE cleaves ZFHL to form the L-histidyl-L-leucine (HL) peptide which was derivatised using o-phthaldialdehyde (Sigma) to form a fluorescent adduct of the HL. This adduct was then quantified fluorometrically using Varian Cary Eclipse Fluorescence Spectrophotometer. An HL (Sigma) standard curve was generated to convert relative fluorescence into milli units (mU) ACE activity where 1mU of ACE is equal to 1 nmol of HL produced per min per mL (1mU ACE = 1nmol min^{-1} $mL^{-1)}$. This method has been published in detail by Schwager et al., (2006).

Western blot was used to identify the ACE protein specifically from the pool of other proteins from the bioreactor samples. The protein samples were first separated by sodium dodecyl sulphate polyacrylamide gel electrophoresis (SDS–PAGE), which separates the proteins based on their sizes (molecular masses). The following workflow was observed for the western blot as illustrated in Figure 3-7.

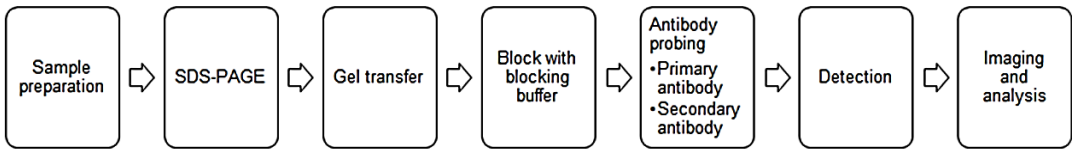

Figure 3-7 Steps involved in the western blot workflow

12 % separating gel and 6.5 % stacking gel was used. Separation was carried out at a constant voltage of 200 V for approximately 90 min. After the completion of the electrophoresis, the gel was stained in a Coomassie Brilliant Blue R-250 solution for 30 min. Thereafter, the gel was de-stained in a 7 % acetic acid and 25 % ethanol solution overnight. The details of reagents and buffers used in casting the gel is given in Table 3-4

Table 3-4 Amounts of chemicals needed for 12 % separating and 6.7 % stacking gel

Chemical	**12 % Separating gel**	**6.7% Stacking gel**
40 % acrylamide, 0.2 % bis- acrylamide	7.5 mL	1 mL
Buffer (Tris-HCl)	8.4 mL (pH 8.8)	2 mL (pH 6.8)
Deionised water	8.8 mL	2.8 mL
10 % SDS	250 µL	150 µL
10 % *Ammonium persulphate (*AMPS)	250 µL	150 µL
TEMED	25 µL	10 µL
TOTAL	25 mL	6 mL

The following reagents and buffers were prepared (i) sample buffer (0.375 M Tris-HCl, (pH 6.8), 10 % SDS, 2 mL glycerol, 0.5 mL 2-mercaptoethanol for 10 mL volume with deionised water), (ii) tank buffer (glycine (30 g), Tris (6 g), SDS (2 g) and for 2 L volume with deionised water), (iii) gel staining buffer (dissolve 0.25 % Coomassie Brilliant Blue R 250 in 500 mL technical methanol, 400 mL deionised H_2O and 100 mL acetic acid) and (iv) gel de-staining buffer (7 % acetic acid, 25 % technical ethanol for 1 L). The detailed procedure is given in CeBER protocol (unpublished).

The SDS-PAGE with separated protein fractions were transferred onto a Nitrocellulose membrane electrophoretically. The sACE was then identified by using a specific primary antibody (polyclonal anti-ACE raised in Rabbit) which corresponds to that of purified somatic ACE. A secondary anti-rabbit antibody linked to reporter enzyme (horseradish peroxidase) was added which cleaved a chemiluminescent agent (Bio-Rad-Immuno-Star Western C kit) and the signal was recorded/visualised using the Syngene G-box system. The protocol for running SDS-PAGE and Western blot (transfer, development of blot, blocking and visualization) was carried out as per established CeBER laboratory manual. The following buffer composition was used in the Western blot.

Blotting buffer: 3.025 g Tris, 14.4 g glycine and 200 mL methanol (pH 8.2- 8.4)

Blocking buffer: 5 % skim milk, 0.1 % Tween 20, 0.2 M NaCl and 0.05 M Tris-HCl (pH 7.4)

Wash buffer (TBST): 0.1 % Tween-20, 0.2 M NaCl and 0.05 M Tris-HCl (pH 7.4)

Primary antibody (1:500- 1:1000) and secondary antibody (1:500-1:2000) in blocking buffer

Alkaline phosphatase detection buffer: 50 mM Tris-HCl, 5 mM $MgCl_2$, pH 9.5

Alkaline phosphatase substrate solution: .015 % (w/v) BCIP, 0.03 % (w/v) NBT in detection buffer.

3.8 Puromycin Aminonucleoside (PAN) cultivation experiments

Experiments were conducted with PAN to establish the effects of this anti-cancer drug on the viability and vitality of the cell culture after exposure to the drug.

3.8.1 Determination of inhibitory dose (IC_{50}) for Puromycin Aminonucleoside (PAN)

The time-dependent inhibitory dose of PAN was evaluated through the CellTiter-Blue® Cell Viability Assay. This viability assay uses the resazurin dye (a tetrazolium salt) as an indicator of measuring viability (metabolic activity). The viable cells reduce the resazurin into highly fluorescent resorufin compound. Unhealthy cells/ Dead cells after exposure to the drug rapidly lose their metabolic activity and hence generate weak or no fluorescent signal (Riss et al., 2016). The stock solution of PAN was prepared in DMSO with a final concentration of 5.0 mg mL^{-1}

Three 96-well plates of Vero cells were seeded with 75,000 cells 200 μL^{-1} $well^{-1}$. These plates were rested overnight at 37°C in the CO_2 incubator. Cells were then treated with PAN (reconstituted in DMSO, degassed with N_2 gas and filtered through 0.22 µM syringe filter). A two-fold serial dilution was prepared from 200 to 1.56 µg mL^{-1}. Blank controls were used consisting of media (no-cell), untreated cells and vehicle control (2.0 % DMSO). The vehicle control was to determine whether DMSO alone contributed to the cytotoxicity of the cells. After 24 h of exposure, one 96-well plate was taken out and processed. 20 µL of cell titre blue (Promega, Cat # G8081) was added in the wells and incubated for 4 h at 37°C in the CO_2 incubator. Following incubation, the plate was read at 570 nm using a spectrophotometer (Molecular Device). Similarly, results were obtained at 48 h and 72 h post-exposure of PAN to determine the IC_{50} dose. The data obtained from the plate reader was further analysed by software Graph-Pad prism 7.02 using inhibitor Vs normalized response- variable slope function.

3.8.2 Suspension of Vero at different concentrations of Puromycin Aminonucleoside in shake flasks

Two sets of experiments were done using different concentration ranges of PAN on Vero cells grown in DMEM with 1 % FBS in T-25 cm^2 flasks. In the first experiment, the concentration ranges of PAN considered were 100, 50, 10, 5, 2.5, 1.25, 0.625 and 0.3125 µg mL^{-1}. In the second experiment, higher concentration ranges of PAN were used: 100, 90, 80, 70, 60 and 50 µg mL^{-1}.

Experiments were also carried out with Vero cells grown in serum-free media (SFM4 MegaVir with 4 mM stable glutamine and 0.1 % Poloxamer 188) exposed to a higher concentration range of PAN: 100, 200 and 250 µg mL^{-1}. In all the experiments, plain complete media was kept as negative control and normal cells (without PAN exposure) considered as a positive control.

The Vero cells which were detached from the surface of the TC-flasks grown in serum-free medium (SFM4 MegaVir) or DMEM + 1 % FBS medium were collected in separate shake flasks and kept inside the CO_2 incubator at 37 °C on an orbital shaker at 100 rpm. The detached cells grown from the serum-free medium were kept in the same medium whereas, detached cells detached from DMEM + 1 % FBS medium were mixed with serum-free medium in 1:1 ratio.

3.8.3 Re-culturing of Vero cells in complete growth medium

The cells harvested from the previous experiments mentioned in the 3.8.2 were re-seeded in serum-containing medium (DMEM + 10 % FBS) for their growth without PAN. The aim of the experiment was to check whether the effect of PAN on the cells was reversible or irreversible. The viability of the harvested cells was checked using the trypan blue exclusion method and isothermal microcalorimetry (IMC).

3.9 Isothermal microcalorimetry (IMC) and mammalian cells

3.9.1 Setup of the TAM III IMC instrument

The Thermal Activity Monitor III (TAM III) isothermal microcalorimeter was used to measure the metabolic activity of the biological samples, in this case, CHO and Vero cells. The TAM III instrument was equipped with a multi-channel calorimeter (6-channel) module. The module shared a single thermostat which operated within the range of 15 - 150 ^{o}C, which was controlled and monitored to within 0.0001 ^{o}C. The instrument has an accuracy of < ± 0.1 °C and long-term stability of < ± 100 µK per 24-hour (TA Instruments, 2012). The detailed working of TAMIII instrument is outlined in Myers (2017).

Figure 3-8 shows the TAM III instrument and (A) and (B) depict the side and top view of the 6-channel module arranged in a circular pattern. Each channel accommodated a 4 mL glass ampoule which was sealed/crimped with aluminium cap containing rubber and Teflon sealing disks. All the experiments in the multi-channel TAM III instrument were performed at 37 °C and the volume in each ampoule was fixed at 2 mL to leave 50 % headspace for oxygenation of the culture. The CHO and Vero cells (treated and non-treated/adherent and non-adherent cells) were subjected to IMC studies.

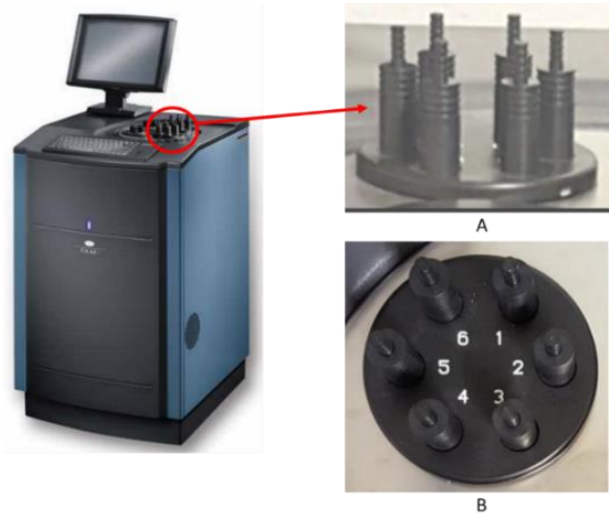

Figure 3-8 TAM III Isothermal Microcalorimeter (A) Side view of multichannel showed with red arrow (B) Top view of multichannel

Before starting of the IMC studies, calibration of the instrument is the first priority to ensure the reliable, robust and repeatable results. The main purpose behind the calibration of TAM III was to ensure the heat flow data represent the actual heat flow by the sample and account for any heat losses.

The TAM III instrument was calibrated frequently by running a general performance test (GPT) through TAM III assistant software each time the instrument was re-started or when the temperature of the thermostat and the experimental conditions were changed. The general performance test (GPT) was executed by TAM III assistant software which made use of the inbuilt calibration heater.

After calibration, the results obtained were compared to factory calibration and deviation was calculated as unit-less constant called gain constant. The gain constant was used to re-calculate the time constants based on heat pulses to establish a new baseline for 24 h. The values of the gain constant were between 0.95 -1.06 (TA Instruments, n.d.)

3.9.2 Experimental plan

An initial experiment with adherent CHO cells (Item no. CCHO-C; CHO-K1) grown in DMEM with 1 % FBS was carried out to obtain optimum cell densities for significant heat generation response (thermograms). During the execution of the experiments, all the samples were prepared carefully in the biosafety cabinet (BSC II). After loading the cells into the ampoules, these ampoules were briefly flamed before putting the aseptic rubber septum. Thereafter metal cap was crimped without tilting the ampoules.

Another important issue observed was the attachment of the cells on the inner wall of the glass ampoules. To mitigate the cells attachment of the suspension-adapted cells onto the inner wall of the glass ampoules, siliconization was done with Sigmacote. Before using the siliconized ampoules, they were thoroughly cleaned and sterilised at 121 ^{o}C for 20 min.

In two separate experiments, initially, 10k cells (duplicate), 50k cells (duplicate), 100k cells (single) and medium blank (single) were measured. In the second set of experiment, 100k cells (single), 200k cells (duplicate), 500k cells (single) and two blanks water and media were measured. Thereafter, suspended CHO-S were also studied to optimise cell densities. The cell numbers used in this experiment were 100k cells (duplicate), 300k cells (duplicate), 500k cells (single) and medium blank (single). Details of the experimental plan are broken down in Table 3-5.

Table 3-5 Experimental plan for CHO cells using Isothermal Microcalorimetry (IMC)

Cell Model	Volume (mL)	Cell numbers in millions					
		Channels					
		1	2	3	4	5	6
CHO cells + 1 % FBS	2	Media blank1	0.01	0.01	0.05	0.05	0.1
CHO cells + 1 % FBS	2	Water	Media blank	0.1	0.2	0.2	0.5
CHO-S	2	Media blank2	0.1	0.1	0.3	0.3	0.5

1 DMEM +1 % FBS
2 SFM 4 CHO + 4 mM Glutamine + 0.1 % Poloxamer 188

The experimental plan was also carried out for Vero cells. The only difference was in the case of Vero cells, Vero with 1 % FBS and Vero grown in serum-free media (SFM) both were exposed to PAN (Anti-cancer) drug. The experimental plan matrix for Vero cells is given below in Table 3-6. The data obtained

from this experimental plan was then used for determining the growth kinetics of the cells under investigation to determine their bioactivity.

Table 3-6 Experimental plan Isothermal Microcalorimetry for Vero cells

Cell Model	Volume (mL)	Cell numbers in millions					
		Channels					
		1	2	3	4	5	6
Vero cells + 1 % FBS	2	Media blank	0.1	0.1	0.3	0.3	0.5
Vero cells - SFM	2	Media blank	0.1	0.3	0.3	0.5	0.5
Vero-treated and resuspended in Serum-free media	2	Media blank	SFM blank[1]	0.5[2]	0.5	0.25[3]	0.25
Vero cells treated with different concentrations of PAN and re-grown in Serum-containing media (no PAN)	2	Media blank	Untreated cells (0.2)	100 µg (0.2)	200 µg (0.2)	200 µg (0.2)	250 µg (0.2)

SFM 4-MegaVir + 4 mM Glutamine + Poloxamer 188
[2]Positive control (channel 3 and 4)
[3] Vero treated cells (channel 5 and 6)

3.9.3 Determination of specific growth rate, doubling time and power generated by per cell

The microcalorimetric data obtained through these experiments were voluminous so data was sliced to get 1h data-point for easy data-handling. For the consistency of the data and to avoid any erroneous reading, data were normalized by subtracting media blank value from the test value using Origin Pro 8.

Click the tab (Analysis - data manipulation - subtract reference data - open dialogue window- Select Input 1 (test column) – Select reference data (media blank) – output.

The normalized data then analysed for the specific growth, doubling time and calculating the averaged power produced by a single cell in pW cell^{-1}.

As the rate of growth of mammalian cells depend on the initial cell density so:

$$\frac{dx}{dt} = \mu X \qquad \text{Equation 3-8}$$

Where $\frac{dx}{dt}$ is rate of cell growth, X is the cell density (cell mL^{-1}) and t is time in (h), and µ is the specific growth rate (h^{-1}). On integration of Equation 3-8 from t=0 and t=t

$$X_t = X_0\, e^{\mu t} \qquad \text{Equation 3-9}$$

Where, X_0 is starting cell number, X_t is the cell number after time t. taking log natural on both sides of the Equation 3-9

$$\mu = (ln\,(\frac{X_t}{X_o})/\Delta t) \qquad \text{Equation 3-10}$$

µ indicate the rate at which the cell number increased in a given time (h^{-1}).

The doubling time was calculated by using growth rate in Equation 3-11

$$t_d = \frac{ln\,2}{\mu} \qquad \text{Equation 3-11}$$

Where t_d is doubling time (h)

The power produced by single cell was calculated by diving the averaged heat flow data produced by the cells divide by the total number of cells harvested by the end of the experiment.

3.10 Overall chapter summary

This chapter was aimed to provide information on the methodologies and the research approach taken while carrying out this PhD research. In the beginning, the context was given to elaborate on the need of developing the new bioreactor design which work on the principle of surface aeration with induced agitation with the novel design of a spiral impeller for enhanced homogeneity, mass and heat transfer capacity of the HTB.

The design of spiral impeller was inspired from observing the nature's design which is spiral from microscopic objects such as mitochondrial cristae/ Endoplasmic reticulum to galactic object like galaxies. The idea of using the spiral impeller (screw) in the horizontal vessel was also complemented by its use in the stirred tank (Holland and Bragg, 1995; Tsui and Hu, 2008) and in moving non-Newtonian fluids.

This chapter further sheds light on the abiotic and biotic characterisation of HTB with spiral impeller primarily focused on explaining the research methodology and approach to determine the fluid flow pattern and mixing time, mass transfer efficiency with and without cells by dynamic method, power consumption profile and minimum agitation speed. The evaluation of the shear conditions was done by measuring the cell death constant (k_d) which indirectly indicate the shear conditions inside the bioreactor.

The approach to evaluating the suitability of the HTB was tested by running three batches with CHO cells. CHO and Vero cells were used in this research where the methodology of their cryopreservation, revival, subculturing and adaptation into serum-free media were discussed in detail. The chapter also described the methods of bioreactor design and assembly, the medium used, seed inoculum preparation and overall process conditions for the batches.

Additionally, spent media profile was also done by explaining the HPLC methods for glucose and lactate estimation, $NH4^+$ from calorimetric methods, osmolality was measured by using freezing point Osmometer SLAMED 800 CL, and quantity and quality of proteins by fluorimetric assay.

Vero cells with serum and without serum, were exposed to various concentrations of PAN to establish its effect on the suppression of integrin. The cell detached from the substratum collected and re-seeded into the fresh T-flasks to find out its attachment and morphological behaviour in serum-containing medium. Furthermore, the activities of treated and non-treated cells were also studied through isothermal microcalorimetry (IMC) to elucidate its biological activities.

4 Designing, fabrication and abiotic characterisation of Horizontal Tubular Bioreactor (Results and Discussion - Part I)

The objective of this chapter is to give a detailed account of the design, fabrication and abiotic characterisation of the horizontal tubular bioreactor (HTB). The engineering characterisation of the HTB was carried out to evaluate the mixing time, fluid flow pattern by tracer and phenolphthalein method, oxygen mass transfer ($k_L a$) through the dynamic gassing-in method, power consumption through heat calorimetry (temperature method) and, minimum stirring speed (N_{js}) through alginate beads and, modelling through modifying Zwietering equation at different agitation speeds. Thereafter, obtained results were analysed and compared to other bioreactor systems such as STR, Wave bioreactor and CelCradle.

4.1 Criteria for bioreactor design

The primary purpose of the bioreactor is to establish a biosphere ("Ideal" environment) that would be suitable to carry-out the bioreactions based on the organism used such as bacteria, yeast, algae, moulds and mammalian cells. They required different environment for their growth and to carry-out bioreactions. To achieve the "Ideal" environment, the following major tasks need to be considered. 1. Physical entity - Bioreactor design which ensures the transportation of solid, liquid and gases over the period of time 2. Suitability of the bioreactor design with the biological system used, in this case, mammalian cells 3. Operability of the bioreactor at a large scale (Mandenius, 2016). Various bioreactor types as discussed in chapter 2 have been employed at lab scale and an industrial scale for the production of biologicals. The growing knowledge of the cellular behaviour of different cell lines and their interaction with the macroenvironment has led to the improvement of the bioreactor design to satisfy the industry requirements as shown in the List 4-1.

List 4-1 Basic requirements for bioreactor design- adapted from Margaritis and Wallace (1984)

1. Wider suitability for different cell systems
2. Mass and heat transfer characteristics
3. Hydrodynamics characteristics
4 Adaptability to perform batch, fed batch & perfusion culture
5. Aseptic design (sterilizable/single use)
6. Easily controllable process parameters (macro and microenvironment)
7. Suitability of the design for easy down streaming/separation of the product
8. Scalable design
9. Suitability for the integration with process analytical tools (PAT)
10. Lower capital and running cost of the bioreactor
11. Material acceptance from industry and regulators

List 4-1 shows the basic characteristics/requirements of the bioreactor design, which are critical for designing a successful bioreactor. The above design criteria take a comprehensive approach to integrate

old knowledge of bioreactor design to the new knowledge which works in unison with different process analytical tools (PAT). PAT enables online real-time monitoring of the processes and associated process improvements by controlling parameters stringently and reducing the risk of batch failure (Kontoravdi et al., 2013; Mandenius, 2016; Marasco et al., 2013; Read et al., 2010).

In the current research, a horizontal tubular bioreactor (HTB) was designed to achieve appropriate cell density with extended viability of the culture in an optimised process which stringently controls the process parameters. The bioreactor suitability for culturing mammalian cells is majorly influenced by fluid flow regimen, transport phenomena (minimum agitation speed, mass and heat transfer efficiency), power consumption and hydrodynamic shear stress.

4.2 Working principle of the spiral impeller in a horizontal tubular design

The helical mixer has been reported in the literature which works in a vertical vessel. This mixer aid in pumping fluid from the bottom of the vessel to the top surface of the vessel which creates movement of fluid elements (freshly-oxygenated) from the top surface layer to the bottom (Holland and Bragg, 1995) as shown in Figure 4-1 (a). Taking cues from this study, it was expected that the horizontal vessel would also show a similar fluid flow pattern with a spiral impeller, hence, a proposed bidirectional fluid flow pattern was expected in HTB as shown in Figure 4-1 (b).

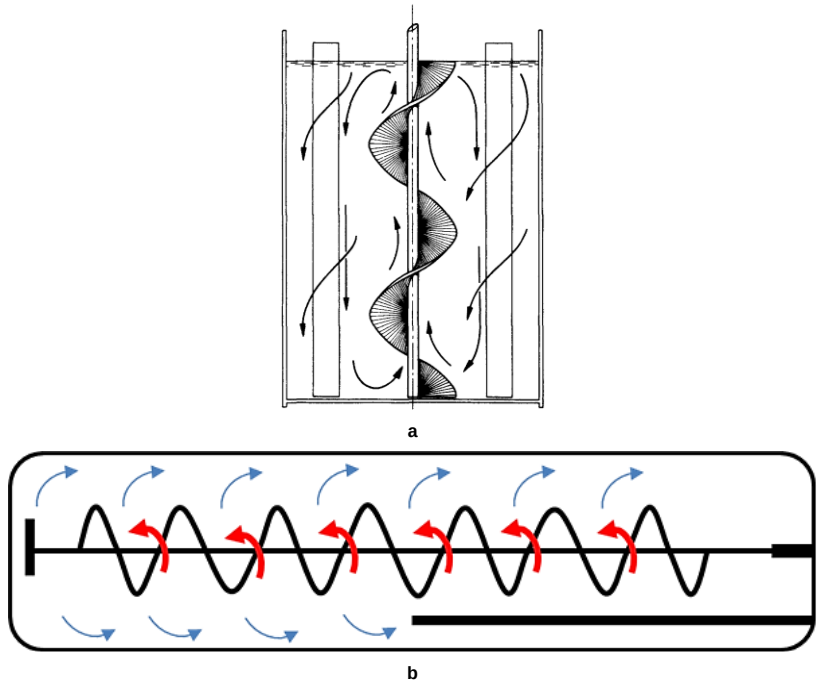

Figure 4-1 Illustration of fluid flow pattern in vertical and horizontal geometries with spiral impeller. (a) showed the fluid flow in a vertical vessel with baffles where helical screw, pump the fluid from bottom to the top surface and thereafter from top to bottom as shown with the black arrows (b) depicted the proposed fluid flow pattern in HTB where red curved arrow showed forward motion of fluid and blue arrows represented the backward flow which created a counter-current fluid flow that creates turbulences required for mixing, mass and heat transfer

4.2.1 Designing and fabrication of HTB prototype

Sections 3.1, 3.2, and 4.1 explained the context behind the bioreactor design and how the idea was conceived to build the horizontal tubular bioreactor with spiral impeller, keeping in mind the pre-set criteria mentioned in List 4-1. The current section elaborates on the design criteria adopted and the results obtained from it, which further aid in the fabrication of the bioreactor.

The idea of choosing a horizontal vessel for the cultivation of mammalian cells based on achieving high mass and heat transfer by providing a high surface area and high surface renewal rate. For that, a spiral impeller (a helical screw) was designed at CeBER, UCT. There are certain elements in designing a spiral impeller which is crucial in affecting the fluid flow mainly pitch, pitch angle and diameter of the impeller.

Tsui and Hu, (2008), used a spiral impeller with a draft tube in a stirred tank bioreactor which inspired the design of the spiral impeller in a horizontal tubular vessel. The various dimensions of the spiral impeller for the HTB were modified from the aspect ratio used by Tsui and Hu in 2008. Initially, the aspect ratio of the prototype was calculated using the basic aspect ratio Length / Diameter (L/D ratio) of the vessel. Various lengths of the vessel were considered from 350 mm to 600 mm with the increments of 50 mm. Different combinations of aspect ratios (L/D) from 1:1 to 5:1 were calculated on the spreadsheet to design the impeller diameter, shaft diameter, length of the impeller, pitch, height of the impeller blade, clearance, and total volume it could accommodate (DOI: 10.25375/uct.13570970).

The criteria for the selection of the design (aspect ratio) were kept simple. Firstly, the vessel should accommodate the maximum volume of approximately 5.0 L and the minimum volume must have significant impeller immersion ratio which could generate fluid flow necessary for mass and heat transfer, for that, each vessel lengths (350, 400, 450, 500, 550, and 600 mm) were tried for various L/D ratios such as 1.0, 1.2, 1.5, 1.8, 2.0, 2.5, 3.0, 3.5, 4.0, 4.3, 4.6, and 5.0 to calculate the volume it can accommodate. Secondly, impeller diameter and pitch of the impeller at pitch angle 15, 30, 45 and 60 degrees were considered because of their direct impact on the clearance, mass and heat transfer efficiency of the bioreactor and then, liquid height was considered to select the suitable design of the HTB.

It was found upon calculations that in many aspect ratios, the volume of the vessel exceeds the set criteria. Only a few combinations as depicted in Table 4-1 fulfil the criteria for the maximum volume of approximately 5.0 L. To narrow down the approach of selecting the suitable aspect ratio, the vessel design with volume lower than 5.0 L was considered. Only two options were left where the length of the vessels was 450 mm and 500 mm with L/D ratio of 4.0 and 4.6 respectively. Both the vessels can accommodate 4.5 L and 4.6 L of volume respectively. Out of these combinations, it was decided to consider liquid height when the vessel was at 70 % of fill volume. It was calculated that liquid height in the vessel (450 mm/ (L/D) 4.0) was at 74.23 mm, whereas (500 mm/ (L/D) 4.6) was 71.72 mm. These liquid heights are without the internal parts of the bioreactor which would further displace the liquid and raise the liquid level. To have more headspace for surface oxygenation with appropriate impeller immersion ratio, we have finally chosen the vessel with a length of 500 mmm with L/D ratio of 4.6 with a pitch angle of 15 degree to have a greater number of turns which was expected to facilitate the fluid movement with low shear.

Table 4-1 Aspect ratios fulfilling the selection criteria for the design of the vessel and spiral impeller

	Length (mm)															
	350				450				500				550			
L/D	Pitch angle (θ)	Pitch (m)	No. of spiral turns	Volume (L)	Pitch angle (θ)	Pitch (m)	No. of spiral turns	Volume (L)	Pitch angle (θ)	Pitch (m)	No. of spiral turns	Volume (L)	Pitch angle (θ)	Pitch (m)	No. of spiral turns	Volume (L)
2.5	15	0.032	8.8	5.4	15				15				15			
	30	0.069	4.1		30				30				30			
	45	0.120	2.4		45				45				45			
	60	0.208	1.4		60				60				60			
4.0	15				15	0.026	14.1	4.5	15				15			
	30				30	0.056	6.6		30				30			
	45				45	0.096	3.8		45				45			
	60				60	0.167	2.2		60				60			
4.3	15				15				15	0.027	15.2	5.3	15			
	30				30				30	0.057	7.0		30			
	45				45				45	0.100	4.1		45			
	60				60				60	0.172	2.3		60			
4.6	15				15				15	0.025	16.2	4.6	15			
	30				30				30	0.054	7.5		30			
	45				45				45	0.093	4.3		45			
	60				60				60	0.161	2.5		60			
5.0	15				15				15				15	0.025	17.6	5.2
	30				30				30				30	0.054	8.2	
	45				45				45				45	0.094	4.7	
	60				60				60				60	0.163	2.7	

HTB consisted of a glass column of 500 mm in length (L). The diameter (D) and height of the horizontal vessel (H) were D=H=L/4.6. The diameter of the impeller (d) was d=D/2.2 and the shaft diameter ds=0.2d. The clearance (C) of the impeller was C=0.05 d and the length of the impeller (h) was L/1.235. The pitch (S) of the spiral impeller was determined by the helix (Blade angle) which was 15 degrees, and the pitch of the impeller was calculated from Equation 4-1

$$Tan\ \theta = \frac{S}{\pi d_m} \qquad \text{Equation 4-1}$$

Where S is the pitch of the impeller and d_m is the mean diameter. The width of the impeller blade (W) was fixed at $(d - ds)/2$ and the thickness of the blade was 2 mm. Figure 4-2 visualises the HTB based on the design with labels.

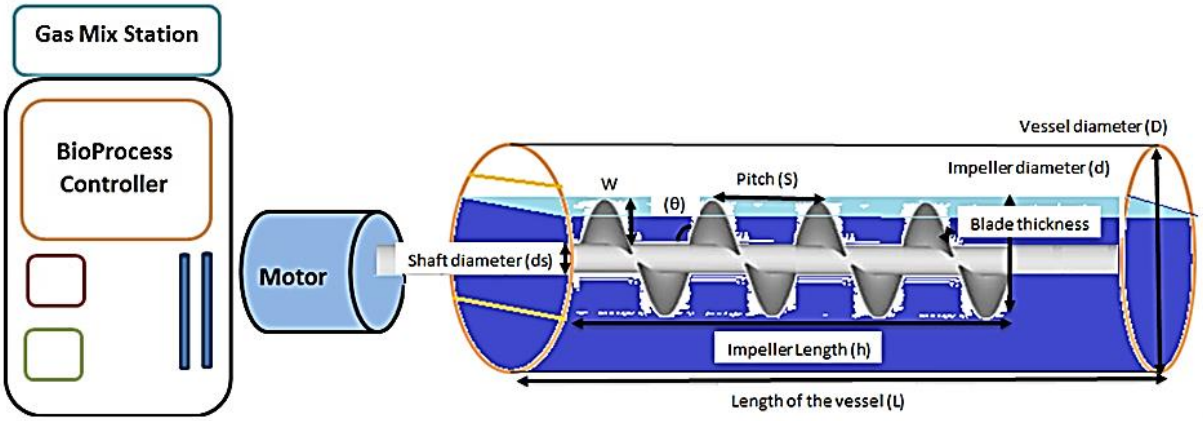

Figure 4-2 Pictorial illustration of presumed horizontal tubular bioreactor (HTB) with the design symbols.

The fabrication of the HTB was outsourced from GlassChem, Stellenbosch, where the glass vessel was fabricated as per User Required Specifications (URS) mentioned in the dataset (DOI: 10.25375/uct.13570970). A locally made bioprocess controller was also fabricated for controlling the process parameters such as pH, temperature, impeller stirring speed and gas flow. The biocontroller was equipped with mass flow controller (MFC) which control the opening and closing of solenoid valves for the air (e.g. to maintain 40 % air saturation) and CO_2 gas (for pH maintenance). A data acquisition software (Terminal IP) was also designed to log the real-time monitoring of the process onto the computer system, which logged the data in comma-delimited (CSV) format. The peculiar feature of this prototype is that it has a magnetic-coupled motor drive on one side (glass side) and addition ports positioned on the other side plate (stainless steel). The bioreactor was equipped with commercially available probes e.g. pH probe (Hamilton) and dissolved oxygen probe (Mettler Toledo Ingold) and temperature sensor (PT-100). A circulatory water heater was connected to the bioreactor for the control of the process temperature. For the regulation of the flow of gases, the biocontroller was also attached with the appropriate rotameters.

Based on the calculations, the 25 mm pitch of the impeller gave 16.22 number of spiral turns (impeller axial length/pitch of the impeller). It was noted that the moulding of stainless steel around the shaft at the given angle was difficult to achieve and a slight modification to the pitch was made to ease production. Table 4-2 shows the adapted configuration for the HTB.

Table 4-2 Design configuration adapted for the fabrication of the horizontal tubular bioreactor (HTB)

Dimensions	Symbol	Measurements	Units
Vessel internal diameter	D	109	mm
Vessel length	L	500	mm
Impeller diameter	d	50	mm
Impeller shaft diameter	d_s	10	mm
Impeller pitch	S_I	29	mm
Impeller axial length	L_I	405	mm
Blade angle	θ	17	degree

The bioreactor has been designed carefully, keeping in mind the sterility of the batch. Therefore, all the materials used in the fabrication of the bioreactor are autoclavable and inert. The following salient features were considered in the design shown in the List 4-2:

List 4-2 Salient features of the horizontal tubular bioreactor (HTB)

1. For glass vessel, Borosilicate glass 3.3 with superior visibility was used
2. For metallic work- Stainless steel 316 L (inside the Vessel) and 304 L (outside the vessel) was used as per industry standards
3. To avoid leakage and to ensure sterility, 'O' rings and gaskets were made up of Silicone material (No leaching material)
4. A brushless DC motor was mounted on a sturdy platform to avoid/dampen the vibrations during operation because the glass vessel was also placed on the same platform. The motor drive was a variable speed control with digital display and has low power input and torque
5. Glass vessel was placed on the platform with proper holding clamps close to the motor drive to ensure the safety of the vessel and the user
6. Detachable side plate for easy cleaning and mounting the impeller for coupling

Apart from that, several ports were also designed. The sizes of these ports were carefully selected so that standard probe can be used in the bioreactor without compromising the sterility of the batch. Figure 4-3 elaborate the schematic diagram of the horizontal tubular bioreactor with the probable set-up for running a batch.

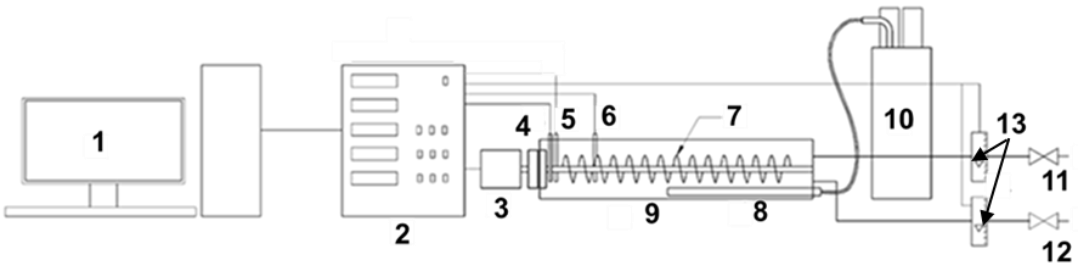

Figure 4-3 Schematic diagram of the horizontal tubular bioreactor showing different part denoted by numbers
1. PC with Terminal program for data logging 2. Bio-controller 3. Magnetically coupled motor drive 4. Dissolved oxygen probe 5. pH probe 6. Temperature probe 7. Spiral impeller 8. Heating finger 9. Horizontal tubular glass reactor vessel 10. Thermostat 11. Compressed air, 12. CO_2 supply, 13. Rotameters.

Figure 4-4 described the external features of the bioreactor which include (a) magnetic coupling, (b) glass vessel and (c) side plate for the addition ports.

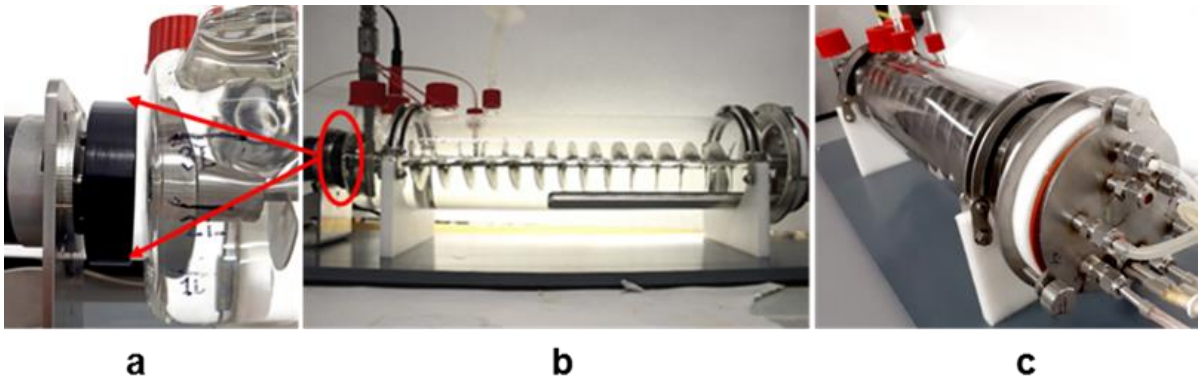

Figure 4-4 Illustration of horizontal reactor vessel with (a) Zoomed-in magnetically-coupled motor drive (b) Central glass reactor vessel with spiral impeller and heating finger and (c) side plate for addition ports

Additionally, Table 4-3 described the number of ports used, their sizes and location of the vessel regarding Figure 3-5.

Table 4-3 Detailed descriptions of the probes and addition ports used in the vessel along with their location on the vessel

Ports	Sizes	Position on the vessel
Dissolved Oxygen sensor	M18 x 1.5 (Universal size)	One corner of the side of the glass wall (near magnetic coupling)
pH Probe	M18X1.5 (Universal size)	Another corner of the side of the glass wall (near magnetic coupling)
Straight Heating Finger	M18X1.5 (Universal size)	At the bottom of the vessel
Triple addition port for base	M18X1.5 (Universal size)	Top of the glass vessel
Temperature sensor PT-100	10 mm OD	Detachable part for the sensor on the vessel (No contact with culture media)
Harvest port	10 mm OD	Bottom of the side plate
Medium addition	10 mm OD	Top of the side plate
Primary and Secondary feed addition	10 mm OD	Top of the side plate
Air Vent filter	10 mm OD	Top of the glass vessel
Seed Addition	10 mm OD	Top of the side plate
Sampling Port	6 mm OD	Middle of the side plate

4.3 Engineering characterisation of HTB

The abiotic characterisation of the horizontal tubular bioreactor was carried out in detail for the parameters described in section 3.4. Generally, all the engineering parameters under investigation are inter-dependent and influence the overall performance of the bioreactor as shown in Figure 4-5. The main components which create a difference are shown in blue boxes like bioreactor design (geometry) and impeller shape, and power input per unit volume. These two-components directly affect the performance of the bioreactor. For instance, bioreactor geometry and impeller shape directly influence fluid flow pattern which later affects the mixing profile in the bioreactor. The impeller speed directly influenced by power input which proportionately affects the mass transfer efficiency of the bioreactor and mixing time.

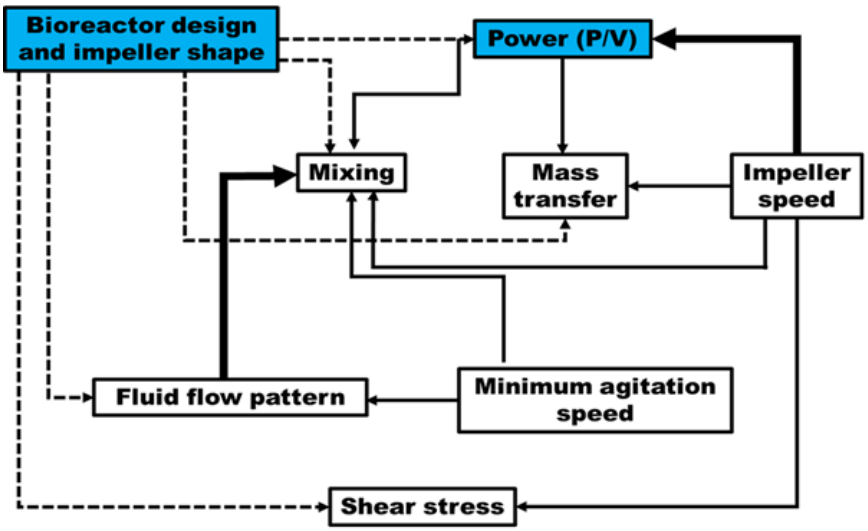

Figure 4-5 Represented the interdependence of engineering parameters. The bioreactor design and impeller shape and power are the two primary influencers (Blue boxes). The thick black solid arrows (↑) represent the direct effect of impeller speed on power consumption and fluid flow pattern has direct impact on mixing. Solid black arrows (↑) show interdependence among various parameters whereas dotted lines (⇡) represented indirect influence on the engineering parameters

4.3.1 Fluid flow pattern and homogeneity through Phenolphthalein method

To identify the pattern of flow of fluid in the horizontal tubular vessel with spiral impeller, images were captured at each impeller immersion of 4 %, 42 %, 79 % and fully immersed (121 %), which corresponds to 1 L, 2 L, 3 L and 4 L fill volume at each impeller speed of 100 rpm with an increment of 100 until 500 rpm. For visualization, three images of decolourization of phenolphthalein dye were shown in Figure 4-6 at each fill volume at an impeller speed of 300 rpm. The last image (right-hand side) shows a slight streak of pink colour which indicate the moment before complete decolourization.

4.3.1.1 Effect of impeller immersion on the fluid flow pattern

The different impeller immersions show different profiles of fluid flow at the same impeller speed which can be seen through the pictorial representation of Figure 4-6 at each impeller immersion (fill volume).

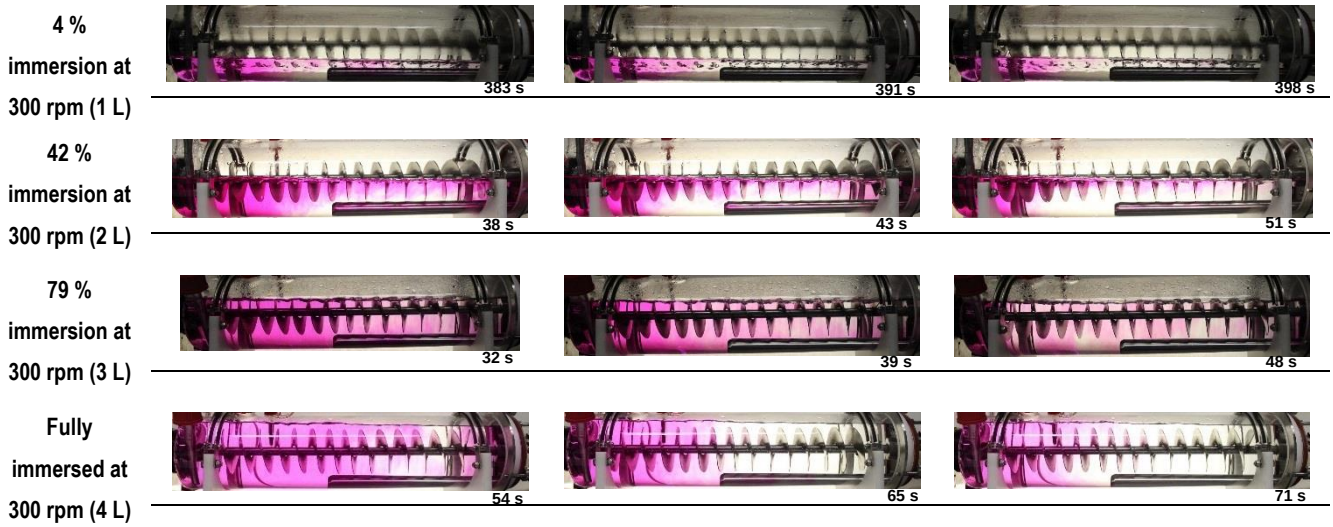

Figure 4-6 Schematic progression of homogeneity attained at different impeller immersion at 300 rpm

The mixing time for 95 % homogeneity at 4 % impeller immersion was the longest for all the volumes tested at all the impeller speeds. It is because of the low impeller immersion ratio which is not capable of generating axial flow motion of fluid or simply able to push the fluid along the length of the vessel. It was also observed that in the empty vessel, 1 L liquid height just touched the lower blades of the impeller. When the liquid displaced by the heating element was taken into account, it increases the liquid height by 2 mm (DOI: 10.25375/uct.13570970) and shown in Figure 4-7. The bottom of the blade immersed in the fluid at 1 L volume (4 % immersion) was the only section capable of moving the fluid.

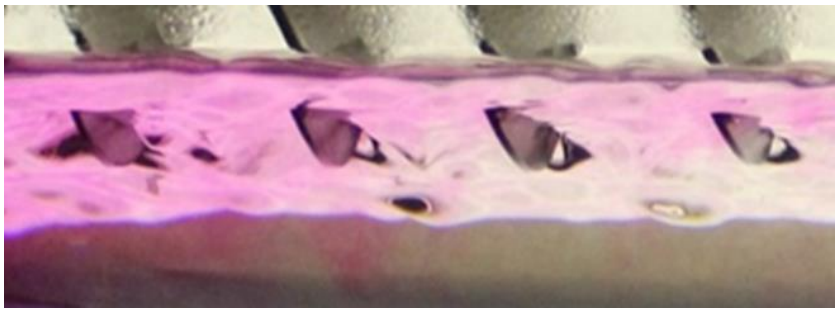

Figure 4-7 Showing the lower tip of the blades immersed at 4% impeller immersion (1 L) responsible for moving the fluid across the length of the vessel

In the case of 42 % impeller immersion (2 L), decolourization occurred faster than 4% immersion. This is primarily because the improved impeller immersion ratio at 2 L (42 %) is 10 times that of 1 L (4 %), which continuously pushes the liquid and generate axial motion along the length of the vessel. The region near to the heating element decolourize faster than the area without it (near the end of the vessel) and generally faster at the bottom as compared to the region near to the gas-liquid interface. It is mainly because the presence of the heating element acted as a baffle in the vessel and aid in creating turbulent eddies as shown in Figure 4-8 with black circles.

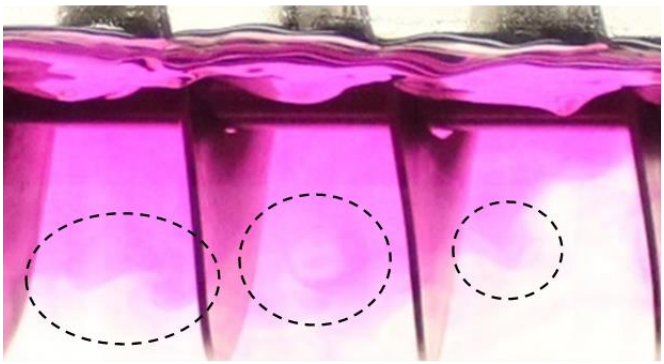

Figure 4-8 Turbulent eddies formed (circled) between impeller blades above the heating finger

These turbulent eddies formed between the impeller blades and near the tip (shown within the black dotted circles). It indicates that the turbulent flow (eddies) formed are normal to the viewing plane.

If the horizontal vessel was assigned with the cylindrical coordinate, the angle of shaft rotation (ω), and the rotation of the shaft would move the fluid simultaneously in both axial and tangential directions as described in Figure 4-9.

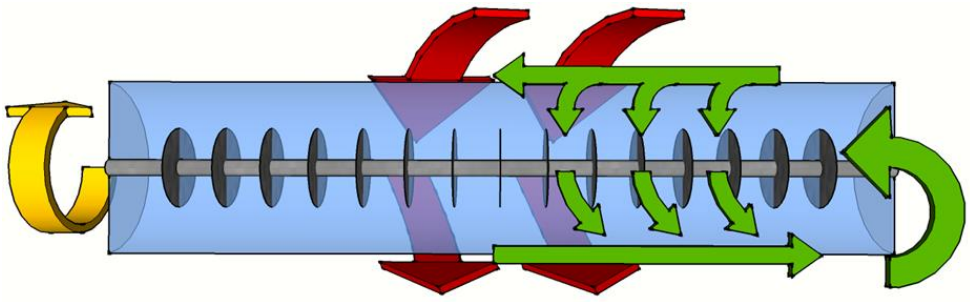

Figure 4-9 Illustrating the proposed fluid flow pattern. The yellow arrow represents impeller rotation, red arrows indicate the spiral movement of the fluid, small green arrows draw fluid inside, between the blades and pushed out whereas big green arrows showed that fluid motion due to pressure gradient formed by the impeller pumping

Fluid flow can be visualized in a simplistic way as depicted in Figure 4-1 (b), where the red arrows depict the liquid moving backwards from right to left whereas blue arrows depict the liquid moving forward form the tip of the blades. Both the fluid movements occurred simultaneously thus in addition to the heating finger, this movement created turbulence and formed eddies between the blade for enhanced mixing.

79 % impeller immersion follows the similar fluid flow patterns of the 42 % immersion except that the mixing time was shorter. The decolourization of the reactor occurred uniformly across the length of the vessel in different regions as shown in Figure 4-10

Figure 4-10 Homogenous patches of fluids shown with rectangular boxes at 3 L

It was observed that the point of addition of decolouriser (1 M HCl) (top of side plate) Figure 4-4 (c), decolourises first at the point of injection and soon after small patches of fluid decolourise along the length of the vessel as shown in Figure 4-10. It was observed again in 79 % immersion (3 L fill volume) that the regions close to the heating element decolourise faster than the end without the heating element. The spiral fluid flow pattern created by the impeller can be seen by the sweeping movement of pink colour at the bottom curvature of the glass vessel throughout the length.

With the fully submerged impeller at 4 L, the fluid flow pattern was not completely distinguishable. The time taken to decolourise the entire length of the bioreactor was much longer than 3 L. It could be because the axial flow generated by the fully immersed impeller is not of turbulent behaviour as compared to 3 L with 79 % immersion, where the partial immersion of the stirring blade across the length of the vessel generated turbulent axial motion. Additionally, backflow mixing occurred between the blades due to the counter current flow of fluid. The region closes to heating finger took a similar time as in 3 L and showed the same pattern of decolourisation as shown in Figure 4-6.

4.3.1.2 Effect of impeller agitation speed on homogenization

The effect of agitation speed was observed for 42 % (2 L) and 79 % (3 L) impeller immersion. These impeller immersions demonstrated the shortest mixing time and clear fluid flow pattern. At each volume, the agitation speed from 100 rpm to 500 rpm was observed with an increment of 100 rpm as shown in Figure 4-11. The time mentioned in the Figure 4-11 represented the time of photograph taken.

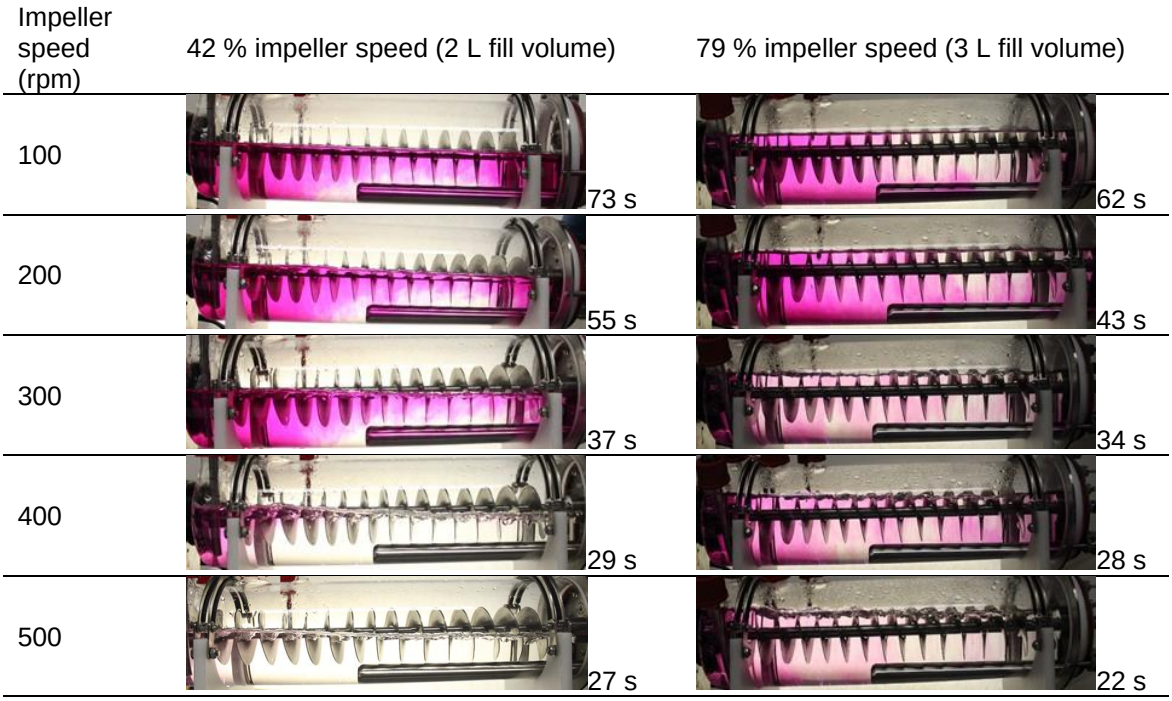

Figure 4-11 Visualization of fluid flow at different impeller agitation speed at 42 % impeller immersion (2 L) and 79 % impeller immersion (3 L)

As the impeller agitation increases, the time of decolourization decreases, whilst the flow of fluid become more turbulent. This chaotic turbulence at high speed makes the system well mixed, thus reduces the concentration gradient of the tracer (pink colour) quicker. The agitation speed at 300 rpm or above, showed surface vortices formed and continue to grow as the impeller agitation increases. At 500 rpm, the spiral impeller entrained air bubbles from the headspace through the impeller blade into the bulk liquid as shown in Figure 4-12 (a), which would increase the oxygen transfer into the liquid but may lead to cell death due to bubble bursting (Chalmers and Ma, 2015; Chisti, 2000).

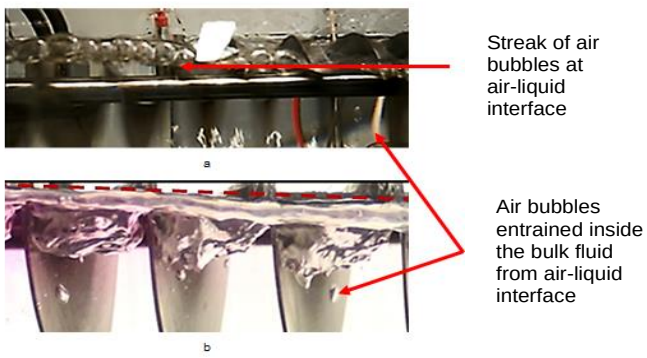

Figure 4-12 Illustrate (a) the formation of bubble streak at the air-liquid interface and (b) bubble entrainment from the headspace at an impeller speed of 500 rpm

The other peculiar phenomena were observed in the HTB, where the moving fluid (liquid surface) made a slight slope downward (from motor drive to stainless steel side plate) as can be seen in Figure 4-12 (b) denoted with the red dotted lines. This phenomenon could be because of the pressure gradient formed across the length of the vessel by the pumping action of the impeller which pushes the fluid with uniform acceleration at a particular impeller speed. It can be assumed that this hydrodynamic pressure gradient could be the main driving force for the circulatory flow of bulk liquid and the slope formed at the liquid surface.

In the case of 79 % impeller immersion (3 L), mixing time decrease as the impeller speed increases as depicted in Figure 4-11. At a low impeller speed from 100 - 200 rpm, it has been observed that decolourization occur faster in the regions close to the heating elements as compared to the far end of the vessel but at high impeller speed, the effect of decolourization was less pronounced. The impeller speed above 200 rpm generates fully turbulent fluid flow regimen which can be seen through colour gradient formed in Figure 4-11 at an impeller speed of 300, 400 and 500 rpm, which was further confirmed by calculating impellers' Reynolds number as shown in Table 4-4.

Table 4-4 Impellers' Reynold Numbers at tested impeller speeds

Impeller speed (rpm)	Impeller Reynold's number
100	5985
200	11970
300	17960
400	23940
500	29930

The fluid is said to be fully turbulent if their Reynolds number (R_e) is greater than 10,000, at that stage, impeller power number is constant and independent of the Reynolds number (Chapple et al., 2002). In other words, it is called the power number for the fixed impeller. From the result obtained from the decolourisation method, it has been concluded that the decolourization method was highly dependent on visual and therefore may be influenced by the operator. This method is acceptable and appropriate for fluid flow pattern studies, but may not be consistent for mixing studies., Therefore, the conductivity method was used to quantify the mixing time

4.3.2 Mixing time through conductivity method

Mixing time is the time taken to achieve 95 % homogeneity in the fluid which is given by Equation 3-1. This method was used to determine the mixing time at different fill volumes or impeller immersion ratios and different impeller speed in the HTB in the presence of tracer (5 M NaCl) as shown in Figure 4-14. The residence time distribution (RTD) profile of HTB directly correlates the mixing profile of the reactor.

Figure 4-13 represented the graphical illustration of mixing time profile for each volume at different impeller speed in the form of F(t) curve. All the conductivity curves obtained were generally smooth after normalization with some small oscillations. The mixing time (95 % homogeneity) can be determined by the slope of the conductivity profile of each volume at different impeller speed. The point on the F (t) curve where it begins to rise-up to show the exponential increase indicates the response time. Small oscillations observed accounted for the potential noise from the conductivity meter, small concentration gradient near probe and human error.

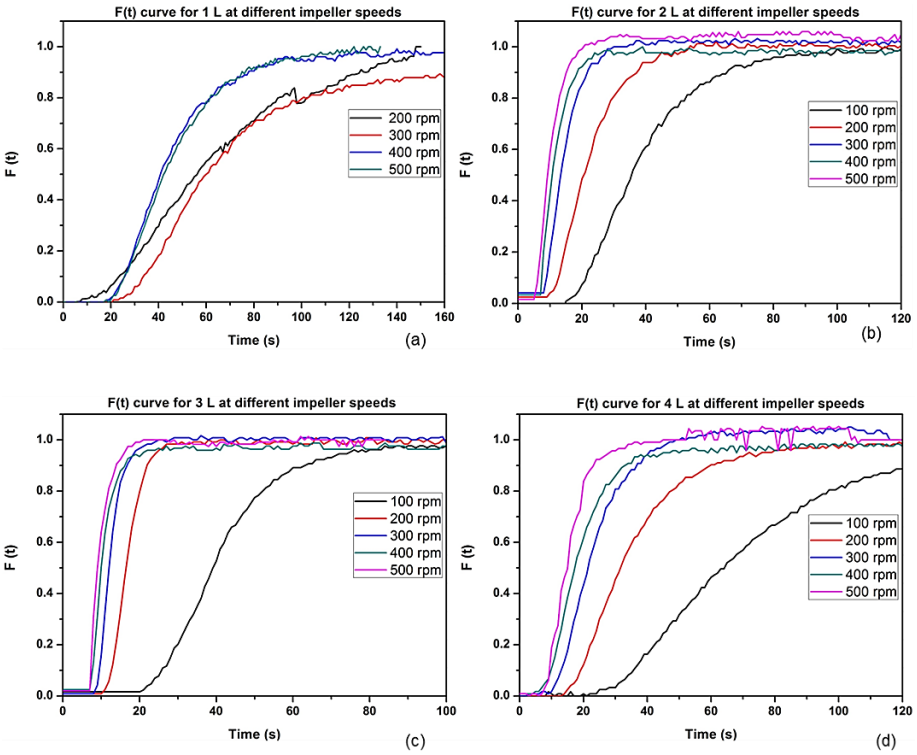

Figure 4-13 The F (t) curves representing the conductivity profile of different fill volumes at a different impeller speed (a) F (t) curve for 4 % impeller immersion without 100 rpm (b, c, and d) represented the conductivity profile of 42 %, 79 % and fully immersed impeller at different agitation speed

To simplify the mixing time profile, the cumulative distribution function F(t) curve was prepared. The conductivity profile of each impeller speed at different fill volume was plotted as a normalised conductivity value F (t), which represent the normalised concentration of the tracer with time in seconds as illustrated in Figure 4-13. The curve for the fill volume of 1 L at 100 rpm was not shown because of the prolonged mixing time.

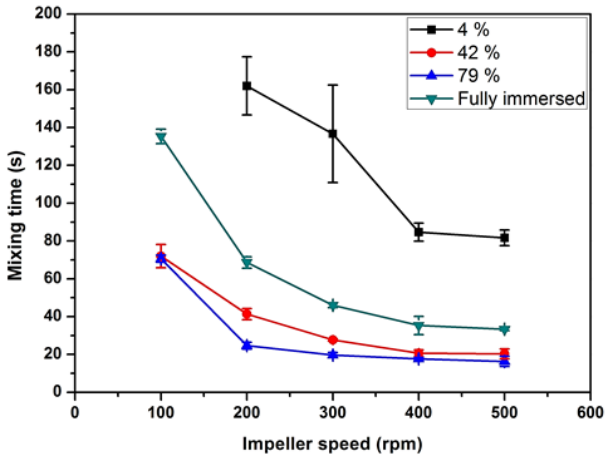

Figure 4-14 Relationship between mixing time and impeller speed at different fill volumes. The mixing time data for 1 L volume has not been shown in the graph due to large error bars. Error bars show the standard deviation of n=3 replicate samples.

The mixing profile of HTB follows the general trend which is, with the increase in agitation, mixing time decrease at all the fill volumes (impeller immersion). It was seen that the fluid flow regimen was turbulent

at impeller speed ≥ 200 rpm. In the case of 1 L fill volume when the impeller immersion is 4 %, it took a long time because of the low impeller-fluid interaction which results in low turbulence.

Figure 4-14 showed that mixing time decreases dramatically for all impeller immersions from 100 – 200 rpm and gradually becomes steady as it approached 500 rpm. This trend is less noticeable at 42 % (2 L) and 79 % immersion (3 L), adequately observed at fully immersed impeller at 4 L and substantial at 1 L (4 % impeller immersion). The error bars represent the low uncertainty in the mixing times obtained at 2 L to 4 L volume. However, the error bars were larger for 1 L at 100 rpm because of the low fluid-impeller interaction. The experiments also showed that the mixing time was lowest in 3 L volume for all impeller speeds. The mixing time was progressively worst when the volume of the reactor was decreased from 2 L, 4 L and mixing was least effective at 1 L volume. This research was limited to fluid flow pattern and measuring mixing time. It did not undertake the in-depth study on the Kolmogorov number and the eddy formation on the hydrodynamic behaviour of the HTB.

4.3.3 Mixing time models for HTB

Mixing is a key unit operation in bioprocessing. Mixing time of a reactor primarily is a function of reactor shape and geometry, impeller design, and impeller agitation which directly contributed to the Reynolds' number, energy dissipation and circulation and impacted the mass and heat transfer efficiency of the bioreactor (Nienow, 2006; Tsui and Hu, 2008). Three models have been evaluated for effectively ascertain the mixing time for the HTB which evaluated the already tested operating range. Model 1-adapted from Tsui and Hu (2008)

Tsui and Hu in 2008 developed the mixing modelled to describe the mixing properties of a helical screw impeller used in STR using CFD technique as shown in Equation 4-2.

$$\boldsymbol{\theta_m = \frac{\pi}{nN_Q}\left(\frac{H}{D}\right)\left(\frac{D}{d}\right)^3} \qquad \text{Equation 4-2}$$

They studied the effect of vessel and impeller geometry on the parameters such as power number (N_P), circulation number (N_Q), and energy of dissipation (E). They also reported that the impeller design and vessel geometry played a crucial role in achieving homogeneity with minimum energy. Despite the vertical design of the vessel and the draught tube of the system they studied, their findings may be applicable to the geometrically similar vessels, therefore their model was evaluated for its suitability for the horizontal tubular bioreactor.

The model only undertakes the vessel geometry and not the impeller immersion as in the case of STR. As the impeller immersion ratio is an important parameter which drastically changes the mixing time in HTB. Hence, the Equation 4-2 is not capable of modelling the mixing time for HTB and the relationship of impeller speed and mixing time may not follow 1st order proportionality for mixing time as in the case of STR. Therefore, Equation 4-2 modified to accommodate the impeller immersion and impeller speed as shown in Equation 4-3

$$\boldsymbol{\theta_{m,model\ 1} = \frac{\pi}{n^a N_Q}\left(\frac{L}{D}\right)\left(\frac{D}{d}\right)^3\left(\frac{h_{L,d}}{d}\right)^b} \qquad \text{Equation 4-3}$$

The exponents a and b were assigned to impeller speed and impeller immersion respectively to find out their relationship to the mixing time. The unknown parameters were calculated using Microsoft Excel's solver method by minimising the overall sum of square errors between experimental and predicted data. The value of a and b found to be 1.15 and 0.46 respectively (DOI: 10.25375/uct.13570970), hence Equation 4-3 rewritten as Equation 4-4 which is applicable to HTB

$$\theta_{m,model\ 1} = \frac{\pi}{n^{1.15} N_Q}\left(\frac{L}{D}\right)\left(\frac{D}{d}\right)^3\left(\frac{h_{L,d}}{d}\right)^{0.46} \quad \text{Equation 4-4}$$

4.3.3.1 Model 2- further modification to Tsui and Hu (2008) mixing model

Model 1 incorporated the desired parameters to elucidate the mixing profile of HTB, yet there are uncertainties whether these parameters represented the mixing profile in the correct form. In order to explicate the relationship between impeller speed, impeller immersion ratio and mixing time, best fit trendlines have been plotted at all the impeller speeds and for all the immersion ratios (volumes) as shown in Figure 4-15.

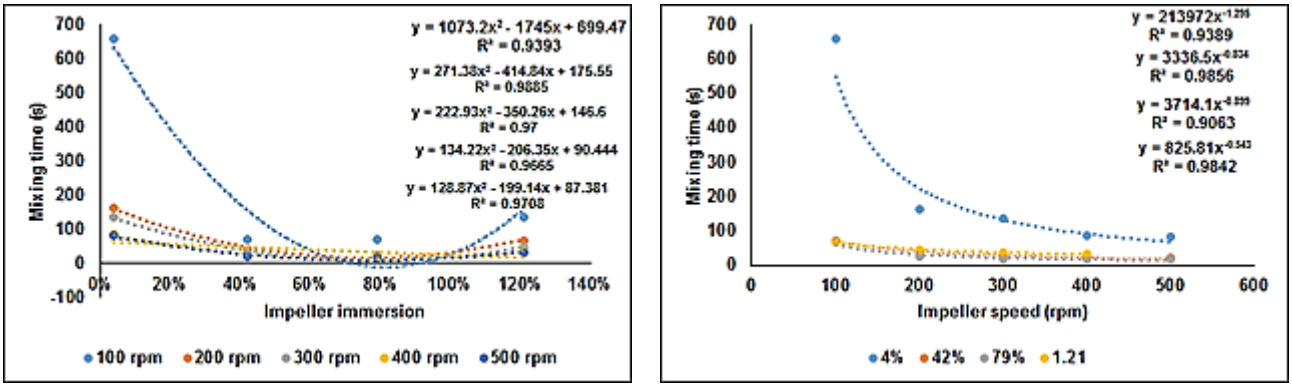

a b

Figure 4-15 Best-fit trendline elucidating the relationships of mixing time with (a) impeller immersion and (b) with impeller speed

Figure 4-15 (a) exhibited the best fit with 2nd order polynomial and R^2 value of 0.9393 for 100 rpm indicated the degree of fluctuation in data whereas in Figure 4-15 (b) represented the best-fit with power curve where the exponent is greater than 1 which directly indicated that the impeller speed may not follow the 1st order inversely proportionality of the mixing time. Therefore model 1 further modified to accommodate the above relationship. Keeping in mind, model 1 further modified to below relationship as shown in Equation 4-5

$$\theta_{m,model\ 2} = \frac{\pi}{n^a N_Q}\left(\frac{L}{D}\right)\left(\frac{D}{d}\right)^3\left[\left(\frac{h_{L,d}}{d}\right)^b - c\left(\frac{h_{L,d}}{d}\right) + d\right] \quad \text{Equation 4-5}$$

Like model 1, the value of a, b, c and d were calculated by least square regression by using solver method that led to Equation 4-6

$$\theta_{m,model\ 2} = \frac{\pi}{n^{1.0} N_Q}\left(\frac{L}{D}\right)\left(\frac{D}{d}\right)^3\left[\left(\frac{h_{L,d}}{d}\right)^{0.98} - 0.45\left(\frac{h_{L,d}}{d}\right) + 0.19\right] \quad \text{Equation 4-6}$$

4.3.3.2 Model 3- through Buckingham π-Method

A new model was developed using Buckingham π-Method as a function of dimensionless groups which can accommodate power number, Reynolds' number and circulation number as shown in Equation 4-7. These parameters directly take part in the mixing and overall performance of the bioreactor. The detailed derivation can be found in the dataset (DOI: 10.25375/uct.13570970).

$$\theta_{m,model\,3} = K\left(\frac{h_{L,d}}{d}\right)^{\alpha}(N_P)^{\beta}(N_{Re})^{\gamma}(N_Q)^{\delta} \quad \text{Equation 4-7}$$

Like model 1 and 2, the value of $K, \alpha, \beta, \gamma, \delta$ were calculated by least square regression by using solver method that led to Equation 4-8.

$$\theta_{m,model\,3} = 160945\left(\frac{h_{L,d}}{d}\right)^{0.51}(N_{Re})^{0.06}(N_P)^{-0.89}(N_Q)^{-1.19} \quad \text{Equation 4-8}$$

Re-arranging and simplifying the Equation 4-8, it becomes Equation 4-9

$$\theta_{m,model\,3} = 160945\frac{h_{L,d}{}^{0.51}\cdot d^{7.63}\cdot \rho^{0.95}\cdot n^{3.92}}{\mu^{0.06}\cdot P^{0.89}\cdot Q^{1.16}} \quad \text{Equation 4-9}$$

4.3.3.3 Statistical analysis of mixing time and models

Statistical analysis was done with a Two-way ANOVA with replication method. This method was chosen to investigate the significance of the two independent variables such as impeller immersion and impeller speed on the mixing time. The data analysis was carried out in Microsoft Excel's ANOVA with replication method using the Data Analysis Tool pack with the confidence level of 95 % (α = 0.05). As the sample was taken in triplicate, the sample frequency was 3 in the analysis. In general, Two-way ANOVA test three null hypothesis namely

- Means of observation (mixing time) grouped by one factor (impeller immersion) are the same
- Means of observation (mixing time) grouped by another factor (impeller speed) are the same
- That there is no interaction between the two factors i.e. impeller immersion and impeller speed have no interaction

Table 4-5 represented the results of Two-way ANOVA where *F-test* and *P-test* value were used to reject/accept the null hypothesis. In the table *SS* represented the sum of the square, *df* indicated the number of degrees of freedom (which is usually the number of sample-1), *MS* stands for the mean square value of the data, *F* indicated the F statistic (distribution of data from the mean), *P-value* is the probability and *F crit* represented the critical value of F distribution to accept or reject the null hypothesis.

Table 4-5 Analysis of mixing time data with Two-way ANOVA with replication

Source of Variation	SS	df	MS	F	P-value	F crit
Impeller immersion	380337	3	126779	99.04	1.48E-18	2.84
Impeller speed	328219	4	82054.8	64.10	7.34E-17	2.61
Interaction	427309	12	35609.1	27.81	1.20E-15	2.00
Within	51203	40	1280.08			
Total	1187069	59				

From the Table 4-5, it has been observed that *F* value of 99.04 is greater than the F_{crit} value of 2.84 which means that there is statistically significant effect of impeller immersion on the mixing time hence first null hypothesis was rejected. Likewise, from impeller speed, $F > F_{crit}$ (64 > 2.61), therefore second null hypothesis was also rejected which indicated that the impeller speed had a significant effect on the mixing time. *P test* represented the probability of distribution of data. For the *P-test,* the null hypothesis is that there is no statistical significance if the P-value < α-value i.e. 0.05, the null hypothesis is rejected. The *P-test* is an indication of the reliability of the data gathered and the conclusions drawn from the *F-test*. For both the parameters, the P value is less than 0.05 hence rejected the null hypotheses. Finally, the interaction value of 27 is more than the F_{crit} value which signifies that the impeller immersion and impeller speed are significantly interdependent and have a cumulative effect on the mixing time when the impeller immersion is above 79 % (3 L) in the HTB as shown in Figure 4-16

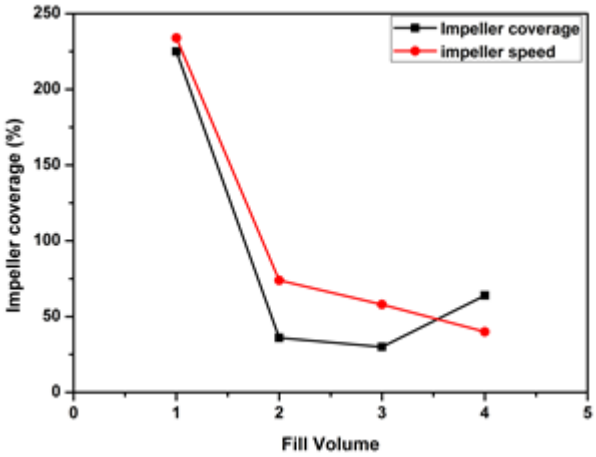

Figure 4-16 Means of observation of the two factors depicting the interaction

Table 4-6 indicated that the impeller immersion has more significance in mixing time determination than impeller speed. This observation can be made from the F value of 99.04 than to 64.10 from impeller speed. This means the working volume of the batch is crucial for its success.

Table 4-6 Conclusion from F-test and P-test

Test	*F-value vs. Fcrit*	Conclusion	*P-value vs. α*	Conclusion
Impeller immersion	99.04 >> 2.839	Highly significant effect	1 e-18 << 0.05	Very high statistical significance
Impeller speed	64.10 > 2.606	Significant effect	7 e-17 << 0.05	Very high statistical significance
Interaction	27.82 > 2.004	Significant effect of interaction	1 e-15 << 0.05	Very high statistical significance

The immersion *P-value* is many orders of magnitude lower than the α-value and therefore the relationship between impeller immersion and mixing time is statistically significant and the results from the *F-test* are reliable. Similarly, impeller speed has a significant effect on mixing time. Again, this result is expected as the impeller speed is related to the rate at which energy is dissipated from the impeller to the liquid volume. This energy acts against viscous and drag forces in the liquid, moving liquid elements throughout the fluid. The faster the rate of energy dissipation, the faster fluid elements move around the

vessel, leading to a faster mixing time. However, this effect is less significant than the immersion effect, confirming a trend observed earlier concerning the small change in mixing times with impeller speed at 42 % and 79 % immersion. The impeller speed *P-value* is many orders of magnitude lower than the α-value as with impeller immersion, and therefore the relationship between impeller speed and mixing time is statistically significant and the results from the *F-test* are reliable.

Finally, both the *P-test* and *F-test* for interaction reject the null hypotheses and it can be said that there is a significant effect on mixing time from the interaction between the independent variables. This means that impeller speed and impeller immersion interact with respect to affecting mixing time; keeping one variable constant is not necessarily the same as removing the effect of that variable on mixing time.

Comparison of mixing models were carried out numerically using percentage error, R^2-values and residuals plots to find out the best fit model which corresponds to the experimental data. Table 4-7 summarised the percentage error associated with each model with respect to impeller immersion and impeller speed together with an overall error. The acceptable limit considered for error, in this case, is 15 %.

Table 4-7 Percentage error of each mixing model with respect to impeller speed and impeller immersion

Parameter	**Percentage error (%)**		
Impeller speed (rpm)	Model 1	Model 2	Model 3
100	25	0.56	5
200	17	0.56	7
300	14	0.56	5
400	12	0.56	7
500	12	0.56	10
Impeller immersion (%)	Percentage error (%)		
4	12	0.01	2
42	29	0.60	20
79	15	1.5	4
121	8	0.16	3
Overall	16	0.56	7

It has been clear from Table 4-7 that the percentage error values in all the models came out to be under or around the acceptable error limits of 15 %. Model 2 appears to be the best fit as it showed less error than other models. Model 2 also showed the same amount of error with respect to impeller speed which means experimental values falls away from the predicted value which needs to be addressed. Model 1 at 100 rpm impeller speed has the highest error which was expected because HTB did not perform well at 100 rpm. In the case of impeller immersion, Model 1 and 3 exhibited high percentage error at 42 % impeller immersion (2 L) whereas model 2 showed at 79 % (3 L) which was under acceptable limit.

The coefficient of determination (R^2) is a statistical measure that represents the ratio of explained variance to that of the total variance in a regression model. So, if the R^2 value of a model is above 0.90, This can be explained as 90 % of the observed variation is due to the model's inputs and 10 % variance is unexpected and it can be due to multiple factors such as sampling error, human error and so on. Hence, R^2 data was considered to find the suitability of the model which closely represented the experimental data. Table 4-8 showed the R^2 values for impeller immersion and impeller speed.

Table 4-8 Coefficient of variance (R^2-values) of each model with respect to impeller speed and impeller immersion

Parameter	**R^2 values**		
Impeller speed (rpm)	Model 1	Model 2	Model 3
100	0.990	1.000	0.999
200	0.960	1.000	0.988
300	0.951	1.000	0.996
400	0.916	1.000	0.992
500	0.894	1.000	0.986
Impeller immersion (%)	R^2 values		
4	0.995	1.000	1.000
42	0.210	1.000	0.887
79	0.748	0.999	0.996
121 (Fully immersed)	0.891	1.000	0.992
Overall	0.990	1.000	0.999

The threshold error for R^2 analysis considered was above 0.8. The overall R^2-value of Models 1, 2 and 3 were well above this threshold and from this perspective, all models satisfactorily match the experimental data. However, on closer inspection of each parameter tested, Models 2 and 3 fit the experimental data well whereas Model 1 at 42 % and 79 % exhibited some anomalies. This is primarily because Model 1 did not consider impeller immersion ratio while calculating mixing time.

The final tool used was the residual plot, which represented the distribution of the data on the negative and positive axis. There does not seem to be a defined shape in these residual plots, though this is difficult to confidently conclude with 5 data points; a larger sample size will better determine whether the distribution of residuals was indeed random. Generally, the data point sits close to the axis are a better fit than those sit far from the horizontal axis.

Residual plot for impeller speed differs greatly for all the 3 models (Figure 4-17). For Model 1, 42 %, 79 % and 121 % have a similar and defined shape. The shape at 4 % is similar with a small amount of variation. This is also true for Model 2, where 4 %, 42 % and 121 % clearly have similar defined shapes, while 79 % has a defined shape in the opposite direction. Model 3 shows a more erratic residual plot, although 79 % and 121 % may still have a defined shape.

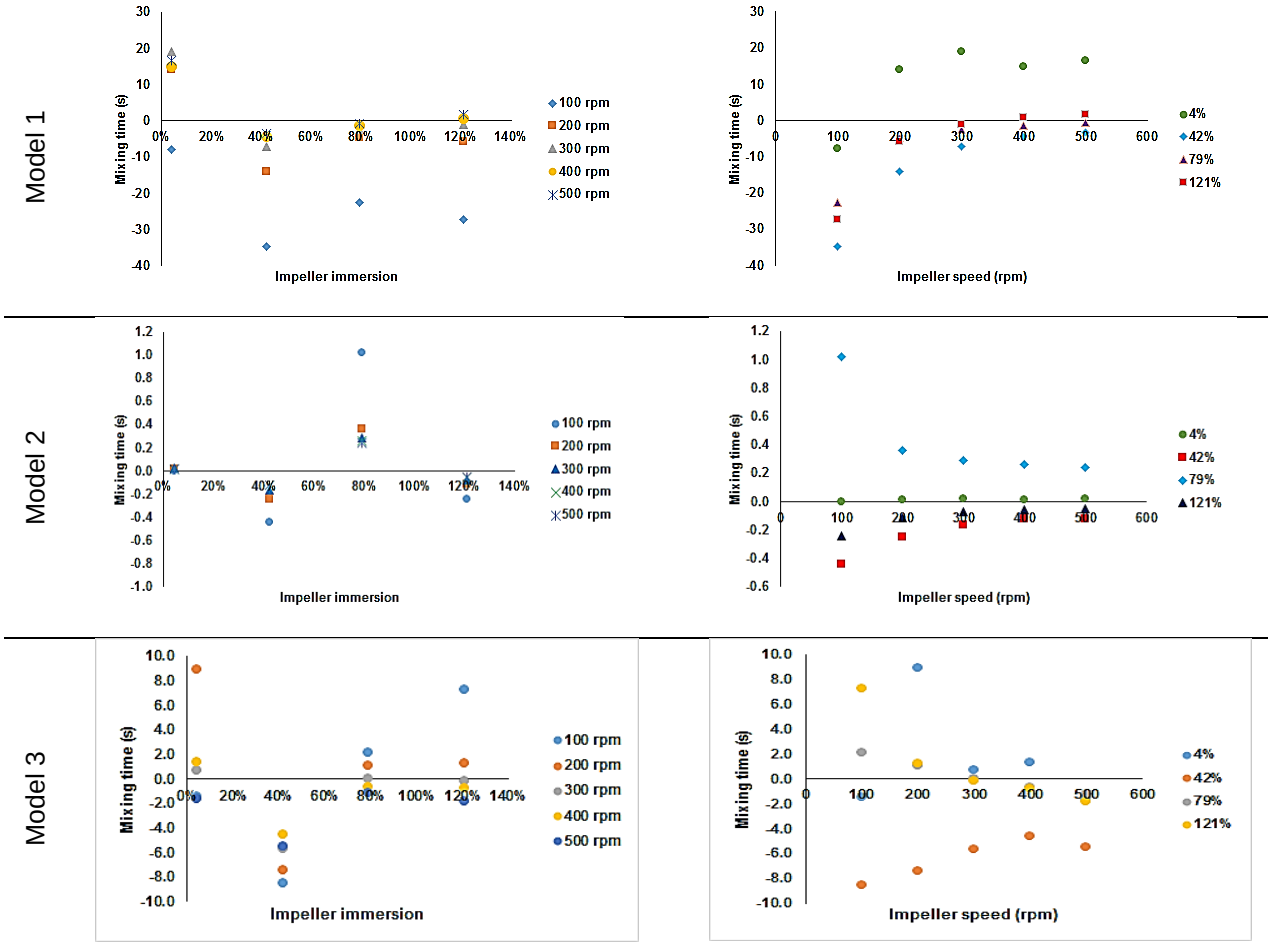

Figure 4-17 Residual plots for all the mixing models with respect to impeller immersion and impeller speed

From the results obtained from the predicted models, it was imperative to decide which model would mimic the actual mixing behaviour of the HTB. The model must be as accurate and robust as possible which means that the error percentage and R^2-values must be in the acceptable range, and the residuals data points must be as close to the horizontal axis as possible to that of randomly distributed data points. Table 4-9 summarised the model assessment based on the percentage error, coefficient of determination and residual plot. The models were evaluated qualitatively in the scale of very poor, poor, good, and very good. Additionally, the criteria for model development were also taken into consideration.

Table 4-9 Mixing models assessment based on Percentage error, R^2 values and from residual data

Criteria	Model 1	Model 2	Model 3
Error percentage	Very poor	Very good	Good
R^2-value	Good	Very good	Good
Randomly distributed residual plots	Very poor	Very poor	Good

While Model 2 meets the first two criteria very well, the defined shapes in the residual plots cast doubt over its widespread applicability. Defined shapes in residual plots are usually an indication that the model has the wrong form, despite being able to accurately predict experimental values. The model will be

accurate but not robust, as there will be uncertainty in the applicability of the model at values outside of those used to fit the model. To rectify this phenomenon, the model can be transformed by taking the logarithms of variables in the model by making the model non-linear or adding other variables that may be lacking in the formula. A number of these solutions were tested generating residual plots with still some definable shape, and sometimes increasing the percentage errors. If through more analysis, Model 2 can be modified to meet the criterion of randomly distributed residuals without compromising its accuracy, it will be a more suitable model.

Model development further indicates the applicability of the models. Models 1 and 2 were developed from a model proposed by Tsui and Hu (2008), which was used for a vertical screw impeller system. Although Tsui and Hu's (2008) model appears elsewhere in the literature and is generally accepted, its applicability for the horizontal screw impeller system is uncertain. Model 3 was derived using the Buckingham π-method. This method is widely accepted as a robust way to develop empirical models, though the core variable selection procedure may sometimes arbitrary. While both methods come with uncertainties, the empirical model derived using the Buckingham π-Method is more favourable. In conclusion, Model 3 meets all criteria satisfactorily. Figure 4-18 show the experimental data with Model 3's predicted values illustrating the fitting data.

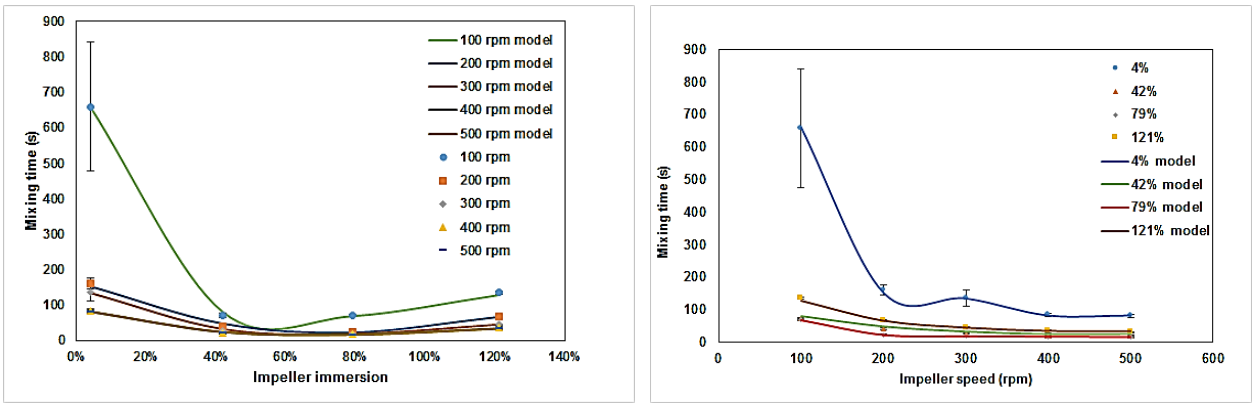

a b

Figure 4-18 Relationship of mixing time with (a) impeller immersion and (b) impeller speed in comparison with model 3

How this model is applied will be affected by and inform decisions surrounding operating points and reactor performance. For example, the goal is to minimise mixing time for efficient mass transfer, and from results obtained, it happens between an impeller immersion of 42 % and 90 % at moderate to high impeller speeds (DOI: 10.25375/uct.13570970). However, at high impeller speeds, Model 3's error increases to 10 % at 500 rpm. Similarly, the error is highest at 42 % impeller immersion for this model but decreases to 3 % as immersion increases. Therefore, operating at high impeller speeds and in the lower range of optimum impeller immersion runs the risk of introducing more error into the predictions of mixing time. It would be wise to operate at a higher impeller immersion and lower impeller speed to minimise error, although impeller speed is limited by the constraint of minimum suspension speed.

4.3.4 Oxygen mass transfer and model

As it was clear from the mixing studies that 1 L and 4 L volume are not suitable to run batches in the HTB, therefore, the mass transfer studies were conducted for only 2 L and 3 L volumes with impeller immersion at 42 % and 79 % respectively. The aeration rate of 0.2 LPM to 0.5 LPM was considered with an increment of 0.1 LPM whereas the impeller speed tested was 100 – 500 rpm with the increment of 100 rpm as explained in Table 3-3 (DOI: 10.25375/uct.13570970). The following assumptions were taken into consideration while measuring the mass transfer coefficient

- Henry's Law applies for dynamic equilibrium.
- The mass transfer coefficient ($k_L a$) is constant at a given dissolved oxygen concentration with respect to time
- The liquid temperature was at 37 °C at all times of study (Isothermal liquid).
- The driving force (partial pressure of oxygen-pO_2) was constant for a given set of aeration and agitation, therefore, is constant with respect to dissolved oxygen concentration (DO)
- Regression DO readings used for less than 80 % saturation only.

The mass transfer values of 2 L and 3 L volumes were calculated experimentally and populated in Table 4-10 and Table 4-11 given below

Table 4-10 Experimentally calculated values of $\boldsymbol{k_L a}$ (h^{-1}) for 2 L volume (42 % impeller immersion)

Impeller speed (rpm)	Aeration rate (LPM)			
	0.2	0.3	0.4	0.5
100	5.4 ± 0.2	6.6 ± 0.3	7.4 ± 0.3	8.2 ± 0.3
200	6.9 ± 0.2	8.8 ± 0.3	10.0 ± 0.4	10.0 ± 0.3
300	7.2 ± 0.26	10.0 ± 0.4	10.6 ± 0.4	12.8 ± 0.4
400	7.6 ± 0.3	10.9 ± 0.4	13.0 ± 0.5	12.6 ± 0.4
500	8.5 ± 0.3	11.4 ± 0.4	13.7 ± 0.5	16.0 ± 0.5

Table 4-11 Experimentally calculated values of $\boldsymbol{k_L a}$ (h^{-1}) for 3 L volume (79 % impeller immersion)

Impeller Speed [rpm]	Aeration rate [LPM]			
	0.2	0.3	0.4	0.5
100	5.3 ± 0.2	6.0 ± 0.2	6.0 ± 0.2	6.8 ± 0.2
200	6.9 ± 0.2	8.2 ± 0.3	8.5 ± 0.3	9.7 ± 0.3
300	7.8 ± 0.3	10.2 ± 0.3	10.5 ± 0.4	10.0 ± 0.3
400	8.9 ± 0.3	10.8 ± 0.4	12.0 ± 0.4	13.2 ± 0.4
500	9.3 ± 0.3	11.6 ± 0.4	14.3 ± 0.4	15.7 ± 0.4

Table 4-10 and Table 4-11 indicated that with the increase in impeller speed, mass transfer efficiency increases. Alternatively, with the increase in airflow rate at a given impeller speed, $\boldsymbol{k_L a}$ value increases. The difference in $\boldsymbol{k_L a}$ value was not prominent at 42% and 79 % impeller immersion. This could be explained through the impeller immersion ratio, or the liquid height increased from 2 L to 3 L volume. The mass transfer range exhibited by the HTB at all the agitation speeds fall in between 5 - 16 h^{-1} which is in accordance with the widely reported range for mass transfer of 1-15 h^{-1} for STR in animal cell cultures (Nienow, 2006).

The mass transfer efficiency in a horizontal bioreactor primarily depends on the agitation speed, impeller immersion ratio, airflow rate and surface renewal rate. The use of spiral impeller with multiple blades along the length of the vessel having provides a large surface area to volume ratio for mass and heat transfer. The spiral design of the impeller also imparts uniform distribution of energy to the fluid due to high fluid movement between the blades across the length of the vessel. It is possible because of the multiple energy distribution points available across the length in the form of impeller blades, this would enhance gas hold-up volume due to this redistribution and result in increased mass transfer efficiency (Gogate et al., 2000).

The geometric configuration of the bioreactor plays a key role in determining the three main parameters such as mixing time, circulation number (N_Q), and power number (N_p) which include tank diameter, length of the impeller, the pitch of the impeller and width of the impeller blade (Tsui and Hu, 2008). Carreau et al., (1992) used these parameters to establish their applicability for a screw impeller in a fixed geometry in the form a dimensionless number for Newtonian fluids at high Reynolds numbers (N_{Re}) above 10000

$$\frac{N_p N_{Re}}{N_Q} = \text{Constant} \qquad \text{Equation 4-10}$$

Tsui and Hu, (2008) modelled the Equation 4-10 to find out the value of the constant using CFD analysis for a screw impeller with the draft tube as shown in Equation 4-11, which has similar impeller clearance ratio (D/d=2.18) as of the HTB under investigation in the current research.

$$\frac{N_p N_{Re}}{N_Q} = 600 \qquad \text{Equation 4-11}$$

Using Equation 4-11, Reynolds numbers were calculated for each impeller speed and power numbers were also predicted from estimated circulation number through mixing time (Table 4-12). The ratio of $\boldsymbol{N_Q/N_p}$ was also calculated. The significance of the ratio of circulation number to power number is that larger the ratio results in better bulk mixing at the lower shear rate at the same power input (Godoy-Silva et al., 2010)

Table 4-12 Predicted values of power numbers and circulation flow numbers

Liquid volume	Impeller speed [rpm]	Mixing time $\boldsymbol{\theta_m}$ [s]	$\boldsymbol{N_{Re}}$	$\boldsymbol{N_Q}$ Predicted	$\boldsymbol{N_p}$ Predicted	$\boldsymbol{\frac{N_Q}{N_p}}$
2 L	100	72.0	5985	0.533	0.054	9.87
	200	41.3	11970	0.465	0.023	20.22
	300	27.7	17955	0.463	0.015	30.87
	400	20.7	23940	0.465	0.012	38.75
	500	20.3	29927	0.378	0.008	47.25
3 L	100	70.7	5985	0.815	0.082	9.94
	200	24.7	11970	1.168	0.059	19.80
	300	17.7	17955	0.976	0.033	29.58
	400	16.3	23940	0.815	0.020	40.75
	500	20.3	29927	0.705	0.014	50.36

It was hypothesized that for the HTB, $k_L a$ is a function of the following parameters

$$k_L a = f\left(h_{L,d}, d, n, P, \rho, \mu, V_s, Q, D, L, S\right)$$

Where, $h_{L,d}$ is a height of liquid, d is impeller diameter, n impeller speed, P power input, ρ density of the fluid, μ fluid viscosity, Q volumetric bulk fluid pumping rate. Some parameters are fixed such as D and L (diameter and length of the vessel) and S is the impeller pitch and DO_2 is the diffusivity of oxygen in water. All these fixed parameters are included in the pre-exponential constant K_1. To investigate the inter-dependence of the power input, Reynolds numbers, flow number and impeller clearance, the dimensional analysis was done using the Buckingham π-Method, which provided the following non-linear expression for $k_L a$ in Equation 4-12. (Refer DOI: 10.25375/uct.13570970)

$$k_L a\ (h^{-1}) = K_1 \left(\frac{h_{L,d}}{d}\right)^{\alpha} \left(\frac{P}{\rho n^3 d^5}\right)^{\beta} \left(\frac{\rho n d^2}{\mu}\right)^{\gamma} \left(\frac{V_S}{nd}\right)^{\delta} \left(\frac{Q}{nd^3}\right)^{\varepsilon} \qquad \text{Equation 4-12}$$

The value of these exponents (α, β, γ, δ, ε) was determined by the method of non-linear least-squares regression of the measured $k_L a$ data for all liquid volumes using Microsoft Excel's solver method.

$$K_1 = 0.36, \quad \alpha = 0.08, \quad \beta = -0.90, \quad \gamma = -0.03, \quad \delta = 0.48, \quad \varepsilon = 0.79$$

The values of these exponents were substituted in Equation 4-12, with a coefficient of determination of R2 = 0.941, the new Equation 4-13 is proposed for a surface aerated horizontal tubular bioreactor with screw impeller, under abiotic conditions:

$$k_L a\ (h^{-1}) = 0.36 \left(\frac{h_{L,d}}{d}\right)^{0.08} \left(\frac{P}{\rho n^3 d^5}\right)^{-0.90} \left(\frac{\rho n d^2}{\mu}\right)^{-0.03} \left(\frac{V_S}{nd}\right)^{0.48} \left(\frac{Q}{nd^3}\right)^{0.79} \qquad \text{Equation 4-13}$$

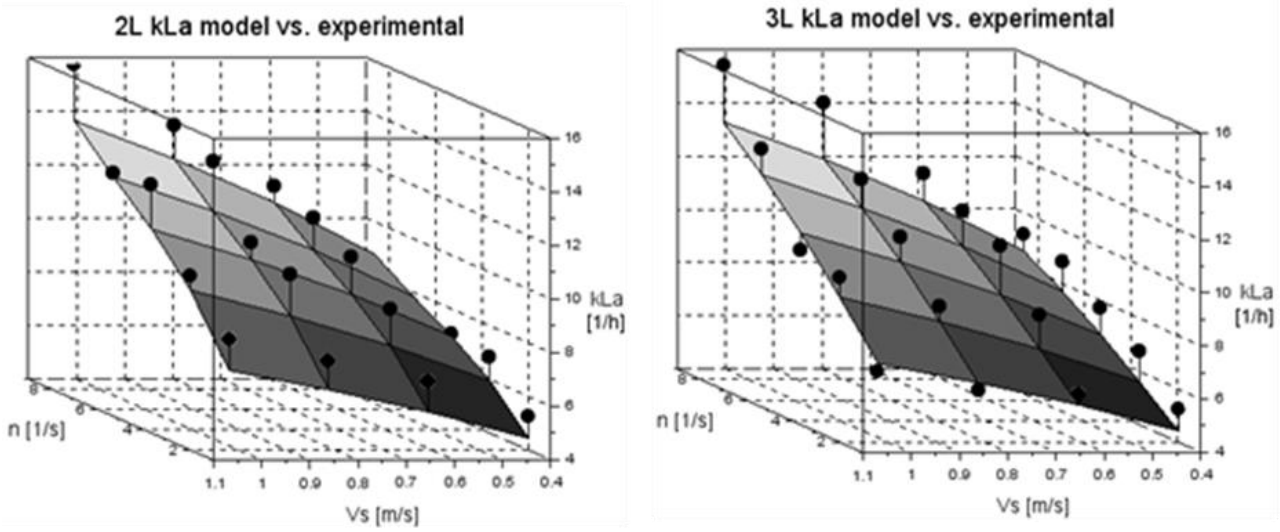

Figure 4-19 $\boldsymbol{k_L a}$ model comparison to experimental values for 2 L (left), and 3 L (right) volumes using the same proposed model where x-axis represented by volumetric airflow rate, y-axis with impeller speed and z-axis represented by $k_L a$. The dots indicate the experimental data

Only two independent parameters could be plotted simultaneously with $k_L a$. For this reason, experimental $k_L a$ measurements (black dots) were compared to the model (Equation 4-13) plotted as a

shaded grey surface as a function of impeller speed and superficial gas velocity. The comparison was made separately for impeller immersions of 42 % and 79 %, respectively as shown in Figure 4-19.

An alternative approach was to use different models for the 2 L (42 %) and 3 L (79 % impeller immersions). Non-linear regression was used to derive the following expressions in Scilab 6.1.0, in the form of Equation 4-12, resulting in the following two equations:

$$k_L a_{V=2L}\ (h^{-1}) = 0.37\left(\frac{h_{L,d}}{d}\right)^{0.32}(N_P)^{-0.89}(N_{Re})^{-0.02}(N_{VS})^{0.55}\left(N_Q\right)^{0.63} \quad \text{Equation 4-14}$$

$$k_L a_{V=3L}\ (h^{-1}) = 0.34\left(\frac{h_{L,d}}{d}\right)^{0.17}(N_P)^{-0.87}(N_{Re})^{-0.00}(N_{VS})^{0.41}\left(N_Q\right)^{0.81} \quad \text{Equation 4-15}$$

With a coefficient of determination of R^2 = 0.957 for 42 % and 0.959 for 79 % immersion, the surface plots are represented in Figure 4-20.

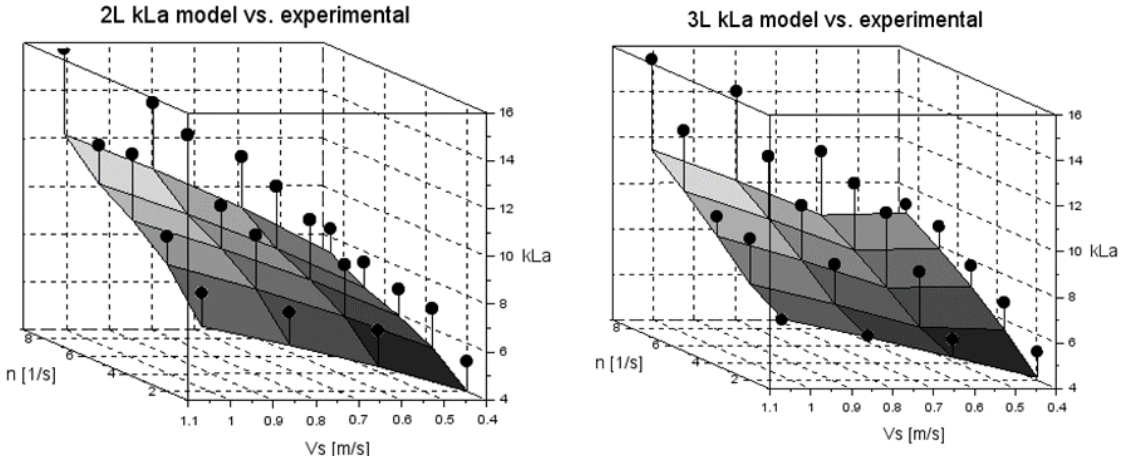

Figure 4-20 $\boldsymbol{k_L a}$ model comparison to experimental values for (left) 2 L, and (right) 3 L volumes using different models given in Equation 4-14 and Equation 4-15.

Equation 4-13 was further simplified by substituting the value of the fixed impeller diameter ($d = 0.50\ \mathrm{m}$) in the Equation 4-13 and then solving the d and n exponents to calculate the pre-exponential constant which resulted in Equation 4-16 for that increases the dimensionless groups. Assuming that the temperature of the liquid phase was at set to 37°C throughout the observation (DOI: 10.25375/uct.13570970).

$$\boldsymbol{k_L a\ (h^{-1}) = 1.29\frac{h_{L,d}{}^{0.08} V_S{}^{0.48} Q^{0.79} n^{1.41}}{P^{0.90}}} \quad \text{Equation 4-16}$$

Statistical analysis was carried out with two-way ANOVA with replication method using experimental data with the aid of the Microsoft Excel Data Analysis Tool Pack. Due to the large number of data obtained, a separate ANOVA was done for each impeller immersion 42 % (2 L) and 79 % (3 L). As the sample was taken in duplicate the sampling frequency was 2 in the analysis. In general, Two-way ANOVA test three null hypothesis namely.

1. Means of observation ($\boldsymbol{k_L a}$) grouped by one factor (airflow rate) are the same
2. Means of observation ($\boldsymbol{k_L a}$) grouped by another factor (impeller speed) are the same
3. That there is no interaction between the two factors i.e. airflow rate and impeller speed have no interaction

Table 4-13 showed that F value for airflow rate and impeller speed is greater than $Fcrit$ ($F > Fcrit$), which means that the null hypotheses 1 and 2 were rejected. The results showed that the effect of airflow rate and impeller speed on the mass transfer efficiency is significant. It has been established that with the increase in impeller speed and airflow rate, $\boldsymbol{k_L a}$ increases. The interaction between the two parameters is slightly greater than the Fcrit value which indicated that both the parameters may or may not interact with each other to impact the mass transfer efficiency. The mass transfer efficiency can be increased when impeller speed ramped up at a fixed airflow rate or airflow can be increased at a fixed impeller speed to increase the $\boldsymbol{k_L a}$.

Table 4-13 Two-way ANOVA with replication for $\boldsymbol{k_L a}$ data at 2 L

Source of Variation	SS	df	MS	F	P-value	F crit
Airflow rate	0.038	3	0.013	57.99	4.78E-10	3.10
Impeller speed	0.039	4	0.010	45.10	9.81E-10	2.87
Interaction	0.006	12	0.001	2.33	4.58E-02	2.28
Within	0.004	20	0.000			
Total	0.087	39				

Table 4-14 Two-way ANOVA with replication for $\boldsymbol{k_L a}$ data at 3 L

Source of Variation	SS	df	MS	F	P-value	F crit
Airflow rate	0.009	3	0.003	6.653	2.69E-03	3.10
Impeller speed	0.050	4	0.012	28.275	5.57E-08	2.87
Interaction	0.006	12	0.001	1.185	3.56E-01	2.28
Within	0.009	20	0.000			
Total	0.074	39				

In the case of 79 % impeller immersion at 3 L,

Table 4-14 illustrate the result of the analysis of variance (ANOVA). It has been observed that the F value for airflow rate and impeller speed is greater than their respective *Fcrit* value hence both the null hypothesis was rejected, which means that the airflow rate and impeller speed both have a significant effect on the mass transfer efficiency of the bioreactor. To compare the results with 2 L at 42 % impeller immersion, it was found that F value for airflow rate for 3 L is 9 times lower than 2 L and a half for impeller speed. This could be due to increased liquid height and less headspace available at 3 L than at 2 L. This indicated that the availability of headspace to aerate the bulk fluid is limited, the only option left is to increase the impeller speed to fulfil the $\boldsymbol{k_L a}$ requirement. This null hypothesis was supported by the low interaction value of 1.19, which is lower than *Fcrit*. This indicated that there could be a low level of interaction between airflow and impeller speed. These observations find support from the P value for 3 L for airflow rate and impeller speed which are lower than α (0.05). The difference in the P value of airflow rate and impeller speed indicated that airflow rate has much less effect than impeller speed.

4.3.5 Minimum agitation speed (N_{js}) for suspension

The minimum agitation speed (N_{js}) for solids suspension was determined for 42 % (2 L), 79 % (3 L) and fully immersed impeller with 4 L volume. The minimum agitation speed was not determined at an impeller immersion ratio of 4 % due to poor contact between the liquid surface and impeller blades. The solid loading used for each volume was in the order of 0.25 %, 0.50 %, 0.75 % and 1.00 % by mass/volume of liquid in the reactor. The average size of the beads falls in the range of 200 ± 50 µm. During the experiments, the heating finger was removed to avoid the beads from getting stuck between the heating finger and the bottom of the reactor.

Zwietering (1958) carried out series of experiments on vertical stirred tank reactors with different geometries such as impeller type, different ratios of vessel and impeller dimensions, solids with different densities and loadings, and fluid viscosity with a purpose to develop an empirical formula as shown in Equation 4-17.

$$N_{js} = \frac{S \cdot \nu^{0.1} \cdot d_p^{0.2} \cdot \left(\frac{g \cdot \Delta\rho}{\rho}\right)^{0.45} \cdot \chi^{0.13}}{d^{0.85}} \qquad \text{Equation 4-17}$$

The S is a dimensionless parameter required to calculate N_{js}, which is a function of vessel geometry, impeller type and vessel to impeller ratio and can be expressed as Equation 4-18

$$S = f\left(\frac{T}{D}; \frac{T}{C}; \textit{impeller type}\right) \qquad \text{Equation 4-18}$$

Many researchers exploited the Zwietering equation to determine the minimum speed required for complete off-bottom suspension by determining the dimensionless parameter (S) specific for their design. Some are critical, primarily because it is a visual technique hence it is subjective, especially when used with fine suspension material. Another disadvantage is that it did not consider the stagnant part of the vessel, where the particle may take a long time to off-bottom that would lead to overestimation of power consumption. (Armenante and Nagamine, 1998; Chitra and Muruganandan, 2014; Collignon et al., 2010).

In this study, S coefficient was determined based on the geometry of the horizontal tubular bioreactor (HTB). The aspect ratio (T/D) of STR was replaced with the aspect ratio of HTB by L/D and clearance ratio (T/C) by the impeller diameter by vessel diameter (d/D). Another important feature which played a crucial role in defining the S, is the ratio of liquid height from the bottom of the impeller $(h_{L,d})$ to the impeller diameter (d). This ratio changed with the change in fill volume. As L/D and d/D are fixed geometries for the HTB, so the only variable will be $\frac{h_{L,d}}{d}$, The Equation 4-18, therefore modified to Equation 4-19 to express the dimensionless parameter (S) for HTB. It was expected that the value of S to be the same for all 4 solids loadings.

$$S = f\left(\frac{L}{D}; \frac{d}{D}; \frac{h_{L,d}}{d}; \textit{impeller type}\right) \qquad \text{Equation 4-19}$$

The value of S was determined experimentally by measuring the minimum impeller speed (N_{js}) to off-bottom the beads at each impeller speed at each impeller immersion ratio with each solid loading. Thereafter, modelled (N_{js}) value was determined by Equation 4-17, and comparison was carried-out

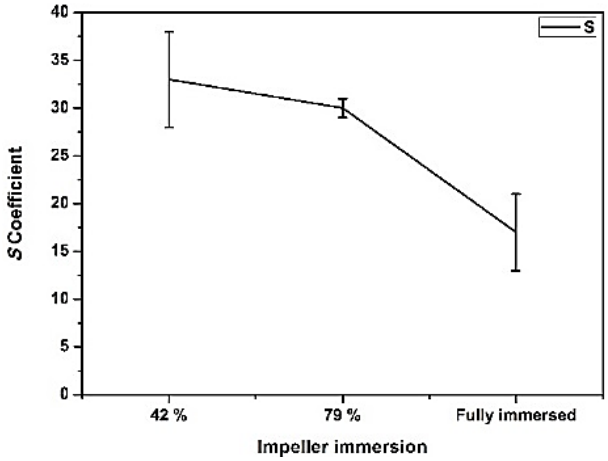

Figure 4-21 Relationship between Zwietering's S coefficient and impeller immersion. The error represents the standard deviation in the mean.

Figure 4-21 indicated that with the increase in impeller immersion, the value of S decreases significantly.

Table 4-15 Percentage error and R^2-values with respect to solids loading and impeller immersion

Solids loading (%)	Error (%)	R^2
0.25	17	0.71
0.50	13	0.88
0.75	4	0.95
1.00	15	0.32
Impeller immersion (%)		
42	13	0.54
79	4	0.82
Fully immersed	20	0.33
Overall	12	0.83

The tabulated information given in Table 4-15 displayed the percentage error and the coefficient of determination (R^2-values) concerning both solids loading and impeller immersion, as well as overall values. The acceptable threshold for error should be less than 15 %, while that for the R^2-value is above 0.8 (Kuncewicz et al., 2005). The error associated with overall N_{js} calculation in Table 4-15 indicated that the Zwietering equation satisfy the criteria with an overall 12 % error and R^2 = 0.83. However, the error and R^2 at 0.25 % solids loading and the R^2 at 1.00 % does not meet this criterion as highlighted with yellow. The error and the R^2 value of the impeller immersion of 42 % and fully immersed impeller at 4 L also showed large error bars for the determination of S as shown in Figure 4-21. Alternatively, the residual plot of impeller immersion and N_{js} with solid loading indicated the random distribution of data points as illustrated in Figure 4-22. The data points which are close to the baseline at zero are the best fit than the points which are distantly placed. The red rectangle enclosed the data points which satisfied the criteria of the Zwietering equation.

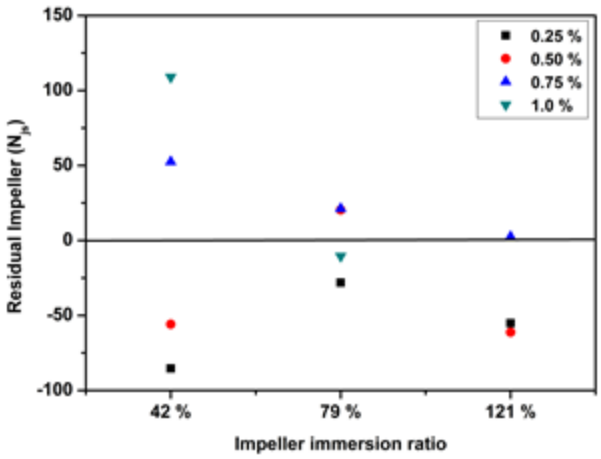

Figure 4-22 Residual plot of Zwietering equation with respect to impeller immersion.

As Zwietering model was initially developed for the STR, Using the same Zwietering model was modified for the HTB. The coefficients were recalculated by least squares regression to minimise the sum of squares error and improve the fit of the model. Through this analysis, Equation 4-20 was formed from Equation 4-17

$$N_{js} = \frac{S^{0.965} \cdot \nu^{0.048} \cdot d_p^{0.046} \cdot \left(\frac{g \cdot \Delta\rho}{\rho}\right)^{0.092} \cdot \chi^{0.32}}{d^{0.10}} \qquad \text{Equation 4-20}$$

The percentage error and R^2-values for this equation are shown in Table 4-16 and the residuals plot represented the distribution of the data points in Figure 4-23

This modified Zwietering equation meet both the criteria of overall % error at 9 % and R^2 values at 0.992 with both the solid loadings and at each impeller immersion (volume). R^2-values and the % error with respect to the independent solid loading and impeller immersion parameters, however, show some notable deviations below the threshold. The values are highlighted in yellow in the Table 4-16. The R^2-values at 79 % immersion (3 L) and at fully immersed impeller at 4 L came out to be 0.083 and 0.669 respectively. The deviation occurred may be due to the impeller immersion ratio which influenced the value of S and then N_{js}. However, this modified Zwietering equation is better in determine the value of N_{js}. The residual plot showed a better fit of the distribution of data points to the residual plot obtained using the original modified Zwietering equation.

Table 4-16 Percentage error and R^2-values with respect to solid loadings and impeller immersion of modified Zwietering equation

Solids loading (%)	Error (%)	R^2
0.25	7	0.984
0.50	13	0.970
0.75	4	0.996
1.00	12	0.952
Impeller immersion (%)		
42	4	0.934
79	8	0.083
Fully immersed	15	0.669
Overall	9	0.992

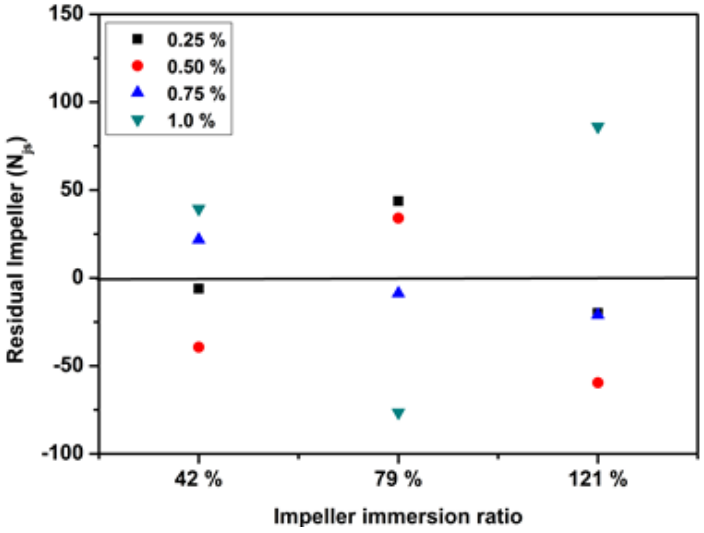

Figure 4-23 Residual plot of modified Zwietering equation with respect to impeller immersion

Apart from that, Figure 4-24 explains the effect of impeller immersion on the minimum agitation speed by plotting the experimentally determined N_{js} with that of modified Zwietering Equation 4-20

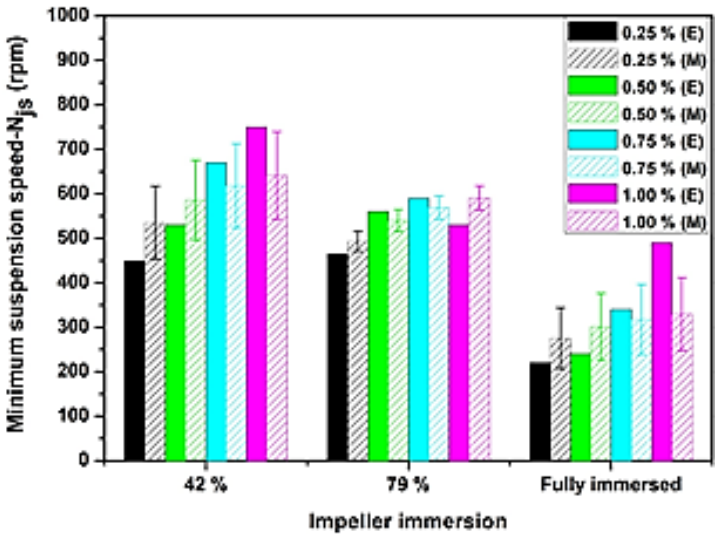

Figure 4-24 Experimental and predicted values of minimum suspension speed with respect to impeller immersion. The solid column represented the experimental values (E) and modelled (M) values denoted by column with medium pattern.

Figure 4-24 showed the two sets of data, one is experimental denoted by (E) with solid columns and the predicted values through Zwietering equation denoted by (M) by column with medium pattern. The modelled values follow the experimental values. With the increment in solid loading at 42 % and at fully immersed impeller at 4 L, the value of N_{js} exponentially increases wherein 79 % immersion (3 L), the increase was not proportional. It indicated that off-bottom clearance is much better at all the solid loading at 3 L volume than at 2 L and 4 L. The modelled values also followed the experimental value. However, at 0.25 % and 0.50 % of solid loading, there is a maximum in experimental N_{js} near 79 % immersion, a trend which the model does not predict. However, 0.75 % and 1.00% does not show a maximum in N_{js}, and it can be said that the model follows this trend more so than that of 0.25 % and 0.50 %. This error was calculated by propagating

the error in S to N_{js} (DOI: 10.25375/uct.13570970). With the error in S, the error in predicted N_{js} is large, varying from 5 % to 25 %. Although most of the data points do not lie on the lines generated by the model, they lie within the error margins in N_{js}, showing that the modified Zwietering equation is able to predict the experimental values.

4.3.6 Power consumption profile in HTB

The power consumed by HTB was measured using the temperature method as described in section 3.4.4. The power consumption profile of HTB is shown in Figure 4-25

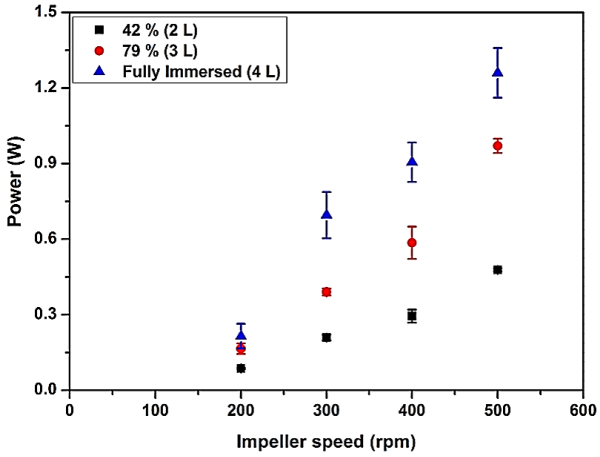

Figure 4-25 Power consumption profile of HTB at different volumes at various agitation speeds

It has been observed that as the impeller speed increases power consumption increase. Power consumption also increases as the impeller immersion ratio increases. This is the energy imparted to the bulk fluid by the impeller to counter the viscous and drag forces. In the case of 4 L, when the impeller is fully immersed, agitated impeller experienced more drag forces as compared to 2 L and 3 L volume, when the impeller was 42 % and 79 % immersed. This has impacted the mixing behaviour of the bioreactor as well.

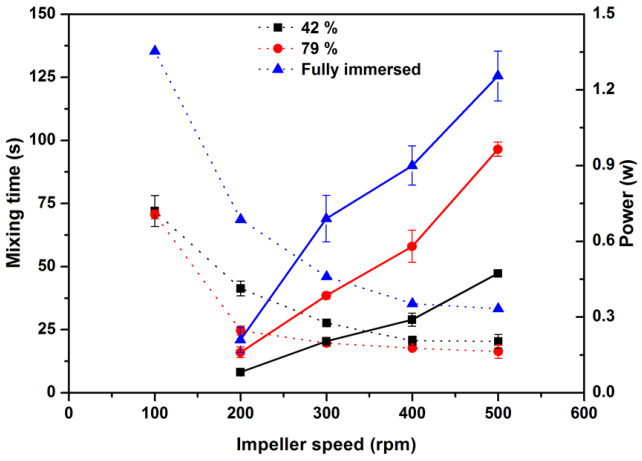

Figure 4-26 Mixing time Vs power consumption with different impeller immersion ratios at different impeller speeds. Solid lines represented the power consumption at different impeller immersion ratios whereas dotted lines indicated mixing time. The error bars represented the standard deviation with n=3 repeats

Figure 4-26 explains the mixing time profile versus power consumption for each impeller immersion. It has been in a common knowledge that as the impeller speed increases, mixing time decreases so as the power consumption increases. The main purpose of the impeller design is to reduce mechanical shear and mixing time while improving mass transfer efficiency. This could be achieved by installing specific impeller that can provide high flow number and low power number (Np). For a specific impeller geometry at a given impeller speed, mixing time is inversely proportional to flow number and directly proportional to power number (Varley and Birch, 1999). From Table 4-12, it can be concluded that as the impeller speed increases at a specific impeller immersion (fill volume), Reynolds number increases and power number decreases. It has been suggested that to maximise the pumping capacity and reducing the mixing time, it is better to use large agitator with slow speed than small agitator with high speed, therefore the spiral impeller is present across the length of the horizontal vessel, agitating the liquid at a low impeller speed consuming low power as compared to STR (Nienow, 2015, 1997). It has been observed that power density (P/V) for HTB increases more than double when impeller speed increased from 200 rpm to 300 rpm for 42 % and 79 % impeller immersion whereas the difference increases to nearly 6 times when impeller speed ramped up to 500 rpm. This is evident that at lower impeller speed, power consumption is low while mixing is effective.

The power consumption has also a direct relationship with the mass transfer efficiency of the bioreactor. In the case of the HTB, the spiral impeller has multiple blades which distribute the energy across the length of the vessel, when the contact between the liquid surface and impeller blades are optimum, mixing time and mass transfer profile increases as thus improving the mass transfer efficiency as shown in Figure 4-27

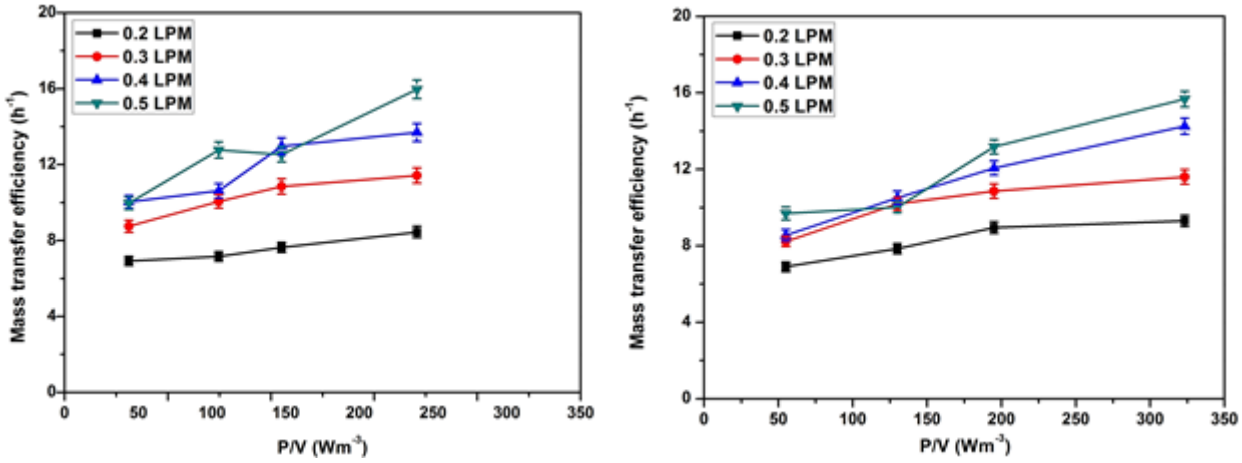

a b

Figure 4-27 Mass transfer efficiency Vs power input at (a) 42 % and (b) 79 % impeller immersion

Figure 4-27 explains that as the power input increases at a fixed airflow rate, mass transfer increases. Furthermore, with the increase in airflow rate also mass transfer value increases in 2 L and 3 L volume. This is mainly because air hold up and residence time increase as the power input increases which directly impacted the mass transfer efficiency.

4.3.7 Comparison of HTB with other bioreactor systems

This section aims to compare the performance of the various bioreactors using different operating principles of working in terms of mixing, mass transfer and the power utilisation profile. The efforts have been made to compare the engineering characteristics of the horizontal tubular bioreactor (HTB) with other designs such as conventional stirred tank, horizontal oscillatory baffled photobioreactor (PBR) (designed at CeBER, specifically for algal culture), wave-induced bioreactor, shaken bioreactor and CelCradle. It is known that the mass transfer efficiency, mixing time and power consumption collectively define the appropriateness of the bioreactor for the growth of biological organisms. Type of agitation alone (with or without impeller type) responsible for the fluid motion that further influence the mixing, mass and heat transfer and shear conditions inside the bioreactor. The interdependence of fluid motion, stirring speed and power input dictates the overall suitability of the bioreactor which dynamically change with the change in scale (liquid height), shown in Figure 4-5. Therefore, the comparison of the HTB with STR, wave-induced, shaken, PBR and CelCradle was considered.

Nienow, (2006) reported that, for the wide range of animal cells to grow, the value of $\boldsymbol{k_L a}$ required in the media and the power density (P/V) falls in the range of 1 - 15 h^{-1} and 10 - 250 W m^{-3} respectively. Table 4-17 showcased the values of mixing time, mass transfer coefficient and power density of various types of bioreactors found in the literature, where the fluid flow was generated by different working principles. For comparison of HTB with STR, single-use stirred bioreactor-Mobius CellReady (3L) was considered because of its similarity in design and set-up with that of a conventional system. Wave bioreactor and Biowave were used for wave-induced motion, horizontal oscillatory baffled photobioreactor employed three different kinds of baffles to study the fluid motion namely donut, half-moon and perforated half-moon baffles, orbitally shaken bioreactor make use of periodically oscillation of media and CelCradle represented packed-bed bioreactor where surface-aeration was used to oxygenate the media.

Table 4-17 Comparison of different bioreactor systems w. r. t. mixing time, mass transfer efficiency and power consumption profile. NA: Not available

Type of Bioreactor	Mixing time (s)	Mass transfer ($k_L a$) (h^{-1})	Power consumption (P/V) (Wm^{-3})	References
HTB	16 - 72	5.25 - 16	43.5 - 323	This work
Stirred tank bioreactor (Stirred Mobius Cell Ready 3L bioreactor)	3.4 – 27	6.5 - 35	0.26 – 38.3	Kaiser et al., (2011)
Wave-induced	5 – 10 s/ 10 L	4 (10 – 100 L)	NA	Singh, (1999)
Oscillatory baffled PBR	12 - 45	4.9 - 17.2	216 - 461	Jones, (2015)
Orbitally shaken bioreactor (OSR)	10 – 30 s	4 - 30	500 (120 rpm) 1.5 L	Tissot et al., (2011)

Mixing time is the simplistic tool to evaluate the performance of the bioreactor. Different fluid flow pattern in different bioreactor displayed a varied profile of mixing. In this research, HTB was run at 1, 2, 3 and 4 L volume with different impeller immersion ratios, but for comparison, values taken were of 2 and 3 L only. Mixing time in HTB fall in the range of 16 – 72 s with the impeller speed of 100 to 500 rpm, whereas in the case of Mobius CellReady 3L bioreactor, it was reported in the range of 3.4 – 27 s, when ran for 1.5 to 2.5 L with the stirring speed ranged from 100 – 250 rpm. It is a common phenomenon that with the increase

in agitation (rpm), mixing time decrease. It has also been reported that in stirred tank bioreactor, the mixing time of 54.7 and 7.0 s was reported for 2 L volume when the stirring speed was adjusted to 50 and 250 rpm respectively (Kaiser et al., 2011), whereas in the case of HTB, mixing time of 41 s was reported when ran at 200 rpm. The low mixing time in STR could be because of axial motion generated by the marine impeller and continuous sparging of air, whereas HTB used surface aeration and motion generated in HTB was bidirectional as shown in Figure 4-9. Liquid height also played a crucial role in determining the engineering parameters. Mixing time significantly varies in the case of HTB for 2 L (41 s) and 3 L (25 s) for the same stirring speed of 200 rpm. The same applies to the wave and shaken bioreactor where rocking (up-down) and orbital motion at varied angle and speed generate a liquid-air interface that enhances bulk mixing and mass transfer. Singh, (1999) reported that mixing time for wave-induced bioreactor fall between 5 -10 s for 10 L working volume (20 L bag) and around 60 s for 100 L (200 L bag). In an orbital shaken bioreactor, Tissot et al., (2011) revealed that 10 – 30 s is the range for mixing time at a scale range from 5 mL to 1500 L, on the contrary, mixing time in STR increases with the increase in scale and it may reach to more than 60 s at large-scale bioreactor. The horizontal oscillatory baffled PBR (plug-flow) bioreactor showed good mixing with different impeller types, donut, half-moon and perforated moon which came out in the range of 12 – 45 s. No mixing time data was found in the case of CelCradle for comparison. For lab scale CelCradle system, complete cell culture media vertically oscillates periodically by decompression and compression of the bellows holding the culture medium and for large scale “Tide Cells” mixing was done externally before pumping the media inside the tide cells (Cesco Bioengineering, n.d.)

From the above discussion about mixing time, the inference can be drawn that although the working principle of the bioreactor under consideration are different yet with the increase in agitation (rpm), rocking angle, frequency of orbitally shaking enhances the mixing efficiency. The comparison of these bioreactor seems unjust because stirred tank uses vertical marine impeller whereas HTB uses spiral impeller along the length of the vessel and wave and OSR performed mixing without impeller. Among these bioreactors, HTB also showed good mixing profile at 2 L and 3 L. The data for 1 L and 4 L has not been considered for comparison because impeller immersion ratios at 1 L (4 %) and 4 L (fully immersed) does not correlate to the literature values.

Mixing profile directly related to the distribution of gases and material homogenously to the growing cells which influenced the mass and heat transfer capabilities of the bioreactor. The mass transfer efficiency of these bioreactors (mentioned in the above table) differed greatly because of the method of oxygen transfer. HTB with a spiral impeller depends on surface aeration, Mobius Cell Ready with a marine impeller and air sparging whereas, wave and OSR depends on rocking and orbital shaking for the fluid motion rather than using any mechanical devices (stirrer) for surface aeration. The $k_L a$ value found to be 5 – 16 h^{-1} for HTB when the airflow rate was 0.2 to 0.5 LPM in the headspace and the stirrer speed kept between 100 rpm to 500 rpm. In the case of Mobius Cell Ready, this falls in the range of 6.5 – 35 h^{-1} when the flow rate of air was 0.5 LPM and the impeller speed was 200 rpm maximum (Kaiser et al., 2011). The surface aerated bioreactor without agitator also exhibited good mass transfer capabilities e.g. wave bioreactor showed the maximum value of 4.0 h^{-1} at 10 L and, a glass spinner flask (10 L) showed the $k_L a$ value of 0.4 h^{-1} at the same scale (Singh, 1999). On the other hand, horizontal baffled bioreactor reached to 4.9 – 17.2 h^{-1} (Jones, 2015). Orbitally shaken bioreactor showed mass transfer efficiency in the range of 5 – 15 h^{-1}, when operated at 1.5

L capacity at 0.3 LPM of airflow rate with the agitation rate of 80 – 150 rpm. In general, various OSR including Tube spin, the value of $k_L a$ falls between 4 – 30 h^{-1} at a volume of 1 L - 2000 L with an agitation rate appropriate for cell culture growth (Tissot et al., 2011).

Power per unit volume or power density is the measure of energy dissipated while mixing the volume under consideration. Temperature method was employed to measure the power input in HTB for 2 L and 3 L volume which measured the power input of 43.5 – 323 Wm^{-3}. The computational fluid dynamic (CFD) method was used in determining the power input in Mobius Cell Ready 3 L bioreactor, where fluid momentum acted on the impeller and impeller shaft. The values predicted through this method was 0.26 – 38.3 Wm^{-3}. Singh, (1999) did not mention the power input in wave bioreactor, although Eibl et al (2009) have given a detailed account of the engineering aspect of the wave-induced bioreactor where they had mentioned the peculiarities of the different bag-based bioreactor whose working is based on the wave motion of the fluid such as Wave Bioreactor, BioWave, BIOSTAT CultiBag RM, CELL-tainer, AppliFlex and Tsunami bioreactor. In the case of BioWave, specific power input was calculated by means of CFD using 'Static Model', which can be explained as a fluid system move with a constant velocity if the sum of all the momentums acting on the system are in equilibrium that showed static behaviour of fluid in the bag. Furthermore, by determining the point of gravity of the bag and the total surface area of the fluid and the resulting momentum acting on the system, the necessary work-done was calculated. By this method, Eibl et al., (2009) determined the power input of 80 – 561 Wm^{-3} in BioWave bioreactor at 2 L with 50 % fill volume at 10^o of rocking angle with 6 – 30 rpm. Jones, (2015) reported the power input for Horizontal baffled PBR of 131 – 634 Wm^{-3} at a rocking angle of 10^o with an increase rocking frequency from 10 – 40 rpm and 50.8 – 482 Wm^{-3} with an increase rocking angle of 2 - 10^o and at rocking rate of 30 rpm. In the case of OSR, power input of 500 – 1500 Wm^{-3} was reported at 120 – 150 rpm with 2 L volume.

4.3.8 Summary

The focal point of this chapter was to discuss the designing, fabrication and abiotic engineering characterisation of the horizontal tubular bioreactor with the spiral impeller. In the beginning, a criterion was set out for the "ideal" bioreactor design which can satisfy the current industrial requirements by flexibly accommodating wide varieties of processes in batch mode to continuous processes in combination with PAT with lower capital and running cost. Thereafter, the working principle and proposed fluid flow pattern in HTB was anticipated from the literature where vertical helical mixer design was discussed by Holland and Bragg in (1995).

A detailed account of designing and fabrication of the HTB was given, where a design parameter for a spiral impeller was adapted from the Tsui and Hu (2008) for different combinations of aspect ratios (L/D) for the horizontal vessel. A criterion was set for the selection of the best combination of the aspect ratio which can accommodate the maximum volume of 5 L and a minimum volume which can have significant impeller immersion ratio. Upon calculations in Microsoft Excel, the best-fit aspect ratio D=H=L/4.6 was decided. A detailed User's requirement specifications based on the design configuration was established and then the bioreactor was fabricated for further engineering evaluation.

Engineering characterisation of the HTB was initially carried out to visualise the fluid flow pattern through phenolphthalein method and mixing time through conductivity method for different impeller

immersions and at different impeller speeds. Thereafter, three mixing time models were analysed for their best fit to the experimental data. Statistical analysis was carried out with Two-way ANOVA with replication. It has been observed that 4 % impeller immersion (1 L) does not prove enough contact between impeller blades and the bulk liquid to move the fluid effectively for proper mixing, and mass and heat transfer. Hence 1 L volume was not in the scope of working volume in subsequent experiments. Fully immersed impeller (4 L) experienced greater fluid drag forces as the impeller speed increase and exhibited more power consumption as compared to 42 % (2 L) and 79 % (3 L) impeller immersion. The mixing time profile also showed that the 2 L and 3 L volume provide the optimum window for the HTB performance.

Mass transfer efficiency of the bioreactor was then calculated only for 2 L and 3 L fill volume. It has been found that with the increase in airflow rate (0.2 – 0.5 LPM) and impeller speed (10 – 500 rpm), $k_L a$ value increases, which fell in the range of 5 – 16 h^{-1}. A mass transfer model was also made which considered Reynolds number, impeller circulation number and impeller power number along with geometric specific function like impeller immersion ratio. The model was fitted with experimental value and Two-way ANOVA with replication test was performed. It was found that the interaction between variables such as impeller speed and $k_L a$, aeration rate and $k_L a$ vary for 2 L and 3 L. This could be due to the impeller immersion directly influencing the impeller's mixing capacity.

This chapter also covered the minimum suspension speed applied to the spiral impeller. The alginate beads with the size of 200 ± 50 µm were used for the solid loading of 0.25, 0.50, 0.75 and 1.0 wt % for reactor volumes of 2 (42 % impeller immersion), 3 (79 % immersion) and 4 L (full immersion). The S value was calculated which is a function of vessel geometry and impeller type and vessel to impeller ratio (impeller immersion). It has been found that the S value decreases when the impeller immersion (Volume) increases. The mean S value for 42 % impeller immersion (2 L) came out to be 33 ± 5. Zwietering equation was modified to apply for the HTB model, and the suitability was observed by plotting residuals plots.

Power consumption profile of the HTB was also determined through temperature method and a comparison was drawn to elucidate the effect of power input on the mixing time, and mass transfer. The maximum power drawn was around 1.0 W for 2 L and 3 L fill volume.

At the end, a comparative study was carried out to find the appropriateness of the HTB among other commercial bioreactor systems using different operating principles in terms of mixing, mass transfer and the power utilisation profile. For that, conventional STR, horizontal oscillatory baffled photobioreactor (PBR), wave-induced bioreactor, shaken bioreactor and CelCradle were used. It was found that the engineering performance of the HTB is comparable with other bioreactor systems.

5 Biotic characterisation of Horizontal Tubular Bioreactor (Results and Discussion - Part II)

This chapter explores the biotic characterisation of the HTB and evaluates its suitability for the cultivation of mammalian cells. The performance of the HTB was tested by using suspended wild-type CHO cells and transfected CHO cells expressing somatic angiotensin converting enzyme (sACE) protein. The maximum cell densities and protein production were compared to those of other cultivation platforms. The media screening was performed in shaker flasks with six different commercially available media. Thereafter, shear studies were performed to assess the effects of impeller stirring on the mammalian cells during cultivation, using the cell death constant (k_d) as an indicator. An operational window for the HTB was established based on these results (abiotic and biotic).

5.1 Media screening for enhanced cell growth

The Six new commercial media (Table 3-1) were evaluated for their ability to achieve maximum cell density. CHO cells were initially adapted in SFM4CHO powder media, and therefore SFM4CHO was designated as the reference medium (M6). The cells grown in medium M1 reached a maximum cell density of 2.15 x 10^6 cells mL^{-1} on day 5. Medium M2 supported a cell density of 2.0 x 10^6 cells mL^{-1} and cells grown in M3 attained a cell density slightly above 1.0 x 10^6 cells mL^{-1} on day 8. Cells grown in M4 and M5 did not reach a cell density of 1.0 x 10^6 cells mL^{-1}, whereas cells grown in M6 reached a cell density of 2.18 x10^6 cells mL^{-1} on day 4, with a viability of 95 %. The cell density and viability of these different media was measured until day 6, as the cells reached stationary stage on day 4 (Figure 5-1). Cells grown in M1 and M2 remained at above 90% viability at the end of day 8, whereas cells grown in M3, M4, M5 and M6 had cell viabilities of 87.2%, 86.9%, 85.7% and 89.7%, respectively. Based on their ability to support higher cell densities, M1 and M6 were superior to the other media.

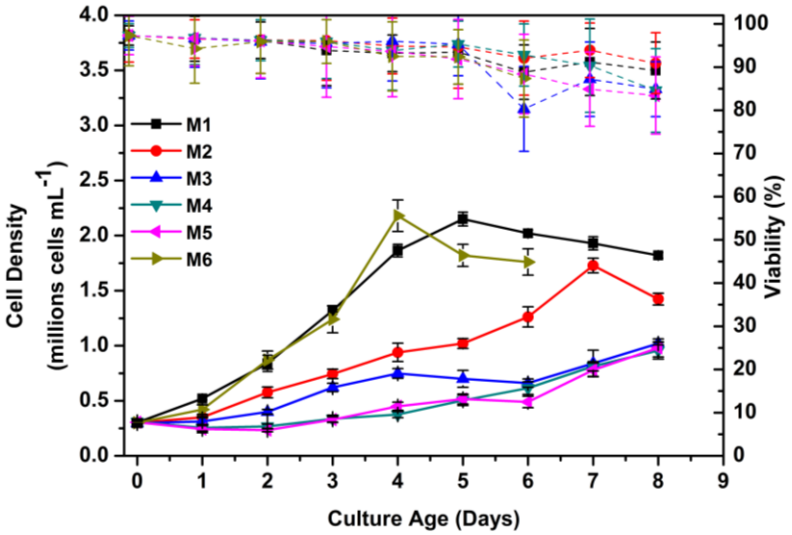

Figure 5-1 Screening of six commercially available media for their ability to support the growth of CHO cells. The media M1 is represented by the symbol (–■–), M2 (–●–), M3 (–▲–), M4 (–▼–), M5 (–◄–), and M6 (–►–). The cell density is denoted by solid lines, whereas viability percentage is represented by dotted lines. Data represents the mean ± the standard deviation of 3 independent replicate

Another important selection criterion is the production of sACE by cells grown in various media. The sACE expression level was measured in cells grown in each medium on day 4 and day 8 of culturing, except for M6 where sACE expression was measured on day 4 and day 6 (Figure 5-2). All the media tested supported sACE production, with cells grown in M1 showing the highest concentration of protein (17.63 mg mL^{-1}) on day 8. This could be because M1 has all the necessary nutrients for cell growth, such as hypoxanthine and thymidine, except for stable glutamine, which was supplemented externally at a concentration of 4.0 mM. Reconstituted M6 powder media also contained the necessary nutrients for protein expression. M2 lacks hypoxanthine and thymidine, which play crucial roles in nucleic acid synthesis and energy metabolism and is more suited for the purpose of selecting a clone. M3 medium is specifically designed for producing human antibodies and recombinant protein production using the PER.C6 platform technology. Cells grown in M2 and M3 media reached the maximum protein production of approximately 10.16 and 6.84 mg mL^{-1} respectively on day 8. M4 and M5 media are devoid of growth factors such as insulin and other peptides and hydrolysates, and therefore supported limited protein production of slightly more than 3 mg mL^{-1}. Both M4 and M5 are meant to be used in combination, in addition with added cell boost supplement 7a and 7b, to support cell growth and protein production (Hyclone, 2016a, 2016b, 2015a, 2015b). Large clumps of cells formed in the shaker flasks of M2, M3 and M4 (data not shown). This could be caused by intrinsic factors of the media, and from the stress experienced by cells during shaking.

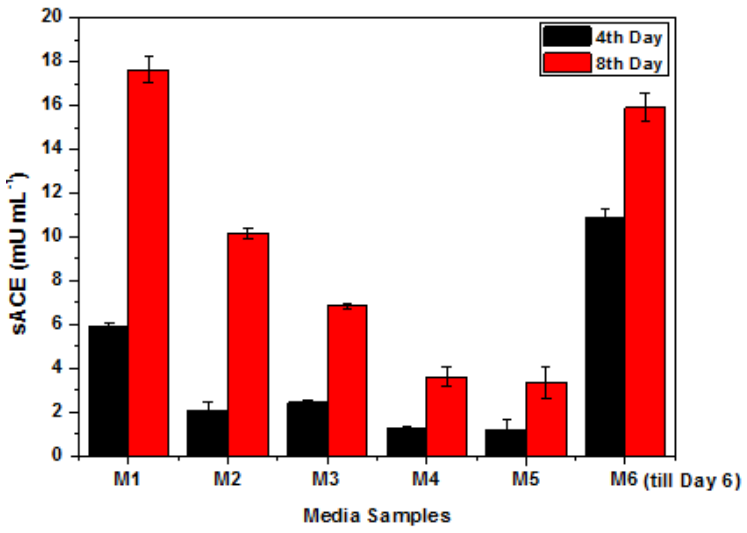

Figure 5-2 sACE expression levels in CHO cells grown in different commercially available media (M1-M5) on day 4 and on day 8 and M6 on day 4 and day 6 represented by black and red bars, respectively. M1 (HyCell CHO), M2 (HyCell CHO w/o hypoxanthin, w/o thymidine), M3 (CDM4PerMAb), M4 (ActiPro), M5 (ActiSM) and M6 (SFM 4CHO – Powder). Data represents the mean ± the standard deviation of 3 independent replicates

When protein concentration was expressed as per unit biomass (per 1x 10^6 cells mL^{-1}), the protein production profile showed a similar trend as in Figure 5-3. When the cell density factor was accounted for, it could be seen that M2 and M3 also supported protein expression, despite the poor cell density achieved during the experiment (Figure 5-3). Cells grown in media M4 and M5 showed comparatively poor protein expression.

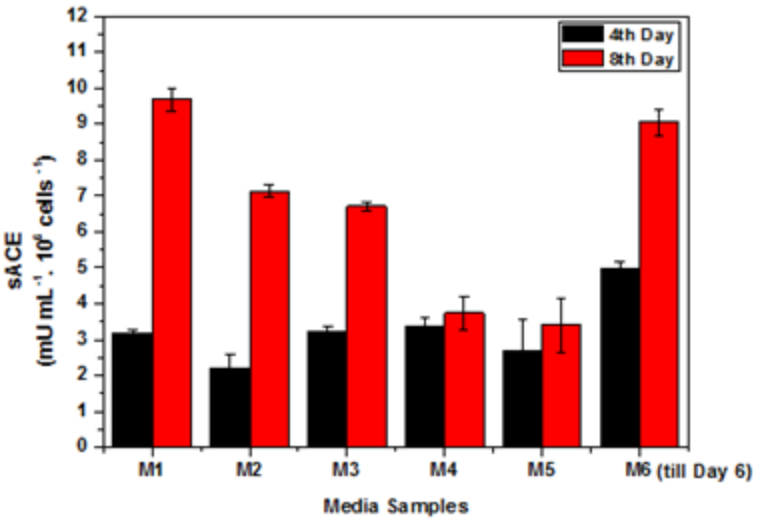

Figure 5-3 The profile of sACE expression in different commercially available media (M1-M6) on (A) day 4 and (B) day 8 after normalizing cell density to 1 x 10^6 cells, except for M6, which was grown until day 6. Data represents the mean ± the standard deviation of 3 independent replicates

To select a suitable and affordable medium, a cost analysis was performed. The price (in ZAR) to produce 1 mg mL^{-1} x 10^6 $cells^{-1}$ was calculate and is shown in Table 5-1. Out of the six commercially available media tested, the most cost-effective medium for producing sACE is M6. Although both M1 and M6 had similar results for cell density and protein expression, M1 costs R9.54 to produce 1 mg mL^{-1} x 10^6 $cells^{-1}$ of sACE, while M6 only costs R3.69. The price of M1 (liquid medium - HyCell CHO) is ZAR 3079 per litre as compared to M6 (SFM4 CHO - powder) media, which is ZAR 1114 per litre, which is nearly three times that of M6. The production cost of the other media is comparatively high, and they were therefore not considered further. Powder media requires extra care while reconstituting into complete liquid growth media, with filtration through a 0.22 µ filter required after dissolving. It is advisable that the freshly prepared media should be incubated at 37°C for 48 h to ensure sterility before use.

Table 5-1 Cost analysis of the media (M1 - M6) to determine the price per mg of sACE produced in HTB

Media	VCD on day 8	sACE mg x 10^6 $cells^{-1}$ mL^{-1}	Media Cost (ZAR) +15 % VAT		Price in ZAR per 1 mg sACE produced
			L	30 mL	
M1	1.82	9.68	3079	92	9.54
M2	1.42	7.14	3674	110	15.44
M3	0.89	7.69	2984	90	11.65
M4	0.96	3.75	3879	116	31.01
M5	1.04	3.22	3998	120	37.28
M6	1.76	9.05	1114	33	3.69

In the current research, M6 medium was selected, particularly given that the CHO cells were already growing in M6 medium at the beginning of the research, and because of its ability to support cell growth and its relative affordability. Therefore, based on these media screening experiments, M6 (SFM4 CHO - powder) was selected as the preferred medium for cultivation of CHO cells in the HTB.

5.2 Batch fermentation of CHO cells in an HTB

Next, the batch fermentation of CHO cells was tested in an HTB. The first batch was CHO cells expressing somatic ACE (sACE), while the second and third batches were wild-type CHO cells. The starting seed inoculum for all the batches was 0.3 x 10^6 cells mL^{-1} and the process conditions were kept the same until the batch attained peak cell density (Refer section 3.3.2).

5.2.1 Cell growth and protein production

The primary objective of growing cell culture batches inside the HTB was to establish its suitability for attaining peak cell density under a given set of process parameters. In the current research, the target was to achieve a cell density of ≥ 5.0 x 10^6 cells mL^{-1} with a viability ≥ 85 % as a criterion to harvest the batch. This is because the cell density of ≥ 5.0 x 10^6 cells mL^{-1} falls within the limits of middle-range cell density, as per current industry norms and viability below 85 % can generate cellular debris in the culture broth, which would further increase the concentration of impurities such as host cell proteins and host cell DNA complicating the downstream processing steps (Gronemeyer et al., 2014; Pörtner, 2015; Shukla and Gottschalk, 2013). Additionally, the protein product produced in the batch would be at risk of degradation because of the action of proteases.

Figure 5-4 shows that batch 1 had a short lag phase, thereafter the CHO cells started actively dividing, and attained a peak cell density of 4.06 x 10^6 cells mL^{-1} on day 5, when the viability of the culture was above 90%. Figure 5-4 also shows that the protein production was directly linked to the cell density, with the cell density increasing alongside the concentration of the protein. The sACE productivity was at maximum of 465 mg mL^{-1} on day 9. The day 8 sample was not analysed for sACE productivity and is not present on the graph. The kinetic parameters (doubling time and growth rate) of batch 1 between 24 h and 96 h were 22 h^{-1} and 0.031 h^{-1}, respectively (DOI: 10.25375/uct.13570970).

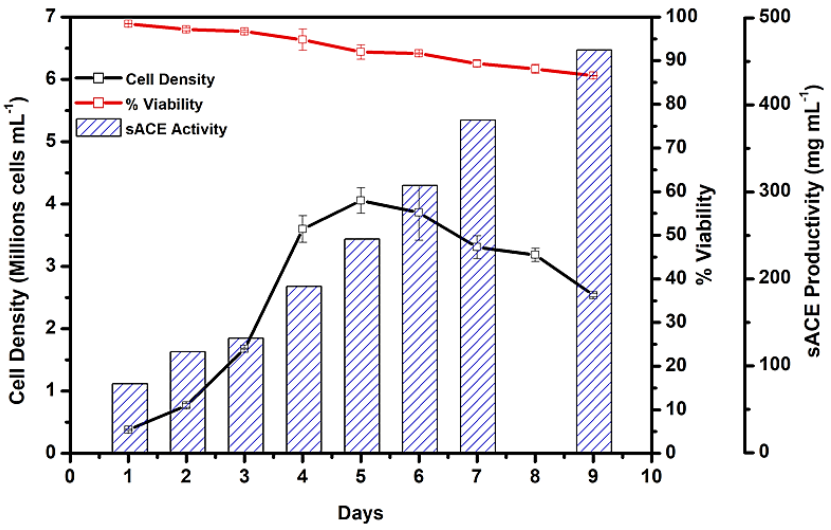

Figure 5-4 Growth profile of CHO cells during batch 1 in the HTB. The black solid line represents the cell density, % viability is denoted by the red line, and the blue columns indicate the profile of sACE production. Data represents the mean ± the standard deviation of 2 independent replicates.

Batch 2 was CHO cells without the expression of any recombinant protein. The peak cell density achieved in batch 2 was in the order of 5.5 x 10^6 cells mL^{-1}, and the cell viability decreased to 92.8 % on day 8. The hydrodynamic shear sensitivity test was initiated on day 8. The dropline on Figure 5-5 segregates the two different phases in the HTB. Until day 8, the bioreactor was operated at pre-defined process conditions, with an impeller speed of 150 rpm, thereafter, the impeller speed was increased to 300 rpm. The impact of increasing the impeller stirring from 150 to 300 rpm resulted in a rapid drop in cell density and viability over Day 9 and 10, as illustrated in Figure 5-5. The kinetic parameters (doubling time and growth rate) of batch 2 between 48 h and 96 h were 30 h^{-1} and 0.023 h^{-1} respectively.

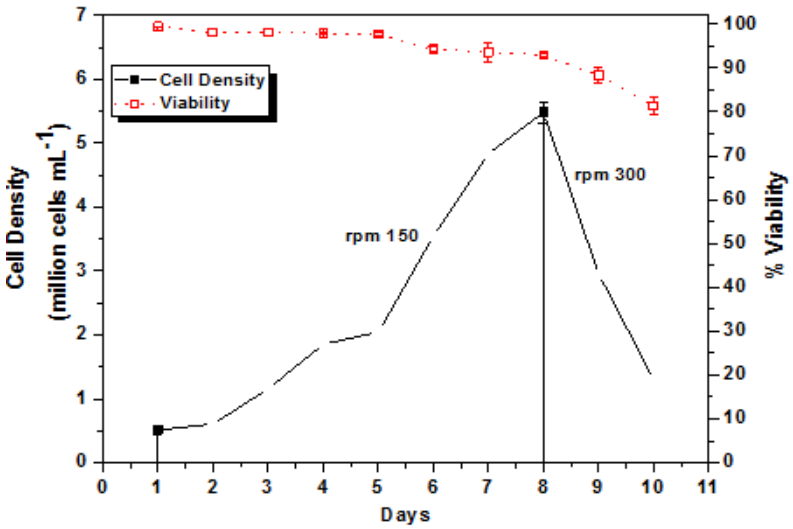

Figure 5-5 Growth profile of CHO cells during batch 2 in the HTB. The black broken line represents the cell density, and % viability is denoted by the dashed red line. The dropline segregates the growth phases of the batch at 150 rpm from the batch at 300 rpm. Data represents the mean ± the standard deviation of 2 independent replicates.

Figure 5-6 showed the different levels of batch 2 in the HTB where change in turbidity at day 3 and 5 was clearly seen which signify the increase in cell number. The magnified sample, from the bioreactor (Figure 5-6 (d)), onto the haemocytometer showing the cellular health inside the bioreactor. The cells were single-cell suspended in the culture and were bright and healthy when treated with trypan blue.

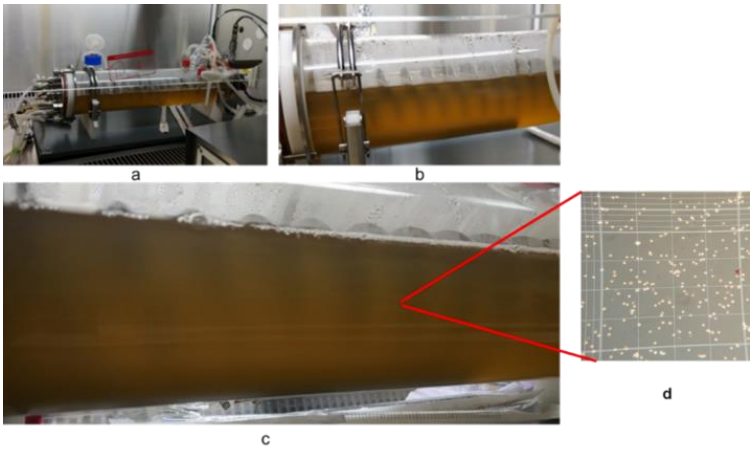

Figure 5-6 Pictures of batch 2 in HTB (a) complete horizontal tubular bioreactor (b) culture medium at day 3 (c) culture medium at day 5 indicated the increase in turbidity of the culture, indirectly signify the conducive conditions for the cell growth (d) sample from the bioreactor on the haemocytometer showing a healthy state of the cultured cells

Batch 3 followed the same growth pattern of CHO cells as batch 1, where the highest cell density achieved was 4.14 x 10^6 cells mL^{-1} and the viability were 92 % on day 5 under normal process conditions. During the stationary phase, the % viability dropped from 92 % on day 5 to 86.45 % on day 7, as shown in Figure 5-7, before subjecting the batch to hydrodynamic shear exerted by the spiral impeller at different speeds. The kinetic parameters (doubling time and growth rate) of batch 3 between 24 h and 96 h were 23 h^{-1} and 0.030 h^{-1} respectively.

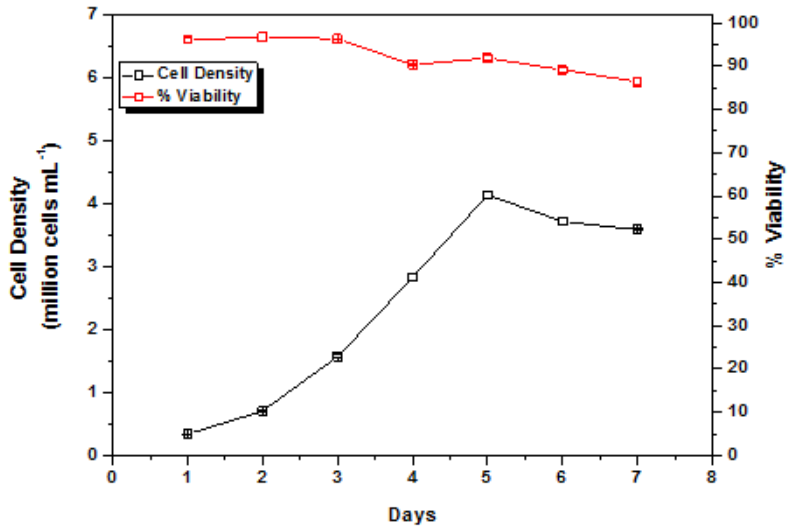

Figure 5-7 Growth profile of CHO cells for batch 3 in an HTB bioreactor. The cell growth profile depicted in black line with % viability with a red dotted line. Data represents the mean ± the standard deviation of 3 independent replicates.

The first key indicator for the suitability of the HTB with a spiral impeller was to achieve middle to high-range cell density for the suspended CHO cells. The target was achieved in all the three batches, where cell densities in the range of 4.0 – 6.0 x 10^6 cells mL^{-1} were attained. The high cell densities achieved also indicated the reproducibility and robustness of the bioreactor operations, which indirectly signify the efficiency of the biocontroller at maintaining conducive process conditions for cellular growth, such as temperature, pH, continuous air flow and the removal of gasses from the system. The growth rate across all three batches fell in the range of 0.023 - 0.031 h^{-1} which was in-line with values reported by Leelavatcharamas et al., (1994) as of 0.031 h^{-1} and Kornecki and Strube, (2019) of 0.029 h^{-1}.

The HTB was able to provide conducive growth conditions for the propagation of cells, and the expression of the protein of interest (sACE). This could only be possible if the bioreactor was producing sufficient oxygen mass transfer and exerting less hydrodynamic shear stress. The shear studies of the HTB are discussed further in section 5.2.5 to establish its suitability for the growth of mammalian cells in terms of its capacity to exert hydrodynamic shear.

5.2.2 Qualitative and quantitative analysis of sACE

The ACE activity in the bioreactor samples was measured using a fluorometric assay (Schwager et al., 2006). The maximum protein productivity achieved during batch 1 was 465 mg mL^{-1}.

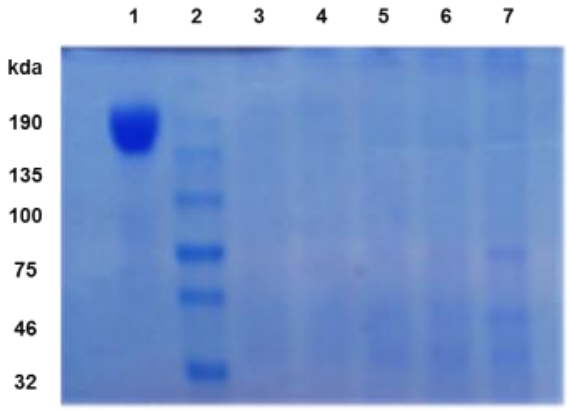

lane	Samples
1	sACE purified
2	MW marker
3	96 h
4	120 h
5	144 h
6	168 h
7	216

a b

Figure 5-8 SDS-PAGE analysis of purified sACE, as well as aliquots taken from Batch 1 after 96, 120, 144, 168, and 216 hours. The sACE expected molecular weight is between 150-180 kDa.

The SDS-PAGE analysis was performed with the purified sample to confirm the presence of sACE (Figure 5-8). The marker used was purified sACE (in-house) with a molecular weight in the range of 150-180 kDa (Guang et al., 2012). Although the band on the gel is in the correct range of molecular weight indicating the presence of sACE protein, SDS-PAGE does not guarantee unequivocal proof of identity. Therefore, western blot analysis was carried out using a specific primary antibody (polyclonal anti-ACE raised in rabbit) and secondary antibody (anti-rabbit linked to horseradish peroxidase) to establish sACE identity and purity.

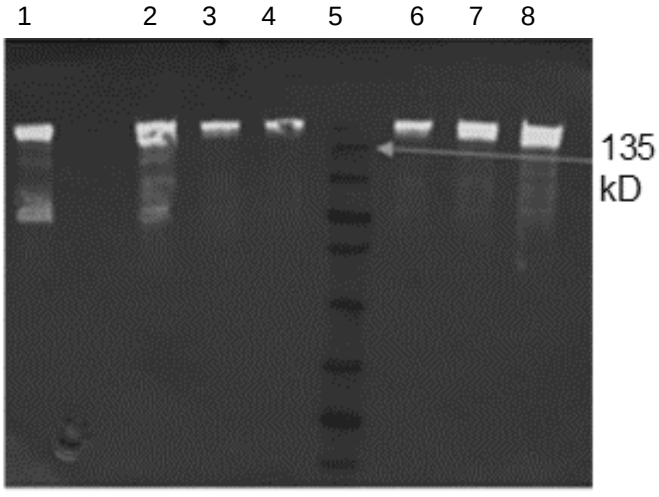

Lanes	Samples
1	**sACE standard**
2	**Sf1 (Inoculum)**
3	**Sf2 (Inoculum)**
4	**48 h**
5	**MW standard**
6	**96 h**
7	**144 h**
8	**216 h**

Figure 5-9 Western blot analysis of batch 1 for confirming the identity and purity of the sACE protein with sACE in-house standard

The band intensity of the western blot represents the quantity of the ACE protein expressed during culturing (Figure 5-9). A semi-quantitative comparative analysis and identification of the protein was

performed for the different samples. However, the absolute concentration of the protein is could not be measured using western blotting (Yang and Mahmood, 2012).

5.2.3 Comparison with other culture systems

Various culture systems have been employed in the industry (Table 2-1) to achieve high cell density with extended longevity whilst minimising the hydrodynamic shear. In this section, a comparison between HTB and other culture systems was carried out, with emphasis given to select culture systems belonging to different categories resulting in varying cell densities achieved in the system.

Table 5-2 Comparison of different cell densities achieved in various culture systems

Culture system	Cell line	Category	Cell density (x10^6 cells mL^{-1})	Working Volume	Comments	References
Tube spin	CHO	Dynamic/rotational	>10	5-20 mL	Gentle mixing and efficient gas transfer rate	De Jesus and Wurm, (2011)
Spinner	Vero	Dynamic	1.8 ± 0.25	500 mL	Microcarriers/ stirring	Toriniwa and Komiya, (2007)
Conventional Membrane aeration	CHO	Dynamic	10	1.5 L	Agitator wrapped with aeration tubing	Frahm et al., (2009)
DMA	CHO	Dynamic/ Membrane aeration	15-20	12 L	Perfusion	Frahm et al., (2009)
CelCradle	CHO	Oscillating/ packed bed	9	500 mL	BioNOC II carriers for adherent cells	Vaccixcell, (n.d.)
Smart rocker	CHO	Wave mixed	16		Medium change	Perepelitsa et al., (n.d.)
Mobius Cell Ready	CHO	Disposable STR	3.3	2.4 L	Conventional stirring	Eibl et al., (2010)
Helical track	CHO	Orbital shaking	7.7	36 L	Batch	Zhang et al., (2008)
PBS	CHO	Pneumatically-driven	6-7	250 L	Fed-batch	Hashimura, (2011)
HTB	CHO	Dynamic/ surface- aerated	5.5	3 L	Novel spiral impeller	Current research

In Table 5-2, most of the representative culture systems use surface aeration as their preferred mode of aeration except Mobius Cell Ready where the air is sparged inside the bioreactor similar to a stirred tank bioreactor. Tube spin bioreactor demonstrated excellent mixing and mass transfer efficiency with the orbitally shaken motion of fluids which could yield cell density >10 x 10^6 cells mL^{-1} whereas, in the spinner flask of 500 mL culture volume, the cell density of 1.8 x 10^6 cells mL^{-1} was reported when cells were grown on microcarriers. Membrane aeration systems such as conventional (when aeration basket was fixed with head-plate and the culture fluid is moved through impeller stirring) and dynamic membrane aeration (explained in 2.15.2) reported supporting cell density ≤ 10 x 10^6 cells mL^{-1} in batch and 15 - 20 x 10^6 cells mL^{-1} with perfusion culture respectively. CelCradle (mimicking the functionality of the lungs) can support the cell density of ≤ 9 x 10^6 cells mL^{-1} in single bellow and wave-induced motion in smart rocker can support 16 x10^6 cells mL^{-1} with medium changes during the cultivation time. Shaken helical track and vertical wheel support the cell density around 7 - 8 x 10^6 cells mL^{-1}. The horizontal tubular bioreactor has shown to support the cell density of 5.5 x 10^6 cells mL^{-1} in a batch mode. As the $k_L a$ value of HTB fall in the range of 5.25 - 16 h^{-1}, it

can support cell densities of ≥ 10 x 10^6 cells mL^{-1} in fed-batch and/or perfusion mode for a longer duration of the cultivation.

5.2.4 Mass transfer studies - Dynamic gassing out method

Delivery of the oxygen to the growing cells is a key aspect of bioreactor operation, owing to its low solubility in the culture media. Traditionally, direct sparging has been employed for high cell density culture to cater the oxygen demand. Surface aeration alone may not be sufficient to meet the required demand hence bubble-free aeration with effective impeller mixing was employed in HTB. The determination of the mass transfer coefficient ($k_L a$) with the growing cells is a complex phenomenon. This is because of the changing demand for the oxygen with respect to cell density and culture age which was directly impacted by hydrodynamic conditions and the macroenvironment inside the bioreactor during the batch. The oxygen uptake rate of mammalian cells and the required $k_L a$ for the cell density of 10 x10^6 cells mL^{-1} was discussed in section 2.11. It was reported that for the OTR of 0.5 – 8.0 mmol L^{-1} h^{-1} and for the cell density of 5 x 10^6 cells mL^{-1}, the $k_L a$ required would be 2 – 33 h^{-1} when operated at 40 % air saturation.

In the current studies, the bioreactor batches were operated at an impeller speed of 150 rpm with airflow rate of 0.2 LPM through the headspace (surface aeration). The values of oxygen uptake rate and $k_L a$ were determined using the Excel solver method (DOI: 10.25375/uct.13570970).

Table 5-3 comparison of the $k_L a$ during different time of the culture age

Parameters	Batch 1			Batch 2		
$k_L a$ (h^{-1})	1.9	2.5	2.9	0.90	1.46	0.43
Q (cell^{-1} mL min^{-1})	1.06	1.08	1.17	0.67	0.43	0.71
VCD (x10^6 cells mL^{-1})	2.54			4.84	5.48	1.31
Culture age (days)	9 (Last day)			7	8	10 (Last day)

The mass transfer values in batch 1 and 2 is shown in Table 5-3. It was observed that the specific oxygen uptake rate (Q) is almost consistent (triplicate) on day 9, where the average $k_L a$ is 2.4 ± 0.54. In the case of batch 2, mass transfer value varies every day so as its specific oxygen uptake rate which ranges from 0.90 – 1.46 (h^{-1}) and 0.43 – 0.71 (cell^{-1} mL min^{-1}) respectively.

Shakibaie et al., (2011) reported that, the $k_L a$ of 8.0 h^{-1} for packed bed reactor when operated at 50 % air saturation with 2.2 x 10^6 cells mL^{-1} at a culture age of 120 h. The comparison of HTB values with other surface-aerated bioreactor systems have not been done because of the lack of relevant data in the literature.

5.2.5 Shear stress

The hydrodynamic shear generated by the moving spiral impeller in the HTB was determined by evaluating the cell death constant (k_d). The cell death kinetics was assessed by plotting the natural log of viable cell density (ln VCD) vs time (h) at the stationary phase. The slope of the graph represents the specific cell death constant (k_d) at a particular impeller speed. At the stationary phase of each batch, cell death kinetic experiments were performed as described in 3.5.2. The emphasis was given to elucidate the effect of shear stress generated by the increased impeller speed and to differentiate the long-term and short-term effect on the culture health and overall batch performance.

5.2.5.1 Effect of long-term exposure to hydrodynamic shear on the culture health

A comparison has been drawn to show the effect of impeller speed on the cultured cells at the stationary phase to predict the cell death constant in all the three batches. Figure 5-10 represents the total viable cells in batches 1, 2 and 3, where the batches 1 and 3 ran at 150 rpm after attaining peak cell density during the stationary phase, and batch 2 ran at 300 rpm. Batch 1 was taken with CHO cells expressing the recombinant protein sACE whereas batch 2 and batch 3 were taken with plain CHO. It was assumed that both the cell types (recombinant and plain CHO) showed no morphological and physical changes, and both behave identically. This assumption can be verified by the doubling time and growth rate of batch 1 (22.07 h^{-1} and 0.0314 h^{-1}) and in batch 3 (23 h^{-1}, 0.031 h^{-1}) respectively which were comparable.

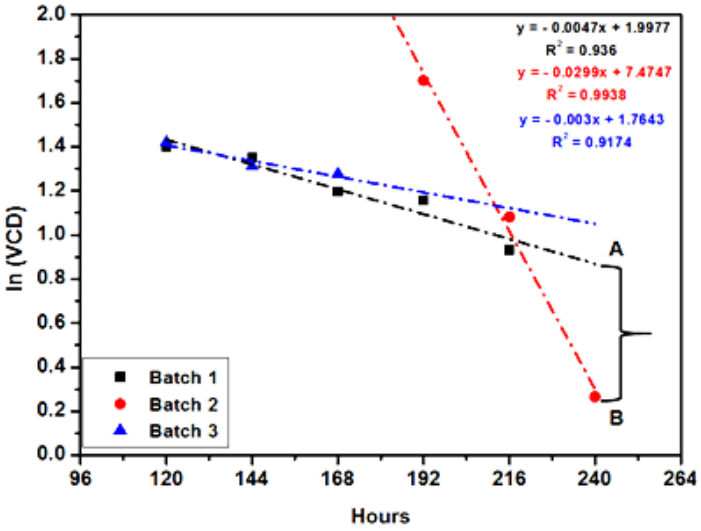

Figure 5-10 Long-term effects of impeller speed on the culture health in all three batches after attaining the stationary phase. The trend line was extrapolated for the batch 1 and 3 up to 240 h to visualize the difference in cell death with the assumption that culture conditions and the rate of cell death were constant till 240 h. Batch 1 is represented by (■), batch 2 (●) and batch 3 with (▲). The extrapolated trend lines were represented by dashed lines and the difference between point A (batch 1) and B (batch 2) indicated the difference in the extent of cell death when exposed to hydrodynamic shear from 150 rpm to 300 rpm

The experimental data of batch 1 and batch 3 were extrapolated until 240 h (black and blue dashed line) to allow comparison in all the batches. The point A on the black dashed line (Batch 1) and point B on the red dashed line (Batch 2) indicate the extent of cell death (0.005 h^{-1}) occurring in batch 1 and batch 2 (0.030 h^{-1}) respectively and the difference between A and B (indicated by a curly bracket) described the amount of cell death induced by impeller stirring at 300 rpm (from the last 2 days at stationary phase) from that of natural cell death occurred at 150 and 300 rpm respectively. The difference in the magnitude of cell death accounted for 0.025 (h^{-1}) at 300 rpm in batch 2 denoted by a red box in Table 5-4, as compared to natural cell death in batch 1 at 150 rpm denoted by a green box. From the above 3 batches, it has been found that the magnitude of cell death at 300 rpm (batch 2) was 6.36 times greater than 150 rpm (batch 1) and 10 times than that of batch 3 (150 rpm for 48 h) (Table 5-4). Therefore, it can be concluded that at 300 rpm, CHO cells were exposed to a high shear stress condition that has a negative impact on the culture health as compared to rpm 150.

Table 5-4 Impeller induced cell death in all the three batches as (k_d)

Batches	Impeller speed (rpm)	Stationary phase span (h)	Cell death (k_d) (h^{-1})			Ratio of cell death	
			Long-term effect at stationary phase (Natural cell death)	Short-term effect after stationary phase, (one hour at each rpm)	Due to increased impeller speed	Long-term	Short-term
1	150	120 - 216	0.005	0.006	0.001	6.36	24.33
	300			0.146	0.141		
2	300	192 - 240	0.030	NA	0.025		
3	150	120 - 168	0.003	0.006	0.003	9.97	
	200			0.046	0.043		7.14
	250			0.071	0.068		11.14
	300			0.145	0.142		22.67
	400			0.200	0.197		31.25
	500			0.815	0.812		127.40

5.2.5.2 Effect of short-term exposure to hydrodynamic shear on the culture health

In batch 1, after acting as the control experiment at 150 rpm, the impeller speed was step-up from 150 to 300 rpm after 216 hours to determine the short-term effect of impeller speed on the culture health for an hour. The cell death (k_d) value measured was 0.006 h^{-1} and 0.145 h^{-1} for 150 rpm and at 300 rpm respectively (Figure 5-11). These values pointed-out that the magnitude of cell death at 300 rpm, was around 25 times higher as compared to 150 rpm for a short duration of time (one hour) as shown in Table 5-4. Figure 5-11 show point A and B, which represented the extrapolated lines for 150 and 300 rpm and the gap between them shown with the curly bracket indicate the difference of 0.142 (h^{-1}) in cell death constant due to increased impeller speed.

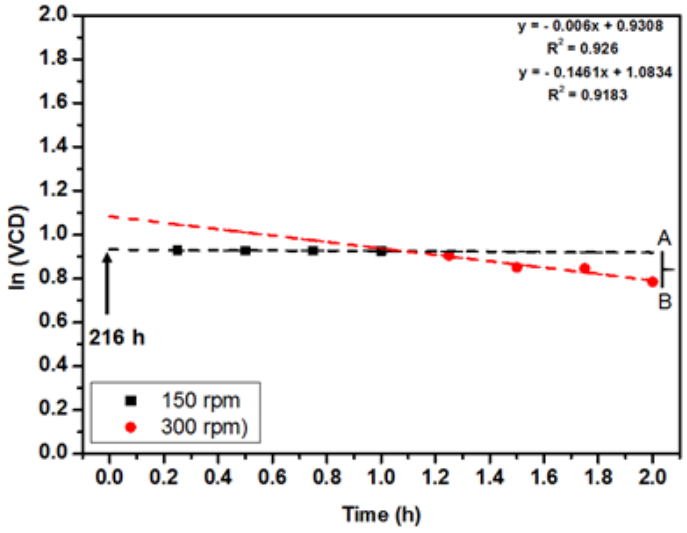

Figure 5-11 Short-term effects of impeller speed on culture health when exposed to 150 rpm and 300 rpm for an hour each after 216 h in batch 2. The impeller speed at 150 rpm is denoted by (■), and 300 rpm with (●). The extrapolated trend lines were represented by dashed lines and the difference between point A (150 rpm) and B (300 rpm) indicated the difference in the extent of cell death when exposed to hydrodynamic shear at 300 rpm from that of 150 rpm

To determine the short-term effect of the increased impeller speed to the cells, the experiment was designed at the end of 168 h of batch 3 as shown in Figure 5-12. An attempt was made to envisage the full spectrum of hydrodynamic shear induced by impeller agitation from 150 rpm to 500 rpm. The impeller speed

was step-up at a regular interval (after 1 h each) with the increment of 50 rpm from the previous impeller speed until the speed reached to 300 rpm and thereafter, 100 rpm increment was made till 500 rpm as depicted in the legends of Figure 5-12. The cells were subjected to different shear conditions to interpret the effect of various impeller speeds on culture health. Cell death (k_d) obtained from this experiment ranged from 0.006 h^{-1} at rpm 150 to 0.815 h^{-1} at 500 rpm as shown in Figure 5-12.

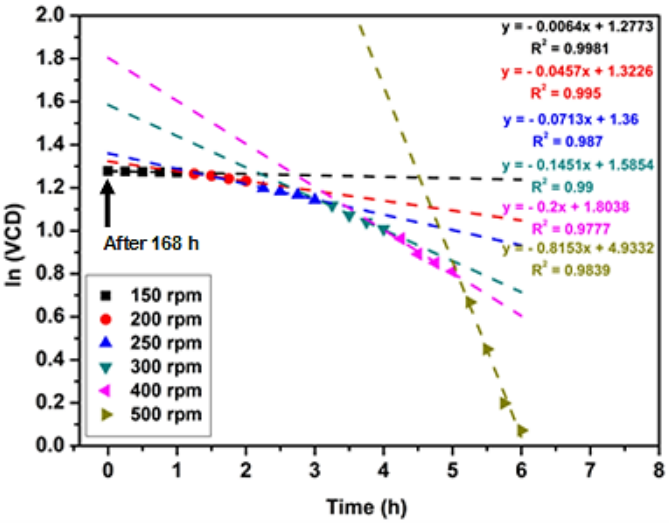

Figure 5-12 Comparing the effect of various impeller speeds on culture health for short exposure to hydrodynamic shear. The trend line for each impeller speed was extrapolated to 6 h (denoted by dashed lines) to visualize the difference in cell death. The 150 rpm is represented by (■), 200 rpm (●), 250 rpm (▲), 300 rpm (▼), 400 rpm (◄) and 500 rpm (►). The gaps between the trend lines showed the extent of cell death occurred between them with their respective impeller speeds

From Figure 5-12, it was established that the magnitude of cell death at 300 rpm was 20 times higher than the cell death at 150 rpm merely after 4 h. It has also been found that at every 50 rpm increase from 200 rpm onwards up to 300 rpm, the shear stress almost doubled, precisely, at 200 - 250 and 250 - 300, the difference in magnitude of cell death accounted for 1.56 and 2.04 respectively. Thereafter, from the impeller speed of 300 - 400 and then 400- 500, the cell death ratio accounted for 1.38 and 4.08 respectively. The difference lies in the fact that in batch 3, the cells were subjected to a sequential increase in agitation speed at regular interval of time which means cells were at 200 and 250 rpm for one hour each before subjected to 300 rpm. There was striking similarity found in batch 1 and 3 where cell death constant in two different batches running at 300 rpm came out to be similar as denoted by black boxes in Table 5-4.

Above discussion concluded that the increase in impeller speed, increases the shear stress exerted on the cells, which resulted in accelerated cell death. Short-term exposure to cultured cells at the later stages of fermentation had shown a negative effect on cellular health. Long – term exposure (batch 2) of increased impeller speed (300 rpm) to growing cells at stationary phase shown better results as compared to short term exposure (batch 3), which stands out to be 0.030 and 0.145 h^{-1} respectively. Therefore, short-term exposure to increased impeller speed is detrimental to the growth of cells. For long-term, appropriate impeller speed may fall in the range of 150 – 300 rpm, which may yield cell death constant in-between 0.005 - 0.030 h^{-1} which may produce extended longevity of the culture with enhanced mass and heat transfer capability whilst with tolerable shear conditions.

5.2.6 Operational Window for HTB

Chalmers (2015) reported the specific oxygen demand (SOD) of CHO cells fell in the order of 5.3 x 10^{-17} - 9.0 x 10^{-17} molO_2.cell^{-1}s^{-1}. To maintain the cell densities (X) of 5 x 10^6 - 10 x 10^6 cells mL^{-1}, which are common at industrial scale, It is recommended that the dissolved oxygen concentration in the bioreactor be maintained in the range of 30 % to 50 % (Godoy-Silva et al., 2010; Nienow, 2015).

From these values, four cell culture scenarios have been evaluated for the minimum k_La required as shown in Table 5-5. These scenarios were: low biomass concentration (0.5 x 10^6 cells mL^{-1}) and low SOD (2.6 x 10^{-11} mol mL^{-1} s^{-1}), low biomass (0.5 x 10^6 cells mL^{-1})) and high SOD (4.5 x 10^{-11} mol mL^{-1} s^{-1}), high biomass concentration (10 x 10^6 cells mL^{-1}) and low SOD (5.3 x 10^{-10} mol mL^{-1} s^{-1}), and high biomass (10 x 10^6 cells mL^{-1}) and high SOD (9 x 10^{-10} mol mL^{-1} s^{-1}). In addition, these four scenarios were calculated for maintaining the culture conditions at 30 % and at 50 % of oxygen saturation (DOI: 10.25375/uct.13570970).

Table 5-5 k_La value required for the mammalian cells to grow

Scenarios				
Biomass	low	low	High	high
SOD	low	high	Low	high
X [cells mL^{-1}]	0.50 x 10^6	0.50 x 10^6	10 x 10^6	10 x 10^6
SOD [mol mL^{-1} s^{-1}]	2.65 x 10^{-11}	4.50 x 10^{-11}	5.30 x 10^{-10}	9.00 x 10^{-10}
$\boldsymbol{k_La}$ (h^{-1}) at dO_2 30 %	0.59	1.01	11.85	20.12
$\boldsymbol{k_La}$ (h^{-1}) at dO_2 50 %	0.83	1.41	16.59	28.17

These target values of k_La, and the measured k_La values would be used in combination with the parametric model (section 4.3.4) to find a satisfactory operating 'window' of HTB through impeller speed and aeration rate required to meet the oxygen demand of CHO cell culture at high density. If the axes of the plots given in Figure 4-20 may be assumed such that rpm, Vs (flow rate), and k_La correspond to the x, y and z axes: The minimum k_La value required for any given scenario given in Table 5-5, X and SOD represented in a plane in the x y dimension, and minimum k_La. Shown on the z axis. The intersection of this plane with the parametric model surface derived in section 4.3.4 represents the boundary of the viable operating window for the HTB. A two-dimensional (2 D) projection of this region onto the x-y axis will yield an operating window in terms of agitation speed and superficial gas velocity. An example of this type of window is given in Figure 5-13.

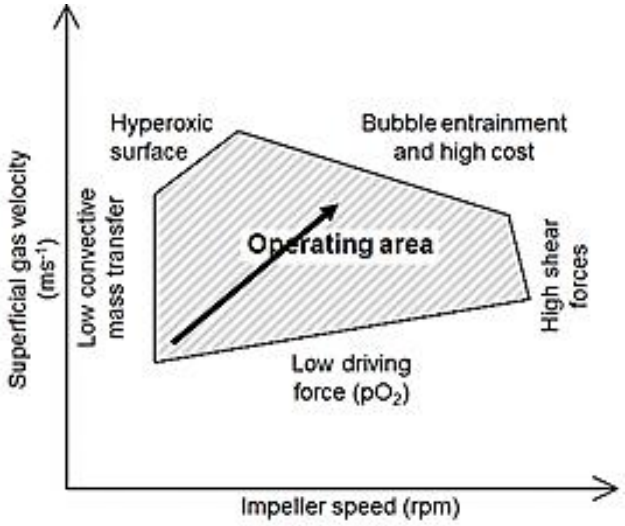

Figure 5-13 Satisfactory operational window of HTB with black arrow indicating the direction of optimum performance of HTB for meeting the required oxygen demand for high cell density culture

It has been evaluated that HTB performance is satisfactory and suitable for batch operations. It can deliver the required amount of oxygen to the cells. The k_La values of 5.4 ± 0.2 and 16.0 ± 0.5 h^{-1} were measured at impeller speeds of 100 – 500 rpm at an aeration rate of 0.2 – 0.5 LPM (Table 4-10 and Table 4-11). This would be able to cater the oxygen demand (k_La) values of 12 – 17 h^{-1}, however at high cell density and high SOD, the HTB would not be able to meet the required k_La value of 20 – 28 h^{-1} (Table 5-5). The desired operating window with the oxygen demand (k_La) of 20 – 28 h^{-1} can be achieved when the OTR will be greater than OD (OTR > OD) for the various scenarios occurring in different growth phases of the culture. In general, at low biomass, k_La values and OD requirement are low that can be met with slow impeller speed and low airflow rate. As the culture density increases, so as the demand of k_La and high airflow rate and increased impeller speed can be used. Alternatively, it has also been observed that there is a limit to increase the impeller speed to avoid the hydrodynamic shear which may cause cell death. The optimum speed observed was in the range of 150 - 300 rpm which could satisfy the required oxygen demand of the cell density (0.5 x 10^6 - 10 x 10^6 cells mL^{-1}) while operating at 50 % air saturation with maximum airflow rate of 0.5 LPM whilst reducing hydrodynamic shear and minimising cell deaths.

In the case of HTB, as the cell density increases, aeration and impeller speed can be ramped up to meet the required oxygen demand of the cells and to maintain a desired dissolved oxygen concentration range. When the culture is at maximum sustainable density, the optimised maximum impeller speed and aeration rate used should not induce hydrodynamic shear to cells. Figure 5-13 illustrates operating conditions (window) for the optimum working of the HTB and black arrow indicate the increase in airflow rate with the increase in agitation that may be able to cater the desired oxygen demand whilst minimising the shear to the cells.

5.2.7 Cell metabolism and Metabolite analysis

The primary aim of the bioprocess development is to formulate strategies that enhance cell density, extend the viability of the culture and increase the protein titre. Protein productivity has over time increased from mg L^{-1} to g L^{-1} in mammalian cell cultures, due to demands for the biological drugs with cost-effective

processes (De Jesus and Wurm, 2011). Detailed studies of cellular metabolism offer insight into the type of metabolites (Biological and chemical entities) and their role in cellular processes by using available energy resources (Lu et al., 2017). For example, the replication of genetic material which leads to cell division is a key process that requires energy to control and regulate the process with precision. The availability of the nutrients is a must for building blocks and to provide energy for all the processes (Krause et al., 2020). Therefore, during the batch run, it is important to quantify the depletion of nutrients (energy sources) and the production of secondary metabolites which may negatively impact the growth and productivity (Lao and Toth, 1997).

Reitzer et al., (1979) reported that HeLa cells grew at the same rate when cultured in the media containing sugar either glucose, galactose or fructose. They also reported that the utilisation of sugar and carbon flow through glycolysis and citric acid cycle (TCA) depends on the type of sugar and its concentration in the media. When the concentration of sugar in the media is ≥ 1.0 mM, around 80 % of carbon from the glucose was metabolized through glycolysis to produce lactic acid and only 4 - 5 % went through the TCA. Fructose and galactose metabolism also do not contribute to the energy requirements of the cells. Therefore, they concluded that there could be another source present in the culture media which impart energy to the cells.

Glutamine is an alternative next available carbon-source other than sugars. It is primarily required for the biosynthesis of protein and nucleic acid material (by providing amino group to purine and pyrimidine). It has also been reported that L-glutamine decomposes at a rate of 10 % per day at 37 ^{o}C to produce ammonia, which is a by-product of glutamine metabolism (Bell et al., 1995). Glutamine metabolizes quickly in the presence of sugars. It has been reported that the glutamine oxidation alone contributes around 30 - 50 % of cellular energy requirements through aerobic oxidation through the citric acid cycle. During cellular metabolism, the glutamine oxidation is regulated by the concentration of glucose in the culture media. Generally, when the concentration of glucose is decreased or replaced by other sugars, the extent of glutamine oxidation increases, and it becomes the sole energy supplier for the growing cells. The utilisation of the glucose and other sugars are meant only for anabolic activities by delivering precursors for biosynthesis and they do not take part in bioenergetics of the cells (Reitzer et al., 1979; Zielke et al., 1984).

It has been reported that in a batch culture, inefficient and unregulated consumption of glucose and glutamine produced higher amount of metabolic waste products, such as lactate, ammonia, and amino acids, like alanine or proline. It is because the cells were exposed to the high concentration of glucose and glutamine in the batch culture and cells keep on metabolizing these nutrients at a much high rate than normal to maintain the cell growth (Slivac et al., 2010).

Generally, under stress conditions (mechanical or oxidative stress), the growing cells produced a large amount of lactate and ammonia as a by-product (Blaschczok et al., 2013). Mammalian cells have the capability of producing ATP through glycolysis (aerobic glycolysis) and/or mitochondrial respiration (Fan et al., 2013). At high cell density culture, when the rate of oxygen consumption is more than the rate of oxygen supply (Hypoxia), and the point where, DO concentration touches the critical oxygen concentration level, below that point, the rate of oxygen consumption and mitochondrial activity slow down. As a result, glucose

and glutamine consumption rate increases to meet the energy demand (ATP compensation) of the cells. As a consequence, the rate of lactate and ammonia production also increases (Berdugo, 2010).

It has been widely accepted that lactate and ammonia have negative effects on the cell growth of mammalian cells and cell lines behave differently in the presence of these metabolites based on their tolerance levels (Lao and Toth, 1997). Martínez-Monge et al., (2019) reported recently through flux balance analysis (FBA) that during glucose metabolism, around 69 % of pyruvate obtained through glycolysis is converted to lactate to cater the need for nicotinamide adenine dinucleotide (NADH) regeneration in the cytoplasm and 31 % of pyruvate entered the citric acid cycle (TCA) via *acetyl-CoA*. Hence, only 31 % of glucose carbon is utilized in the TCA cycle for bioenergetics. It has also been reported by Martínez-Monge et al., (2019) that glucose and lactate can be co-metabolize by CHO even during the growth phase. It could be due to Warburg effect which explains the production of lactate from glucose consumption, instead of glucose being metabolized into CO_2 and H_2O when oxygen is not even a limiting factor (Fan et al., 2013; Martínez-Monge et al., 2019).

5.2.7.1 Glucose and Lactate

The profile of glucose consumption and lactate formation during the batch indicates the overall culture health in the vessel and assist in anticipating the scale of cell growth and protein productivity in the batch. Generally, as the cell density increases in the batch, glucose consumption increases so as the lactate production rate, but glucose metabolism is affected by culture conditions such as temperature, pH and osmolality. At low temperature, glucose consumption decreases, and the rate of lactate production also reduces. In all the batches, the starting glucose concentration was around 6.0 g L^{-1}. As the culture progresses, glucose concentration lowers down to 1.0 g L^{-1} except batch 3 where it stayed above 2.0 g L^{-1}. The lactate concentration was in all the three batches were measured below 3.0 g L^{-1} at the end of the batch (Figure 5-14).

Mammalian cell culture metabolism generally specified as glucoglutaminolysis which means a high concentration of glucose and glutamine was metabolised to produce high concentrations of lactate and non-essential amino acids (Quek et al., 2010). The amount of glucose consumed, and the lactate produced in all the three batches falls within the range of literature. Hartley et al., (2018) reported that CHO culture worked optimally when the lactate concentration is below 1.8 g L^{-1} (20 mM) and showed a negative effect on the culture heath and protein productivity when the concentration exceeded 3.6 g L^{-1} (40 mM) which is in-line with literature values. Glucose concentrations in batch 2 and 3 were above 1.0 g L^{-1} at the end of the batch, which indicated that the substrate was not limiting but in the case of batch 1, it fell with the glucose-limiting conditions (Meuwly et al., 2006). It could be due to the higher glucose uptake rate due to the expression of sACE protein and the hydrodynamic stress conditions experienced by the cultured cells.

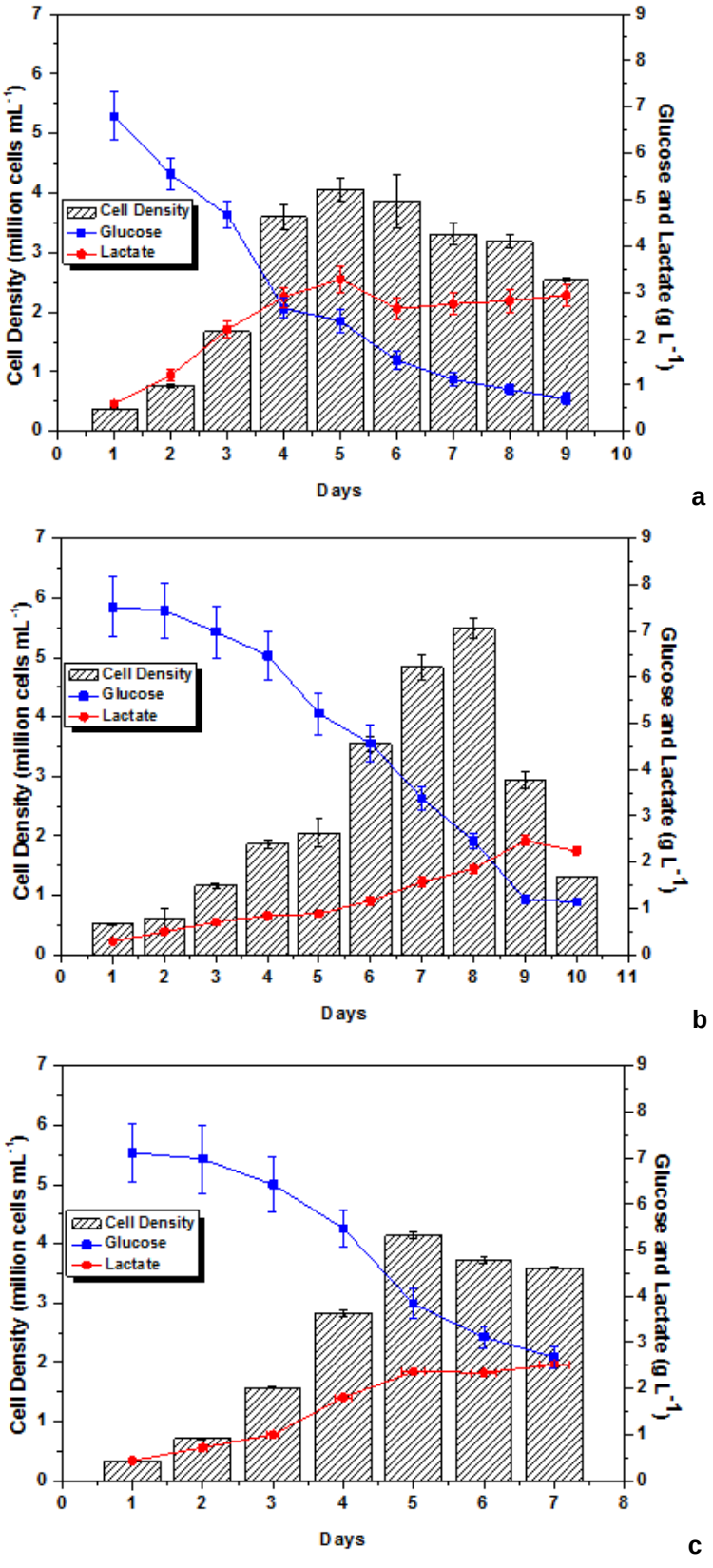

Figure 5-14 Glucose and Lactate profile of the batches w.r.t their respective cell densities (a) batch 1 (b) batch 2 and (c) batch 3. The error bars indicated the mean standard deviation n=3 replicates

5.2.7.2 Ammonia

Ammonia is a by-product of glutamine catabolism which affect the cell growth rate and impair the glycosylation of recombinant proteins (Yang and Butler, 2000). Glutamine is an amino acid which is required for the nucleic acid formation and energy needs in the culture. Accumulation of ammonia in the culture is toxic to cells and affect product quality (Butler, 2005). The inhibitory effect of ammonia on cell growth is cell line dependent. The removal of exogenous ammonia from the culture media would also utilize less adenosine triphosphate (ATP) molecules for transporting NH^{4+} into the cells through Na^{+}/K^{+}-ATPase (Bell et al., 1995). Hence, in the current study, stable glutamine which is a dipeptide of L-alanyl-L Glutamine and stable at 37 ^{o}C was used. The ammonia production in all the three batches ranged between 2.0 - 3.5 mmol L^{-1} which is considered safe for the production of proteins (Figure 5-15). It has been reported that recombinant CHO cells are tolerant up to 10 mmol L^{-1} of ammonia concentration and show no negative effect on the growth of cells (Yang and Butler, 2000).

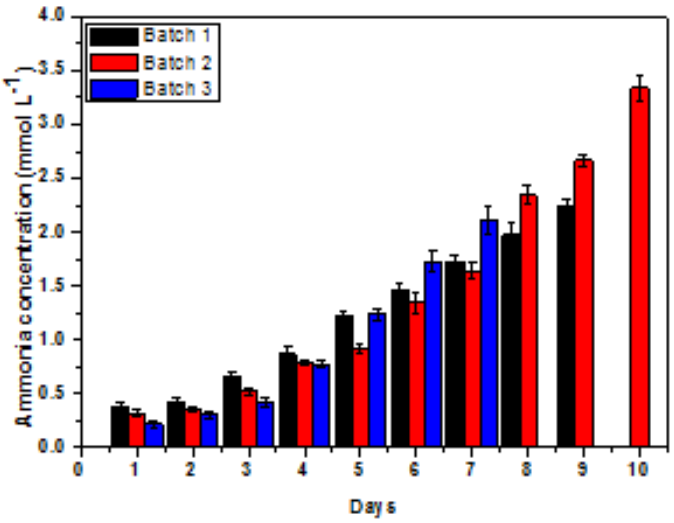

Figure 5-15 Ammonia profile in bioreactor batches where black, red and blue represented the batch 1, 2 and 3 respectively. Data for batch 1 available to day 9, batch 2 to day 10 and batch 3 to day 7. The error bars indicated the mean standard deviation n=3 replicates

5.2.7.3 Osmolality

Mammalian cells lack a cell wall and because of this, they are sensitive to various physiological conditions such as temperature, pH, nutrient depletion, hydrodynamic shear and culture osmolality (Zhu, 2012; Zhu et al., 2008). Osmolality not only impacts the culture health but also affect the glycosylation of the recombinant proteins (Pacis et al., 2011; Zanghi et al., 1999).

In all the three batches taken in the HTB, pH of the culture medium was maintained through CO_2 in the gaseous phase and sodium bicarbonate ($NaHCO_3$) in the media. During the lag phase of the batch, there has not been much shift in the culture pH as cells are acclimatizing with the dynamic culture conditions. With the low cell density and low cellular metabolism, the amount of CO_2 produced is also insignificant which is evident from the Figure 5-16, where till day 3, the osmolality in all the three batches rest at 320 - 330 mOsmol kg^{-1}.

As the batch progresses and the culture entered the log phase of the growth cycle, actively dividing cells start metabolising medium nutrients such as glucose and glutamine. The by-product formation (lactate

and ammonia) in the culture would drift the pH equilibrium. To maintain the pH equilibrium, CO_2 and $NaHCO_3$ play a crucial role as shown in Equation 5-1 and Equation 5-2

$$CO_2+H_2O \longleftrightarrow H_2CO_3 \longleftrightarrow H^+ + HCO_3^- \quad \text{Equation 5-1}$$

$$NaHCO_3 \longleftrightarrow Na^+ + HCO_3^- \quad \text{Equation 5-2}$$

As the cell density increases so as the glucose consumption which directly increases the concentration of dissolved CO_2 and lactate in the medium and turn it acidic. To compensate it, it is necessary to strip CO_2 continuously by addition of the base solution, sodium bicarbonate (8 %). The addition of sodium bicarbonate elevates the high osmolality issue of the culture.

The significance of the HTB is the high surface area which aids in stripping of CO_2 from the culture medium which indirectly defers the addition of bicarbonate. In batch 1, CHO cells were expressing the sACE protein. It has been reported that the high osmolality in the range of 450 - 550 mOsmol kg^{-1} directly affect the growth rate and induce cell death, but on a positive note, increases the protein yields by increasing the specific productivity (Hu and Aunins, 1997; Kim et al., 2002; Zhang et al., 2010). Figure 5-16 (a) shows the osmolality profile of batch 1 where culture entered the stationary phase at day 5 with an osmolality of 388 mOsmol kg^{-1}. Thereafter, osmolality increases which retard the cell growth but gradually increases the sACE productivity which supported the findings of Kim et al., (2002) and Zhang et al., (2010).

In batch 2, the maximum peak cell density achieved was on day 8 when the osmolality and lactate concentrations were 439 mOsmol kg^{-1} and 186 g L^{-1} respectively. Thereafter the impeller speed was stepped-up to 300. The cumulative effect of increased stirring speed, sensitivity of the cells towards culture conditions, the viability drop rapidly due to excessive cell death which then steeply elevate the osmolality of the culture at 483 mOsmol kg^{-1} as shown in Figure 5-16 (b) in the span of 3 days.

The osmolality profile of batch 3 was also similar to batch 1 and 2. The maximum peak cell density achieved on day 5 when the osmolality and lactate concentrations were 410 mOsmol kg^{-1} and 2.3 g L^{-1} respectively. The maximum osmolality observed at day 7 was 445 mOsmol kg^{-1} when the day 5 viability also came down to below 90 %. During the stationary phase of the growth, lactate production did not change much, which may indicate the co-metabolism of lactate along with glucose for the energy requirements of the batch as osmolality was also not increasing steeply as seen in Figure 5-16 (c).

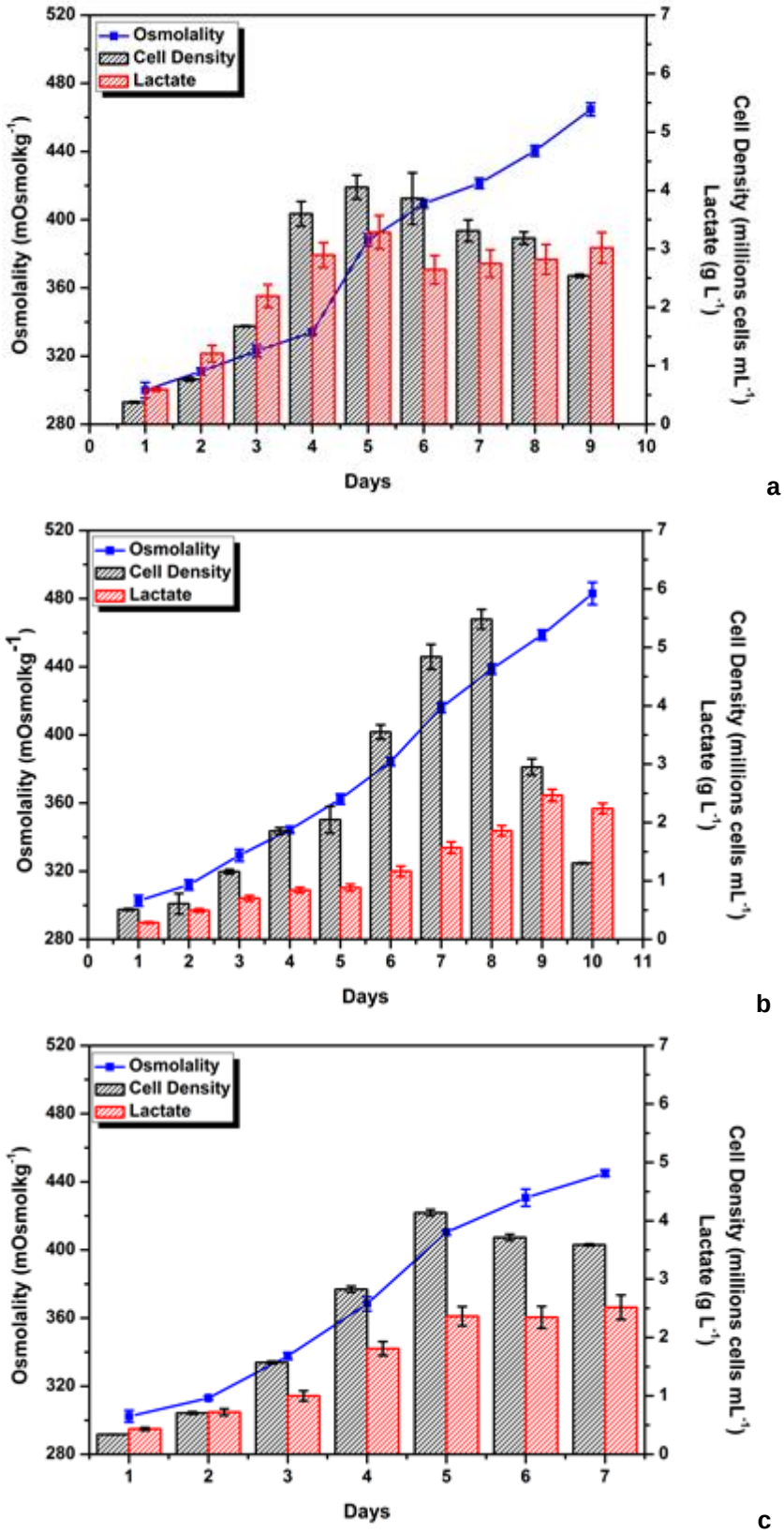

Figure 5-16 Osmolality profile w. r. t. cell density and lactate production during the of bioreactor batches. (a) batch 1, (b) batch 2 and (c) batch 3. The error bars indicate the standard deviation of n=3 replicates

5.2.8 Summary

The present chapter described the biotic aspects of the HTB, which encompasses the screening of suitable media, replicate batches in the bioreactor, and the quantitative and qualitative analysis of the target protein (sACE). A comparative study was also carried out to place HTB alongside other surface-aerated culture systems. Thereafter, shear stress was analysed to differentiate the cell death from the impeller from overall cell death. Furthermore, an operating process window for the HTB was also predicted based on abiotic and biotic characterisation, which satisfy the optimum operation. Finally, metabolite analysis was also discussed.

Six commercially available media were screened for their ability to support the growth of CHO cells. M6 (SFM4 CHO- powder) media supported high cell density and high protein productivity and was a relatively cheaper option compared to M1 (HyCell CHO) media, which showed comparable cell growth results. Hence, M6 media was selected for subsequent bioreactor experiments.

A total of three HTB batches with CHO cells were carried out with M6 media. The first batch cultivated was CHO cells expressing the sACE protein, where cell density of 4.15 x 10^6 cells mL^{-1}, and protein productivity of 465 mg mL^{-1} were achieved. Thereafter, two batches of wild-type CHO cells were grown. In the second batch, the cell density attained was 5.6 x 10^6 cells mL^{-1}, and in the third batch the peak cell density was 4.2 x 10^6 cells mL^{-1}.

Shear studies were performed by measuring the cell death constant from the hydrodynamic profile of the HTB. During the stationary phase of each batch, the bioreactor induced impeller shear on the cultured cells to determine the cell death constant (k_d). A short exposure to stress, due to increased impeller speed, killed more cells than long-term exposure. During long-term exposure, the growing cells could adapt to the microenvironment, possibly enabling them to better survive long-term shear stress exposure. This behaviour is similarly observed with cold or heat shock stress experiments, where gradual or long-term exposure to suboptimal temperatures allowed the cells to adapt to the stress, resulting in less overall stress.

Furthermore, an operating window for the HTB was devised based on its satisfactory abiotic and biotic engineering characterisation. The bioreactor can deliver a mass transfer (k_La) of 5.4 ± 0.2 – 16.0 ± 0.5 h^{-1} at impeller speeds of 100 – 500 rpm, with aeration rates of 0.2 – 0.5 LPM. However, stirring speeds of between 150 - 300 rpm are appropriate for cell culture, which can deliver a k_La in the range of 10 – 12 h^{-1} at high flow rates of 0.5 LPM (Table 4-10 and Table 4-11). For high density and high SOD cell cultures, the required k_La of 20 – 28 h^{-1} may not be delivered by the HTB with the current design. The maximum sustainable culture density can be achieved in the HTB when the OTR is always more than the OD, with stirrer speeds and air flow rates that pose no threat of hydrodynamic shear stress to the growing cells.

A comparative study has been performed between the HTB and other surface aerated bioreactors, which are operated using different operating principles. In addition, spent media analysis was carried out to measure the glucose consumption, lactate and ammonia production, and sACE productivity. The rate at which glucose was consumed and lactate and ammonia were formed fall within the range of cited literature values, suggesting that the HTB is suitable for the cultivation of mammalian cells. It is recommended that

further experiments related to fed-batch and perfusion should be performed to confirm the suitability of the HTB for the cultivation of mammalian cells.

6 Exploiting puromycin aminonucleoside (PAN) to bring strongly adherent Vero cells into suspension

The primary focus of this chapter is to test and evaluate the second hypothesis (1.3.2), which emphasized the use of the anti-cancer drug, Puromycin aminonucleoside (PAN) to suppress the expression of integrin (surface receptors), that could result in bringing the strongly adherent Vero cells into suspension in serum-free conditions. In this chapter, the 50 % inhibitory dose (IC_{50}) was determined for Vero cells and subsequently, PAN was evaluated on the Vero cells at various concentrations below and above the IC_{50} values. This was done because our objective was to test the inhibitory dose of the drug and to find the appropriate concentration of the drug which could detach the cells from the attachment surface and bring them into suspension culture. The post PAN-treated Vero cells were visually inspected under a microscope every day for visualizing the effect of PAN on the cells morphology and eventually detachment from the surface. No cell biology experiments were done to evaluate and validate the findings as those were beyond the scope of this thesis although the recommendation is given in chapter 8 for future research on this topic.

6.1 Determination of Inhibitory dose 50 (IC_{50})

The IC_{50} value of the drug is the response correlates with the 50 % inhibition efficiency of the drug as compared to the controls (which includes the means of 0 % and 100 % assay controls) (Sebaugh, 2011). The IC_{50} value directly aids in evaluating the suitability and performance of the drug. In this thesis, the IC_{50} value of the PAN was determined as given in section 3.8. The effect of PAN was evaluated on the time-dependent manner as shown in Figure 6-1

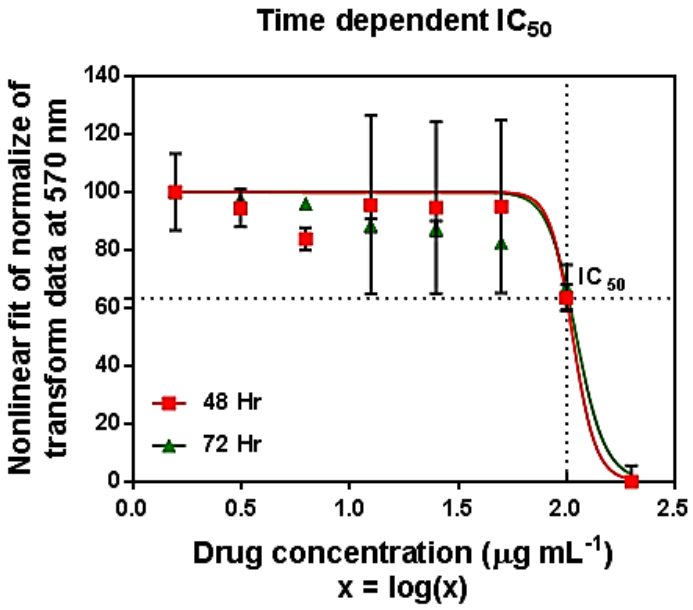

Figure 6-1 Time-dependent profile of inhibitory dose (IC_{50}) of PAN on the Vero cells post-exposure at 48 and 72 hours. Error bars show the standard deviation of n=3 replicates. The intersection of the dotted lines indicates the value of IC_{50}

The data points from the 24 h post-exposure of the drug did not show a good correlation and thus was not considered in the calculations. This could be due to the human error in dispensing an accurate number of cells in the 96 well plates without any clumps, therefore may have resulted in an outlier reading. The IC_{50} value for 48 h and 72 h were 2.03 and 2.05 on log (X) scale which amounts for 107 µg mL^{-1} and 111 µg mL^{-1} respectively. This signifies that below this concentration, the cytotoxic effect of the drug is minimal, and cells perform normal metabolic activities. The effect of exposure time on the Vero cells (48 h and 72 h) also showed that Vero cells are resistant to PAN *in-vitro*. Hence, it would be interesting to evaluate further the effect of PAN on Vero cells for an extended period.

6.2 Effect of different concentrations PAN on the growth of Vero cells

Initially, the effect of PAN was evaluated by using the PAN concentration from 0.3125 (lowest concentration) to 100 µg mL^{-1} (maximum concentration) which was lower than the IC_{50} value. This was to evaluate the appropriate dose of PAN which could dislodge the Vero cells from their surface and bring them in suspension without altering their metabolic function. Post-exposure TC flasks of Vero cells (T-25 cm^2) were visually inspected under the microscope and photographs were taken daily to monitor the growth and detachment of cells under the influence of PAN.

It was observed that the positive control flask (cells without PAN exposure) grew as adherent culture normally and the flask was fully confluent on day 7 (Figure 6-2). Vero cells at a PAN concentration of 10 µg mL^{-1} to 0.3125 µg mL^{-1} showed little effect on the growth pattern as compared to the positive control. At these PAN concentrations, cells remained confluent and did not detach from the flask surface. There was a significant difference in growth when Vero cells were exposed to 50 µg mL^{-1} to 100 µg mL^{-1}. The cells exhibited slower growth which was measured by the percentage confluency achieved every day. The morphology of the cells also changed as these concentrations approached the IC_{50} value. Gonçalves et al., (2006) also reported similar changes (growth rate and morphological) in Vero cells, when exposed to various concentration of Cisplatin (an anti-cancer agent).

On day 4, few cells detached from the surface and came into suspension in the TC flask when treated with 100 µg mL^{-1} and 50 µg mL^{-1} of PAN. Cell viability was tested with 0.4 % trypan blue. It was observed that around 10 - 20 % of cells experienced cell death and left cell plaques behind. Interestingly, the percentage of plaques in 50 µg mL^{-1} flask was almost half from that of 100 µg mL^{-1} (Visual observation). On day 5, 70 % of spent media was removed from the TC flasks and replenished with an equal amount of fresh media (containing the respective PAN concentrations) to minimise the effect of media toxicity due to secondary metabolite and the change in pH conditions (change in media colour). The free Vero (suspended) cells that were removed from the spent media were re-collected after centrifugation at 700 rpm for 5 min. The cell pellet was resuspended in 50 % DMEM media with 1 % FBS and 50 % SFM4 MegaVir media and kept at 100 rpm on the orbital shaker inside the CO_2 incubator at 37 ^oC for further evaluation of cell growth in suspension culture, which will be discussed in section 6.3.

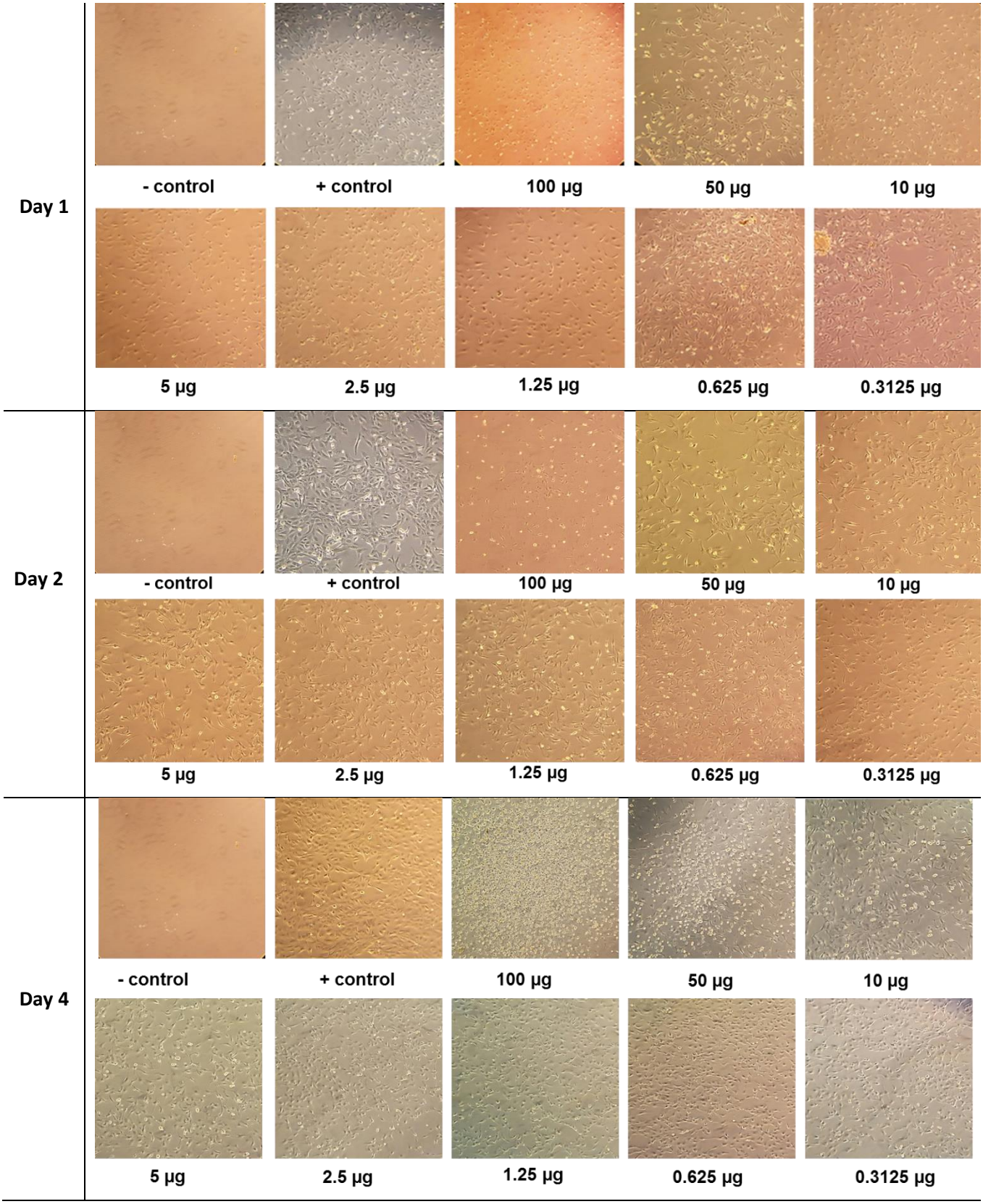
Day 1
- control
+ control
100 µg
50 µg
10 µg
5 µg
2.5 µg
1.25 µg
0.625 µg
0.3125 µg
Day 2
- control
+ control
100 µg
50 µg
10 µg
5 µg
2.5 µg
1.25 µg
0.625 µg
0.3125 µg
Day 4
- control
+ control
100 µg
50 µg
10 µg
5 µg
2.5 µg
1.25 µg
0.625 µg
0.3125 µg

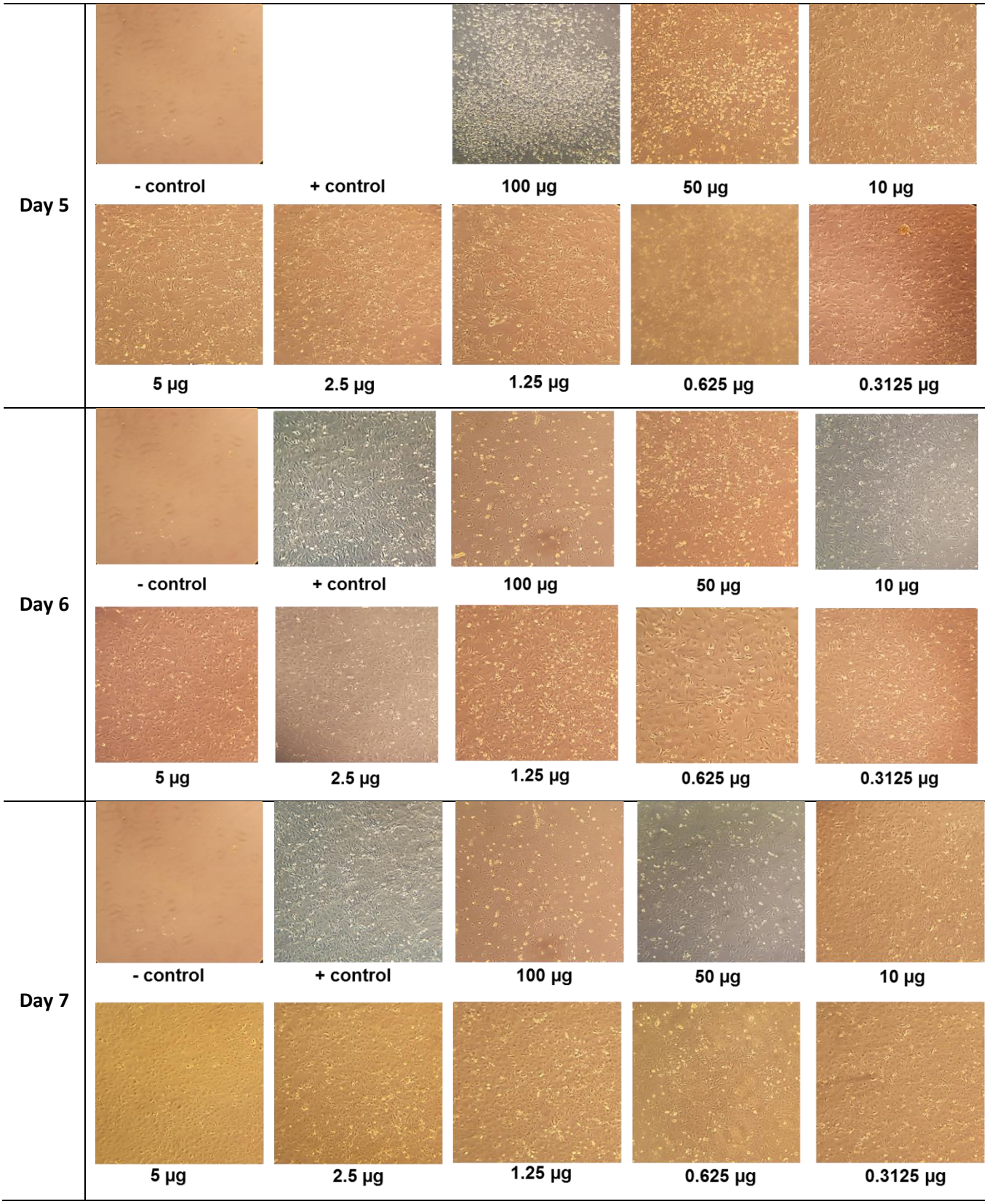

Figure 6-2 Visual illustration of the Vero cells growth pattern under the influence of different PAN concentrations ranging from highest 100 µg mL^{-1} to minimum 0.3125 µg mL^{-1}. Photographs were taken every day under an inverted microscope at 100 X magnification to visualize the change in cell morphology under the influence of various concentrations of PAN. The positive control picture on day 5 was not available

In the second experiment, PAN concentration used was in the range of 50 - 100 µg mL^{-1} with the difference of 10 µg mL^{-1} (e.g. 100, 90, 80, 70, 60 and 50 µg mL^{-1}). This experiment was designed to explore the effect of PAN within the concentration range of 100 - 50 µg mL^{-1} to determine the effective dose of PAN to dislodge the cells from the surface of the TC flask whilst retaining the normal cellular behaviour such as growth rate, doubling time, morphology and response to external stresses. A visual illustration of the experiment can be seen in Figure 6-3.

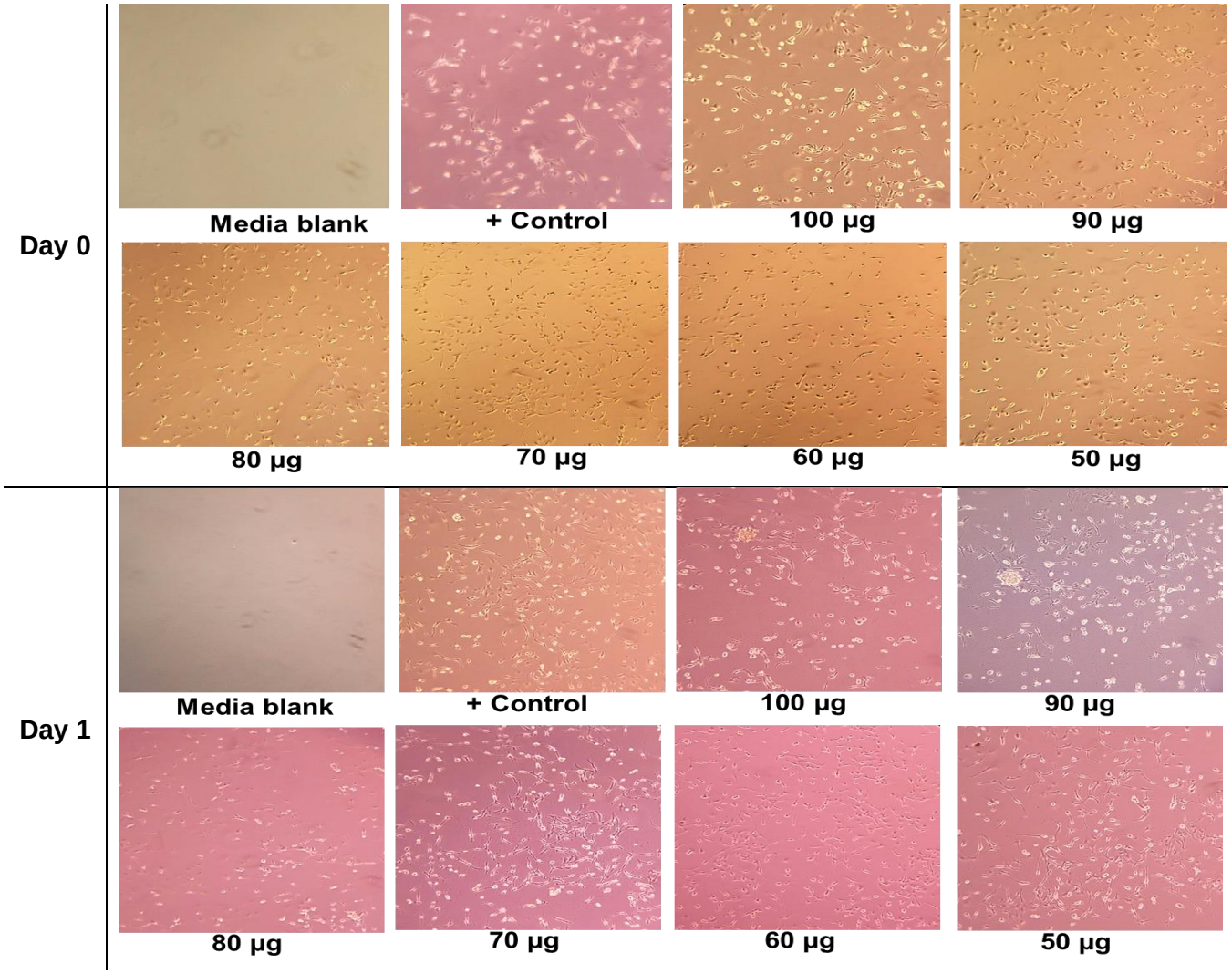

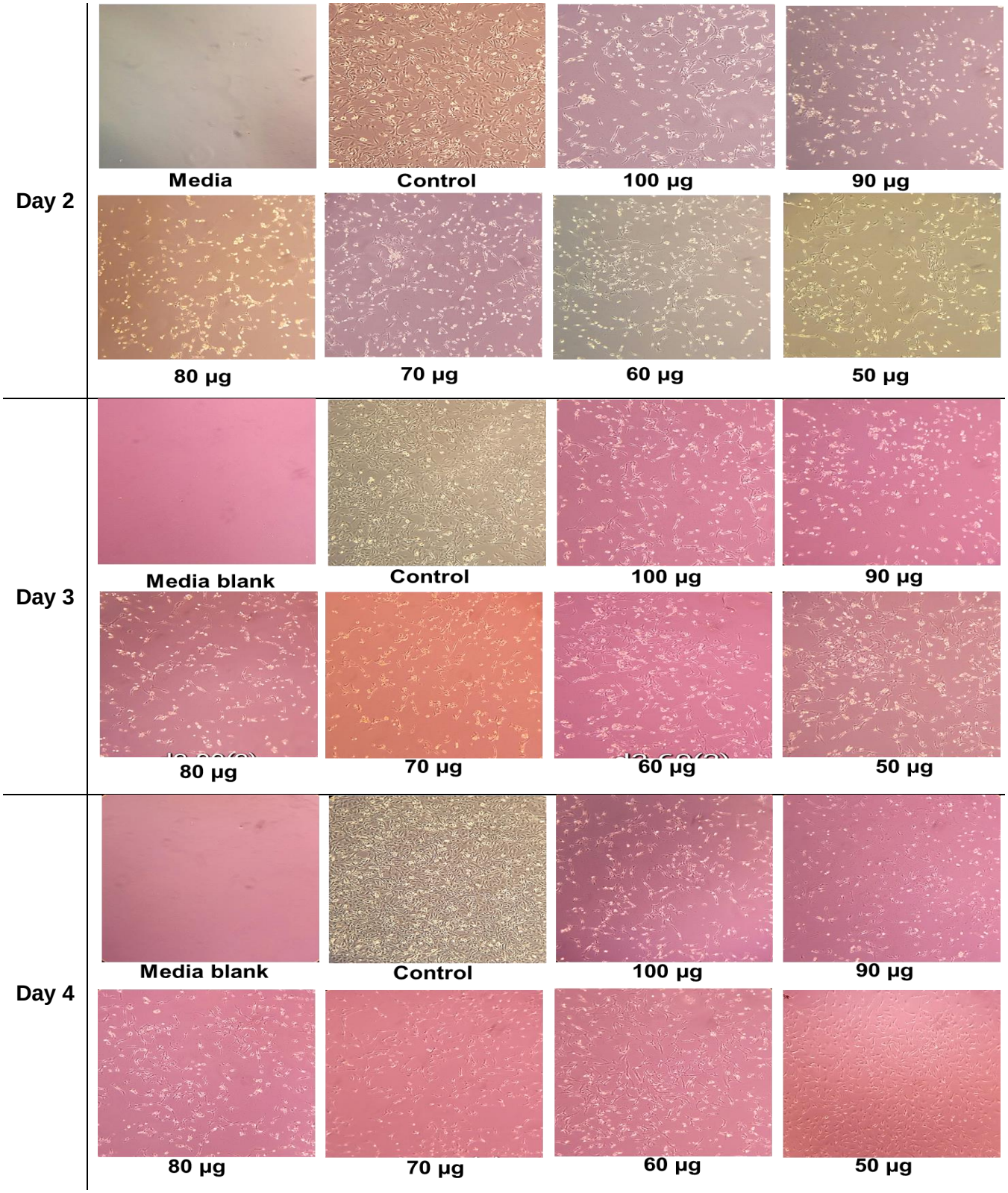
Day 2
Media
Control
100 µg
90 µg
80 µg
70 µg
60 µg
50 µg
Day 3
Media blank
Control
100 µg
90 µg
80 µg
70 µg
60 µg
50 µg
Day 4
Media blank
Control
100 µg
90 µg
80 µg
70 µg
60 µg
50 µg

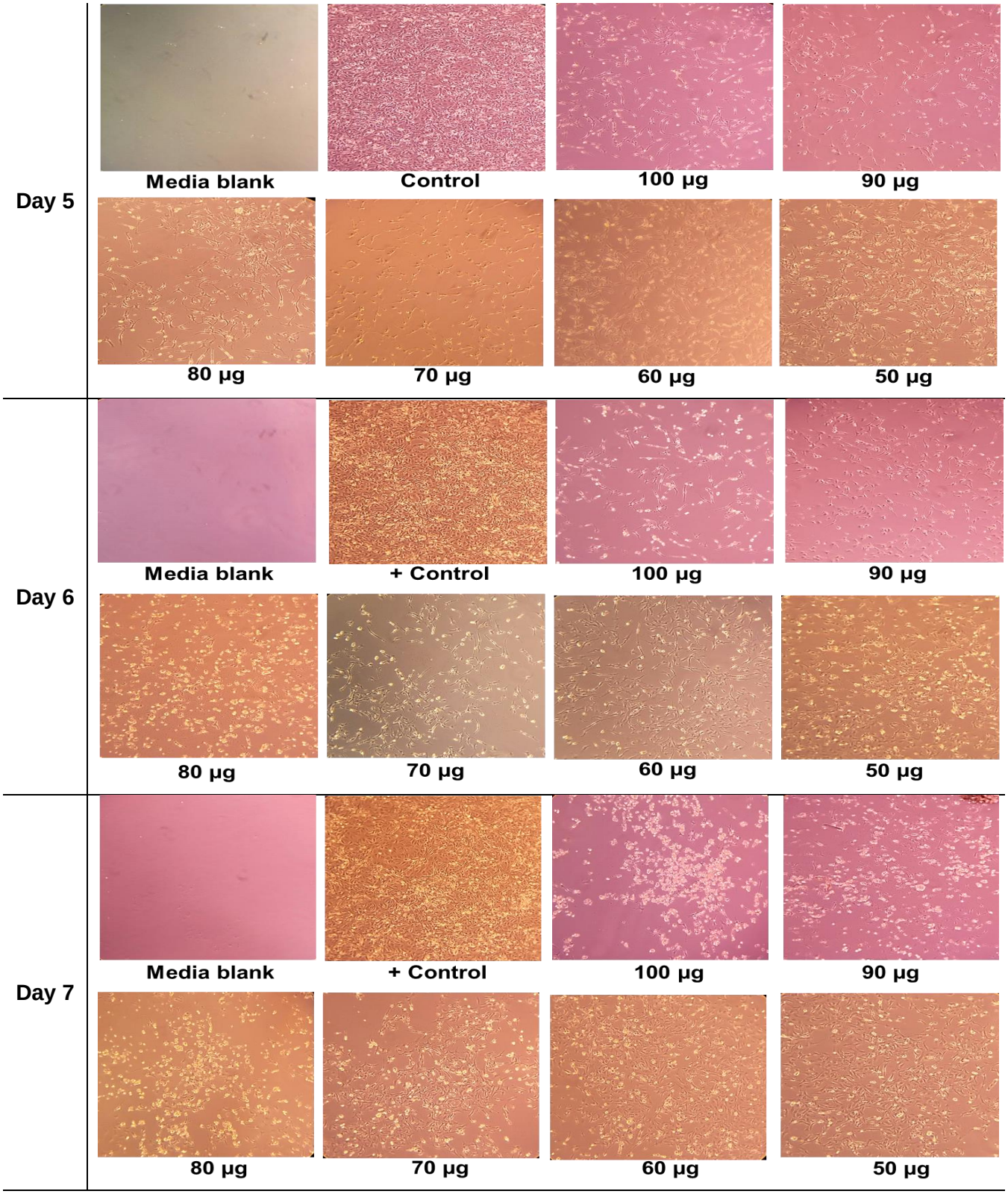

Figure 6-3 Visual illustration of the Vero growth pattern under the influence of different PAN concentrations ranging from highest 100 µg mL^{-1} to 50 µg mL^{-1}. Photographs were taken daily under an inverted microscope at 100 X to visualize the change in cell morphology under the influence of various concentrations of the PAN

A similar result was seen in the second experiment, where cells were dislodged at higher concentration i.e. 100 µg mL^{-1} and proportionately reduced as the concentration decreases which can be seen clearly in Figure 6-3 (day 7).

It has been noticed from these two experiments (Figure 6-2, Figure 6-3), that the PAN concentration near the 50 % inhibitory dose (IC_{50}) detached the cells more effectively than the lower concentrations. The low concentration of PAN from 0.3125 μg mL^{-1} to 50 μg mL^{-1} did not detach the cells from the surface effectively as compared to 50 to 100 μg mL^{-1}. The gradual increase from 50 to 100 μg mL^{-1} also confirmed the increased number of cells suspended, consistent with the overall findings. To further expand the horizon on the effect of PAN on Vero cell's attachment/ detachment behaviour, high concentrations of PAN (> 100 μg mL^{-1}) were also investigated.

The higher concentrations of PAN (100, 200, 250 and 500 μg mL^{-1}) were explored. The selection of these concentrations was taken broadly to evaluate the effect of PAN on Vero cells between 100 to 500 μg mL^{-1} where 100 to 200, and 250 to 500 μg mL^{-1} provide two windows for analysis. Figure 6-4 visually illustrate the changes that occurred to the Vero cells under the influence of high doses of PAN. The photographs were taken every day from day 2 onwards. It was observed from the Figure 6-5 that on day 2, Vero cells detached from the surface and came into suspension under the influence of 100 - 200 μg mL^{-1} concentration whereas at 250 μg mL^{-1} concentration, monolayer peeled off from the surface and formed cellular aggregates (clumps). The peeling of monolayer and formation of clumps indicated the cellular stress experienced by the cells due to the high concentration of the PAN. The highest concentration used in this experiment was 500 μg mL^{-1} which killed all the cells and left the plaques behind on day 2 (Figure 6-4).

On day 3, spent media was replaced with the fresh serum-containing media (with PAN) into the TC flasks. Some cells came into suspension after the media change. Suspended cells were collected in a shake flask and kept on an orbital shaker at 100 rpm inside the CO_2 incubator at 37 ^oC (discussed in Section 6.3). Consequently, photographs were taken until day 6 when the control flask (untreated cells) and the TC flasks with 100 and 200 μg mL^{-1} of PAN were fully confluent. The flask with 250 μg mL^{-1} of PAN was more than 80 % confluent at this stage. It was discerned from the Figure 6-2, Figure 6-3, and Figure 6-5 that the PAN concentrations between 100 μg mL^{-1} to 200 μg mL^{-1} showed a workable window of concentrations which were capable of dislodging cells whilst retaining their cellular activities. Because of this, cells reattached to the surface and formed a monolayer.

Figure 6-4 Visual inspection of Vero cells treated with PAN with highest concentration of 500 μg mL^{-1} depicting plaques after cellular death. Photograph was taken on day 2 (48 h of post PAN exposure) under an inverted microscope at 100 X magnification.

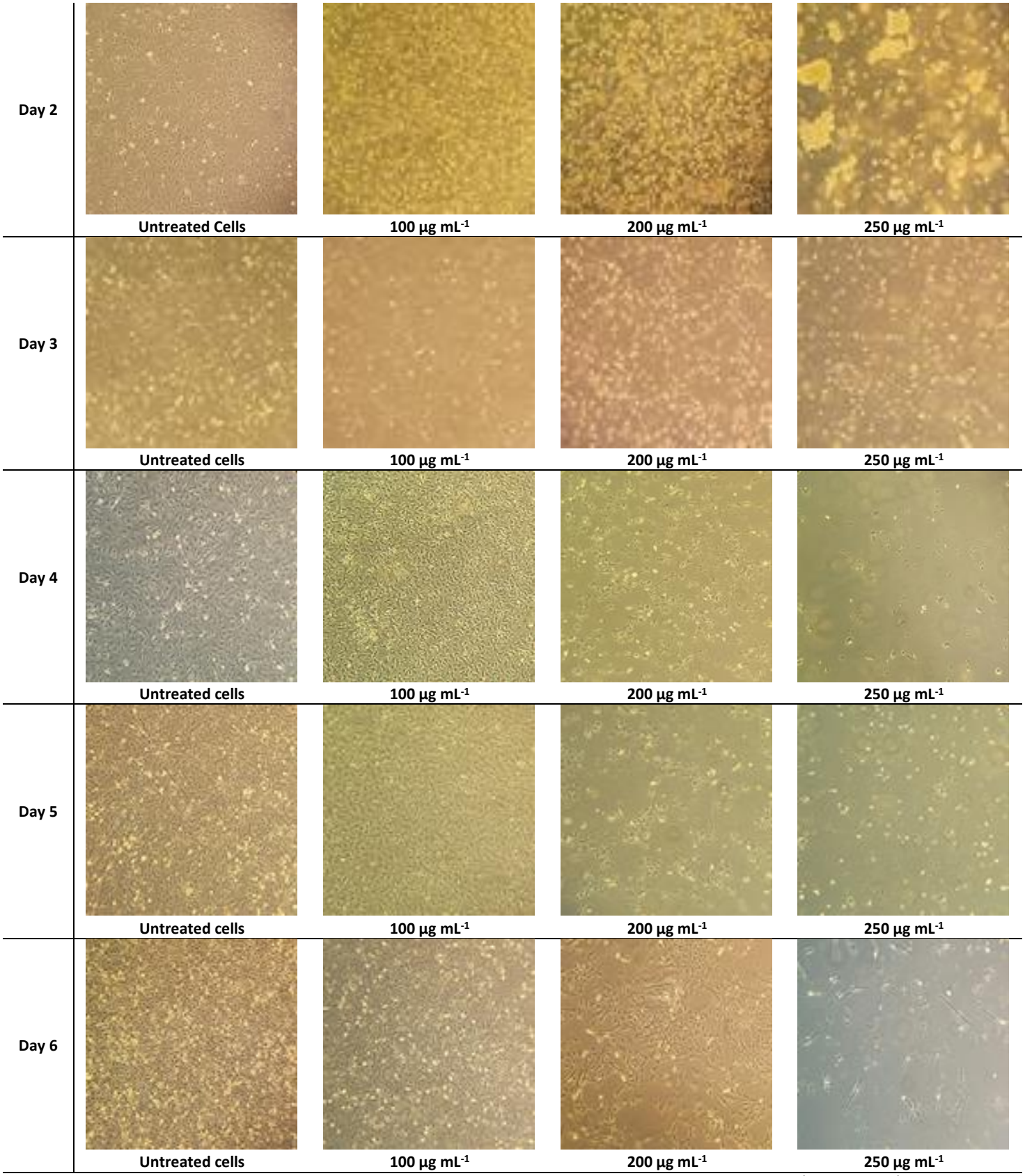

Figure 6-5 Visual illustration of the Vero cells under the influence of different PAN concentrations ranging from highest 100 µg mL^{-1} to 250 µg mL^{-1}. Photographs were taken every day after 48 h of incubation under an inverted microscope at 100 X magnification to visualize.

6.3 Re-culturing of suspended Vero cells in complete growth medium

The suspended cells from the above experiments (Figure 6-2, Figure 6-3, and Figure 6-5) were collected and kept on shaking platform in a medium which constituted 1:1 ratio of complete DMEM with 1 % FBS and SFM4 MegaVir. It was observed that cells remained viable for a couple of days without multiplying in numbers but formed cellular aggregates with the existing cells in the flask as shown in Figure 6-6 (b). Figure 6-6 (a) showed free Vero cells were viable whereas Figure 6-6 (c, d) showed the necrotic cells (lysed) due to overexposure to high concentrations of PAN.

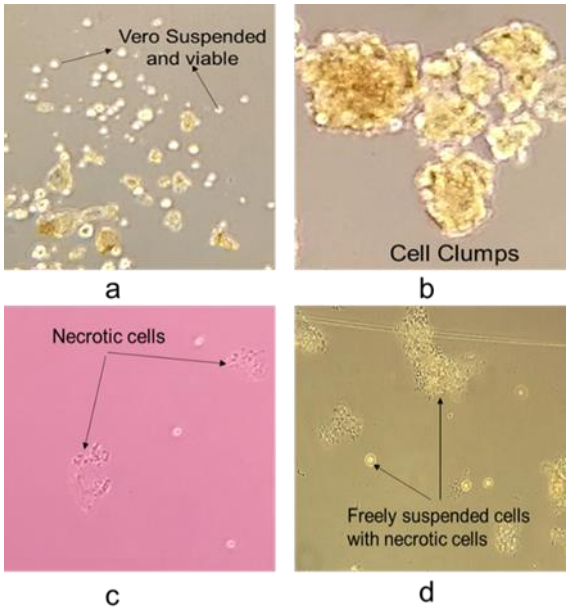

Figure 6-6 State of Vero cells post PAN treatment (a) harvested cells formed clumps and few cells are in single-cell suspension (b) big clumps of Vero cells where dark core indicated the dead cells in the centre (c and d) showed the floating necrotic and few suspended cells in the supernatant. Photographs were taken every day under an inverted microscope at 100 X magnification

The suspended Vero cells were triturated, and part of suspended cells were transferred to complete serum-free media to check if it may trigger cell growth. The cells were collected and evaluated for their biological activity and viability through isothermal microcalorimetry (discussed in chapter 7). The remaining suspension of Vero cells were re-seeded in the TC flask with DMEM constituted with 10 % FBS (No PAN). The cells started to grow adherently as shown in Figure 6-7.

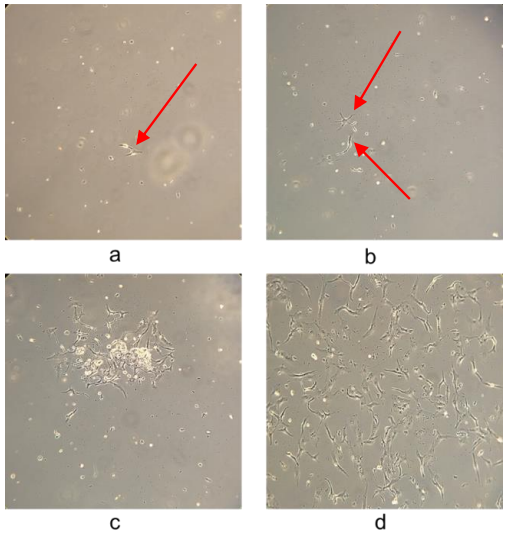

Figure 6-7 Suspended Vero cells re-attachment on the surface in the presence of serum-containing media (a) few cells attached (b) attached cells started to attain their normal fibroblast morphology from circular suspended cells (c, d) cells started multiplying and attained their normal activities

Vero cells which remained attached to the surface despite the exposure of PAN were re-fed with DMEM with 10 % FBS. The cells started to attain their activity and re-gained their morphology and confluency. Figure 6-8 showed sequential stepwise progress of the Vero cell monolayer. After day 5 of incubation, the monolayer was fully confluent, and cells attained their morphology.

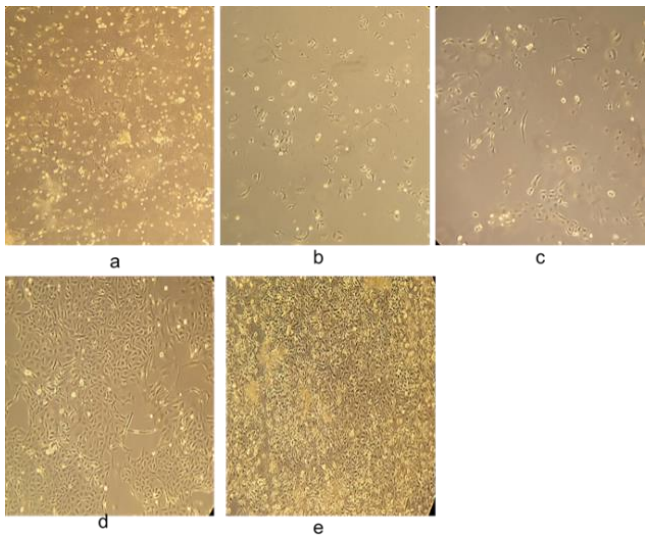

Figure 6-8 Step-wise growth pattern of non-suspended Vero cells after adding fresh media (DMEM with 10 % FBS) post-exposure of PAN. The photographs were taken every day to monitor the growth (a) Few cells remain attached to surface while media containing floating suspended cells along with cellular debris (b) after media change (c) cell growth after day 1 (post-medium change) (d) cell growth after day 3 (post-medium change), and (e) cell growth after day 5 (post-medium change)

So far from these results, it is postulated that PAN interferes in the integrins' signal transduction pathways which resulted in dislodging of the cells in the presence of PAN and when in contact with serum-containing media, it reversibly regains their morphology. The detailed answer may lie in the realm of cell biology and its plethora of signal transduction pathways. A brief justification is put forward below.

6.4 Reasoning and analysis

As mentioned before, integrins play a crucial role in bi-directional transmembrane communication which aid in cell adhesion, migration, proliferation, differentiation, and gene regulation as shown in Figure 6-9 (a). On the surface of the resting cell, it is present in the form of non-adhesive inactive state which upon activation, quickly and reversibly assist in cell adhesion by changing the integrin's affinity for its ligands (Legate et al., 2009; Shattil et al., 2010). Integrin activation is the best-suited example of inside-out signalling which can be explained through immune cells.

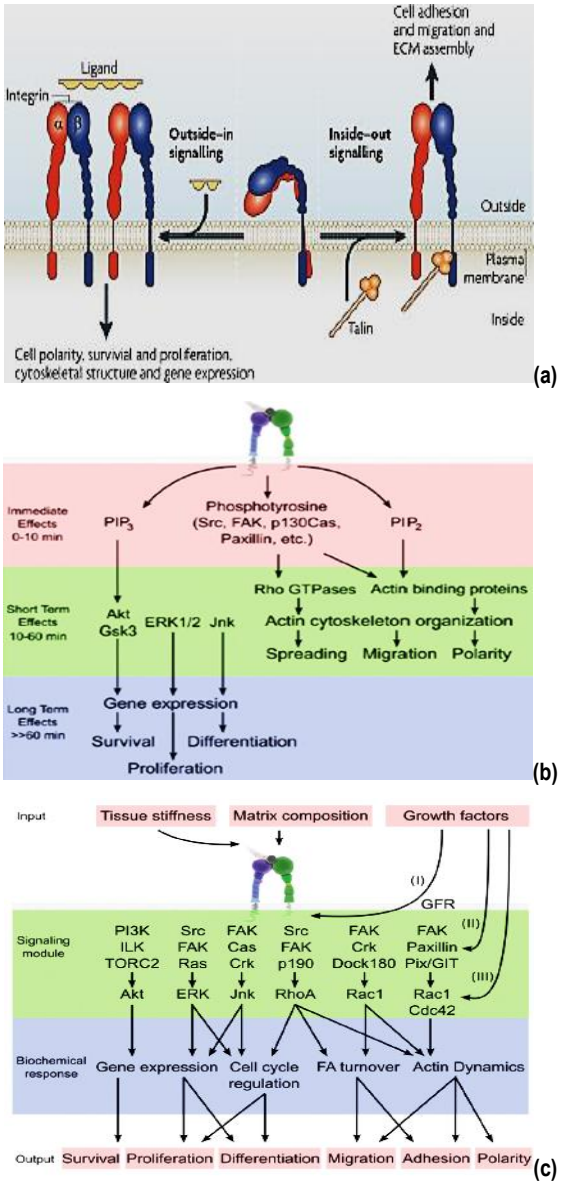

Figure 6-9 Illustration of step-wise role of integrin in cell adhesion, migration, proliferation, differentiation, and gene regulation (a) depicts the bidirectional transmembrane communication (inside-out and outside-in), (b) described the consequences of integrin activation based on the time that leads to downstream signalling and (c) illustrate the examples of downstream signalling after integrin activation - taken from Legate et al., (2009) and Shattil et al., (2010)

Immune cells freely circulate in the bloodstream without attaching to the walls of the vessels and the platelet's cells. Improper activation of integrin on these immune cells may form thrombosis (blood clot), which

can be life-threatening. Upon activation, integrin transduces intracellular changes which is an example of outside-in signalling (Legate et al., 2009).

The transduction of outside-in signalling from the activated integrin immediately bring intracellular changes by increasing the tyrosine phosphorylation of specific substrate and increasing the lipid concentration (Legate et al., 2009). The composition of the plasma membrane plays a key role in two-way communication across the membrane. It has been reported that it is constituted by large domains of cholesterol and sphingolipids, along with proteins caveolins, flotillins, glycosylphosphatidylinositol (GPI) and src kinases which is collectively termed as *lipid raft* that further assist in signal transduction at the plasma membrane (del Pozo et al., 2004). Based on the extracellular stimulus, integrin initiates short – term changes to the effector cells by impacting the cytoskeletal rearrangement that changes the morphology of the cells by interacting with the actin filaments. On the other hand, long-term attachment to ECM changes the signal transduction pathways and gene expression that have direct influence the cell proliferation, differentiation and survival Figure 6-9 (b). The detailed review of the pathways was explained in (Legate et al., 2009).

Additionally, integrin activation also controls the composition and assembly of the extracellular matrix (ECM). The ECM, its mechanical strength and the growth factor environment regulate the outside-in signalling through interaction with integrin and growth factor receptors (GFR). The growth factors play a key role for integrin binding to specific ligands and regulating signalling proteins such as FAK, Src, PI3 K (II) and downstream effectors such as Akt, Erk, JNK, Rho-GTPase (III) (Legate et al., 2009).

In simple words, activated integrin binds to the specific ligand and the ligands are multivalent entities, which interact with various subunits of integrins that forming integrin clusters which produce signals that regulate and control cell polarity, cytoskeletal rearrangement, growth, differentiation survival and gene regulation as shown in Figure 6-9 (c) (Legate et al., 2009; Shattil et al., 2010). Furthermore, integrin activation is also useful for anchorage-dependent cellular events such as platelets aggregation and leukocyte (WBC's) movement to the effector cells. Moreover, integrin activation can control the polarity of the migrating cells and regulate metastasis, therefore blocking of the integrin inactivation could be a useful tool for non-adherent therapies (Shattil et al., 2010).

In the current study, Vero cells were suspended from the adherent state under the influence of PAN. Integrins generally mediate cell adhesion to the ECM and when in culture conditions, group of proteins (e.g. phospho-caveolin-1) with various signalling properties and cytoskeletal proteins, cluster at the focal adhesion scaffold (Gaus et al., 2006). Focal adhesion is large macromolecular assemblies which directly connects with ECM and established mechanical linkage and transmit regulatory signals to the effector cells (Wehrle-Haller, 2012) as shown in Figure 6-10.

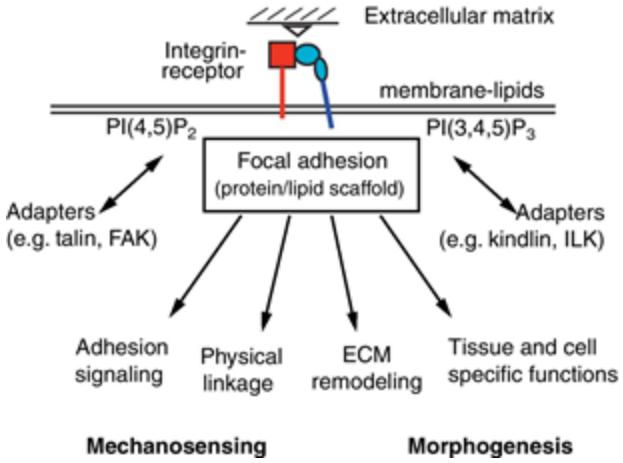

Figure 6-10 Construction of focal adhesion and their function – taken from Wehrle-Haller (2012)

It is known that GTP-binding protein Rac1 is required for integrin-mediated adhesion which binds to adherent cell membrane more effectively than planktonic free fibroblast cells. As a result, GTP-binding protein Rac1 in suspended cells remains in the cytoplasm bound to Rho guanine nucleotide dissociation inhibitor (RhoGDI) (del Pozo et al., 2004; Echarri and Del Pozo, 2006).

del Pozo et al.,(2004) further elaborated that the RhoA and Rac 1 proteins are present in the lipid raft and caveolae that play a significant role in signalling. Cell detachment also triggers internalisation of the plasma membrane which can be prevented in adherent cells by inhibiting the translocation of Rac1 to the plasma membrane Figure 6-11. The Lipid raft and caveolins play a key role in Integrin-mediated internalisation of the membrane. Therefore, integrin-mediated adhesion cells came into suspension (del Pozo et al., 2004; Del Pozo et al., 2005; Echarri and Del Pozo, 2006). Figure 6-11 described the process of internalization.

Echarri and del Pozo (2006) described the model of integrin-dependent regulation of caveolae/Cholesterol-Enriched Membrane Microdomains (CEMM) internalization. In the case of adherent cells, integrin-dependent signalling regulates the caveolae/CEMMs present at the plasma membrane targeting Rac protein. This pathway is likely to regulate at least the localization of phospho-caveolin-1 at focal adhesions, that prevent caveolae internalization (Figure 6-11 (a)). In the case of suspension cells, integrin signalling is interrupted, and the pathways inhibiting caveolae/CEMM internalization are blocked, resulting in endocytosis of the caveolae/CEMMs. Internalization is mediated by translocation of phospho-caveolin-1 to caveolae/CEMMs, triggered by an unknown mechanism. Caveolae/CEMM internalization results in uncoupling of Rac from downstream effectors, resulting in a shut-down of the signal. In the cytosol, Rac is bound by RhoGDI, further blocking downstream signalling (Figure 6-11 (b)).

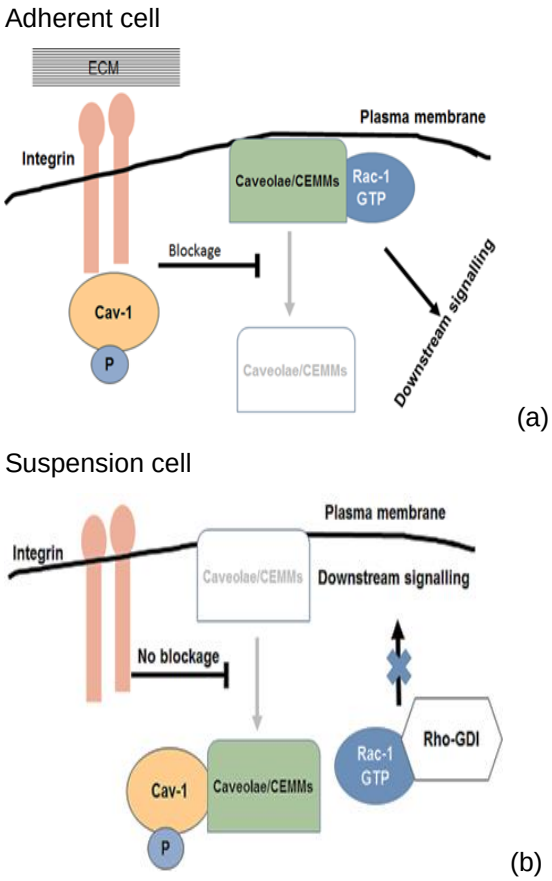

Figure 6-11 Illustration of integrin-dependent regulation of Caveolae/CEMM internalization. (a) For adherent cells, caveolae/CEMM present on the plasma membrane which permits the Rac1 GTP protein to transduce a signal. The integrin-mediated localised phosphor-caveolins1 block the internalization of the Caveolae/CEMM. (b) For suspension cells, due to impaired integrin signalling, the internalization of caveolae/CEMM is mediated by translocation of phosphor-caveolin-1 to caveolae/CEMM, as a consequence, Rac-1 GTP coupled with Rho-GDI block the downstream signalling- adapted from Echarri and Del Pozo, (2006)

Krishnamurti et al., (2001) reported that the main integrin (α3β1) was expressed by glomerular epithelial kidney cells which mediate the cell attachments to the ECM. As Vero cells are also kidney cells, the similar mechanism was presumed to occur in the case of Vero cells where PAN acts as an external ligand. It is therefore postulated that time-dependent exposure of PAN reduces the expression of α3 and β1 at protein and mRNA levels and assist in detachment of the cells. Due to outside-in communication, re-organisation of plasma membrane occurs, which result in the internalization of the lipid component of the Vero cells' membrane thus allowing cell detachment from the surface and eventually into suspension.

When the suspended Vero cells were again re-seeded into the TC flask with serum-containing media, the cells re-attached to the surface and attained their morphology and activities as illustrated in Figure 6-7. This phenomenon can be explained through the re-organisation of membrane order. Generally, in adherent cells, loss of adherence triggers internalization/endocytosis of multiple lipid raft components such as GPI-linked proteins, ganglioside GM1 and cholesterol which downgrade the membrane order (constituents). Lipid rafts are endocytosed through caveolae by phosphorylation of caveolins 1 on tyrosine 14 which suppress the expression of Rac1, Erk, PI-3 kinase-dependent pathways (Balasubramanian et al., 2007).

The crosstalk between integrin and growth factor receptors occurred during integrin-mediated cell adhesion. Exposing the drug-treated Vero cells to serum-containing media reversibly stimulate the re-modulation of integrins via Akt1 signalling that regulates the assembly of fibronectin through the activation of integrin particularly α5β1 (Danen and Yamada, 2001; Izmailyan et al., 2012; Somanath et al., 2007) Because of this, it was assumed that Vero cells re-attached to the surface and attained their morphology and activity upon exposing to serum-containing medium.

Another important aspect of Vero cell line is their susceptibility to various viruses. Altering the integrin pathways may negatively influence the susceptibility of the Vero cells. Guo et al., (2014) published a proteomic analysis of membrane proteins of Vero cells. The total of 627 membrane proteins were mapped, out of which 17 were identified as virus receptor proteins responsible for virus entry. The 627 membrane proteins constitute a part of the pool of membrane proteins which are not fully extracted due to the complexity and extraction efficiency of the methods used (shotgun LC-MS/MS approach).

Integrins are common receptor for a of viruses such as rotavirus, West Nile virus, dengue virus, foot and mouth disease virus, Japanese encephalitis virus, hepatitis C virus, feline immunodeficiency virus, canine distemper virus in human and animals. This is due to their inability to express signal peptide (interferon) upon virus infection which impaired their defence mechanism (Kiesslich and Kamen, 2020). Vero cells expresses α3/ α5/ β1/ β3/ β4/ β6 subunits of integrins. The integrins such as αVβ3 is a cellular receptor of rotavirus, cytomegalovirus, West Nile virus whereas β integrin is a receptor for spot syndrome, β3 for Hantaan virus, αVβ1 and αVβ6 for foot and mouth disease are few examples which showed that integrins played a crucial role in virus entry. Since integrins are important proteins for virus entry, care must be taken in manipulating its expression as it may interfere the cells function as a host cell for infection. Further investigation on this needs to be carried out but is not in the scope of this thesis.

It can be concluded that integrins play a paramount role in adhesion or suspension of the cells. Their mechanism of signal transduction is complex and requires a thorough understanding of cell biology and its mechanism. The knowledge of the cell-specific integrin expression (e.g. Vero) could lead to identifying the pathways, where activation/deactivation might bring the Vero cells in suspension irreversibly without changing their morphology, genotype and virus susceptibility.

6.5 Summary

The focus of this chapter was to bring Vero cells into suspension culture which is otherwise difficult. This is primarily because of the high expression of the surface receptor proteins integrins, which control and regulate the binding of the cells to the substratum (ECM) through bidirectional signalling (inside-out and outside-in).

In this research, efforts have been made to make use of the anticancer drug, PAN to bring the cells into suspension. The use of PAN to detach the cells (Podocyte-kidney cells) from the ECM is well documented in the literature.

Initially, IC_{50} studies were carried to find out the 50 % inhibitory dose of PAN in a time-dependent manner. The effect of PAN was observed till 72 h. The value of 48 h and 72 h of post exposure was turned out to be 107 and 110 μg mL^{-1}. The value of 24 h of post-exposure was not considered due to erroneous results.

After obtaining the IC_{50} value, various concentrations of PAN were tested to evaluate the effect of PAN on cell growth or cell detachment. The concentration tested covered the range from 0.3125 μg mL^{-1} to 500 μg mL^{-1}.

It can be seen that the cells started detaching from the surface after 50 μg mL^{-1} concentration and above, however, at 500 μg mL^{-1} led to cell death within 2 days of exposure. The detached cells were collected and suspended into 1:1 ratio of DMEM medium with 1 % FBS and serum-free medium (SFM4 MegaVir) shaken on an orbital shaker inside the CO_2 incubator at 37°C. The cells survived for a week and formed clumps and did not grow in number. But when re-seeded into the serum-containing basal medium (10 % FBS), they resurrected their metabolic activity and started multiplying and formed the monolayer.

The reason behind this behaviour of the Vero cells has been explained in the section Reasoning and analysis. In brief, integrin mediates cell adhesion to the ECM. There are many sets of protein which aid in signal communication such as RhoA and Rac. These proteins are present in the lipid raft and caveolin, which play an important role in integrin-mediated membrane internalization. The membrane internalization caused the cells to come into suspension after detachment from the ECM. The re-attachment of the cells to the TC flasks is because of the re-organisation of the membrane order. It happened when the drug-treated cells re-seeded into serum-containing media that reversibly stimulate the re-modulation of integrins via Akt1 signalling which regulates the assembly of fibronectin through the activation of integrin subunit α5β1.

7 Investigating isothermal microcalorimetric profile of post-drug-treated Vero cells for the suspension culture

The objective of this chapter is to incorporate isothermal microcalorimetry, a technique used to investigate the metabolic heat produced at different cell densities and physiological states of CHO and Vero cells. A correlation was drawn between the responses obtained from Vero cells treated with PAN with those not-treated with PAN in the form of heat generation (μW and J). CHO cells were used as a positive control to optimise the cell density for obtaining the measurable calorimetric signals for processing. The scope of using this technique in this research is limited to monitor the changes in the heat profile of the Vero treated cells from that of non-treated cells to determine the bioactivities of the cells.

7.1 Growth profile of CHO cells

CHO cells are usually adapted to suspension culture with ease in serum-free conditions and exhibit nearly the same growth rate, doubling time and other metabolic activities as compared to native adherent cells (Sinacore et al., 2000). Therefore, in the current research, CHO cells were considered as the control specimen. CHO cells were used to determine the appropriate cell densities required to generate the detectable calorimetric response as the cell numbers are crucial in determining the value of heat dissipation during the experiment. For that, the adherent CHO cells cultured in DMEM with 1 % FBS and CHO-S cells suspended in complete SFM4 CHO medium were used. Their respective media were used as a negative control (media blank).

Figure 7-1 depicts the graphical representation of the heat flow and heat data obtained from the three separate experiments with adherent and suspended CHO cells with different initial cell densities. The heat flow signal signifies the net response of all the activities in the ampoule which encompasses the physical or chemical processes particularly metabolic reactions (anabolic/catabolic). As a result, the exothermic and endothermic reaction can occur simultaneously which may yield a negative signal. To mitigate the negative values in the samples, the value of the negative blank (media control) was subtracted from the test samples to normalize all the samples.

Heat flow data reflect the bioactivity of the samples which is measured as the rate at which overall chemical and physical processes take place in the ampoules over the run-time (metabolic activities carried out by the cells) and the heat thermogram indicate the anabolic/catabolic reactions occurring inside the cells while consuming nutrients (substrate) and producing the metabolic products (Braissant et al., 2010).

For typical single bacterial cells, the heat flow activity was assumed to be ~ 2 pW and 100k bacteria required to produce a detectable signal. Similarly, it has also been reported that mammalian cells' heat production rates fall in the range of 0.2 – 50 μW and a single active mammalian cell produces heat in the order of 1 - 100 pW (Braissant and Daniels, 2011).

To find out the optimum cell number required for the detectable signal and find out the bioactivity profile, different cell number of CHO cell were tested in the IMC.

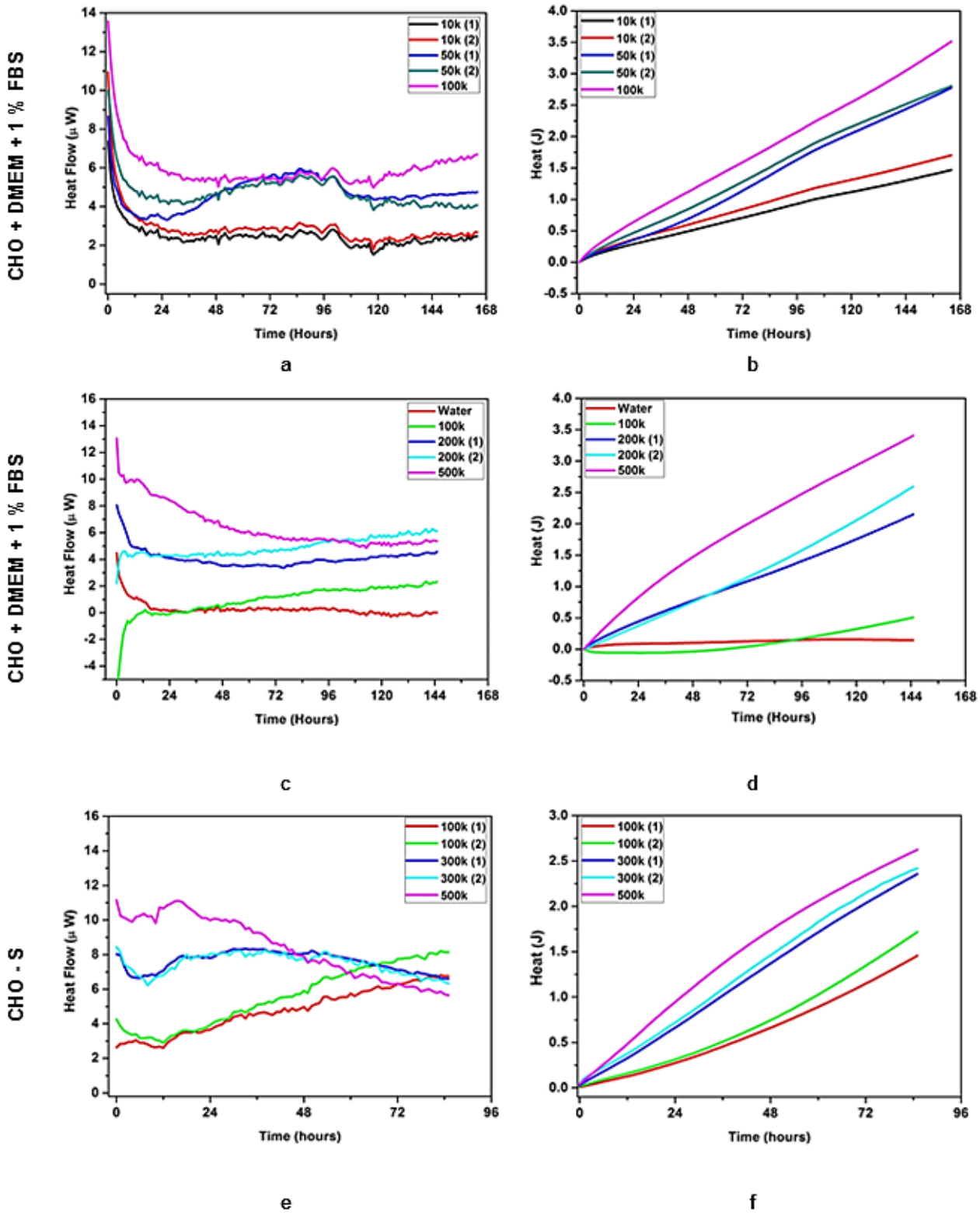

Figure 7-1 Microcalorimetric profiles of CHO cells (adherent and suspension) at different cell densities. Measurements were reported every 1 hour. (a) and (b) indicated the heat flow and heat generation data for adherent CHO cells with cell density 10k, 50k and 100k cells in 2 mL culture volume. (c) and (d) represented the data for adherent CHO cells with cell density 100k, 200k and 500k in 2 mL culture volume with water and (e) and (f) represented the heat flow and heat generation data for suspended CHO-S cells with 100k,300k and 500k cells. The data have been normalised with media blank in all the experiments. (k = 1000)

The thermograms obtained from the CHO cells are different from the recently published thermograms in the literature, more likely of other specimens such as fungus and bacteria. Myers, (2017) has conducted a study on yeast (Saccharomyces cerevisiae CBS8803) investigating the stress response using microcalorimetry. He demonstrated that the heat flow profile of yeast showed a bell-shaped curve while optimising the inoculum sizes (cell number) as shown in Figure 7-2 (a) and integrated heat profile showed sigmoid “S” curve Figure 7-2 (b)

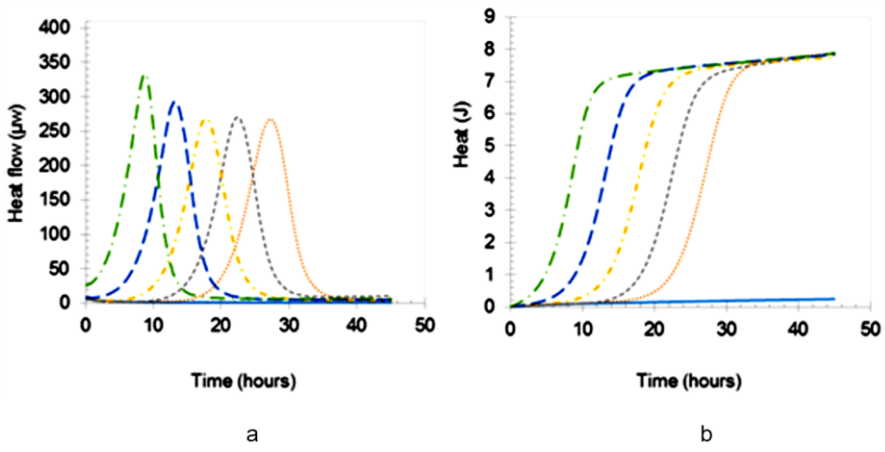

Figure 7-2 Microcalorimetric profile of yeast (*Saccharomyces cerevisiae* CBS8803) showing (a) heat profile and (b) heat curve of different cell concentrations (inoculum sizes). The lines (▬) represented the YPD blank, (▪▪▪▪) 0.1k, (▪▪▪▪) 1k, (▪ ▪ ▪) 10k, (▬ ▬) 10k and (▬ ▪ ▬) 1000k cells mL^{-1}. –taken from Myers, (2017)

In a separate study, Di Luca et al., (2019) showed the similar bell-shaped heat flow pattern and “S” shaped heat curve for various *Candida* species as shown in Figure 7-3 (a, b). In another study, (Bravo et al., (2011) also reported similar bell-shaped curve with various species of bacteria when grew in Angle medium with potassium oxalate as a sole carbon source as shown Figure 7-4.

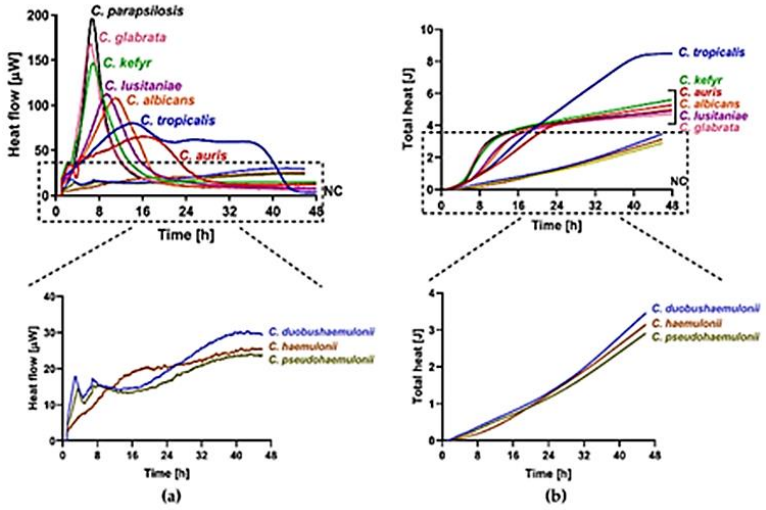

Figure 7-3 Microcalorimetry analysis of Candida spp. Heat flow (a) and total heat (b) curves generated by planktonic *C. parapsilosis*, *C. glabrata*, *C. kefyr*, *C. lusitaniae*, *C. albicans*, *C. tropicalis*, *C. auris*, *C. duobushaemulonii*, *C. haemulonii,* and *C. pseudohaemulonii* in RPMI 1640 at 37 °C. – taken from Di Luca et al., (2019)

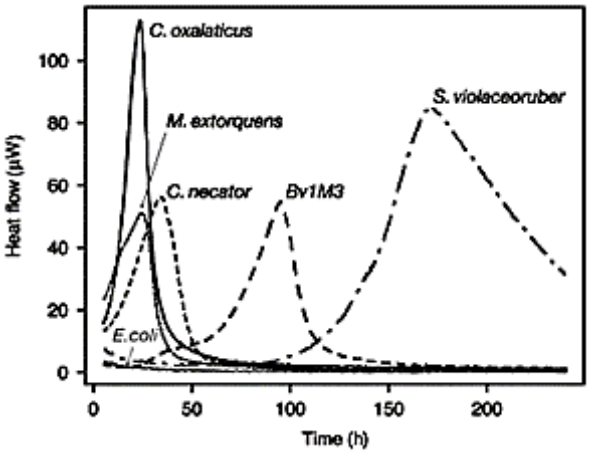

Figure 7-4 Heat flow pattern recorded for *Cupriavidus oxalaticus, Methylobacterium extorquens*, *Cupriavidus necator*, *Streptomyces violaceoruber, Sptreptomyces* sp. BV1M3, and *Escherichia coli* inoculated in Angle medium with potassium oxalate as the sole carbon source - taken from Bravo et al., (2011)

The observation made from the Figure 7-2, Figure 7-3, and Figure 7-4, it appeared that the Bell-shaped curve for heat flow curve is the norm but the heat curves (thermograms) for the CHO cells (adherent and suspension) at different cell numbers shown in Figure 7-1 is different from the heat flow curves of yeasts and bacteria, rather mammalian cells have initial peak activity and thereafter formed a plateau.

Guan et al., (1997) demonstrated that in a batch culture, CHO 320 cells followed the heat flow pattern as shown in Figure 7-5 which is not bell-shaped but resemble the pattern as shown in Figure 7-1. Hence, the thermograms obtained for the CHO cells in this study, are in-line with the pattern reported in the literature for mammalian cells.

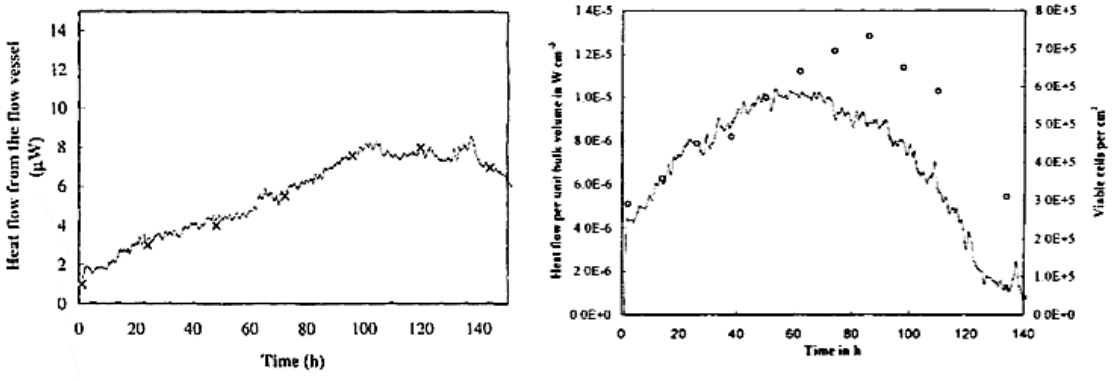

a b

Figure 7-5 Represented the heat flow measurements of (a) CHO 320 cells where (-) indicated the online heat flow and (x) indicated the offline heat flow rate with an insertion vessel and (b) illustrate the heat flow of a small portion of the growth curve of CHO 320 growing cells measured online by the IMC and scaled to the unit bulk volume of RPMI 1640 medium buffered with 20 mM HEPES and 4 mM bicarbonate (-) indicate the number of viable cells per cm^3 bulk volume (o) at discrete time intervals- figures taken from Kemp and Guan, (1997) and Guan et al., (1997)

After normalising, Figure 7-1 (a) showed that the ampoules containing 10 k cells in duplicate showed almost uniform bioactivity with heat flow fell between 2 - 3 µW throughout the run which indicated that the cells become acclimatised to the culture conditions and formed a plateau. The ampoules containing 50k cells in duplicate express the increase in activity started from 48 h and declined after 96 h with highest activity

around 85 h which ranged from 4 – 6 µW, whereas 100k cells showed that the activity of cells stays around 6 µW till 96 h, thereafter, heat flow started increasing as shown with a pink line. Heat curve profile (J) of after normalization of 10k, 50k (duplicates), and 100k showed comparable curves with an increase in activity as the cell number increased Figure 7-1 (b).

The number of cells and the final volume in the ampoule play a crucial role in generating useful data. An insufficient number of cells may not generate a detectable signal and a large number of cells could produce a quick large peak of heat flow data and soon after nosediving to baseline due to medium depletion/toxicity and low oxygen availability. It has been reported that high cell density (≥1 x 10^6 cell mL^{-1}) produce an unstable heat production curve with an initial peak and sharp decline (Nässberger et al., 1988). Therefore, the emphasis was given to optimising the cell density with CHO cells which can produce consistent heat flow data that can be used to study the thermodynamics of treated and non-treated Vero cells.

All the experiments were carefully designed to avoid generating erroneous data. There could be multiple sources of erroneous heat flow signals as described in detail by Braissant and Daniels in 2011. It is also assumed that the negative value of the baseline (negative controls which include blank water) could be because of the faulty crimping of the metallic collar around the rubber septum and loosely inserted screw top in the metallic cap which permit leakage and heat exchange within the system.

Other reasons which can be attributed to the negative drift include the deterioration of serum proteins or the presence of the serum contaminants which trigger an endothermic reaction. The heat flow data produced through IMC is non-specific, which signify that the heat flow signal produced is a net signal produced from all the physical and chemical activities taking place in the ampoule, therefore, experiments were planned with the appropriate controls to avoid erroneous data. To avoid cell attachments on the inner walls of the glass ampoules as shown in Figure 7-6, the ampoules were siliconized with sigmacote (as explained in 3.9.2) to avoid suspended CHO cells forming a biofilm which would compromise the interpretation of the heat flow signal results.

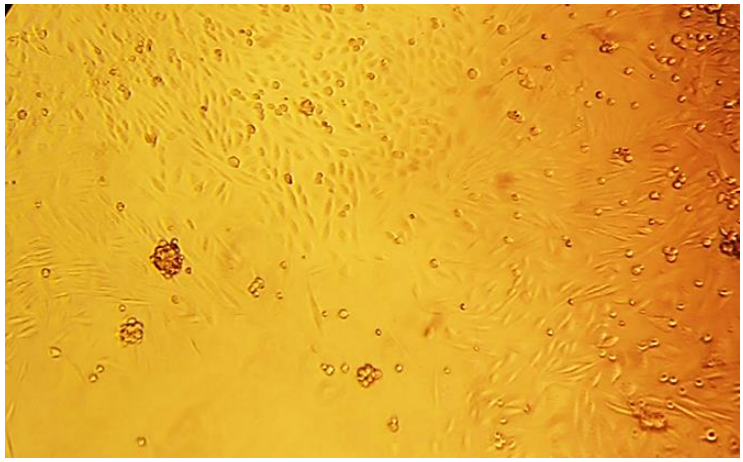

Figure 7-6 Example picture showing CHO (adherent) cell attachment on the inner surface of the ampoule

The metabolic heat flow and heat production of the CHO cells (adherent and suspension) was observed throughout of their respective batches which lasted for 164 h and 145 h with adherent cells grew in serum-containing media (1 % FBS) and CHO-S batch lasted for 85 h Figure 7-1. The average value of heat flow for 10k cells measured from the two thermograms was 2.69 ± 0.28 µW with the maximum bioactivity recorded 10.96 µW at the start of the batch Figure 7-1 (a). On the other hand, the average heat produced by 10k cells in duplicate showed an averaged value of 0.86 ± 0.10 J (Table 7-1). The reason for the error margins encountered in heat flow data can be attributed to the difference in starting cell numbers due to pipetting error and/or change in culture environment such as lactate production leading to pH change. The output of heat flow and heat production from the CHO (adherent and suspension) is summarised in Table 7-1, where cell numbers in duplicate were given as the averaged value in the same experiment. (DOI: 10.25375/uct.13570970).

Table 7-1 Averaged microcalorimetric responses of CHO cells (Adherent and suspension) for the complete duration of the experiments

Experiments	Cell numbers	Average heat flow (µW)	Average heat (J)
CHO + 1 % FBS	10k 10k	2.69 ± 0.28	0.86 ± 0.10
	50k 50k	4.72 ± 0.03	1.41 ± 0.08
	100k	5.95	1.80
CHO + 1 % FBS	100k	0.94	0.11
	200k 200k	4.51 ± 0.58	1.15 ± 0.08
	500k	6.49	1.91
CHO - S	100k 100k	5.51 ± 0.58	0.67 ± 0.07
	300k 300k	7.55 ± 0.09	1.24 ± 0.05
	500k	8.44	1.48

As expected, the thermograms of the 50k cells exhibited the better heat flow pattern and heat generation as compared to 10k cells and the thermograms of 100k cells showed a prominent curve of heat flow and heat production during the experiment (Figure 7-1 (a, b)). The peak from 50k cells were followed the nearly sigmoid curve which indicated the cells were entering into the stationary phase of their growth which contrasts with the thermogram of 100k cells which showed increasing heat flow which can be attributed to a large number of cells (Figure 7-1 (b)). The increased cell number above 100k (e.g. 200k and 500k) showed distinct curves for adherent CHO cells as illustrated in Figure 7-1 (c, d). It signifies that the cell numbers greater than 100k was sufficient to carry out studies which could last for a week without compromising the metabolic activities as compared to cell number less than 100k where the response is comparatively weak as can be seen in Table 7-1.

Additionally, microcalorimetric responses of the above-mentioned CHO cell numbers were analysed for the average heat flow and heat production profile over the complete run-time of the experiments as shown in Table 7-1. A noticeable observation was made from the data obtained for the adherent CHO cells. As the cell number increased from 10k to 50k which is 5 times, the average heat flow increased by 1.76 times and heat production by 1.65 times. When the heat flow and heat production profile of 50k were compared to that

of 200k, the values of heat flow and heat production were similar with only 0.95 and 0.82 times change respectively. Similar trends were observed when the cell numbers increased from 200k to 500k. The values of heat flow and heat produced increased by 1.44 and 1.66 times respectively which is slightly less than the ratio at which cell number increased (2.5 times). The low values of the averaged heat flow and heat signals were probably due to the possible variations in the initial cell number, the change in culture environment inside the ampoule such as accumulation of toxic metabolite, change in pH, oxygen depletion, heterogeneity of the culture (different phases of cell division) and volume of the culture media (available headspace) which all play a significant role in cellular growth and directly influence the thermodynamics of the growing cells.

In the case of CHO-S, the heat flow thermogram of 500k cells showed an initial rapid increase in metabolic activity and then a decline to form a plateau, which indicated that the initial cell numbers were sufficient for a 2 mL culture volume. Because of this, the setup resulted in an initial high activity and subsequently due to either to oxygen or media limitations, activity declined as depicted in Figure 7-1 (e. f). The heat flow profile of 300k cells had also followed the same pattern with an extended plateau. Therefore, it is evident that adherent CHO and CHO-S cells (>100k) were fully acclimatised to their respective growth conditions and produced a measurable microcalorimetric response. Hence, it was decided that for the further studies of Vero cells, the cell numbers above 100k cells were considered, as they produce a distinct measurable signal.

7.2 Growth profile of Vero cells

The microcalorimetric studies of Vero cells in the basal medium (DMEM) with 1 % FBS were carried out with cell numbers ranging from 100k, and 300k (in duplicate) and 500k and media blank as a single sample. The volume of each ampoule was kept at 2 mL

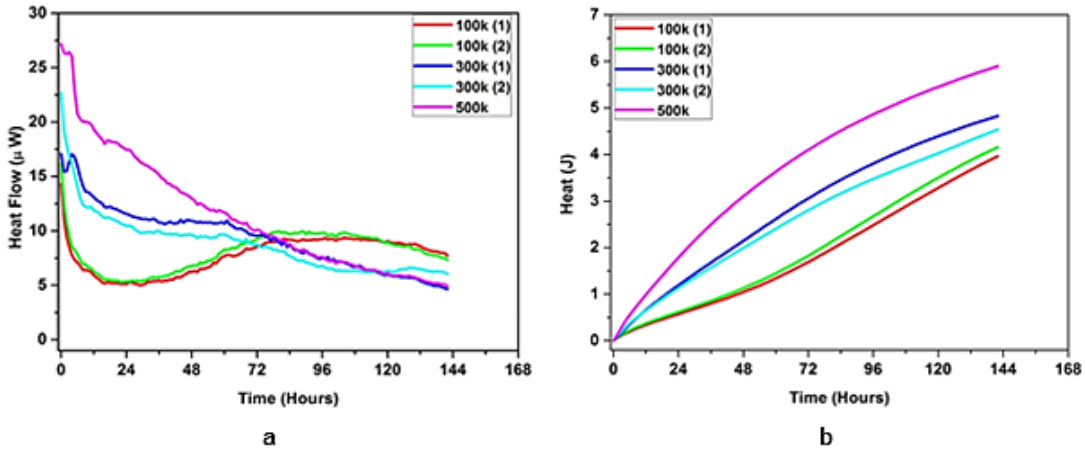

Figure 7-7 Microcalorimetric profile of Vero cells in DMEM with 1 % FBS at different cell densities presented (a) heat flow and (b) heat production profiles, where ampoules containing 100k cells (— and —), 300k (— and —), and 500k (—). Data shown here was normalized with media blank

From Figure 7-7, Vero cells with 300k and 500k cell numbers initially gave a maximum output of heat flow (power) at the beginning of the experiment and thereafter it started coming down slowly and formed a plateau at the end. A peculiar heat flow scenario of 100k (duplicate) cells was observed in Figure 7-7 (a) where heat flow decreases first and then slowly increased and reached to the maximum average heat flow

output of 9.59 ± 0.54 µW at 89 hours. The behaviour of these cells could be because of cell growth at this initial cell concentration.

In the case of Vero-SFM, the heat flow profile of Vero cells adapted to serum-free medium with 300k and 500k cells showed an initial high heat flow data as shown in Figure 7-8 (a) whereas 100k cells adapted to a serum-free medium in adherent culture showed an extended steady production of heat flow (µW). This trend is nearly similar to the Vero cells grown in the serum-containing medium as depicted in Figure 7-7.

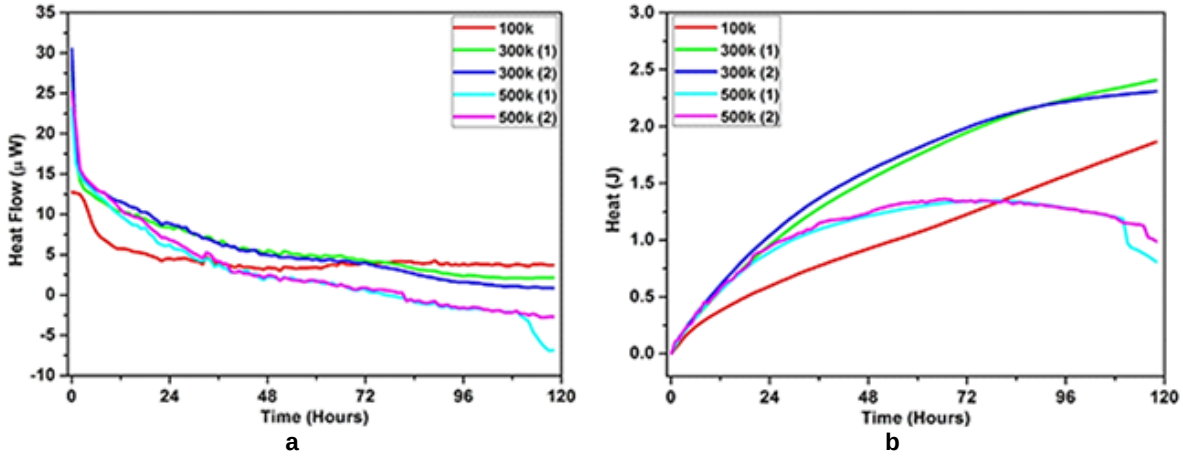

Figure 7-8 Microcalorimetric profile of Vero (adherent) adapted in serum-free media (SFM) with different cell densities (a) heat flow data and (b) heat production. (c) and (d) graphs rescaled to magnifying the dotted line area of the (a) and (b) to illustrate the heat flow and heat production profile to distinguish the pattern. The sample ampoules containing serum-free media control (—), 100k cells represented by (—), 300k (— and —) and 500k (— and —).

To compare the metabolic activity of the Vero with 1 % FBS and Vero-SFM, the averaged heat flow data of Vero cells grown in serum-containing medium (1 % FBS) for 100k, 300k and 500k cells were 1.77, 1.60 and 4.07 times metabolically more active than Vero-SFM (DOI: 10.25375/uct.13570970). This is in line with the notion that serum-containing cultures have better vitality and that serum containing medium sustains growth and the health of cell better.

From the observation made from the thermograms of Vero 1 % FBS and Vero-SFM, it has been decided that cell numbers between 100k to 300k would be the best bet to study the effect of PAN on Vero cells as their metabolic activity seems stable during the batch run (Figure 7-8 (a, b)). With a similar observation on the high heat production, Vero cells grown in DMEM + 1 % FBS at 500 k were used as a positive control.

From Figure 7-9 (a), Vero 250k cells treated with 200 µg mL^{-1} of PAN showed low to no activity of averaged heat flow (-0.13 ± 0.35 µW) as compared to the positive control (13.12 ± 0.18 µW). Similar heat flow diagrams were obtained when Vero at 200k cells were treated with 100, 200 and 250 µg mL^{-1} of PAN (data not shown). There are many possibilities for the low activity of Vero treated cells resuspended in serum-free medium, but the probable reason would be the high concentrations of PAN (>100 µg mL^{-1}) inhibiting metabolic activities in the Vero treated cells.

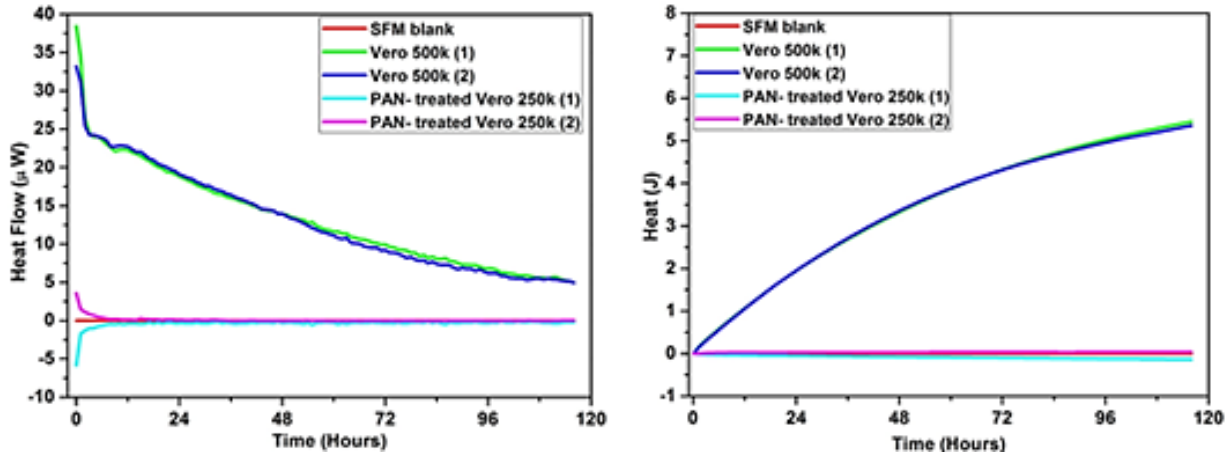

a b

Figure 7-9 Microcalorimetric profile of Vero cells treated with PAN and resuspended in SFM at different cell densities (a) heat flow data and (b) heat production. The serum-free media blank (—), Vero cells normally grown in DMEM with 1 % FBS were denoted by (— and —), Vero cells treated with PAN (200 µg mL^{-1}) was denoted by (— and —)

To verify the viability of these stressed Vero cells subjected to >100 µg mL^{-1} PAN, they were regrown in serum-containing media (DMEM + 10 % FBS) in TC-25 cm^2 flasks without PAN. These PAN-treated Vero cells managed to restore the cellular activities and started multiplying in the flasks. The proof of their viability and restoration of their cellular activities can be interpreted from Figure 7-10, where all PAN treated cells showed significant bioactivity.

The PAN-treated (100, 200 and 250 µg mL^{-1}) Vero cells (200k), when regrown in serum-containing media, showed their activity as 10.12, 10.18 and 9.15 µW, as compared to a positive control (untreated cells) which showed the heat flow value of 9.30 µW. (DOI: 10.25375/uct.13570970)

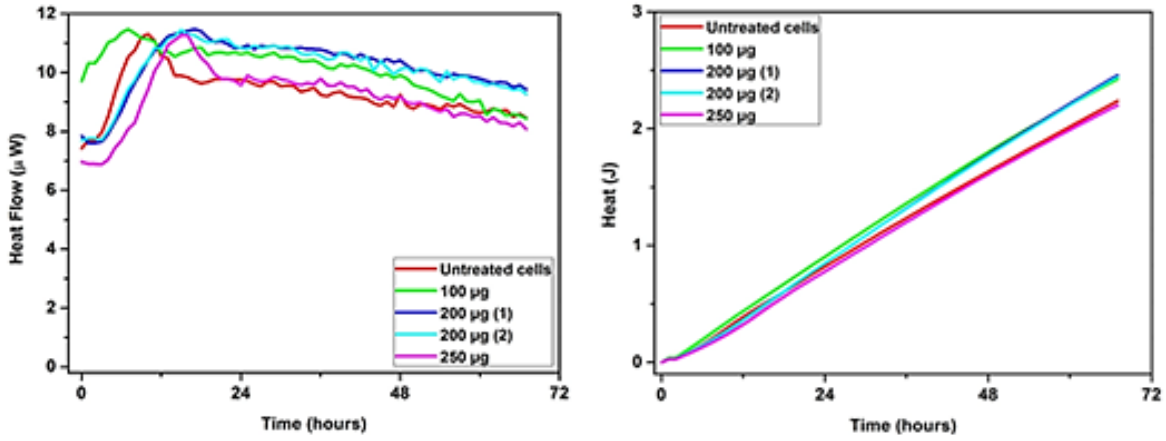

a b

Figure 7-10 Microcalorimetric profile of Vero cells treated with different concentrations of PAN and regrown in serum containing media with the same cell number of 200k per ampoule (a) heat flow data and (b) heat production. untreated cells as a positive control (—), Vero cells treated with 100 µg (—), two ampoules with cells exposed to 200 µg (— and —) and cells exposed to 250 µg was denoted by (—).

The increased value of heat flow and heat production of Vero cells, when regrown in serum-containing media, points out that the cells regained their ability to perform the required metabolic activities

which include the attachment to the surface and proliferation. The qualitative evidence can be seen in Figure 6-7, where Vero cells were re-attached to the surface in the presence of a serum-containing medium.

7.3 Growth kinetics of mammalian cells (CHO and Vero) in the closed ampoule

Efforts have been made to compare the kinetics of CHO (adherent and suspended) and Vero cells (grown in 1 % FBS, Vero-SFM, treated with PAN and Vero cells re-grown in serum-containing medium-10 % FBS) in a closed ampoule. The kinetic parameters for mammalian cells normally characterised by specific growth rate (μ) and doubling time (t_d). Doubling time (t_d) is the average time taken for the initial cell number to double during the log phase or linear phase. The rate at which cell number increases is depends on the cell number at a given time which is given as

$$G = \frac{dx}{dt} = \mu x \qquad \text{Equation 7-1}$$

Where G is volumetric cell growth rate (cell number L^{-1} h^{-1}), μ is specific cell growth rate (h^{-1}) and x is the viable cell number (Adams et al., 2007). The initial cell number (seed inoculum) played a crucial role in determining the doubling time and specific growth rate of the cells, as different cell line respond differently to the culture conditions. Therefore, a pre-optimised cell number is required to obtain optimum growth. Initial cell inoculum lower than required cell number generally shows an elongated lag phase because the culture medium is devoid of sufficient conditioning factors (Adams et al., 2007; Ljunggren and Häggström, 1995). For the reliable growth rate (μ) and doubling time (t_d), cells were carefully seeded into the ampoules at the start of each experiment, in a closed ampoule in a batch mode.

In this study, the initial cell number (inoculum) and cell number at the end of the experiment were used, to calculate the growth rate (μ) and doubling time (t_d). Although this method is not appropriate because it will not account for the delay occurred during the lag phase which would depend on the cell line used, culture conditions and the initial cell number hence end up showing increased doubling time.

Table 7-2 elaborates the power (heat dissipation) production profile per cell of various cell systems under consideration. During the experimentation, along with their growth rates and doubling time. Heat dissipation of the various cell systems with different cell number was calculated as pW $cell^{-1}$. Due to the limitations of the closed ampoule such as oxygen mass transfer, nutrients depletion, and accumulation of the toxic metabolite, the growth rates and doubling times of different cell systems under consideration do not reflect optimal growth scenarios but represent growth profiles of the cells under culture conditions inside the ampoules.

Table 7-2 Growth kinetics of various cell system (CHO and Vero cells) through IMC

Cell system	Sample Ids	Cell density in (x10^6 mL^{-1})		μ (h^{-1})	t_d (h^{-1})	Heat flow (μW)	Average pW $cell^{-1}$
		Initial	Final				
CHO (adherent)	10k (1)	0.01	0.099	0.014	49.36	2.49	25.15
	10k (2)	0.01	0.143	0.016	42.54	2.89	20.21
	50k (1)	0.05	0.391	0.013	55.05	4.70	12.04
	50k (2)	0.05	0.413	0.013	53.62	4.75	11.51
	100k	0.10	0.446	0.009	75.74	5.95	13.36
CHO (adherent)	100k	0.10	0.308	0.008	88.94	0.94	3.06
	200k (2)	0.20	1.353	0.013	52.33	4.10	3.03
	200k (1)	0.20	1.309	0.013	53.25	4.92	3.76
	500k	0.50	1.854	0.009	76.36	6.49	3.50
CHO-S	100k (1)	0.10	0.330	0.014	49.12	4.74	14.37
	100k (2)	0.10	0.336	0.014	48.45	5.56	16.58
	300k (1)	0.30	0.946	0.014	51.07	7.61	8.05
	300k (2)	0.30	0.996	0.014	48.90	7.49	7.52
	500k	0.50	1.359	0.012	58.68	8.44	6.21
Vero 1 % FBS	100k (1)	0.10	0.737	0.014	49.05	7.71	10.47
	100k (2)	0.10	0.770	0.014	48.00	8.10	10.51
	300k (1)	0.30	1.447	0.011	62.28	9.37	6.48
	300k (2)	0.30	1.381	0.011	64.19	8.84	6.40
	500k	0.50	1.782	0.009	77.10	11.47	6.44
Vero SFM	100k (1)	0.10	0.649	0.016	43.53	4.46	6.88
	300k (1)	0.30	1.271	0.012	56.41	5.80	4.56
	300k (2)	0.30	1.386	0.013	53.20	5.56	4.01
	500k (1)	0.50	1.386	0.009	79.86	2.55	1.84
	500k (2)	0.50	1.425	0.009	77.77	3.09	2.17
PAN-treated Vero suspended in SFM	500k (1)	0.50	1.502	0.009	72.79	13.25	8.83
	500k (2)	0.50	1.458	0.009	74.81	13.00	8.92
	250k (1)	0.25	0.506	0.006	113.52	-0.38	-0.75
	250k (2)	0.25	0.523	0.006	108.58	0.11	0.21
Vero treated regrown in DMEM + 10 % FBS	200k (+control)	0.20	0.776	0.020	34.11	9.30	11.99
	100ug-200k	0.20	0.611	0.017	41.43	10.12	16.58
	200ug-200k	0.20	0.787	0.020	33.76	10.21	12.98
	200ug-200k	0.20	0.765	0.020	34.48	10.16	13.28
	250ug-200k	0.20	0.495	0.014	51.01	9.15	18.48

Vero cells grown in DMEM + 1 % FBS medium (positive control)
Vero cells survived in serum-free media post-treatment

The significance of having pW $cell^{-1}$ heat flow data represent the heat dissipated by an average individual cell size of the population of cells under investigation. This implies that at a given point of time, an

average cell is represented by the many cells at different stages of cell division, therefore their sizes in the ampoule.

The varying cellular heat production of Vero and CHO cells under different culture conditions are primarily because of change in physiological conditions inside a closed ampoule. The availability of oxygen in a non-stirring ampoule to the growing cells create a poor growth condition (low oxygen availability, change in pH, accumulation of lactate and ammonia) and result in a decrease in metabolic activities (Kemp and Guan, 1997).

From Table 7-2, the cell number 100k for both Vero and CHO cells were metabolically more active in the ampoules which are reflected by their higher pW $cell^{-1}$ values whereas 500k showed lower values which signify that the cells in the 500k population were less vital and experienced unfavourable culture conditions. This is also evident from the thermograms of 500k cells of Vero and CHO cells where an initial spike in activity was seen and thereafter gradual decline which could be due to the high initial cell number resulting in the rapid exhaustion of nutrients and dissolved oxygen, and accumulation of by-products in the ampoule.

Specific growth rate (μ) of CHO (adherent) and CHO-S cells are comparable which indicated that the CHO cells were fully adapted to grow in suspension and attained the similar growth rate and doubling time (

Table 7-2). It has been reported that the heat flow rate is sensitive to pH changes (Kemp and Guan, 1997). Figure 7-11 (a) demonstrate and differentiate the normal IMC ampoules containing growth media with appropriate pH (7.2) with CHO cells, properly sealed and crimped with a metallic cap.

Figure 7-11 (b) indicate the change in colour of the media after the end of the experiment, where media colour turned yellow due to the change in pH due to CO_2 accumulation or lactate formation (acidic conditions), produced as a by-product due to the metabolic activities of the cells which testify that the culture conditions changed during the microcalorimetric run in a closed ampoule which significantly impacted the metabolic activity and heat production output of the cells.

Before Experiment

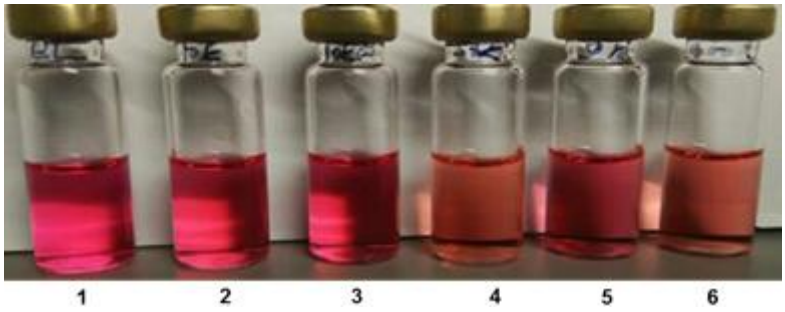

a

After the experiment

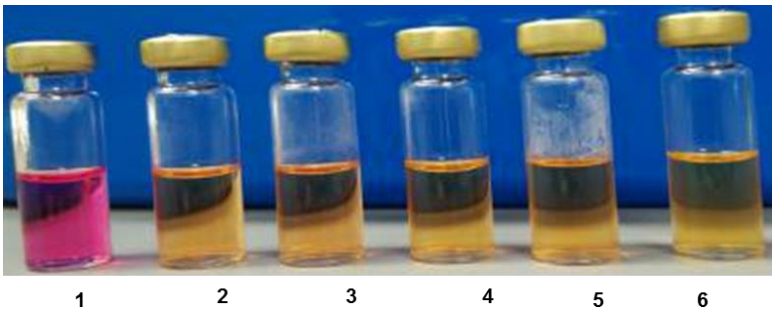

b

Figure 7-11 Illustration of culture conditions (pH change) inside the ampoules over the run-time of experiment represented by the change of colour of culture medium from (a) pink before the experiment and (b) yellow, after completion of the experiment. Ampoules numbers from left to right represented as (1) medium blank, (2) 10k (1), (3) 10k (2), (4) 50k (1), (5) 50k (2) and (6) 100k. The runtime of the experiment lasted for 164 h (Refer Figure 7-1 (a, b) for experiment details)

From the data obtained for CHO adherent cells from the two different experiments, it has been found that more power (pW cell^{-1}) is produced by a smaller number of cells (low cell density) as compared to high cell density. It could be due to better optimisation of appropriate cell number which provides conducive culture condition inside the closed ampoules for the metabolic activities.

In the case of Vero cells grown in 1 % FBS, the power produced by 100k, 300k and 500k cells fall in the range of 7.71 to 11.47 pW cell^{-1}. The power produced by Vero-SFM cells containing 100k cells was 6.88 pW cell^{-1} whereas 500k cells showed an average of 2.0 ± 0.23 pW cell^{-1}. The average power produced by 300k cells was 4.29 ± 0.39 pW cell^{-1}which is much less power as compared to Vero cells grown in 1 % FBS (6.44 ± 0.05 pW cell^{-1}). According to Kemp and Guan, (1997), Vero cells produces 27 ± 2 pW which might be possible if Vero was growing in medium supplemented with 10 % FBS.

Vero cells treated with PAN showed little to no activity in all experiments with PAN, therefore the power produced by one cell was relatively small (0.21 pW cell^{-1}). When Vero cells treated with different concentrations of PAN in serum-free medium were transferred into the serum-containing medium (DMEM + 10 % FBS) in the absence of PAN for rehabilitation (regrown), it was observed that cells regrew in serum-containing media and attained their cellular physiology and started metabolizing actively. In other words, in the absence of PAN, Vero cells grew well in the serum-containing medium. The power generated by a normal Vero cell from the pool of 100k to 500k under culture conditions vary in the range of 7.90 to 11.47 pW cell^{-1} whereas re-growing 200k cells treated with 200 μg mL^{-1} PAN produces an average of 13.13 ± 0.22 pW cell^{-}

[1]. The cells treated with 250 μg mL^{-1} of PAN produced more heat (18.48 pW $cell^{-1}$) than the control 11.99 pW $cell^{-1}$. These pW $cell^{-1}$ values reported are lower than the literature values of CHO 320 (recombinant) ~23, Vero 27 ± 2 and 3T3 mouse fibroblast (17 pW $cell^{-1}$) owing to varied culture conditions.

7.4 Summary

The primary aim of this chapter was to find out the bioactivity in terms of metabolic heat flow of the CHO and Vero cells through analysing the thermograms, which reflects the sum of all the chemical and physical processes occurred in the ampoules during experiments.

Initially, various concentrations of CHO cells were tested to figure out the appropriate cell number required to obtain the detectable and measurable signal through IMC. The cell concentration ranging from 10k, 50k, 100k, 200k, 300k and 500k were tested for CHO (adherent) and CHO-S (Suspension) cells in different experiments. It was found that the cell number above 100k and lower than 300k cells per 2 mL of culture per ampoule would be enough to produce a measurable and detectable signal for analysis. The small error in cell number lower than 100k could significantly change the heat flow pattern, owing to the large lag phase during the growth which end-up in the faulty interpretation of the results. The chances of error above cell density of 100k would be less because of easy cell counting on a haemocytometer and lower dilution of the cell culture soup to obtain the desired number of cells. The other advantage of running the experiments above 100k resulted in getting prominent heat flow peaks in the shortest span of time and short run-time of the experiments. Hence, the cell number more than 100k was considered for the study of Vero cells.

After optimising the cell number appropriate for the IMC studies with CHO cells, various set of experiments were carried-out with Vero cells grown in basal media containing 1 % FBS and Vero adapted in serum-free medium. The Vero cell concentrations (100k, 300k and 500k) were tested for the heat flow generation. Vero cells were also exposed to different concentrations of PAN such as 100, 200, and 250 μg mL^{-1} in T-25 cm^2 TC flasks. It was found that PAN treated Vero cells exhibit low heat flow generation as compared to 500k untreated cells as a positive control. This can be interpreted in the light of chapter 6, when the exposure of PAN dislodged the cell from the surface by modulating the integrin expression and dynamic shaking conditions in serum-free media made them vulnerable and fragile. Though they managed to survive which can be seen from their minimal activity.

The cells that survived for a week in suspension culture in serum-free media did not show prominent heat flow thermogram, but when they were exposed to serum-containing media without PAN, they thrived and started to multiply and formed a monolayer in the TC flask. This indicated that, under the influence of PAN, cells were stressed. Upon removal from PAN, cells resurrected their bioactivity when exposed to serum-containing media. In the end, the chapter summarises the growth kinetics profile of CHO and Vero cells grown under various culture conditions describing their growth rate and doubling time along with power produced by a single cell.

8 Conclusion and Recommendations

This chapter of the thesis conclude the findings of the current research in a nutshell and recommended the probable solution to the issues occurred during the research and suggestions have also made to the improvement of the design and processes for the culturing of mammalian cells

8.1 Significant findings

The role of the bioreactor in the production of biologicals has paramount importance. In the pursuit of achieving high mass transfer, homogeneity and to aerate the bulk fluid, high power input is required which ends up with higher hydrodynamic shear in the bioreactor. The plethora of literature on the bioreactor development have shown that various designs have been developed and researchers are continuing to develop new models, which can provide a conducive environment (low shear and low power consumption) for the growth of mammalian cells.

In the current research, horizontal tubular bioreactor (HTB) with spiral impeller was designed and characterised. The key element which played a major role in the performance of the HTB was the impeller immersion ratio. There is a significant decrease in mixing time from 4 % to 42 % impeller immersion. This is because of the contact between the impeller blades and liquid surface enhance the transfer of energy to the liquid. In the case of 79 % immersion, the change is less prominent when compared to 42 % impeller immersion as the liquid height changed less as liquid volume moved from the widest part of the vessel (from 42 to 79 % immersion) and therefore had less impact on mixing time.

Another aspect of the mixing time vis-à-vis impeller immersion and liquid height can be interpreted from the energy dissipated from impeller agitation. The energy delivered by the spiral impeller to the liquid may not be sufficient to counter the viscous and drag forces, thus the liquid element took longer time to move across the length of the vessel which resulted in delayed mixing and homogeneity particularly at lower impeller speeds. As the impeller speed increased, energy transfer from the impeller to liquid increases, as a result mixing time decreased, and mass transfer increased.

For the minimum agitation speed, the coefficient S is a function of vessel geometry, impeller type and impeller immersion. As the impeller immersion increased, the value of S decreases and consequently N_{js} decreased. This is due to the better contact of the impeller blades with the liquid volume and the total of drag forces acting on the impeller which move the fluid element and solids freely in suspension along the length of the vessel.

The similar trend can be seen in the case of mass transfer efficiency of the HTB. As the impeller speed increased, $k_L a$ increased along with the increase in aeration rate. The maximum $k_L a$ calculated for 3 L at 500 rpm was 16.0 ± 0.5 h^{-1} with 0.5 LPM airflow rate. The $k_L a$ values calculated for HTB fall in the 5.4 ± 0.2 – 16.0 ± 0.5 h^{-1} Table 4-10 and Table 4-11, which is comparable to the $k_L a$ value of 15 h^{-1} reported for the STR for mammalian cells (Nienow, 2006). With this oxygen mass transfer efficiency (16.0 ± 0.5 h^{-1}), HTB may not be able to cater the oxygen demand of the culture with high specific oxygen demand (SOD) (Table 5-5), which required the $k_L a$ of 20 - 28 h^{-1}. Another important observation was on the heating element acting

as a baffle that improved the mixing and mass and heat transfer efficiency, so it can be assumed that if the full length of the heating element is used in the reactor, it would make a significant difference in the mass transfer efficiency of the bioreactor.

The cell densities achieved in the three batches of CHO cells was in the range of 4.0 - 5.5 x 10^6 cell mL^{-1}. From these results, it is believed that HTB design is good enough to cater to the oxygen demand of middle cell density culture by surface aeration and without generating high hydrodynamic shear by the moving impeller. There is however scope for improvement of this design which will be discussed in the recommendations section.

The major observation in adapting Vero cells in suspension by using PAN was that the Vero cells came into suspension and survived for a week. Later they re-modulate themselves and adhere onto the surface when resuspended into the serum-containing medium without PAN. The use of the wide range of concentrations of PAN on the Vero cells indicated that low concentration needs more exposure time to show its effect than the high dose of PAN concentration. The concentration above 100 μg mL^{-1} which is near to IC_{50} value proved to be more effective to dislodge the cells and brings them in suspension. This concentration above 100 μg mL^{-1} is applicable to both culture conditions when cells grew in serum-containing media and in serum-free media.

It was also observed that when cells came in suspension under the influence of PAN, cells were expected to be in stressful conditions. In this study, cells formed clumps despite the media having surfactant (poloxamer 188) at 100 rpm. Therefore, it has been recommended that cells should be exposed to slow shaking condition or intermittent shaking so that they will not form clumps and remain viable for a long duration of time. Partial change of media should be done at an alternate day to slowly wean out PAN from the culture media. This strategy might yield good results in allowing the cells to remain suspended in the absence of PAN. At the end, it has been recommended that the role of integrins need to be explored in detail through the tools of cell biology and advanced microscopy particularly when exposed to agents that suppress the expression.

In this research, the isothermal microcalorimetry was used to elucidate the effect of PAN on the cells. It has been found that 100k cells produce a measurable and detectable signal for both Vero and CHO cells. The metabolic heat produced vary significantly according to the phases of cell growth and their source of origin. The peak value of heat flow measured when the cells are actively dividing at log phase. The value of heat flow for 100k cells of CHO cells grown as adherent and suspension culture measured to be 5.95 and 5.15 μW whereas, in the case of Vero cells grown in serum-containing media and in serum-free, the values found to be 7.9 and 4.5 μW. This indicated that the CHO cells were successfully adapted to suspension culture and exhibited comparable metabolic heat production, whereas, in the case of Vero cells, opposite was happening, where Vero cells in serum-free conditions seem to be less metabolically active than the cells in serum-containing media. There is still ambiguity to relate the viable cell number with the heat flow signal because cells might release more heat when they are in stress to keep themselves alive. Under the effect of PAN, Vero cells almost ceased their activities as shown in Figure 7-9 as compared to normal cells (500k). The average heat flow produced by 500k cells was 13.12 μW compared to PAN treated Vero cells, which produced -0.13 μW of heat flow with 250k cells indicated that the cells were in shock and absorbed heat from

the sink for their survival. When the PAN-treated Vero (various concentration of PAN) were re-seeded into the serum-containing media without PAN, they resurrected themselves and produced metabolic heat. The cells treated with 100 μg mL^{-1} produced almost similar heat flow profile as of normal cells.

8.2 Recommendations

During this PhD work, the scope of the research was fixed. Expanding and furthering the scope of research, the following recommendations have been made based on the research finding and the shortcomings in the design.

8.2.1 HTB design

In this doctoral thesis, the aspect ratio of the HTB was fixed so as the dimensions of the impeller with a fixed pitch and blade angle. Although the fluid flow achieved with the current pitch angle (17$^{o.}$) was in turbulent range, it is expected that if we increase the pitch angle to 45^{o}, it will enhance the fluid flow and surface renewal which would then improve the mass transfer and mixing. The above-said assumption is because when the blade angle increased, the pitch of the impeller increased, which reduces the number of turns. Due to the increased pitch, it is expected that the impeller blades push the liquid with more force than at 17^{o} blade angle. In other words, at low impeller speed, the transfer of energy to the bulk fluid would be enhanced which would improve mass and heat transfer and expected to have low power consumption.

8.2.2 Fluid flow

It has been observed that the presence of the heating element in the bioreactor acted as a baffle thereby improving the mixing time. The fluid flow around the heating element is a complex phenomenon and is hard to elucidate with the current methods used in this research. To understand the intricate details of the fluid flow pattern generated in the HTB with spiral impeller especially with the presence of a heating element, it is recommended to use the computational fluid analysis (CFD) to predict the mixing pattern with the existing length and with the full length of the heating element. Additionally, it would be interesting to predict the fluid flow patterns with various pitch angles of the spiral impeller with simulations through CFD.

Another aspect of bioreactor characterisation which needs further attention is the minimum agitation speed (N_{js}). Due to high variability found by conducting experiments with alginate beads, more sophisticated and reliable techniques must be used to determine the minimum agitation speed (N_{js}) such as particle image velocimetry (PIV) to track the tracer or beads along the length of the vessel. This would not only produce reliable and robust results but also its applicability allows us to understand better how the solid and fluid move in the horizontal vessel and what would be the minimum suspension speed which could bring the solids in suspension.

8.2.3 Process optimisation

The maximum cell density achieved during the batches fell in the range of 4.0 – 5.5 x 10^6 cells mL^{-1} in a batch mode. The efforts should be made to achieve a cell density of ≥ 10 x 10^6 cells mL^{-1}. For that, it has been recommended that intermittent feeding of the batch with primary feed (during growth phase) and secondary feeding (during the stationary phase for the protein expression) must be added into the culture. It

will not only aid in extending the length of the stationary phase and cell density but also increase protein production.

The bioreactor batches ran at 150 rpm till the time batches attained the peak cell density, and 300 rpm creates hydrodynamic shear to cells. Therefore, it would be interesting to see the results vis-à-vis cell density and protein production, when the bioreactor batches would be operated between 150 - 300 rpm and at an increased air flow rate.

Another important aspect that must be looked into is the starting volume of the batch. It would be interesting to start the batch at 2 L. Later, feed the batch with complete media at alternate days till the cell density reached to ≥ 10 x 10^6 cells mL^{-1}. This could be possible because fresh medium addition replenishes the culture with nutrients and oxygen and dilute the toxic secondary metabolite. It has been seen that mixing time and mass transfer efficiency increases from 42 % impeller immersion ratio to 79 % therefore, as the volume of the batch increases by the addition of fresh media, mass and heat transfer increases which would greatly enhance the macroenvironment of the bioreactor and overall performance.

The other pressing aspect of process development is to evaluate the use of microcarrier in HTB. It was assumed that the microcarriers small than 200 µ in size could be used for the propagation of mammalian cells as the size of beads used for the minimum agitation speed was equal or larger than 200 µ, that got stuck underneath the heating finger. Cytodex 1 and Cytodex 3 could be tested for the growth of mammalian cells in HTB.

For measuring shear due to impeller agitation, it is suggested that more batches should be taken to understand the hydrodynamic shear conditions in the HTB by measuring cell death constant (k_d) along with measuring LDH release or by measuring total DNA from the lysed cells.

8.2.4 Mechanical design

The fixed aspect ratio of the vessel for this study impeded a clear picture of the performance of the horizontal vessel. It has been observed that mixing time decreases with lower L/D ratio. For the optimum design, it is recommended to test the various combinations of L/D ratios of the vessel to evaluate the fluid flow, mixing time profile and mass transfer efficiency.

Another area of improvement would be the smooth design of the spiral impeller as per user required specifications. It has been found that there were some manufacturing defects in fabricating the spiral impeller as shown with white arrows in Figure 8-1. These defects could lead to the improper estimation of fluid flow through the gaps left between impeller shaft and blade Figure 8-1(a) and improper welding of the shaft could also lead to estimate erroneous values of the process parameters, which could have a negative impact on the cell culture. In the future, it has been recommended that when the impeller with different blade angle and pitch would be studied, care must be taken in manufacturing the impeller so that these defects can be addressed.

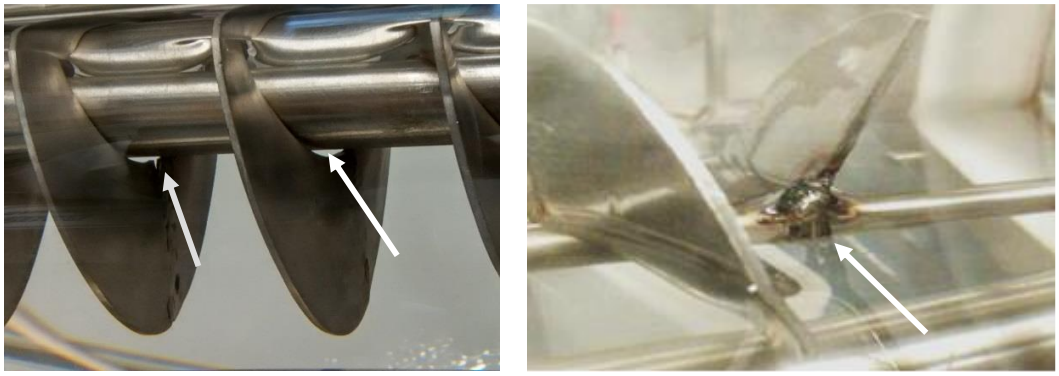

a b

Figure 8-1 Manufacturing defects during the fabrication of spiral impellers

8.2.5 Scale-up and future work

Scalable design is one of the criteria for the successful design of the bioreactor (List 4-1). For the HTB scale-up, height to diameter ratio, liquid height, mixing time, power input and gas mass transfer coefficient are the key parameters, which would determine the scalability of the HTB. The dimensionless numbers of volumetric power input, mixing time and gas mass transfer coefficient can be modelled to fit with the experimental data which would aid in scaling up. This can be achieved once the optimum aspect ratio of the HTB vis- vis impeller design would be achieved as mentioned in the 8.2.1. As a rigid vessel, it can be achieved in the range of cubic meters as horizontal tank can safely place on the platform and operated. This could be challenging in the case of disposable bioreactor.

8.2.6 Integrin work for Vero suspension

As PAN was the only anti-cancer drug used for these studies, literature studies have also reported that sulphonamide derivatives and tellurium containing compounds have also shown the suppression activities of the surface receptors proteins, integrins, therefore, it has been recommended that further study should include these two drugs in pursuit to bring Vero cells into suspension.

Future work on this project should also exploit the knowledge and tools of cell biology to unfold the signal pathways which make the Vero cells adherent and difficult to adapt into suspension culture whereas CHO cells are comparatively easy to adapt into suspension. A thorough investigation of the drug-treated cell's integrin profile through FACS would throw light on the details of the inhibition of the different integrin subunits. This information could form the basis of adapting cell-lines into suspension in a single step, which is otherwise difficult to adapt. Efforts should also be made to identify the novel points in signal transduction pathways or at genetic level which can be manipulated. The advantage of this effort could lay a foundation for new avenues, where difficult to adapt cell lines can be adapted into suspension for commercial use in a bioreactor to produce biologicals.

8.2.7 Recommendations for IMC

Isothermal microcalorimetry is a very sensitive technique which measures a minute change in heat flow in the system therefore, planning of the experiments need to be strict and well planned to minimise the error. The following points should be considered while planning the experiments

1 Count the number of cells carefully before loading the ampoules
2 Keep the volume same in all the ampoules. A small variation could lead to erroneous results
3 Siliconized the glass vessel to avoid cell attachments in the case of suspended cell
4 Crimping of the metallic cap should be accurate so that no heat loss occur

Apart from these precautions, the applications of the IMC can be extended to many domains such as process development. A thorough understanding of the bioactivity profile of cells, expressing a recombinant protein is sought, which could differentiate the viability of the cells from that of the vitality of the cells during the batch run. It has been recommended that dielectric spectroscopy can also be employed to understand the cellular bioactivity of the cells and the outcome can be compared with that of IMC (Cole et al., 2015). It could also aid in monitoring the efficiency of the culture (cell population) to take part in protein production during the stationary phase, where the accumulation of the toxic metabolite is high. With the advanced knowledge of the molecular biology techniques, cell biology and process development, high producer clones of the desired recombinant protein products would be a reality in future which may touch the specific productivity in the range of 50 pg $cell^{-1}$ day^{-1}. This might be sufficient for a single batch to cater to the demand of the desired product.

References

Adams, D., Korke, R., Hu, W.-S., 2007. Application of Stoichiometric and Kinetic Analyses to Characterize Cell Growth and Product Formation, in: Animal Cell Biotechnology. Humana Press, pp. 269–284.

Almo, S.C., Love, J.D., 2014. Better and faster improvements and optimization for mammalian recombinant protein production. Curr. Opin. Struct. Biol. 26, 39–43.

Ammerman, N.C., Beier-Sexton, M., Azad, A.F., 2008. Growth and maintenance of Vero cell lines. Curr. Protoc. Microbiol. Appendix 4, Appendix 4E.

Anderlei, T., Cesana, C., Bürki, C., De Jesus, M., Kühner, M., Wurm, F., Lohser, R., 2009. Shaken bioreactors provide culture alternative. Genet. Eng. Biotechnol. News 29, 44.

Andrews, G., 1988. Fluidized-bed bioreactors. Biotechnol. Genet. Eng. Rev. 6, 151–178.

Anicetti, V., 2009. Biopharmaceutical processes : a glance into the 21st century. Bioprocess Int. 7, 4–11.

Armenante, P.M., Nagamine, E.U., 1998. Effect of low off-bottom impeller clearance on the minimum agitation speed for complete suspension of solids in stirred tanks. Chem. Eng. Sci. 53, 1757–1775.

Asher, W.E., Pankow, J.F., 1991. Prediction of gas/water mass transport coefficients by a surface renewal model. Environ. Sci. Technol. 25, 1294–1300.

ATCC, 2012. ANIMAL CELL CULTURE GUIDE-tips and techniques for continuous cell lines.

Aunins, J.G., Bader, B., Caola, A., Griffiths, J., Katz, M., Licari, P., Ram, K., Ranucci, C.S., Zhou, W., 2003. Fluid mechanics, cell distribution, and environment in cellcube bioreactors. Biotechnol. Prog. 19, 2–8.

Auton, K.A., 2010. Single Use Bioreactors: Expressing Protein in Mammalian Cell Suspension, in: Noll, T. (Ed.), Cells and Culture. Springer Netherlands, Dordrecht, pp. 63–69.

Balasubramanian, N., Scott, D.W., Castle, J.D., Casanova, J.E., Schwartz, M.A., 2007. Arf6 and microtubules in adhesion-dependent trafficking of lipid rafts. Nat. Cell Biol. 9, 1381–91.

Bandaranayake, A.D., Almo, S.C., 2014. Recent advances in mammalian protein production. FEBS Lett. 588, 253–260.

Barczyk, M., Carracedo, S., Gullberg, D., 2010. Integrins. Cell Tissue Res. 339, 269–280.

Bell, S.L., Bebbington, C., Scott, M.F., Wardell, J.N., Spier, R.E., Bushell, M.E., Sanders, P.G., 1995. Genetic engineering of hybridoma glutamine metabolism. Enzyme Microb. Technol. 17, 98–106.

Benyus, J., 2002. Biomimicry: Innovation Inspired by Nature. PerennialHarper, 2.

Berdugo, C., 2010. Cell damage mechanisms and stress response in animal cell culture. [Ph.D Thesis]. Ohio State University.

Berryman, S., Clark, S., Monaghan, P., Jackson, T., 2005. Early events in integrin αvβ6-mediated cell entry of Foot-and-Mouth Disease Virus. J. Virol. 79, 8519–8534.

Blaschczok, K., Kaiser, S.C., Löffelholz, C., Imseng, N., Burkart, J., Bösch, P., Dornfeld, W., Eibl, R., Eibl, D., 2013. Investigations on mechanical stress caused to CHO suspension cells by standard and single-use pumps. Chemie-Ingenieur-Technik 85, 144–152.

Bleckwenn, N.A., Shiloach, J., Bleckwenn, N.A., Shiloach, J., 2004. Large-Scale Cell Culture, in: Current Protocols in Immunology. John Wiley & Sons, Inc., Hoboken, NJ, USA, p. A.1U.1-A.1U.44.

Blume, S., Geesink, I., 2000. A brief history of polio vaccines. Science (80-.). 288, 1593–1594.

Boehm, R., 2007. Bioproduction of therapeutic proteins in the 21st century and the role of plants and plant cells as production platforms. Ann. N. Y. Acad. Sci. 1102, 121–134.

Bouquet, J.-F., 2013. Vaccines and animal cell technology. ACTIP. (accessed 9.13.18).

Bowers, J.S., 2008. Sparger and surface gas transfer for cell culture bioreactors, in: AIChE Annual Meeting, Conference Proceedings.

Braissant, O., Bachmann, A., Bonkat, G., 2015. Microcalorimetric assays for measuring cell growth and metabolic activity: Methodology and applications. Methods 76, 27–34.

Braissant, O., Daniels, A.U. “Dan,” 2011. Closed Ampoule Isothermal Microcalorimetry for Continuous Real-Time Detection and Evaluation of Cultured Mammalian Cell Activity and Responses, in: Stoddart M (Ed.), Mammalian Cell Viability. Methods in Molecular Biology (Methods and Protocols). Humana Press, pp. 191–208.

Braissant, O., Wirz, D., Göpfert, B., Daniels, A.U., 2010. Use of isothermal microcalorimetry to monitor microbial activities. FEMS Microbiol. Lett. 303, 1–8.

Bravo, D., Braissant, O., Solokhina, A., Clerc, M., Daniels, A.U., Verrecchia, E., Junier, P., 2011. Use of an isothermal microcalorimetry assay to characterize microbial oxalotrophic activity. FEMS Microbiol. Ecol. 78, 266–274.

Brecht, R., 2009. Disposable bioreactors: Maturation into pharmaceutical glycoprotein manufacturing, in: Disposable Bioreactors. Springer Berlin Heidelberg, pp. 1–31.

Buckton, G., 1995. Applications of isothermal microcalorimetry in the pharmaceutical sciences. Thermochim. Acta 248, 117–129.

Butler, M., 2005. Animal cell cultures: recent achievements and perspectives in the production of biopharmaceuticals. Appl. Microbiol. Biotechnol. 68, 283–291.

Butler, M., Burgener, A., Patrick, M., Berry, M., Moffatt, D., Huzel, N., Barnabé, N., Coombs, K., 2000. Application of a serum-free medium for the growth of Vero cells and the production of reovirus. Biotechnol. Prog. 16, 854–858.

Butler, M., Meneses-Acosta, A., 2012. Recent advances in technology supporting biopharmaceutical production from mammalian cells. Appl. Microbiol. Biotechnol. 96, 885–894.

Cai, H.H., 2017. Therapeutic monoclonal antibodies approved by FDA in 2016. MOJ Immunol. 5, 00145.

Campbell, I.D., Humphries, M.J., 2011. Integrin structure, activation, and interactions. Cold Spring Harb. Perspect. Biol. 3, a004994.

Carcano, S., 2010. A model for cell growth in batch bioreactors.

Carreau, P.J., Paris, J., Guérin, P., 1992. Mixing of newtonian and non-newtonian liquids: Screw agitator and draft coil system. Can. J. Chem. Eng. 70, 1071–1082.

Cellexus, n.d. Application Data |.

CellTumbler documentation 2014, 2014.

Cesco Bioengineering, n.d. Introduction of bello cell high density cell culture system.

Cesco Bioengineering, n.d. Bello and Tide cells. (accessed 4.16.15b).

Challener, C., 2016. A look at perfusion. Bioprocess Int. 14, 44–45.

Chalmers, J.J., 2015. Mixing, aeration and cell damage, 30+ years later: What we learned, how it affected the cell culture industry and what we would like to know more about. Curr. Opin. Chem. Eng. 10, 94–102.

Chalmers, J.J., 1994. Cells and bubbles in sparged bioreactors. Cytotechnology 15, 311–320.

Chalmers, J.J., Ma, N., 2015. Hydrodynamic Damage to Animal Cells, in: Animal Cell Culture. Cell Engineering, Vol 9. Springer, pp. 169–183.

Chang, H.N., Halard, B., Moo-Young, M., 1989. Measurement of KLa by a gassing-in method with oxygen-enriched air. Biotechnol. Bioeng. 34, 1147–1157.

Chapple, D., Kresta, S.M., Wall, A., Afacan, A., 2002. The Effect of Impeller and Tank Geometry on Power Number for a Pitched Blade Turbine. Chem. Eng. Res. Des. 80, 364–372.

Charcosset, C., 2006. Membrane processes in biotechnology: an overview. Biotechnol. Adv. 24, 482–492.

Cherry, R.S., Papoutsakis, E.T., 1988. Physical mechanisms of cell damage in microcarrier cell culture bioreactors. Biotechnol. Bioeng. 32, 1001–1014.

Cherry, R.S., Papoutsakis, E.T., 1986. Hydrodynamic effects on cells in agitated tissue culture reactors. Bioprocess Eng. 1, 29–41.

Chigaev, A., Smagley, Y., Sklar, L.A., 2011. Nitric oxide/cGMP pathway signaling actively down-regulates α4β1-integrin affinity: an unexpected mechanism for inducing cell de- adhesion Nitric oxide/cGMP pathway signaling actively down-regulates a 4 b 1 -integrin affinity: an unexpected mechanism for . BMC Immunol. 12, 12–28.

Chisti, Y., 2001. Hydrodynamic Damage to Animal Cells. Crit. Rev. Biotechnol. 21, 67–110.

Chisti, Y., 2000. Animal-cell damage in sparged bioreactors. Trends Biotechnol. 18, 420–432.

Chisti, Y., 1993. Animal cell culture in stirred bioreactors: observations on scale-up. Process Biochem.

Chitra, D., Muruganandan, L., 2014. Effect of impeller clearance and multiple impeller combinations on solid suspension in a standard flat bottom agitated vessel. Int. J. ChemTech Res. 6, 973–981.

Chu, J.J.., Ng, M.L., 2004. Interaction of west nile virus with αvβ3 integrin mediates virus entry into cells. J. Biol. Chem. 279, 54533–54541.

Chu, L., Robinson, D.K., 2001. Industrial choices for protein production by large-scale cell culture. Curr. Opin. Biotechnol. 12, 180–187.

Cloete, T.E., Nel, L.H., Theron, J., 2006. Biotechnology in South Africa. Trends Biotechnol. 24, 557–562.

Coco-Martin, J.M., Harmsen, M.M., 2008. A review of therapeutic protein expression by mammalian cells. Bioprocess Int. 6, 28–33.

Cole, H., Demont, A., Marison, I., 2015. The Application of Dielectric Spectroscopy and Biocalorimetry for the Monitoring of Biomass in Immobilized Mammalian Cell Cultures. Processes 3, 384–405.

Collignon, M.-L., Droissart, L., Delafosse, A., Calvo, S., Vanhamel, S., Rodriguez, R., Claes, T., Moncaubeig, F., Peeters, L., Crine, M., Toye, D., 2015. Hydrodynamics in a disposable rectangular parallelepiped stirred bioreactor with elliptic pendulum motion paddle. Biochem. Eng. J. 93, 212–221.

Collignon, M.L., Delafosse, A., Crine, M., Toye, D., 2010. Axial impeller selection for anchorage dependent animal cell culture in stirred bioreactors: Methodology based on the impeller comparison at just-suspended speed of rotation. Chem. Eng. Sci. 65, 5929–5941.

Corning, 2011. CellCube system user's manual Rev. V1.02.

Corning, 2008. HYPER Flask ™ cell culture vessel.

Coulson, B.S., Londrigan, S.L., Lee, D.J., 1997. Rotavirus contains integrin ligand sequences and a disintegrin-like domain that are implicated in virus entry into cells. Proc. Natl. Acad. Sci. U. S. A. 94, 5389–5394.

Cramp, R., Gilmour, M., Cowan, D.A., 1997. Novel thermophilic bacteria producing nitrile-degrading enzymes. Microbiology 143, 2313–2320.

Croughan, M.S., Hamel, J.-F., Wang, D.I.C., 1987. Hydrodynamic effects on animal cells grown in microcarrier cultures. Biotechnol. Bioeng. 29, 130–141.

Croughan, M.S., Hu, W., 2006. From Microcarriers to Hydrodynamics : Introducing Engineering Science into Animal Cell Culture. Biotechnol. Bioeng. 95, 220–225.

Cummings, B.S., Wills, L.P., Schnellmann, R.G., 2004. Measurement of Cell Death in Mammalian Cells. Curr. Protoc. Pharmacol. 0 12.

Cuperlović-Culf, M., Barnett, D.A., Culf, A.S., Chute, I., 2010. Cell culture metabolomics: Applications and future directions. Drug Discov. Today 15, 610–621.

Cypess, R.H., Simione, F.P., 2016. Transformation of an icon: ATCC and the new business model for science., First. ed. American Type Culture Collection (ATCC).

Cytiva, n.d. Xcellerex™ XDR cell culture bioreactor systems. Data file 29-0929-25 AA. (accessed 7.9.15).

Czermak, P., Pörtner, R., Brix, A., 2009. Special Engineering Aspects, in: Cell and Tissue Reaction Engineering: Principles and Practice. Springer, Berlin, Heidelberg, pp. 83–172.

Daelli, M.G., 2007. Vero cell line adapted to grow in suspension. US2007/0111309 A1.

Danen, E.H.J., Yamada, K.M., 2001. Fibronectin, Integrins, and Growth Control . J. Cell. Physiol. 189, 1–13.

Dangi, A.K., Sinha, R., Dwivedi, S., Gupta, S.K., Shukla, P., 2018. Cell line techniques and gene editing tools for antibody production: A review. Front. Pharmacol. 9, 630.

Das, V., Kalyan, G., Hazra, S., Pal, M., 2018. Understanding the role of structural integrity and differential expression of integrin profiling to identify potential therapeutic targets in breast cancer. J. Cell. Physiol. 233, 168–185.

DaSilva, E.J., 2004. The Colours of Biotechnology: Science, Development and Humankind. Electron. J. Biotechnol. 7, 01–02.

Davis, K., 2001. Single-use systems: show me the green! Value Plast. Inc. White Pap.

De Jesus, M., Wurm, F.M., 2011. Manufacturing recombinant proteins in kg-ton quantities using animal cells in bioreactors. Eur. J. Pharm. Biopharm.

de Vos, P., 2014. Cell encapsulation: ready for the next step. Adv. Drug Deliv. Rev. 67–68, 1–2.

de Vos, P., Lazarjani, H.A., Poncelet, D., Faas, M.M., 2014. Polymers in cell encapsulation from an enveloped cell perspective. Adv. Drug Deliv. Rev. 67–68, 15–34.

De Wilde, D., Dreher, T., Zahnow, C., Husemann, U., Greller, G., Adams, T., Fenge, C., 2014. Superior scalability of single-use bioreactors. BioProcess Int. (Innovations Cell Cult. 12, 14).

De Wilde, D., Noack, U., Kahlert, W., Barbaroux, M., Greller, G., 2009. Bridging the gap from reusable to single-use manufacturing with stirred, single-use bioreactors. Bioprocess Int. 7, 36–41.

del Pozo, M.A., Alderson, N.B., Kiosses, W.B., Chiang, H.-H., Anderson, R.G.W., Schwartz, M.A., 2004. Integrins regulate Rac targeting by internalization of membrane domains. Science (80-.). 303, 839–842.

Delon, I., Brown, N.H., 2007. Integrins and the actin cytoskeleton. Curr. Opin. Cell Biol. 19, 43–50.

DeLuca, D., 2016. The power of the Biomimicry Design Spiral. Biomimicry Inst. (accessed 8.5.19).

Demain, A.L., Vaishnav, P., 2009. Production of recombinant proteins by microbes and higher organisms. Biotechnol. Adv. 27, 297–306.

Department of Science and Technology, 2018. White Paper on Science, Technology and Innovation.

Department of Science and Technology, 2013. Bio-economy Strategy.

Di Luca, M., Koliszak, A., Karbysheva, S., Chowdhary, A., Meis, J., Trampuz, A., 2019. Thermogenic Characterization and Antifungal Susceptibility of Candida auris by Microcalorimetry. J. Fungi 5, 103.

Dias, A.M.A., Freire, M., Coutinho, J.A.P., Marrucho, I.M., 2004. Solubility of oxygen in liquid perfluorocarbons, in: Fluid Phase Equilibria. Elsevier, pp. 325–330.

Ding, W., Martin, J., 2010. Implementing single-use technology in biopharmaceutical manufacturing. Bioprocess Int. 8, 52–60.

Doran, P.M., 2013. Mass Transfer, in: Bioprocess Engineering Principles. Academic Press, pp. 379–444.

Duan, G., Walther, D., 2015. The Roles of Post-translational Modifications in the Context of Protein Interaction Networks. PLoS Comput. Biol. 11, 1–23.

Dziejowski, J., Białobrzewski, I., 2011. Calorimetric studies of solid wastes, sewage sludge, wastewaters and their effects on soil biodegradation processes. J. Therm. Anal. Calorim. 104, 161–168.

Echarri, A., Del Pozo, M.A., 2006. Caveolae internalization regulates integrin-dependent signaling pathways. Cell Cycle 5, 2179–2182.

Eibl, D., 2012. Single-use technology in biopharmaceutical production. DECHEMA 1–43.

Eibl, D., Eibl, R., 2009. Bioreactors for mammalian cells: General overview., Cell and Tissue Reaction Engineering: Principles and Practice. Springer Berlin Heidelberg.

Eibl, D., Eibl, R., Portner, R., 2009. Mammalian cell culture technology: An emerging field, in: Cell and Tissue Reaction Engineering: Principles and Practice. Springer, Berlin, Heidelberg, pp. 3–11.

Eibl, R., Kaiser, S., Lombriser, R., Eibl, D., 2010. Disposable bioreactors: the current state-of-the-art and recommended applications in biotechnology. Appl. Microbiol. Biotechnol. 86, 41–49.

Eibl, R., Löffelholz, C., Eibl, D., 2014. Disposable Bioreactors for Inoculum Production and Protein Expression, in: Animal Cell Biotechnology. pp. 265–284.

Eibl, R., Löffelholz, C., Eibl, D., 2011. Single-Use Bioreactors-An Overview, in: Eibl, R., Eibl, D. (Eds.), Single-Use Technology in Biopharmaceutical Manufacture. John Wiley & Sons, Inc., Hoboken, NJ, USA, pp. 33–51.

Eibl, R., Werner, S., Eibl, D., 2009. Bag bioreactor based on wave-induced motion: characteristics and applications., in: Advances in Biochemical Engineering/Biotechnology. pp. 55–87.

Eisenstein, M., 2006. Thinking outside the dish. Nat. Methods 3, 1035–1043.

Fan, J., Kamphorst, J.J., Mathew, R., Chung, M.K., White, E., Shlomi, T., 2013. Glutamine-driven oxidative phosphorylation is a major ATP source in transformed mammalian cells in both normoxia and hypoxia. Mol. Syst. Biol. 9, 1–11.

Fernandes, D., 2004. Reducing risk in biopharmaceutical production by controlling glycosylation. Eur. Biopharm. Rev. 92–97.

Finn, R.K., 1954. Agitation-aeration in the laboratory and in industry. Bacteriol. Rev. 18, 254–274.

Frahm, B., Brod, H., Langer, U., 2009. Improving bioreactor cultivation conditions for sensitive cell lines by dynamic membrane aeration. Cytotechnology 59, 17–30.

Fraser, S.J., Endres, C., 2013. Quorus bioreactor : A new perfusion-based technology for microbial cultivation. Adv Biochem Eng Biotechnol 138, 149–177.

Freshney, R.I., 2005. Culture of animal cells-A manual of basic Technique. Wiley-Liss, New York.

Garcia-Ochoa, F., Gomez, E., 2009a. Bioreactor scale-up and oxygen transfer rate in microbial processes: An overview. Biotechnol. Adv. 27, 153–176.

Garcia-Ochoa, F., Gomez, E., 2009b. Oxygen transfer rate determination: chemical, physical and biological methods, in: Flickinger, M.C. (Ed.), Encyclopedia of Industrial Biotechnology: Bioprocess, Bioseparation, and Cell Technology. John Wiley & Sons, Inc., Hoboken, NJ, USA, pp. 1–21.

Garcia-Ochoa, F., Gomez, E., 2005. Prediction of gas-liquid mass transfer coefficient in sparged stirred tank bioreactors. Biotechnol. Bioeng. 92, 761–772.

Garcia, A.H., Herrmann, A.M., Håkansson, S., 2017. Isothermal microcalorimetry for rapid viability assessment of freeze-dried Lactobacillus reuteri. Process Biochem. 55, 49–54.

Gaus, K., Le Lay, S., Balasubramanian, N., Schwartz, M.A., 2006. Integrin-mediated adhesion regulates membrane order. J. Cell Biol. 174, 725–734. https://doi.org/10.1083/jcb.200603034

Gauthier, L., Thibault, J., LeDuy, A., 1991. Measuring kLa with randomly pulsed dynamic method. Biotechnol. Bioeng. 37, 889–893.

Ghadiri, M., Harrison, S.T.L., Fagan-Endres, M.A., 2018. Influence of X-ray M-Computed Tomography on the microbial activity of a mixed thermophilic and mesophilic bioleaching culture colonising a mineral surface. Biochem. Eng. J. 139, 123–131.

Gimbun, J., Rielly, C.D., Nagy, Z.K., 2009. Modelling of mass transfer in gas–liquid stirred tanks agitated by Rushton turbine and CD-6 impeller: A scale-up study. Chem. Eng. Res. Des. 87, 437–451.

Godoy-Silva, R., Berdugo, C., Chalmers, J.J., 2010. Aeration, mixing, and hydrodynamics, animal cell bioreactors., in: Flickinger, M.C. (Ed.), Encyclopedia of Industrial Biotechnology: Bioprocess,

Bioseparation, and Cell Technology. John Wiley & Sons, Inc., Hoboken, NJ, USA., pp. 1–27.

Goodman, S.L., Picard, M., 2012. Integrins as therapeutic targets. Trends Pharmacol. Sci. 33, 405–412.

Goosen, M.F.A., 1992. Fundamentals of animal cell encapsulation and immobilization. CRC Press.

Goosen, M.F.A., 1988. Animal cell culture in microcapsules. Chem. Eng. Educ. 22, 196–201.

Grigorescu, G., Hunkeler, D., 2003. Cell Encapsulation., in: Freitag, R. (Ed.), Synthetic Polymers for Biotechnology and Medicine. Eurekah.com, pp. 1–18.

Grilo, A.L., Mantalaris, A., 2019. Apoptosis: A mammalian cell bioprocessing perspective. Biotechnol. Adv. 37, 459–475.

Gronemeyer, P., Ditz, R., Strube, J., 2014. Trends in Upstream and Downstream Process Development for Antibody Manufacturing. Bioengineering 1, 188–212.

Guan, Y., Lloyd, P.C., Evans, P.M., Kemp, R.B., 1997. A modified continuous flow microcalorimeter for measuring heat dissipation by mammalian cells in batch culture. J. Therm. Anal. 49, 785–794.

Guang, C., Phillips, R.D., Jiang, B., Milani, F., 2012. Three key proteases - Angiotensin-I-converting enzyme (ACE), ACE2 and renin - Within and beyond the renin-angiotensin system. Arch. Cardiovasc. Dis.

Guerrero, C.A., Mendez, E., Zarate, S., Isa, P., Lopez, S., Arias, C.F., 2000. Integrin αvβ3 mediates rotavirus cell entry. Proc. Natl. Acad. Sci. 97, 14644–14649.

Guo, D., Zhu, Q., Zhang, H., Sun, D., 2014. Proteomic analysis of membrane proteins of vero cells: exploration of potential proteins responsible for virus entry. DNA Cell Biol. 33, 20–28.

Hambor, J.E., 2012. Bioreactor design and bioprocess controls for industrialized cell processing. Bioprocess Int. 10, 22–33.

Handa-Corrigan, A., Emery, A.N., Spier, R.E., 1989. Effect of gas-liquid interfaces on the growth of suspended mammalian cells: mechanisms of cell damage by bubbles. Enzyme Microb. Technol. 11, 230–235.

Hanley, P.J., Mei, Z., Durett, A.G., Cabreira-Hansen, M. da G., Cabreira-Harrison, M. da G., Klis, M., Li, W., Zhao, Y., Yang, B., Parsha, K., Mir, O., Vahidy, F., Bloom, D., Rice, R.B., Hematti, P., Savitz, S.I., Gee, A.P., 2014. Efficient manufacturing of therapeutic mesenchymal stromal cells with the use of the quantum cell expansion system. Cytotherapy 16, 1048–1058.

Harriott, P., 1962. A random eddy modification of the penetration theory. Chem. Eng. Sci. 17, 149–154. h

Hartley, F., Walker, T., Chung, V., Morten, K., 2018. Mechanisms driving the lactate switch in Chinese hamster ovary cells. Biotechnol. Bioeng. 115, 1890–1903.

Hashimura, Y., 2011. PBS Air-Wheel ™ bioreactor offers seamless transition from stirred-tanks in fed-batch CHO process- Application Note [IC03252 Rev. A].

Hatton, T., Barnett, S., Rashid, K., 2012. CHO cell culture with single-use New Brunswick™ CelliGen® BLU packed-bed Fibra-Cel® basket [Application note no. 254].

Haut, B., Ben Amor, H., Coulon, L., Jacquet, A., Halloin, V., 2003. Hydrodynamics and mass transfer in a Couette–Taylor bioreactor for the culture of animal cells. Chem. Eng. Sci. 58, 777–784.

Henry, G., Rees, B., Golightly, C., 2015. Comparison of CHO cell cultivation and mAb production in the Allegro ™ XRS 20 and conventional rocker type single-use bioreactors., in: BMC Proceedings. BioMed Central Ltd.

Henzler, H.-J., Kauling, D.J., 1993. Oxygenation of cell cultures. Bioprocess Eng. 9, 75.

Herholdt, S., Läubli, A., Adams, T., 2013. CHO cultivation in next generation rocking motion single-use bioreactor. [Application Note-6].

Hinz, D.C., 2006. Process analytical technologies in the pharmaceutical industry: the FDA's PAT initiative. Anal. Bioanal. Chem. 384, 1036–1042.

Holland, F.A., Bragg, R., 1995. Fluid Flow for Chemical Engineers., 2nd ed, Butterworth-Heinemann; 2

edition (April 30, 1995). Butterworth-Heinemann.

Houtzager, E., Linden, R. van der, Roo, G. de, Huurman, S., Priem, P., Sijmons, P.C., 2010. Linear scale-up of cell cultures. Bioprocess Int. 8, 56–62.

Hu, W.-S., Aunins, J.G., 1997. Large-scale mammalian cell culture. Curr. Opin. Biotechnol. 8, 148–153.

Hu, W., Berdugo, C., Chalmers, J.J., 2011. The potential of hydrodynamic damage to animal cells of industrial relevance: current understanding. Cytotechnology 63, 445–60.

Hu, Y.-C., Lu, J.-T., Chung, Y.-C., 2003. High-density cultivation of insect cells and production of recombinant baculovirus using a novel oscillating bioreactor. Cytotechnology 42, 145–153.

Hu, Y.C., Kaufman, J., Cho, M.W., Golding, H., Shiloach, J., 2000. Production of HIV-1 gp120 in packed-bed bioreactor using the vaccinia virus/T7 expression system. Biotechnol. Prog. 16, 744–750.

Huang, T.-K., McDonald, K.A., 2012. Bioreactor systems for in vitro production of foreign proteins using plant cell cultures. Biotechnol. Adv. 30, 398–409.

Huang, T.-K., McDonald, K.A., 2009. Bioreactor engineering for recombinant protein production in plant cell suspension cultures. Biochem. Eng. J. 45, 168–184.

Humphries, M.J., Mould, A.P., Tuckwell, D.S., 1993. Dynamic aspects of adhesion receptor function ? integrins both twist and shout. BioEssays 15, 391–397.

Hyclone, G.E.H., 2016a. ActiPro ™ medium.

Hyclone, G.E.H., 2016b. ActiSM ™ medium.

Hyclone, G.E.H., 2015a. HyCell ™ CHO.

Hyclone, G.E.H., 2015b. CDM4PERMAb.

Hynes, R.O., 2004. The emergence of integrins: a personal and historical perspective. Matrix Biol. 23, 333–340.

Hynes, R.O., 2002. Integrins: Bidirectional, Allosteric Signaling Machines. Cell 110, 673–687.

Hynes, R.O., 1992. Integrins: Versatility, Modulation, and Signaling in Cell Adhesion Review. Cell 69.

Ibrahim, S., Nienow, A.W., 2004. Suspension of Microcarriers for Cell Culture with Axial Flow Impellers. Chem. Eng. Res. Des. 82, 1082–1088.

Illing, S., 1996. An investigation of the effect of hydrodynamic stress on the growth, morphology and metabolism of microorganisms. UNIVERSITY OF CAPE TOWN.

Integra Biosciences, 2014. CELLINE disposable bioreactor for efficient protein expression.

Izmailyan, R., Hsao, J.-C., Chung, C.-S., Chen, C.-H., Hsu, P.W.-C., Liao, C.-L., Chang, W., 2012. Integrin β1 Mediates Vaccinia Virus Entry through Activation of PI3K/Akt Signaling. J. Virol. 86, 6677–6687.

Jones, S.M.J., 2015. Mixing, mass transfer and energy analysis across bioreactor types in microalgal cultivation and lipid production. University of Cape Town.

Jones, S.M.J., Louw, T.M., Harrison, S.T.L., 2017. Energy consumption due to mixing and mass transfer in a wave photobioreactor. Algal Res. 24, 317–324.

Kaddar, M., 2013. Global vaccine market features and trends., Workshop on Business Modeling for Sustainable Influenza Vaccine Manufacturing.

Kadzinga, F., 2015. Venturi aeration of bioreactors. University of Cape Town.

Kaiser, P., Werner, M., Jerome, V., Hubner, H., Buchholz, R., Freitag, R., 2014. Cell retention by encapsulation for the cultivation of Jurkat cells in fixed and fluidized bed reactors. Biotechnol. Bioeng. 111, 2571–2579.

Kaiser, S.C., Dittler, I., Steiger, N., Eibl, D., n.d. Cultivation of Sf-9 insect cells and SEAP expression in the Finesse «SmartGlass» bioreactor [Application Note].

Kaiser, S.C., Eibl, R., Eibl, D., 2011. Engineering characteristics of a single-use stirred bioreactor at bench-scale: The Mobius CellReady 3L bioreactor as a case study. Eng. Life Sci. 11, 359–368.

Kaiser, S.C., Perepelitsa, N., Kraume, M., Eibl, D., 2016. Development of the travelling wave Bioreactor. Part II: Engineering characteristics and cultivation results. Chemie Ing. Tech. 88, 86–92.

Kang, H.-N., Xu, M., Rodríguez, V.P., Mefed, K., Hanada, K., Ahn, K.-S., Gangakhedkar, S.J., Pakzad, S.R., Prawahju, E.I., Lee, N., Phumiamorn, S., Nemec, M., Meng, S., Knezevic, I., 2015. Review of the current use and evaluation of cell substrates for producing biologicals in selected countries. Biologicals 43, 153–157.

Kantardjieff, A., Zhou, W., 2014. Mammalian cell cultures for biologics manufacturing, in: Advances in Biochemical Engineering/Biotechnology. Springer Berlin Heidelberg, pp. 1–9.

Kargi, F., 1992. Membrane bioreactors for animal cell culture., in: Vardar-Sukan, F., Sukan, Ş.S. (Eds.), Recent Advances in Biotechnology. Springer Netherlands, Dordrecht, pp. 449–454.

Kato, Y., Peter, C.P., Akgün, A., Büchs, J., 2004. Power consumption and heat transfer resistance in large rotary shaking vessels. Biochem. Eng. J. 21, 83–91.

Kaufman, J.B., Wang, G., Zhang, W., Valle, M.A., Shiloach, J., 2000. Continuous production and recovery of recombinant Ca2+ binding receptor from HEK 293 cells using perfusion through a packed bed bioreactor. Cytotechnology 33, 3–11.

Kauling, J., Brod, H., Jenne, M., Waldhelm, A., Langer, U., Bödeker, B., 2013. Novel, rotary oscillated, scalable single-use bioreactor technology for the cultivation of animal cells. Chemie Ing. Tech. 85, 127–135.

Kemp, R.B., Guan, Y., 1997. Heat flux and the calorimetric-respirometric ratio as measures of catabolic flux in mammalian cells. Thermochim. Acta 300, 199–211.

Kennedy, E., Fecheyr-Lippens, D., Hsiung, B.-K., Niewiarowski, P.H., Kolodziej, M., 2015. Biomimicry: A Path to Sustainable Innovation. Des. Issues 31, 66–73.

Kermani, A., Shen, L., 2009. Surface age of surface renewal in turbulent interfacial transport. Geophys. Res. Lett. 36, L10605.

Kiesslich, S., Kamen, A.A., 2020. Vero cell upstream bioprocess development for the production of viral vectors and vaccines. Biotechnol. Adv.

Kim, M.S., Kim, N.S., Sung, Y.H., Lee, G.M., 2002. Biphasic culture strategy based on hyperosmotic pressure for improved humanized antibody production in Chinese hamster ovary cell culture. Vitr. Cell. Dev. Biol. - Anim. 38, 314–319.

Klemm, F., Joyce, J.A., 2015. Microenvironmental regulation of therapeutic response in cancer. Trends Cell Biol. 25, 198–213.

Klöckner, W., Gacem, R., Anderlei, T., Raven, N., Schillberg, S., Lattermann, C., Buchs, J., 2013. Correlation between mass transfer coefficient kLa and relevant operating parameters in cylindrical disposable shaken bioreactors on a bench-to-pilot scale. J. Biol. Eng. 7, 28.

Knorre, D.G., Kudryashova, N. V, Godovikova, T.S., 2009. Chemical and functional aspects of posttranslational modification of proteins. Acta Naturae 1, 29–51.

Kohler, G., Milstein, C., 1975. Continuous cultures of fused cells secreting antibody of predefined specificity. Nature 256, 495–497.

Koizumi, J., Aiba, S., 1984. Reassessment of the dynamic KLa method. Biotechnol. Bioeng. 26, 1131–1133.

Kontoravdi, C., Samsatli, N.J., Shah, N., 2013. Development and design of bio-pharmaceutical processes. Curr. Opin. Chem. Eng. 2, 435–441.

Kornecki, M., Strube, J., 2019. Accelerating Biologics Manufacturing by Upstream. Processes 7, 166.

Krampe, B., Al-Rubeai, M., 2010. Cell death in mammalian cell culture: molecular mechanisms and cell line engineering strategies. Cytotechnology 62, 175–188.

Krause, K., Maciag-Dorszynska, M., Wosinski, A., Gaffke, L., Morcinek-Orłowska, J., Rintz, E., Bielanska, P., Szalewska-Pałasz, A., Muskhelishvili, G., Wegrzyn, G., 2020. The Role of Metabolites in the Link between DNA Replication and Central Carbon Metabolism in Escherichia coli. Genes (Basel). 11, 447.

Kretzmer, G., 2002. Industrial processes with animal cells. Appl. Microbiol. Biotechnol. 59, 135–142.

Krishnamurti, U., Zhou, B., Fan, W.-W., Tsilibary, E., Wayner, E., Kim, Y., Kashtan, C. liford E., Michael, A., 2001. Puromycin aminonucleoside suppresses integrin expression in cultured glomerular epithelial cells. J. Am. Soc. Nephrol. 12, 758–66.

Kuncewicz, C., Szulc, K., Kurasinski, T., 2005. Hydrodynamics of the tank with a screw impeller. Chem. Eng. Process. 44, 766–774.

Kunert, R., Reinhart, D., 2016. Advances in recombinant antibody manufacturing. Appl Microbiol Biotechnol 100, 3451–3461.

Lai, T., Yang, Y., Ng, S.K., 2013. Advances in mammalian cell line development technologies for recombinant protein production. Pharmaceuticals 6, 579–603.

Langer, E.S., Rader, R.A., 2014. Continuous bioprocessing and perfusion: wider adoption coming as bioprocessing matures. Bioprocess. J. 13, 43–49.

Lao, M.-S., Toth, D., 1997. Effects of Ammonium and Lactate on Growth and Metabolism of a Recombinant Chinese Hamster Ovary Cell Culture. Biotechnol. Prog. 13, 688–691.

Lee, B.-B., Ravindra, P., Chan, E.-S., 2013. Size and Shape of Calcium Alginate Beads Produced by Extrusion Dripping. Chem. Eng. Technol. 36, 10, 1627-1642.

Lee, B., Fang, D., Croughan, M., Carrondo, M., Paik, S.-H., 2011. Characterization of novel pneumatic mixing for single-use bioreactor application. BMC Proc. 5, O12.

Leelavatcharamas, V., Emery, A.N., A1-Rubeai, M., 1994. Growth and interferon-γ production in batch culture of CHO cells. Cytotechnology 15, 65–71.

Legate, K.R., Wickström, S.A., Fässler, R., 2009. Genetic and cell biological analysis of integrin outside-in signaling. Genes Dev. 23, 397–418.

Levine, H.L., Stock, R., Lilja, J.E., Gaasvik, Å., Hummel, H., Ransohoff, T.C., Jones, S.D., 2013. Single-use technology and modular construction. Bioprocess Int. 11, 40–45.

Lewis, W.K., Whitman, W.G., 1924. Principles of Gas Absorption. Ind. Eng. Chem. 16, 1215–1220.

Li, F., Vijayasankaran, N., Shen, A.Y., Kiss, R., Amanullah, A., 2010. Cell culture processes for monoclonal antibody production. MAbs 2, 466–479.

Li, L., Shi, M., Song, Y., Bao, L., Yang, W., Zhang, Xueting, Ruan, M., Rishton, G., Joudi, A., Teng, Y., Xing, Y., Hu, F., Zhao, X., Zhang, Xiuqin, Li, H., Leng, G., Yuan, S., Jia, Q., Hui, M. (Mizhou), 2009. A single-use, scalable perfusion bioreactor system. Bioprocess Int. 7, 46–54.

LifeSciences, G.H., 2013. Microcarrier Cell Culture-Principles and Methods.

Linek, V., Sinkule, J., Benes, P., 1991. Critical assessment of gassing-in method measuring kLa in fermentors. Biotechnol. Bioeng. 38, 323–330.

Litwin, J., 1992. The growth of Vero cells in suspension as cell-aggregates in serum-free media. Cytotechnology 10, 169–174.

Ljunggren, J., Häggström, L., 1995. Specific Growth Rate as a Parameter for Tracing Growth Limiting Substances, in: Beuvery, E.C., Griffiths, J.B., Zeijlemaker, W.P. (Eds.), Animal Cell Technology: Developments Towards the 21st Century. Springer Netherlands, Dordrecht, pp. 229–233.

Löffelholz, C., Husemann, U., Greller, G., Meusel, W., Kauling, J., Ay, P., Kraume, M., Eibl, R., Eibl, D., 2013a. Bioengineering parameters for single-use bioreactors: overview and evaluation of suitable methods. Chemie Ing. Tech. 85, 40–56.

Löffelholz, C., Kaiser, S.C., Kraume, M., Eibl, R., Eibl, D., 2013b. Dynamic single-use bioreactors used in modern liter- and m3 - scale biotechnological processes : Engineering characteristics and scaling up.,

in: Disposable Bioreactors II, Disposable Bioreactors II. Springer Berlin Heidelberg, pp. 1–44.

Lopes, A.G., 2015. Single-use in the biopharmaceutical industry: A review of current technology impact, challenges and limitations. Food Bioprod. Process. 93, 98–114.

Lu, J.-T., Chung, Y.-C., Chan, Z.-R., Hu, Y.-C., 2005. A novel oscillating bioreactor BelloCell: implications for insect cell culture and recombinant protein production. Biotechnol. Lett. 27, 1059–1065.

Lu, W., Su, X., Klein, M.S., Lewis, I.A., Fiehn, O., Rabinowitz, J.D., 2017. Metabolite measurement: pitfalls to avoid and practices to follow. Annu. Rev. Biochem. 86, 277–304.

Lurie-Luke, E., 2014. Product and technology innovation: What can biomimicry inspire? Biotechnol. Adv. 32, 1494–1505.

Ma, N., Mollet, M., Chalmers, J., 2006. Aeration, mixing and hydrodynamics in bioreactors, in: Ozturk, S.S., Hu, W.-S. (Eds.), Cell Culture Technology for Pharmaceutical and Cell-Based Therapies. CRC Press, pp. 225–248.

Makaula, D.X., Huddy, R., Fagan-Endres, M., Harrison, S., 2017a. Investigating the microbial metabolic activity on mineral surfaces of pyrite-rich waste rocks in an unsaturated heap-simulating column system, in: Solid State Phenomena.

Makaula, D.X., Huddy, R.J., Fagan-Endres, M.A., Harrison, S.T.L., 2017b. Using isothermal microcalorimetry to measure the metabolic activity of the mineral-associated microbial community in bioleaching. Miner. Eng. 106, 33–38.

Malerba, F., 2017. Sectoral systems of innovation and production. Res. Policy 31, 247–264.

Mandenius, C.-F., 2016. Challenges for bioreactor design and operation, in: Bioreactors: Design, Operation and Novel Applications. pp. 1–34.

Marasco, D.M., Gao, J., Griffiths, K., Froggatt, C., Wang, T., Wei, G., 2013. Development and characterization of a cell culture manufacturing process using quality by design (QbD) principles., in: Zhou, W., Kantardjieff, A. (Eds.), Mammalian Cell Cultures for Biologics Manufacturing. Advances in Biochemical Engineering/BiotechnologyAdvances in Biochemical Engineering/Biotechnology. Springer, Berlin, Heidelberg, pp. 93–121.

Margaritis, A., Wallace, J.B., 1984. Novel Bioreactor Systems and Their Applications. Nat. Biotechnol. 2, 447–453.

Marks, D.M., 2003. Equipment design considerations for large scale cell culture. Cytotechnology 42, 21–33.

Marshall, A., Lozeva, S., 2009. Questioning the theory and practice of biomimicry. Int. J. Des. Nat. Ecodynamics 4, 1–10.

Martínez-Monge, I., Comas, P., Triquell, J., Casablancas, A., Lecina, M., Paredes, C.J., Cairó, J.J., 2019. Concomitant consumption of glucose and lactate: A novel batch production process for CHO cells. Biochem. Eng. J. 151, 107358.

Maskow, T., Paufler, S., 2015. What does calorimetry and thermodynamics of living cells tell us? Methods 76, 3–10.

Meier, S.J., Hatton, T.A., Wang, D.I.C., 1999. Cell death from bursting bubbles: Role of cell attachment to rising bubbles in sparged reactors. Biotechnol. Bioeng. 62, 468–478.

Merchuk, J.C., 2008. Airlift bioreactors: Review of recent advances. Can. J. Chem. Eng. 81, 324–337.

Merchuk, J.C., Yona, S., Siegel, M.H., Zvi, A. Ben, 1990. On the first-order approximation to the response of dissolved oxygen electrodes for dynamic KLa estimation. Biotechnol. Bioeng. 35, 1161–1163.

Merck Millipore, 2015. Press Release: Merck Millipore introduces the Mobius® 2000 liter single-use bioreactor with industry-leading design for ease-of-use.

Mersmann, A., Schneider, G., Voit, H., Wenzig, E., 1990. Selection and design of aerobic bioreactors. Chem. Eng. Technol. - CET 13, 357–370.

Merten, O.-W., 2006. Introduction to animal cell culture technology—past, present and future.

Cytotechnology 50, 1–7.

Meuwly, F., Papp, F., Ruffieux, P.-A., Bernard, A.R., Kadouri, A., von Stockar, U., 2006. Use of glucose consumption rate (GCR) as a tool to monitor and control animal cell production processes in packed-bed bioreactors. J. Biotechnol. 122, 122–129.

Meuwly, F., Ruffieux, P.-A., Kadouri, A., von Stockar, U., 2007. Packed-bed bioreactors for mammalian cell culture: Bioprocess and biomedical applications. Biotechnol. Adv. 25, 45–56.

Mirasol, F., 2018. Industry adoption of single-use systems remains low. BioPham Int. 31, 33–35.

Mirro, R., Voll, K., 2009. Which impeller is right for your cell line? Bioprocess Int. 7, 52–57.

Mitteregger, R., Vogt, G., Rossmanith, E., Falkenhagen, D., 1999. Rotary Cell Culture System (RCCS): A new Method for Cultivating Hepatocytes on Microcarriers. Int. J. Artif. Organs 22, 816–822.

Mollet, M., Godoy-Silva, R., Berdugo, C., Chalmers, J.J., 2007. Acute hydrodynamic forces and apoptosis: A complex question. Biotechnol. Bioeng. 98, 772–788.

Mordor Intelligence, 2019. Biopharmaceuticals market - Growth, trends, and forecast (2019 - 2024).

Moreno-Layseca, P., Streuli, C.H., 2014. Signalling pathways linking integrins with cell cycle progression. Matrix Biol. 34, 144–153.

Morikawa, N., Iwata, H., Matsuda, S., Miyazaki, J.-I., Ikada, Y., 1997. Encapsulation of mammalian cells into synthetic polymer membranes using least toxic solvents. J. Biomater. Sci. Polym. Ed. 8, 575–586.

Mousa, S.A., 2002. Anti-integrin as novel drug-discovery targets: Potential therapeutic and diagnostic implications. Curr. Opin. Chem. Biol. 6, 534–541.

Moutafchieva, D., Popova, D., Dimitrova, M., Tchaoushev, S., 2013. Experimental determination of the volumetric mass transfer coefficient. J. Chem. Technol. Metall. 48, 351–356.

Müller, M., Ruhl, S., Noack, U., Greller, G., Wilde, D. De, Adams, T., 2015. Large scale cultivation of CHO cells in the stirred single-use bioreactor BIOSTAT® CultiBag STR. Application Note-#1.

Murhammer, D.W., Goochee, C.F., 1990. Sparged animal cell bioreactors: Mechanism of cell damage and pluronic F-68 protection. Biotechnol. Prog. 6, 391–397.

Myers, M., 2017. Investigating process stresses on Saccharomyces cerevisiae using isothermal microcalorimetry. University of Cape Town.

Namdev, P.K., Lio, P., 2000. Assessing a disposable bioreactor for attachment-dependent cell cultures. BioPharm 13, 44–51.

Nässberger, L., Truedsson, L., Monti, M., 1988. Microcalorimetric studies of hybridoma cells. Biol. Cell 62, 33–37.

Nayar, G., 1995. Oxygen transport in animal cell bioreactors with vibrating-plate aerators.[Ph.D Thesis]. Massachusetts Institute of Technology.

Nedergaard, J., Cannon, B., Lindberg, O., 1977. Microcalorimetry of isolated mammalian cells. Nature 267, 518–520.

Negrete, A., Ling, T.C., Lyddiatt, A., 2008. Effect of pluronic F-68, 5% CO2 atmosphere, HEPES, and antibiotic-antimycotic on suspension adapted 293 cells. Open Biotechnol. J. 2, 229–234.

Nienow, A.W., 2015. Mass transfer and mixing across the scales in animal cell culture, in: Al-Rubeai, M. (Ed.), Animal Cell Culture. Cell Engineering, Vol 9. Springer International Publishing, pp. 137–167.

Nienow, A.W., 2010. Impeller selection for animal cell culture., in: Flickinger, M.C. (Ed.), Encyclopedia of Industrial Biotechnology. John Wiley & Sons, Inc., Hoboken, NJ, USA, pp. 1–25.

Nienow, A.W., 2006. Reactor Engineering in Large Scale Animal Cell Culture. Cytotechnology 50, 9–33.

Nienow, A.W., 1997. On impeller circulation and mixing effectiveness in the turbulent flow regime. Chem. Eng. Sci. 52, 2557–2565.

Omasa, T., Onitsuka, M., Kim, W.-D., 2010. Cell engineering and cultivation of Chinese hamster ovary (CHO) cells. Curr. Pharm. Biotechnol. 11, 233–240.

Oosterhuis, N., Junne, S., 2016. Design, applications, and development of single-use bioreactors, in: C.-F. Mandenius (Ed.), Bioreactors: Design, Operation and Novel Applications. Wiley-VCH Verlag GmbH & Co. KGaA, pp. 261–290.

Orive, G., Hernández, R.M., Gascón, A.R., Igartua, M., Pedraz, J.L., 2002. Encapsulated cell technology: from research to market. Trends Biotechnol. 20, 382–387.

Orton, D.R., 1993. Quantitative and mechanistic effects of bubble aeration on animal cells in culture. [Ph.D Thesis]. Massachusetts Institute of Technology.

Ozturk, S.S., 2014. Equipment for Large-Scale Mammalian Cell Culture, in: Advances in Biochemical Engineering/Biotechnology. pp. 69–92.

Ozturk, S.S., 1996. Engineering challenges in high density cell culture systems. Cytotechnology 22, 3–16.

Pacis, E., Yu, M., Autsen, J., Bayer, R., Li, F., 2011. Effects of cell culture conditions on antibody N-linked glycosylation-what affects high mannose 5 glycoform. Biotechnol. Bioeng. 108, 2348–2358.

Paillet, C., Forno, G., Kratje, R., Etcheverrigaray, M., 2009. Suspension-Vero cell cultures as a platform for viral vaccine production. Vaccine 27, 6464–6467.

Pall Life Sciences, 2014. Cultivation of CHO cells in Allegro ™ STR 200 single-use stirred tank bioreactor system. [Application note USD2926].

Park, S., Stephanopoulos, G., 1993. Packed bed bioreactor with porous ceramic beads for animal cell culture. Biotechnol. Bioeng. 41, 25–34.

Patra, S.K., Muchie, M., 2017. Role of innovation system in development of biotechnology in South Africa, Asian Biotechnology and Development Review.

Perepelitsa, N., Kaiser, S.C., Eibl, D., n.d. Cultivation of CHO suspension cells and SEAP expression in the Wave-mixed single-use Finesse smart rocker bioreactor [Application Note].

Perepelitsa, N., Kaiser, S.C., Eibl, D., n.d. Cultivation of CHO Suspension Cells and SEAP Expression in the Wave-mixed Single-use Finesse SmartRocker Bioreactor.

Persistence Market Research, 2015. Biopharmaceuticals market - Global study on biopharmaceuticals: Asia to witness highest growth by 2020.

Pol, L. Van Der, Tramper, J., 1998. Shear sensitivity of animal cells from a culture-medium perspective. Trends Biotechnol. 16, 323–328.

Popović, M.K., Pörtner, R., 2012. Bioreactors and cultivation systems for cell and tissue culture. Encycl. Life Support Syst. (EOLLS), Dev. under Auspices UNESCO.

Pörtner, R., 2015. Bioreactors for mammalian cells., in: Al-Rubeai M (Ed.), Animal Cell Culture. Cell Engineering, Vol 9. Springer International Publishing Switzerland, pp. 89–135.

Pörtner, R., Barradas, O.B.J.P., 2007. Cultivation of mammalian cells in fixed-bed reactors., in: Pörtner R. (Ed.), Animal Cell Biotechnology. Methods in Biotechnology. Humana Press, pp. 353–369.

Pörtner, R., Platas, O.B., Fassnacht, D., Nehring, D., Czermak, P., Märkl, H., 2007. Fixed Bed Reactors for the Cultivation of Mammalian Cells: Design, Performance and Scale-Up. Open Biotechnol. J. 1, 41–46.

Quek, L.-E., Dietmair, S., Krömer, J.O., Nielsen, L.K., 2010. Metabolic flux analysis in mammalian cell culture. Metab. Eng. 12, 161–171.

Raab-Westphal, S., Marshall, J., Goodman, S., Raab-Westphal, S., Marshall, J.F., Goodman, S.L., 2017. Integrins as Therapeutic Targets: Successes and Cancers. Cancers (Basel). 9, 110.

Raval, K., Kato, Y., Büchs, J., 2007. Comparison of torque method and temperature method for determination of power consumption in disposable shaken bioreactors. Biochem. Eng. J. 34, 224–227.

Rawlings, B., Pora, H., 2009. Environmental impact of single-use and reusable bioprocess systems. Bioprocess Int. 7, 18–26.

Read, E.K., Park, J.T., Shah, R.B., Riley, B.S., Brorson, K.A., Rathore, A.S., 2010. Process analytical technology (PAT) for biopharmaceutical products : Part I . Concepts and applications. Biotechnol. Bioeng. 105, 276–284.

Regine, E., Dieter, E., 2011. Single-use technology in biopharmaceutical manufacture. John Wiley & Sons, Inc., Hoboken, NJ, USA.

Reitzer, L.J., Wice, B.M., Kennell., D., 1979. Evidence That Glutamine, Not Sugar, Is the Major Energy Source for Cultured HeLa Cells. J. Biol. Chem. 254, 2669–2676.

Rentschler Biotechnologie, 2015. Employing new single-use technology in bioprocesses. Manuf. Chem. XV 15–16.

Research and Markets, 2017a. Global biopharmaceuticals market growth, trends & forecasts (2017 - 2022).

Research and Markets, 2017b. Global biopharmaceutical market analysis & trends - Industry forecast to 2017-2025".

Riemann, H.K., 2012. CellVessel STR (#21-2000) – Functionality test using CHO cells.

Riess, J.G., 2005. Understanding the Fundamentals of Perfluorocarbons and Perfluorocarbon Emulsions Relevant to In Vivo Oxygen Delivery. Artif. Cells, Blood Substitutes, Biotechnol. 33, 47–63.

Riley, S., 2016. Modular manufacturing. Pharm. Process. (accessed 4.21.18).

Riss, T.L., Moravec, R.A., Niles, A.L., Benink, H.A., Worzella, T.J., Minor, L., 2016. Cell viability assays, Assay Guidance Manual [Internet]. Eli Lilly & Company and the National Center for Advancing Translational Sciences.

Rodrigues, M.E., Costa, A.R., Henriques, M., Azeredo, J., Oliveira, R., 2010. Technological progresses in monoclonal antibody production systems. Biotechnol. Prog. 26, 332–351.

Rodríguez-Hernández, C.O., Torres-García, S.E., Olvera-Sandoval, C., Ramírez-Castillo, F.Y., Muro, A.L., Avelar-Gonzalez, F.J., Guerrero-Barrera, Lilián, A., 2014. Cell culture : History , development and prospects. Int. J. Curr. Res. Acad. Rev. 2, 188–200.

Rogge, P., Müller, P.D.D., 2014. Single-use bioprocesses hype or future technology ? Rentschler Biotechnol. 20, 20–21.

Rourou, S., 2009. Development of an animal-component free medium for Vero cells culture. Biotechnol. Prog. 25, 1752–1761.

Rourou, S., Ben Zakkour, M., Kallel, H., 2019. Adaptation of Vero cells to suspension growth for rabies virus production in different serum free media. Vaccine 37, 6987–6995.

Rourou, S., van der Ark, A., Majoul, S., Trabelsi, K., van der Velden, T., Kallel, H., 2009. A novel animal-component-free medium for rabies virus production in Vero cells grown on Cytodex 1 microcarriers in a stirred bioreactor. Appl. Microbiol. Biotechnol. 85, 53–63.

Ruchti, G., Dunn, I.J., Bourne, J.R., 1981. Comparison of dynamic oxygen electrode methods for the measurement of KLa. Biotechnol. Bioeng. 23, 277–290.

Said, J., Walker, M., Parsons, D., Stapleton, P., Beezer, A.E., Gaisford, S., 2015. Development of a flow system for studying biofilm formation on medical devices with microcalorimetry. Methods 76, 35–40.

Sánchez Pérez, J.A., Rodríguez Porcel, E.M., Casas López, J.L., Fernández Sevilla, J.M., Chisti, Y., 2006. Shear rate in stirred tank and bubble column bioreactors. Chem. Eng. J. 124, 1–5.

Sandadi, Sandeepa, Pedersen, Henrik, Bowers, John S, Rendeiro, D., Sandadi, S, Bowers, J S, Rendeiro, Á.D., Pedersen, H, 2011. A comprehensive comparison of mixing, mass transfer, Chinese hamster ovary cell growth, and antibody production using rushton turbine and marine impellers. Bioprocess Biosyst. Eng. 34, 819–832.

Sandstrom, C., 2009. Disposable vs. traditional equipment- A facility-wide view. CEP 30–35.

Šantek, B., Ivanèiæ, M., Horvat, P., Novak, S., Mariæ, V., 2006. Horizontal tubular bioreactors in biotechnology. Chem. Biochem. Eng. [Quarterly] 20, 389–399.

Sartorius Stedim Biotech, 2014. CultiBag ORB.

Schmidt, K., Keller, M., Bader, B.L., Korytář, T., Finke, S., Ziegler, U., Groschup, M.H., 2013. Integrins modulate the infection efficiency of West Nile virus into cells. J. Gen. Virol. 94, 1723–1733.

Schnitzler, A.C., Verma, A., Kehoe, D.E., Jing, D., Murrell, J.R., Der, K.A., Aysola, M., Rapiejko, P.J., Punreddy, S., Rook, M.S., 2016. Bioprocessing of human mesenchymal stem/stromal cells for therapeutic use: Current technologies and challenges. Biochem. Eng. J. 108, 3–13.

Schwager, S.L., Carmona, A.K., Sturrock, E.D., 2006. A high-throughput fluorimetric assay for angiotensin I-converting enzyme. Nat. Protoc. 1, 1961–1964.

Schwarz, R.P., Wolf, D.A., Trinh, T.T., 1991. Horizontally rotated cell culture system with a coaxial tubular oxygenator. US5026650 A.

Scott, C., 2007. Single-use bioreactors: A brief review of current technology. Bioprocess Int. 5, 44–51.

Seguin, L., Desgrosellier, J.S., Weis, S.M., Cheresh, D.A., 2015. Integrins and cancer: regulators of cancer stemness, metastasis, and drug resistance. Trends Cell Biol. 25, 234–240.

Selker, M., Paldus, B., 2008. Disposable bioreactor system. US20080274541 A1.

Shakibaie, M., Tabandeh, F., Zomorodipour, A.R., Mohammad-Beigi, H., Ebrahimi, S., Habib-Ghomi, H., 2011. Kinetics, experimental and simulation studies of Chinese hamster ovary cell growth in a packed-bed bioreactor. World Appl. Sci. J. 15, 1568–1575.

Shattil, S.J., Kim, C., Ginsberg, M.H., 2010. The final steps of integrin activation: the end game. Nat. Rev. Mol. Cell Biol. 11, 288–300.

Sheets, R., 2000. History and characterization of the Vero cell line. Silver Spring, MD.

Shen, C.F., Guilbault, C., Li, X., Elahi, S.M., Ansorge, S., Kamen, A., Gilbert, R., 2019. Development of suspension adapted Vero cell culture process technology for production of viral vaccines. Vaccine 37, 6996–7002.

Shukla, A.A., Gottschalk, U., 2013. Single-use disposable technologies for biopharmaceutical manufacturing. Trends Biotechnol. 31, 147–154.

Sidoli, F.R., Mantalaris, A., Asprey, S.P., 2004. Modelling of mammalian cells and cell culture processes. Cytotechnology 44, 27–46.

Sinacore, M.S., Drapeau, D., Adamson, S.R., 2000. Adaptation of mammalian cells to growth in serum-free media. Mol. Biotechnol. 15, 249–257.

Singh, V., 1999. Disposable bioreactor for cell culture using wave-induced agitation. Cytotechnology 30, 149–158.

Singh, W., 1996. Communication to the Editor. Biotechnol. Bioeng. 52, 443–448.

Slivac, I., Blajić, V., Radošević, K., Kniewald, Z., Gaurina Srček, V., 2010. Influence of different ammonium, lactate and glutamine concentrations on CCO cell growth. Cytotechnology 62, 585–94.

Smelko, J.P., Wiltberger, K.R., Hickman, E.F., Morris, B.J., Blackburn, T.J., Ryll, T., 2011. Performance of high intensity fed-batch mammalian cell cultures in disposable bioreactor systems. Biotechnol. Prog. 27, 1358–1364.

Somanath, P.R., Kandel, E.S., Hay, N., Byzova, T. V, 2007. Akt1 signaling regulates integrin activation, matrix recognition, and fibronectin assembly. J. Biol. Chem. 282, 22964–76.

Sousa, M.F.Q., Silva, M.M., Giroux, D., Hashimura, Y., Wesselschmidt, R., Lee, B., Roldão, A., Carrondo, M.J.T., Alves, P.M., Serra, M., 2015. Production of oncolytic adenovirus and human mesenchymal stem cells in a single-use, Vertical-Wheel bioreactor system: Impact of bioreactor design on performance of microcarrier-based cell culture processes. Biotechnol. Prog. 31, 1600–1612.

Stanton, D., 2015. Big Biopharma? ABEC launches 4,300L single-use bioreactor [Press release]. Biopharma Report.

Staunton, D.E., Lupher, M.L., Liddington, R., Gallatin, W.M., 2006. Targeting Integrin Structure and Function

in Disease. Adv. Immunol. 91, 111–157.

Stewart, P.L., Nemerow, G.R., 2007. Cell integrins: commonly used receptors for diverse viral pathogens. Trends Microbiol. 15, 500–507.

Szczypka, M., Splan, D., Wools, H., Brandwein, H., 2014. Single-use bioreactors and microcarriers. Bioprocess Int. 12, 54–68.

TA Instruments, 2012. TAM III Brochure/ Microcalorimetry.

TA Instruments, n.d. Calorimetric Principles and Calorimetry Calorimetry.

Takada, Y., Ye, X., Simon, S., 2007. The integrins. Genome Biol. 8, 215.

Tan, A.M., Lu, J.H., 1999. Microcalorimetric study of antiviral effect of drug. J. Biochem. Biophys. Methods 38, 225–228.

Tapia, F., Vázquez-Ramírez, D., Genzel, Y., Reichl, U., 2016. Bioreactors for high cell density and continuous multi-stage cultivations: options for process intensification in cell culture-based viral vaccine production. Appl. Microbiol. Biotechnol. 100, 2121–2132.

Telling, R.C., Elsworth, R., 1965. Submerged culture of hamster kidney cells in a stainless steel vessel. Biotechnol. Bioeng. 7, 417–434.

Terrier, B., Courtois, D., Hénault, N., Cuvier, A., Bastin, M., Aknin, A., Dubreuil, J., Pétiard, V., 2007. Two new disposable bioreactors for plant cell culture: the wave and undertow bioreactor and the slug bubble bioreactor. Biotechnol. Bioeng. 96, 914–923.

The Dolomite Centre Ltd, n.d. CHO cell encapsulation & incubation in gelatin particles [Application note].

Tissot, S., 2011. OrbShake bioreactors for mammalian cell cultures : Engineering and scale-up [Ph.D Thesis]. École Polytechnique Federale De Lausanne.

Tissot, S., Oberbek, A., Reclari, M., Dreyer, M., Hacker, D.L., Baldi, L., Farhat, M., Wurm, F.M., 2011. Efficient and reproducible mammalian cell bioprocesses without probes and controllers. N. Biotechnol. 28, 382–390.

Tolbert, W.R., 1990. Manufacture of biopharmaceutical proteins by mammalian cell culture systems. Biotechnol. Adv. 8, 729–739.

Tolomelli, A., Galletti, P., Baiula, M., Giacomini, D., 2017. Can integrin agonists have cards to play against cancer? A literature survey of small molecules integrin activators. Cancers (Basel). 9.

Toriniwa, H., Komiya, T., 2007. Japanese encephalitis virus production in Vero cells with serum-free medium using a novel oscillating bioreactor. Biologicals 35, 221–226.

Tramper, J., Smit, D., Straatman, J., Vlak, J.M., 1988. Bubble-column design for growth of fragile insect cells. Bioprocess Eng. 3, 37–41.

Tran, T.T., Lee, E.G., Lee, I.S., Woo, N.S., Han, S.M., Kim, Y.J., Hwang, W.R., 2016. Hydrodynamic extensional stress during the bubble bursting process for bioreactor system design. Korea Aust. Rheol. J. 28, 315–326.

Transparency Market Research., 2016. Biopharmaceutical Market - US Industry Size, Market Share, Smart Trends, Analysis and Forecast 2016 - 2024 (accessed 3.13.19).

Tribe, L.A., Briens, C.L., Margaritis, A., 1995. Determination of the volumetric mass transfer coefficient (kLa) using the dynamic ?gas out-gas in? method: Analysis of errors caused by dissolved oxygen probes. Biotechnol. Bioeng. 46, 388–392.

Tsui, Y.-Y., Hu, Y.-C., 2008. Mixing flow characteristics in a vessel agitated by the screw impeller with a draught tube. ASME. J. Fluids Eng. 130, 041103–041110.

Uludag, H., De Vos, P., Tresco, P.A., 2000. Technology of mammalian cell encapsulation. Adv. Drug Deliv. Rev. 42, 29–64.

Uzir, M.H., Don, M.M., 2007. Biochemical engineering: A concise introduction, Universiti Sains Malaysia, Penang.

Vaccixcell, 2016. Vaccixcell cradle for high density cells.

Vaccixcell, n.d. CelCradle-500 Technical Report VI Cultivation of CHO Cells for Protein Secretion Table of Contents.

Van't Riet, K., 1979. Review of measuring methods and results in nonviscous gas-liquid mass transfer in stirred vessels. Ind. Eng. Chem. Process Des. Dev 18, 357–364.

Van't Riet, K., Tramper, J., 1991. Basic bioreactor design, illustrate. ed. CRC Press.

Varley, J., Birch, J., 1999. Reactor design for large scale suspension animal cell culture. Cytotechnology 29, 177–205.

Velez-Suberbie, M.L., Tarrant, R.D.R., Tait, A.S., Spencer, D.I.R., Bracewell, D.G., 2013. Impact of aeration strategy on CHO cell performance during antibody production. Biotechnol. Prog. 29, 116–126.

Villadsen, J., Nielsen, J., Liden, G., 2011. Bioreaction Engineering Principles, 3rd ed. Springer, New York.

von Ah, U., Wirz, D., Daniels, A., 2009. Isothermal micro calorimetry – a new method for MIC determinations: results for 12 antibiotics and reference strains of E. coli and S. aureus. BMC Microbiol. 9, 106.

Vyas, R., Cino, J., 2007. A technique for increasing yields in bioreactors and disposable cell-culture systems. Nat. Methods AN7–AN8.

Wadsö, I., Hallén, D., Jansson, M., Suurkuusk, J., Wenzler, T., Braissant, O., 2017. A well-plate format isothermal multi-channel microcalorimeter for monitoring the activity of living cells and tissues. Thermochim. Acta 652, 141–149.

Walsh, G., 2005. Biopharmaceuticals: recent approvals and likely directions. Trends Biotechnol. 23, 553–558.

Wang, D., Liu, W., Han, B., Xu, R., 2005. The Bioreactor: A Powerful Tool for Large-Scale Culture of Animal Cells. Curr. Pharm. Biotechnol. 6, 397–403.

Wang, G., Zhang, W., Jacklin, C., Freedman, D., Eppstein, L., Kadouri, A., 1992. Modified CelliGen-packed bed bioreactors for hybridoma cell cultures. Cytotechnology 9, 41–49.

Wang, G., Zhang, W., Mirro, R., Gossain, V., 2012. Growing CHO cells in a New Brunswick™ CelliGen® BLU benchtop, stirred-tank bioreactor using single-use Vessels.

Wang, T., Yu, G., Yong, Y., Yang, C., Mao, Z.-S., 2010. Hydrodynamic characteristics of dual-impeller configurations in a multiple-phase stirred tank. Ind. Eng. Chem. Res. 49, 1001–1009.

Wang, Y., Zhang, Y., Li, N., Chen, L., Zhang, D., Sun, D., Lv, G., Yu, W., Guo, X., Ma, X., 2015. Growth and production of microencapsulated recombinant CHO in a stirred tank bioreactor. Bioprocess Biosyst. Eng. 38, 1303–1312.

Warnock, J.N., Al-Rubeai, M., 2006. Bioreactor systems for the production of biopharmaceuticals from animal cells. Biotechnol. Appl. Biochem. 45, 1–12.

Wasan, D.T., Ahluwalia, M.S., 1969. Consecutive film and surface renewal mechanism for heat or mass transfer from a wall. Chem. Eng. Sci. 24, 1535–1542.

Weber, W., Rinderknecht, M., Daoud-El Baba, M., de Glutz, F.-N., Aubel, D., Fussenegger, M., 2004. CellMAC: a novel technology for encapsulation of mammalian cells in cellulose sulfate/pDADMAC capsules assembled on a transient alginate/Ca2+ scaffold. J. Biotechnol. 114, 315–326.

Wehrle-Haller, B., 2012. Structure and function of focal adhesions. Curr. Opin. Cell Biol. 24, 116–124.

Wenzler, T., Steinhuber, A., Wittlin, S., Scheurer, C., Brun, R., Trampuz, A., 2012. Isothermal Microcalorimetry, a New Tool to Monitor Drug Action against Trypanosoma brucei and Plasmodium falciparum. PLoS Negl. Trop. Dis. 6, e1668.

Whitford, W.G., 2010a. Single-use systems as principal components in bioproduction. Bioprocess Int. 8, 34–42.

Whitford, W.G., 2010b. Using disposables in cell-culture based vaccine production. Bioprocess Int. 8.

Williams, J.A., 2002. Keys to bioreactor selections. Chem. Eng. Prog. 98, 34–41.

Wilson, D., 2011. Culture vulture : Building a better bioreactor. Eng.

Wise, W.S., 1951. The Measurement of the Aeration of Culture Media. J. Gen. Microbiol 5, 167–177.

Wolff, C., Beutel, S., Scheper, T., 2013. Tubular membrane bioreactors for biotechnological processes. Appl. Microbiol. Biotechnol. 97, 929–937.

Woodley, J.M., Titchener-Hooker, N.J., 1996. The use of windows of operation as a bioprocess design tool. Bioprocess Eng. 14, 263–268.

Woodside, S.M., Bowen, B.D., Piret, J.M., 1998. Mammalian cell retention devices for stirred perfusion bioreactors. Cytotechnology 28, 163–175.

Wu, S.-C., Liau, M., Lin, Y.-C., Sun, C.-J., Wang, C.-T., 2013. The feasibility of a novel bioreactor for vaccine production of classical swine fever virus. Vaccine 31, 867–872.

Wurm, F.M., 2004. Production of recombinant protein therapeutics in cultivated mammalian cells. Nat. Biotechnol. 22, 1393–1398.

Xiao, T., Takagi, J., Coller, B.S., Wang, J.-H., Springer, T.A., 2004. Structural basis for allostery in integrins and binding to fibrinogen-mimetic therapeutics. Nature 432, 59–67.

Xie, K., Zhang, X.-W., Huang, L., Wang, Y.-T., Lei, Y., Rong, J., Qian, C.-W., Xie, Q.-L., Wang, Y.-F., Hong, A., Xiong, S., 2011. On-line monitoring of oxygen in Tubespin, a novel, small-scale disposable bioreactor. Cytotechnology 63, 345–50.

Xie, Q., Michel, P.O., Baldi, L., Hacker, D.L., Zhang, X., Wurm, F.M., 2011. TubeSpin bioreactor 50 for the high-density cultivation of Sf-9 insect cells in suspension. Biotechnol. Lett. 33, 897–902.

Yang, M., Butler, M., 2000. Effects of ammonia on CHO cell growth, erythropoietin production, and glycosylation. Biotechnol. Bioeng. 68, 370–80.

Yang, P.-C., Mahmood, T., 2012. Western blot: Technique, theory, and trouble shooting. N. Am. J. Med. Sci. 4, 429.

Yeo, D., 2014. Amgen unveils next-generation biomanufacturing facility in Singapore | Singapore Business News (accessed 4.21.18).

Zanghi, J.A., Schmelzer, A.E., Mendoza, T.P., Knop, R.H., Miller, W.M., 1999. Bicarbonate concentration and osmolality are key determinants in the inhibition of CHO cell polysialylation under elevated pCO2 or pH. Biotechnol. Bioeng. 65, 182–191.

Zeng, A.-P., Deckwer, W.-D., 1999. Model simulation and analysis of perfusion culture of mammalian cells at high cell density. Biotechnol. Prog. 15, 373–382.

Zent, R., Srichai, M.B., 2010. Integrin Structure and Function, in: Cell-Extracellular Matrix Interactions in Cancer. Springer, New York, NY, pp. 19–41.

Zhang, J., 2010. Mammalian Cell Culture for Biopharmaceutical Production. Man. Ind. Microbiol. Biotechnol. Third Ed. 157–178.

Zhang, X., Garcia, I.F., Baldi, L., Hacker, D.L., Wurm, F.M., 2010. Hyperosmolarity enhances transient recombinant protein yield in Chinese hamster ovary cells. Biotechnol. Lett. 32, 1587–1592.

Zhang, X., Stettler, M., Reif, O., Kocourek, A., Dejesus, M., Hacker, D.L., Wurm, F.M., 2008. Shaken helical track bioreactors: Providing oxygen to high-density cultures of mammalian cells at volumes up to 1000 L by surface aeration with air. N. Biotechnol. 25, 68–75.

Zhang, Y., Stobbe, P., Silvander, C.O., Chotteau, V., 2015. Very high cell density perfusion of CHO cells anchored in a non-woven matrix-based bioreactor. J. Biotechnol. 213, 28–41.

Zhong, J.-J., 2010. Recent advances in bioreactor engineering. Korean J. Chem. Eng. 27, 1035–1041.

Zhou, T.-C., Zhou, W.-W., Hu, W., Zhong, J.-J., 2010. Bioreactors, cell culture, commercial production, in: Flickinger, M.C. (Ed.), Encyclopedia of Industrial Biotechnology. John Wiley & Sons, pp. 1–18.

Zhu, J., 2012. Mammalian cell protein expression for biopharmaceutical production. Biotechnol. Adv. 30, 1158–70.

Zhu, M.M., Goyal, A., Rank, D.L., Gupta, S.K., Boom, T. Vanden, Lee, S.S., 2008. Effects of elevated pCO2 and osmolality on growth of CHO cells and production of antibody-fusion protein B1: A case study. Biotechnol. Prog. 21, 70–77.

Ziemlewski, J., 2009. The new disposable evolution. Chem. Eng. Prog. Mag. 105, 23–29.

Zijlstra, G.M., Oosterhuis, N., 2010. Cultivation of PER.C6® cells in the Novel CELL-Tainer™ High-performance disposable bioreactor., in: Noll, T. (Ed.), Cells and Culture. Springer Netherlands, pp. 807–808.

Zwietering, T.N., 1958. Suspending of solid particles in liquid by agitators. Chem. Eng. Sci. 8, 244–253.